Scientific and Engineering Studies

Compiled 1990

Signal Processing Studies

A. H. Nuttall

PUBLISHED BY

NAVAL UNDERWATER SYSTEMS CENTER

NEWPORT LABORATORY, NEWPORT, RHODE ISLAND

NEW LONDON LABORATORY, NEW LONDON, CONNECTICUT

Scientific and Engineering Studies

Compiled 1990

Signal Processing Studies

A. H. Nuttall

PUBLISHED BY

NAVAL UNDERWATER SYSTEMS CENTER

NEWPORT LABORATORY, NEWPORT, RHODE ISLAND

NEW LONDON LABORATORY, NEW LONDON, CONNECTICUT

Foreword

This collection of technical reports addresses the following topics: efficient evaluation of attenuation/minimum-phase pairs by means of two fast Fourier transforms; evaluation of integrals and sums involving powers of the ratio sin(Mx)/sin(x); determination of operating characteristics of weighted energy detectors with Gaussian signals; alias-free smoothed Wigner distribution functions and their properties; and an investigation of the filtered complex envelope for improved behavior.

Some of the material presented here is heavily based on the author's earlier work, which can be found in the following volumes in addition to the referenced technical reports:

Performance of Detection and Communication Systems,
NUSC Scientific and Engineering Studies, 1974;

Spectral Estimation,
NUSC Scientific and Engineering Studies, 1977;

Coherence Estimation,
NUSC Scientific and Engineering Studies, 1979;

Receiver Performance Evaluation and Spectral Analysis,
NUSC Scientific and Engineering Studies, 1981;

Signal Processing Studies,
NUSC Scientific and Engineering Studies, 1983;

Signal Processing Studies,
NUSC Scientific and Engineering Studies, 1985;

Signal Processing Studies,
NUSC Scientific and Engineering Studies, 1986;

Signal Processing Studies,
NUSC Scientific and Engineering Studies, 1987;

Signal Processing Studies,
NUSC Scientific and Engineering Studies, 1989.

Dr. William I. Roderick
Associate Technical Director
Research and Technology
NAVAL UNDERWATER SYSTEMS CENTER

Compiled 1990

TABLE OF CONTENTS

NUSC Technical Report 8667
31 January 1990

Evaluation of Attenuation/Minimum-Phase Pairs by Means of Two Fast Fourier Transforms

Albert H. Nuttall

ABSTRACT

A numerically efficient method of obtaining the minimum-phase characteristic corresponding to a measured attenuation (or decibel gain) response of a linear network, by means of two fast Fourier transforms, is presented and programmed in BASIC. A method of extrapolating the measured attenuation to very small and large frequencies, as required by the theoretical transformations, is suggested. The attendant logarithmic singularities in the attenuation are subtracted out and handled separately, leaving a residual which is well behaved for numerical Fourier transformation.

TABLE OF CONTENTS

LIST OF ILLUSTRATIONS

LIST OF SYMBOLS

τ	time delay, (1)
$h(\tau)$	impulse response, (1)
f	frequency, (1)
$H(f)$	transfer function, (1)
$\underline{F}$	Fourier transform, (1)
sub r	real part, (2)
sub i	imaginary part, (2)
sub e	even part, (4),(5)
sub o	odd part, (4),(5)
$\underline{H}$	Hilbert transform, (8)
$⨍$	principal value integral, (8),(A-1)
$\circledast$	convolution, (8)
$U(x)$	unit step function, (9)
$\delta(f)$	delta function, (10)
$\underline{h}(\tau)$	auxiliary function, (19),(20)
$\underline{F}^{-1}$	inverse Fourier transform, (19)
$b_H(\tau)$	Hilbert transform of $b(\tau)$, (28)
$B(f)$	spectrum of $b(\tau)$, (29)
C_1, C_2	contours in complex f-plane, (36),figure 1
$Q(f)$	auxiliary function, (38)
$q(\tau)$	inverse Fourier transform of $Q(f)$, (39)
$\alpha(f)$	attenuation, (42)
$\beta(f)$	phase shift, (42)
$\underline{q}(\tau)$	auxiliary function, (46)
$G(f)$	filter gain in decibels, (47)

$\alpha_1(f)$	singular attenuation, (54)
$\alpha_2(f)$	residual attenuation, (54)
$\beta_1(f)$	minimum-phase pair to $\alpha_1(f)$, (56)
$\beta_2(f)$	minimum-phase pair to $\alpha_2(f)$, (56)
K	frequency range of known values, (63)
U	frequency range of unknown values, (63)
s	argument of Laplace transform, (64)
L(s)	Laplace transform of impulse response $h(\tau)$, (64)
$g'(t)$	first derivative of g(t), (A-5)
ω	radian frequency, $2\pi f$, (B-2)

EVALUATION OF ATTENUATION/MINIMUM-PHASE PAIRS BY MEANS OF TWO FAST FOURIER TRANSFORMS

INTRODUCTION

It is often important to determine whether a given linear device is minimum-phase [1], because if so, it is then possible to compensate the filter characteristic with reciprocal pole-zero locations and obtain an overall all-pass characteristic with flat amplitude and linear phase responses. A relatively simple way of making this determination is to measure the attenuation (or decibel gain) and actual phase shift of the given linear device and then compute the minimum-phase corresponding to the measured attenuation. If this latter calculated phase agrees with the actual measured phase, then the filter is minimum-phase.

The minimum-phase corresponding to a given attenuation function is determined analytically by a Hilbert transform [2; chapter 6, article 22] or [3; section 10-3]. However, this direct integral evaluation is computationally unattractive due to two poles on the line of integration [3; (10-67)]. In addition, it yields only a single value for the phase after each numerical integration. We will circumvent both of these difficulties by first subtracting the singularities (which will be handled analytically) and then employing fast Fourier transforms for efficient numerical evaluation of the entire phase response.

TRANSFER FUNCTION RELATIONS

FILTER CHARACTERIZATIONS

A linear time-invariant filter is characterized by its impulse response $h(\tau)$ or by its transfer function $H(f)$ according to Fourier transform

$$H(f) = \int d\tau \exp(-i2\pi f\tau)\ h(\tau) \equiv \underline{F}\{h(\tau)\} \ . \tag{1}$$

(Integrals without limits are over the range of nonzero integrand.) Both the impulse response $h(\tau)$ and the transfer function $H(f)$ can be complex functions of time delay τ and frequency f, respectively.

The transfer function will be represented in terms of its real and imaginary parts according to

$$H(f) = H_r(f) + i\ H_i(f) \ , \tag{2}$$

where

$$H_r(f) = \frac{1}{2}[H(f) + H^*(f)] \ ,$$

$$H_i(f) = \frac{1}{i2}[H(f) - H^*(f)] \ . \tag{3}$$

It can also be represented in terms of its even and odd parts as

$$H(f) = H_e(f) + H_o(f) \ , \tag{4}$$

which are generally defined according to

$$H_e(f) = \frac{1}{2}[H(f) + H(-f)] = \int d\tau \cos(2\pi f\tau)\, h(\tau) ,$$

$$H_o(f) = \frac{1}{2}[H(f) - H(-f)] = -i\int d\tau \sin(2\pi f\tau)\, h(\tau) . \tag{5}$$

Functions $H_e(f)$ and $H_o(f)$ are both complex generally, whereas $H_r(f)$ and $H_i(f)$ are always real. Impulse response $h(\tau)$ can be complex.

(In the special case where impulse response $h(\tau)$ is real, then

$$H_e(f) = H_r(f) = \int d\tau \cos(2\pi f\tau)\, h(\tau) ,$$

$$H_o(f) = i\, H_i(f) = -i\int d\tau \sin(2\pi f\tau)\, h(\tau) .) \tag{6}$$

CAUSAL FILTER

A filter is said to be causal when its impulse response $h(\tau)$ is zero for negative arguments; that is,

$$h(\tau) = 0 \quad \text{for } \tau < 0 . \tag{7}$$

However, $h(\tau)$ can still be a complex function of τ. In this causal case, the real and imaginary parts of the transfer function $H(f)$ satisfy a pair of Hilbert transform relationships, provided that $h(\tau)$ does not contain any impulses at the origin; see also [3; page 198]. The Hilbert transform of an arbitrary complex function $G(x)$ is defined as

$$\underline{H}\{G(x)\} = \frac{1}{\pi} \fint du \, \frac{G(u)}{x-u} = \frac{1}{\pi x} \circledast G(x) \ , \tag{8}$$

where the tic mark on the integral sign denotes a principal value integral [4; section 3.05] and $\circledast$ denotes convolution. Principal value integrals are considered in appendix A.

In order to derive the Hilbert relations of interest, let U(x) be the unit step function,

$$U(x) = \begin{Bmatrix} 1 \text{ for } x > 0 \\ 0 \text{ for } x < 0 \end{Bmatrix} . \tag{9}$$

Then, because $h(\tau)$ is causal, transfer function (1) becomes

$$H(f) = \int d\tau \, \exp(-i2\pi f\tau) \, h(\tau) \, U(\tau) = \underline{F}\{h(\tau) \, U(\tau)\} =$$

$$= \underline{F}\{h(\tau)\} \circledast \underline{F}\{U(\tau)\} = H(f) \circledast \left[\frac{1}{2}\delta(f) + \frac{1}{i2\pi f}\right] =$$

$$= \frac{1}{2} H(f) - \frac{i}{2} \underline{H}\{H(f)\} \ . \tag{10}$$

Here, we used the Fourier transform of the unit step function $U(\tau)$ [3; (3-13)] and definition (8). Equation (10) yields

$$H(f) = -i \, \underline{H}\{H(f)\} \tag{11}$$

or, more explicitly,

$$H_r(f) = \underline{H}\{H_i(f)\} = \frac{1}{\pi f} \circledast H_i(f) \ ,$$

$$H_i(f) = - \underline{H}\{H_r(f)\} = - \frac{1}{\pi f} \circledast H_r(f) \ . \tag{12}$$

We repeat that transfer function relations (12) hold true even when impulse response $h(\tau)$ is complex; only causality is used. Analogous properties to (12) hold between the even and odd parts, $H_e(f)$ and $H_o(f)$, of the transfer function $H(f)$ as well. Namely, because the Hilbert transform of an even (odd) function is odd (even), there follows, for a causal (but possibly complex) $h(\tau)$,

$$H_e(f) = -i\ \underline{H}\{H_o(f)\}\ , \quad H_o(f) = -i\ \underline{H}\{H_e(f)\}\ . \tag{13}$$

If $h(\tau)$ contains an impulse at the origin, both parts of (12) are false, even though $h(\tau)$ may be causal. Consider

$$h(\tau) = (a + ib)\ \delta(\tau), \quad a \text{ and } b \text{ real}\ . \tag{14}$$

Then (1) yields constant transfer function

$$H(f) = a+ib,\ H_r(f) = a,\ H_i(f) = b,\ H_e(f) = a+ib,\ H_o(f) = 0. \tag{15}$$

But since the Hilbert transform of a constant is zero [4; section 3.05], neither part of (12) is satisfied, and the first part of (13) is false. On the other hand, if

$$h(\tau) = (a + ib)\ \delta(\tau - T)\ , \quad a \text{ and } b \text{ real}\ , \tag{16}$$

then (12) and (13) are satisfied only if $T > 0$. Here, we used the facts that

$$\underline{H}\{\cos(2\pi fT)\} = \sin(2\pi f|T|),\ \underline{H}\{\sin(2\pi fT)\} = -\text{sgn}(T)\ \cos(2\pi fT), \tag{17}$$

where sgn(T) is the polarity of T. Henceforth, we assume that components like (14) and (15) are not present in the filters of interest; see also [3; page 198].

For a causal filter, (2) and (12) afford a method of obtaining the complete transfer function from its real part alone, according to

$$H(f) = H_r(f) + i\,H_i(f) =$$

$$= H_r(f) - i\,\underline{H}\{H_r(f)\}\ . \qquad (18)$$

However, a more attractive approach, computationally, is to use Fourier transforms, as follows. Define inverse Fourier transform

$$\underline{h}(\tau) \equiv \underline{F}^{-1}\{H_r(f)\} = \int df\,\exp(i2\pi f\tau)\,H_r(f) \qquad (19)$$

for any real part $H_r(f)$. (The notation $h_r(\tau)$ cannot be used instead of $\underline{h}(\tau)$, because $\underline{h}(\tau)$ is not the real part of $h(\tau)$, nor is $\underline{h}(\tau)$ necessarily real.) Substitution of (3) into (19) immediately yields

$$\underline{h}(\tau) = \frac{1}{2}\Big[h(\tau) + h^*(-\tau)\Big]\ ; \quad \underline{h}(-\tau) = \underline{h}^*(\tau)\ . \qquad (20)$$

(These particular relations in (20) actually hold true for any filter $h(\tau)$, noncausal as well as complex.) Then because $h(\tau)$ is causal, there follows directly

$$h(\tau) = \left\{\begin{matrix} 2\underline{h}(\tau) & \text{for } \tau > 0 \\ 0 & \text{for } \tau < 0 \end{matrix}\right\} = 2\,\underline{h}(\tau)\,U(\tau)\ . \qquad (21)$$

In summary, the method for obtaining the complete transfer function $H(f)$ from just its real part $H_r(f)$, for a causal filter, is to perform, in order, the following operations:

$$\underline{h}(\tau) = \underline{F}^{-1}\{H_r(f)\} ,$$
$$h(\tau) = 2\ \underline{h}(\tau)\ U(\tau) ,$$
$$H(f) = \underline{F}\{h(\tau)\} . \qquad (22)$$

This procedure requires two Fourier transforms, which can be accomplished very quickly and efficiently by means of two fast Fourier transforms. Furthermore, a fast Fourier transform output sweeps out the complete range of argument values, whereas the brute force Hilbert transform integral of (18) and (8) requires an additional numerical integration for each frequency f of interest. Functions $h(\tau)$ and $\underline{h}(\tau)$ in (22) can be complex.

An accuracy check on the procedure in (22) is afforded by comparing the real part output of the Fourier transform in the bottom line with the input $H_r(f)$ utilized in the top line. The complete set of function values of $H_r(f)$ for all f is required for this procedure; in return, the complete set of values of $H_i(f)$, for all f, results. The operations in (22) are linear insofar as the overall transformation of $H_r(f)$ is concerned, and so superposition can be used for any breakdown of $H_r(f)$ into components, if desired.

The rule for obtaining H(f) or $H_i(f)$ from $H_r(f)$, as given in (22), applies whether filter H(f) is minimum-phase [1] or not. The only prerequisite for the validity of (22) is the causality of impulse response $h(\tau)$.

If only $H_e(f)$ were available (instead of $H_r(f)$), a more attractive procedure for obtaining H(f) or $H_i(f)$ than using (4) and Hilbert transform (13), is to observe that, in general, for <u>any</u> filter, the inverse Fourier transform

$$\underline{F}^{-1}\{H_e(f)\} = \int df \exp(i2\pi f\tau)\, H_e(f) = \frac{1}{2}[h(\tau)+h(-\tau)] = h_e(\tau). \quad (23)$$

Here, we used (5), the inverse to (1), and the general definition of the even part of an arbitrary complex function. Then, if $h(\tau)$ is causal, we have

$$h(\tau) = 2\, h_e(\tau)\, U(\tau)\ . \quad (24)$$

Thus, the procedure for obtaining $H(f)$ is identical to (22) if we replace $H_r(f)$ and $\underline{h}(\tau)$ by $H_e(f)$ and $h_e(\tau)$, respectively.

ONE-SIDED SPECTRAL FUNCTIONS

The analogous situation in the frequency domain (to causality in the time delay domain) is as follows: if (complex function) $A(f)$ is zero for negative arguments, that is,

$$A(f) = 0 \quad \text{for } f < 0\ , \quad (25)$$

then a procedure similar to (10)-(11) reveals that the inverse Fourier transform of $A(f)$ is given by

$$a(\tau) \equiv \underline{F}^{-1}\{A(f)\} = i\ \underline{H}\{a(\tau)\}\ . \quad (26)$$

That is, in terms of real and imaginary parts,

$$a_r(\tau) = -\ \underline{H}\{a_i(\tau)\}\ , \quad a_i(\tau) = \underline{H}\{a_r(\tau)\}\ . \quad (27)$$

The function $a(\tau)$ is called an analytic waveform, for reasons to become apparent shortly.

GENERAL SPECTRAL RELATIONS

For future purposes, the Hilbert transform of a completely arbitrary complex waveform $b(\tau)$,

$$b_H(\tau) \equiv \underline{H}\{b(\tau)\} = \frac{1}{\pi\tau} \circledast b(\tau) , \tag{28}$$

has spectrum (Fourier transform)

$$\underline{F}\{b_H(\tau)\} = -i \ \mathrm{sgn}(f) \ B(f) = \begin{Bmatrix} -i \ B(f) \text{ for } f > 0 \\ i \ B(f) \text{ for } f < 0 \end{Bmatrix} , \tag{29}$$

where $B(f)$ is the spectrum of $b(\tau)$. Here, we used the fact that the following two functions are a Fourier transform pair [3; apply (2-34) to (3-9)]:

$$\frac{1}{\pi\tau} \longleftrightarrow -i \ \mathrm{sgn}(f) . \tag{30}$$

The left-hand side of (29) is the Fourier transform of the Hilbert transform of $b(\tau)$. It cannot be labeled as $B_H(f)$, which is the Hilbert transform of the Fourier transform $B(f)$ of $b(\tau)$. The two operations of Hilbert transformation and Fourier transformation are not interchangeable, in general.

It follows from (29) that

$$\underline{F}\{b(\tau) + i \ b_H(\tau)\} = 2 \ B(f) \ U(f) , \tag{31}$$

which is a one-sided spectrum. Also, $b(\tau) + i \ b_H(\tau)$ is an analytic waveform. Waveform $b(\tau)$ is completely arbitrary here.

ANALYTICITY OF TRANSFER FUNCTION

Consider the causal exponential impulse response

$$h(\tau) = \exp(-\tau)\ U(\tau)\ . \qquad (32)$$

The corresponding transfer function is

$$H(f) = \frac{1}{1 + i2\pi f}\ , \qquad (33)$$

which has a pole in the upper-half f-plane at $f = i/(2\pi)$, but which is analytic in the lower-half f-plane. (The lower-half f-plane corresponds to the right-half s-plane of Laplace transforms.)

This analyticity of the transfer function H(f) in the lower-half f-plane is generally true for causal finite-energy filters, as may be seen by the following argument. Let frequency f be a complex variable with real and imaginary parts according to $f = f_r + if_i$. Then, for a causal filter, (1) can be expressed more explicitly as

$$H(f) = \int_0^{+\infty} d\tau\ \exp(-i2\pi f_r \tau)\ \exp(2\pi f_i \tau)\ h(\tau)\ . \qquad (34)$$

The first exponential in (34) has magnitude 1 for all τ on the contour of integration. And if $f_i < 0$, the second exponential term in (34) decays with increasing τ, keeping the integral convergent, as it was for $f_i = 0$. That is, transfer function H(f) is analytic in the lower-half f-plane for a causal impulse response $h(\tau)$. Notice, however, that no statements can be made about the locations of the zeros of transfer function H(f) in the complex f-plane. Thus we have

$$\text{causal } h(\tau) \longrightarrow \text{analytic } H(f) \text{ in lower-half f-plane .} \qquad (35)$$

The converse is also true, namely, that analyticity implies causality. To develop this point, express the inverse Fourier transform to (1) in the form

$$h(\tau) = \int_{C_1} df \, \exp(i2\pi f\tau) \, H(f) =$$

$$= \int_{C_2} df \, \exp(i2\pi f_r\tau) \, \exp(-2\pi f_i\tau) \, H(f) \, , \qquad (36)$$

where contours C_1 and C_2 are depicted in the complex f-plane in figure 1. Because transfer function H(f) is analytic in the (crosshatched) region between contours C_1 and C_2, we are allowed to move the integration freely between them, as done in (36),

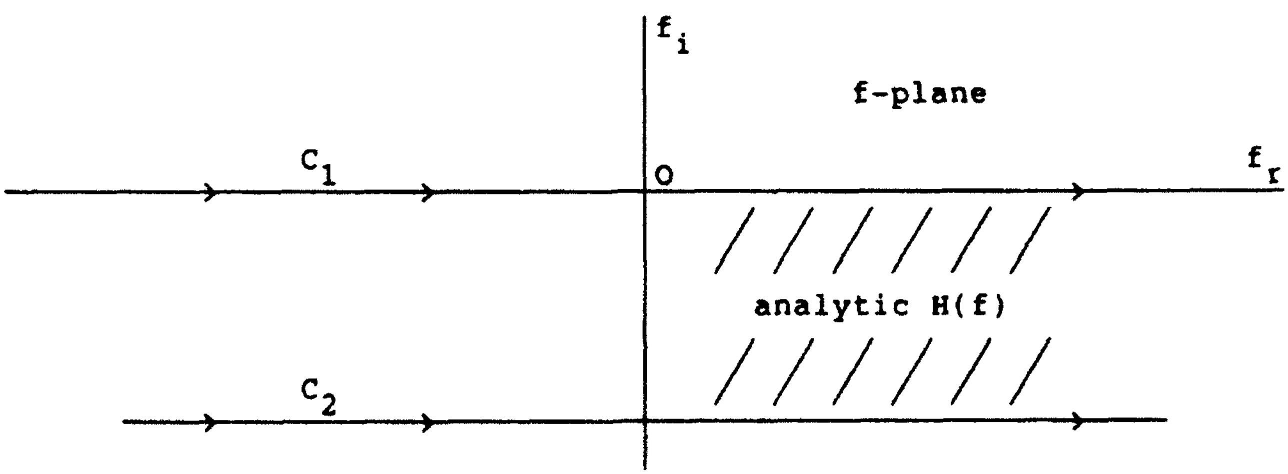

Figure 1. Complex f-Plane Contours

without altering the value $h(\tau)$ of the integral. On contour C_2, we have $f_i < 0$ everywhere. Therefore, if $\tau < 0$ in (36), the second exponential decays to zero as contour C_2 is moved farther down in the f-plane. Because $H(f)$ is analytic in the lower-half f-plane, we can move C_2 arbitrarily far down, causing the integrand of (36) to go to zero, thereby leading to a zero value for $h(\tau)$ whenever $\tau < 0$. Thus, we have

$$\text{analytic } H(f) \text{ in lower-half f-plane} \longrightarrow \text{causal } h(\tau) \ . \qquad (37)$$

This equation is the converse to (35).

Because we have already shown in (10)-(12) that a causal impulse response $h(\tau)$ leads to a transfer function $H(f)$ with Hilbert transform relations between its real and imaginary parts, it follows from (37) that an analytic transfer function $H(f)$ leads to the same conclusions. This means that, for an <u>analytic</u> transfer function $H(f)$ in the lower-half f-plane, we can use the efficient procedure given in (22), in terms of two (fast) Fourier transforms, to find the imaginary part $H_i(f)$, given only the real part $H_r(f)$.

For the example given earlier in (33), we have real part

$$H_r(f) = \frac{1}{1 + (2\pi f)^2} \ .$$

Then from (22), we obtain, in order,

$$\underline{h}(\tau) = \frac{1}{2} \exp(-|\tau|) \ , \quad h(\tau) = \exp(-\tau)\, U(\tau) \ , \quad H(f) = \frac{1}{1 + i2\pi f} \ ,$$

which corroborates (32) and (33).

MINIMUM-PHASE TRANSFER FUNCTIONS

From this point on, we presume that impulse response $h(\tau)$ is causal and that transfer function $H(f)$ contains only poles and zeros. It then follows from (35) that transfer function $H(f)$ has no poles in the lower-half f-plane. We also assume now that $H(f)$ has no zeros in the lower-half f-plane; that is, the filter is minimum-phase [1,2,3]. In this case, the function

$$Q(f) = -\ln H(f) \tag{38}$$

is analytic in the lower-half f-plane, because the function ln z is nonanalytic only at $z = 0$ and $z = \infty$ in the complex z-plane. Accordingly, by analogy to (37), inverse Fourier transform

$$q(\tau) = \int df \exp(i2\pi f\tau)\, Q(f) \tag{39}$$

is causal. (An example is given in appendix B.) Therefore, just as shown in (10)-(12), the real and imaginary parts of $Q(f)$,

$$Q(f) = Q_r(f) + i\, Q_i(f) , \tag{40}$$

can be found from each other by means of Hilbert transforms. In particular, as in (12),

$$Q_r(f) = \underline{H}\{Q_i(f)\} , \quad Q_i(f) = -\underline{H}\{Q_r(f)\} . \tag{41}$$

Alternatively, according to the sequel to (37), because $Q(f)$ is analytic in the lower-half f-plane, the imaginary part $Q_i(f)$ can be found from real part $Q_r(f)$ according to procedure (22) involving two Fourier transforms.

Interesting interpretations of minimum-phase filters, in terms of their group delay and rate of energy flow through the filter, are given in [5; pages 132 - 133]. In particular, the minimum-phase filter has the smallest group delay of any stable filter with specified magnitude transfer function.

ATTENUATION AND PHASE

There is another way of describing a transfer function H(f) rather than by its real and imaginary parts, which is very useful in some applications. Namely, let

$$H(f) = \exp[-\alpha(f) - i\,\beta(f)] \,, \tag{42}$$

where

$$\left.\begin{aligned} \alpha(f) &= \text{attenuation} \\ \beta(f) &= \text{phase shift} \end{aligned}\right\} \text{ of filter .} \tag{43}$$

Reference to (38) and (40) immediately reveals that

$$\alpha(f) = Q_r(f) \,, \quad \beta(f) = Q_i(f) \ . \tag{44}$$

Therefore, if filter H(f) is minimum-phase, according to the discussion in (38)-(41), $\alpha(f)$ and $\beta(f)$ can be found from each other by means of Hilbert transforms. In particular,

$$\beta(f) = -\,\underline{H}\{\alpha(f)\} = -\,\frac{1}{\pi f} \circledast \alpha(f) \ . \tag{45}$$

(Strictly, this relation is not usable and must be modified to allow for attenuations $\alpha(f)$ with logarithmic singularities; for example, see [3; pages 206 - 208]. This manipulation is discussed in appendix C.)

Alternatively, the procedure in (22) can be employed in the form

$$\begin{aligned} \underline{g}(\tau) &= \underline{F}^{-1}\{\alpha(f)\} \ , \\ q(\tau) &= 2\ \underline{g}(\tau)\ U(\tau) \ , \\ \alpha(f) + i\ \beta(f) &= \underline{F}\{q(\tau)\} \ . \end{aligned} \tag{46}$$

The function $\underline{g}(\tau)$ is defined by the inverse Fourier transform in the top line of (46). Phase shift $\beta(f)$ for a minimum-phase filter is given by the imaginary part of the Fourier transform in the bottom line of (46).

A common alternative descriptor of the frequency behavior of a filter is the gain $G(f)$ in decibels, defined as

$$G(f) = 20 \log_{10} |H(f)| \ . \tag{47}$$

Because the attenuation follows from (42) as

$$\alpha(f) = -\ln |H(f)| \ , \tag{48}$$

the gain $G(f)$ and the attenuation $\alpha(f)$ are related by

$$G(f) = -\frac{20}{\ln(10)}\ \alpha(f) = -\ 8.686\ \alpha(f) \ . \tag{49}$$

Measurement of either one is sufficient to find the other and to thereby determine the phase shift $\beta(f)$ of a minimum-phase filter.

EXAMPLE AND LIMITATION

We again consider the example given in (32)-(33), namely

$$h(\tau) = \exp(-\tau)\ U(\tau)\ , \quad H(f) = \frac{1}{1 + i2\pi f}\ . \tag{50}$$

The attenuation and phase follow from (42) according to

$$\alpha(f) = \frac{1}{2}\ \ln(1 + 4\pi^2 f^2)\ ,$$

$$\beta(f) = \arctan(2\pi f)\ . \tag{51}$$

If we attempt to apply the inverse Fourier transform in the top line of (46) to the attenuation $\alpha(f)$ in (51), we encounter a divergent integral because $\alpha(f) \sim \ln|f|$ as $f \to \pm\infty$.

More generally, if filter $H(f)$ has a zero at a frequency f equal to any finite real value, the attenuation $\alpha(f)$ has a logarithmic singularity at that real frequency, and the inverse Fourier transform in (46) diverges. Because typical filters very often have this feature (and almost always at $f = 0$ and $f = \pm\infty$), a way must be found to circumvent the divergent part of the inverse Fourier transform integral, so that the efficient procedure of (46) can be salvaged.

SUBTRACTION OF SINGULARITY

The procedure to be used here is one commonly adopted to numerically evaluate convergent integrals with singular integrands; it is illustrated by the example

$$I = \int_0^a dx \, \frac{\cos x}{x^\nu} \, , \qquad \nu < 1 \, . \tag{52}$$

If ν is positive, the integrand has an infinite cusp at the origin, yet the integral converges, because $\nu < 1$. We express

$$I = \int_0^a dx \, \frac{\cos x - 1 + 1}{x^\nu} = \int_0^a dx \, \frac{\cos x - 1}{x^\nu} + \int_0^a dx \, \frac{1}{x^\nu} \, , \tag{53}$$

which is allowed, because both integrals converge. The last integral in (53) can be done in closed form, yielding $a^{1-\nu}/(1-\nu)$. Also, the middle integrand now behaves as $x^{2-\nu}$ as $x \to 0+$, which is zero at the origin, because $2-\nu > 1$; this behavior enables a straightforward numerical evaluation of the middle integral.

The key to this procedure is to find a component that can be integrated in closed form and that, when subtracted from the given integrand, yields a well-behaved residual for numerical integration.

APPLICATION TO FILTERS

The way we apply this subtraction procedure to a given attenuation $\alpha(f)$ with logarithmic singularities is to break it into two parts,

$$\alpha(f) = \alpha_1(f) + \alpha_2(f) \ , \tag{54}$$

where attenuation $\alpha_1(f)$ contains all the singular components and has a known closed form minimum-phase pair $\beta_1(f)$. (An example is furnished by (50) and (51); some additional examples are listed in appendix D.) Then residual attenuation $\alpha_2(f)$ is found according to

$$\alpha_2(f) = \alpha(f) - \alpha_1(f) \tag{55}$$

and is well-behaved for all f. Residual $\alpha_2(f)$ is subjected to the repeated Fourier transform procedure detailed in (46), resulting in phase shift function $\beta_2(f)$. Finally, the complete minimum-phase corresponding to the given attenuation $\alpha(f)$ is obtained from

$$\beta(f) = \beta_1(f) + \beta_2(f) \ . \tag{56}$$

The procedure can be summarized as follows:

$$\alpha(f) \longrightarrow \beta(f) \quad \text{desired} \ ;$$

$$\alpha_1(f) + \alpha_2(f) \longrightarrow \beta_1(f) + \beta_2(f) \quad \text{used} \ . \tag{57}$$

The exact choice of attenuation/minimum-phase pair $\alpha_1(f)$, $\beta_1(f)$ is not critical, except that residual $\alpha_2(f)$ must not have any singularities and must decay (rapidly) to zero for large f.

Of course, the given attenuation $\alpha(f)$ must be known for all f in order to apply this (or any) procedure for obtaining minimum-phase shift $\beta(f)$, whether obtained directly by Hilbert transforms or by means of a Fourier procedure. The actual numerical evaluation of the Fourier procedure delineated in (46) is accomplished by means of fast Fourier transforms; the details are presented in appendix E.

SHORTCOMING OF HILBERT TRANSFORM

Suppose that two minimum-phase filters $H_a(f)$ and $H_b(f)$ differ only by a complex scale factor:

$$H_b(f) = c\, H_a(f) \; . \tag{58}$$

Then

$$\alpha_b(f) = \alpha_a(f) - \ln|c| \; ,$$

$$\beta_b(f) = \beta_a(f) - \arg(c) + 2\pi n \; , \quad n \text{ integer} \; . \tag{59}$$

However, if $\alpha_a(f)$ and $\beta_a(f)$ are a Hilbert transform pair, $\alpha_b(f)$ and $\beta_b(f)$ cannot possibly be (unless $c = 1$ and $n = 0$) because the Hilbert transform of a constant is zero. Functions $\alpha_b(f)$ and $\beta_b(f)$ are both "incomplete," in that attenuation $\alpha_b(f)$ contains no information about $\arg(c)$, while phase $\beta_b(f)$ contains no information about $|c|$. This means that the Hilbert transform of a given attenuation (phase) yields a phase (attenuation) function that can differ from the actual phase (attenuation) of a minimum-phase filter by an arbitrary additive constant. Some information is inherently absent from a given attenuation (phase) function. In addition, because the Hilbert transform of a constant is zero, additive constants are lost through this transformation. (The situation is somewhat similar for the Fourier transform procedure given in (46).)

Alternatively, suppose that

$$h_b(\tau) = h_a(\tau - T) \; , \quad H_b(f) = H_a(f) \exp(-i2\pi fT) \; . \tag{60}$$

Then filter $H_b(f)$ contains a transfer function component of $\exp(-i2\pi fT)$, with corresponding attenuation 0 and phase $2\pi fT$. Thus, the attenuation contains no information about a pure time delay. However, it should be noted that this component $\exp(-i2\pi fT)$ does not possess poles and zeros at all, but in fact has an essential singularity at $f = \infty$.

APPLICATION TO MEASURED DATA

In this section, we will apply the previous Fourier procedure to a measured pair of attenuation and phase shift functions in an effort to determine if the filter is minimum-phase. The particular filter is a J15-1 transducer used as a continuous-wave source in the 10 to 900 Hertz range. The transmitting current response of this device is defined as the ratio

$$\frac{\text{output pressure}}{\text{input current}} \tag{61}$$

and is the transfer function of interest. The reference level is taken as 1 μPa/Amp. The measurements procedure include a water-path propagation delay (of unknown value) between the transducer and a calibrated receiving hydrophone.

The measured decibel gain, (47)-(49), of transfer function (61) is displayed in figure* 2 for the range of frequencies from 30 to 500 Hertz, on a logarithmic frequency abscissa. Also superposed are the decibel gain responses of filters with 1 or 2 or 3 poles at the origin, which plot as straight lines on this type of paper. This information is required for determining the behavior of the filter from 30 Hertz down to f = 0 and is necessary because the Hilbert and Fourier procedures both require knowledge of the complete attenuation (or gain) for <u>all</u> frequencies, in order to determine the value of the corresponding minimum-phase shift at just one frequency. It may be reasonably concluded from the fits in figure 2 that the transducer of

*Figures 2 through 11 are collected at the end of this section.

interest here has a double zero at $f = 0$.

In addition, the same fitting procedure has been attempted in the neighborhood of 500 Hertz in figure 2, as may be seen by the superposition of responses for filters with decays corresponding to 0 or 1 or 2 or 3 poles at $f = \infty$. However, the situation is rather poor at this upper end of the measured frequency range, because, as seen in figure 2, the transducer has not yet developed its asymptotic behavior at $f = 500$ Hertz. This behavior is consistent with the information mentioned above, which describes the use of this device as a source up to 900 Hertz. Thus, we have a situation where we have insufficient measurements to fully apply the theoretical developments presented earlier. Nevertheless, we will attempt to circumvent the inadequacy by extrapolating the given measurements into the frequency range above 500 Hertz and then using the combination of measured and extrapolated gains to determine the minimum-phase response.

PHILOSOPHY OF EXTRAPOLATION

A situation of frequent occurrence is the following. We have a measured residual attenuation $\alpha_2(f)$, but it is available only for $0 \le f_1 < f < f_2$; see (54)-(57). We presume that attenuation $\alpha_2(f)$ is even about $f = 0$. Call this total frequency range of known values, K. Denote the remainder of the frequency range, where $\alpha_2(f)$ is unknown, by U.

We want to evaluate the minimum-phase corresponding to $\alpha_2(f)$, namely

$$\beta_2(f) = - \underline{H}\{\alpha_2(f)\} = - \frac{1}{\pi} \int_{-\infty}^{+\infty} du \, \frac{\alpha_2(u)}{f - u} \, . \tag{62}$$

Our approach is to extrapolate $\alpha_2(f)$ beyond K into the unknown frequency range U. Call this extrapolated function $\alpha_{2e}(f)$; it exists for all f. This extrapolation <u>must</u> be rather close to the true (unknown) attenuation $\alpha_2(f)$ in U, but $\alpha_{2e}(f)$ need not agree with $\alpha_2(f)$ inside K. In particular, $\alpha_{2e}(f)$ and $\alpha_2(f)$ should match in value <u>and</u> slope at the boundaries of K.

Then, we can obtain the following approximation to phase (62), namely

$$\beta_{2a}(f) = - \frac{1}{\pi} \int_K du \, \frac{\alpha_2(u)}{f - u} - \frac{1}{\pi} \int_U du \, \frac{\alpha_{2e}(u)}{f - u} =$$

$$= - \frac{1}{\pi} \int_K du \, \frac{\alpha_2(u) - \alpha_{2e}(u)}{f - u} - \frac{1}{\pi} \int_{-\infty}^{+\infty} du \, \frac{\alpha_{2e}(u)}{f - u} \, . \tag{63}$$

The first (finite) integral in (63) is done numerically, by employing the Fourier procedure presented here. The second integral in (63) is actually divergent and is instead replaced by use of a known attenuation/minimum-phase pair, $\alpha_{2e}(f)$, $\beta_{2e}(f)$.

The key to this procedure is a shrewd choice for the extrapolated attenuation $\alpha_{2e}(f)$. Several candidates, along with the corresponding minimum-phase functions, are listed in appendix D.

LAPLACE TRANSFORM NOTATION

For convenience of notation, we employ here the Laplace transform of the impulse response, namely

$$L(s) = \int_0^{+\infty} d\tau \exp(-s\tau)\, h(\tau) \ , \tag{64}$$

where we have specifically limited consideration to causal filters. The connection with the Fourier transform (1) is

$$H(f) = L(i2\pi f) \ . \tag{65}$$

EXAMPLE A

The first attempted fit to the measured gain in figure 2 is by means of filter

$$L(s) = \frac{c\ s^2}{(s + a)(s + b)} \ , \tag{66}$$

with constants $a = 260$, $b = 330$, and $c = -.55E8$. This filter has the desired double-order zero at the origin, but does not decay for large frequencies. The gain of (66) is superposed on the measured gain in figure 3; it is seen that the constants have been chosen to give a fit that matches in value and slope for small frequencies and that matches the measured gain value at 500 Hertz.

The difference in decibels between the measured gain and the fitted gain is displayed in figure 4; it goes to zero at 30 and 500 Hertz and is assumed to be zero outside this range. This assumption is not likely to be correct for f greater than 500 Hertz, but it is necessary in order to proceed with the numerical manipulations. The difference in attenuations, $\alpha_2(f)$ of (55), is available by dividing the result in figure 4 by -8.686; see (47)-(49).

The residual attenuation $\alpha_2(f)$ is subjected to the cascaded Fourier procedure of (46), and the resultant phase $\beta_2(f)$ is added to the minimum-phase $\beta_1(f)$ corresponding to (66). The final total phase $\beta(f)$ is shown in figure 5, with the label A&T, meaning analytic and transform, that is, $\beta_1(f)$ plus $\beta_2(f)$. Superposed on this figure is the measured phase, with the label M&D, meaning measured and time-delay adjusted. Recall in the discussion surrounding (61) that there is an unknown time delay, between the transducer and receiving hydrophone, included in the measurements taken. Accordingly, a selection of time delay was made that yielded the best eyeball fit of the two phases over the range of frequencies from 0 to 400 Hertz in figure 5; this corresponds to an additive linear phase function of frequency, as indicated by example (60). The time delay was 1.43 ms.

The agreement between the minimum-phase and the measured results in figure 5 allow us to conclude that the J15-1 transducer is indeed a minimum-phase filter, at least over the frequency range up to 400 Hertz. The difference between the two results is 17° at 500 Hertz, which is significant. However, the reason for this discrepancy is undoubtedly due to the fact that (66) is not the correct fit for $f > 500$ Hertz, because (66) has no decay for large frequencies.

EXAMPLE B

In an effort to find a better phase match, another fit was also tried, namely filter

$$L(s) = \frac{c\ s^2}{(s + a_o)[(s + a)^2 + b^2]} , \qquad (67)$$

with constants a_o = 4000, a = 260, b = 400, and c = – .275E12. The measured and analytical decibel gains are plotted in figure 6, while the decibel difference is plotted in figure 7. The corresponding two phase plots, obtained by an identical procedure to that described in example A above, are presented in figure 8. Now, the difference in the two phase curves at 500 Hertz has decreased, but only slightly, to 14°. Apparently, the unmeasured decibel gain, in the frequency range above 500 Hertz, is causing inaccurate calculations of the minimum-phase in the region just below 500 Hertz, due to our inability to correctly extrapolate, by means of (66) and (67), to what the filter gain truly was in that frequency range. This supposition is consistent with the observation that the minimum-phase at a particular frequency is largely governed by the (rate of change of the) attenuation in the neighborhood of that frequency [2; page 345]. The agreement in phase results for the lower frequencies comes about because errors in gain measurements above 500 Hertz have a much reduced effect on the calculated phase at low frequencies.

EXAMPLE C

In an attempt to justify this conjecture, an estimate of the unmeasured gain in the frequency range from 500 to 900 Hertz was made and is illustrated in figure 9. A droop of 7 dB, centered at 565 Hertz, has been added and is annotated by the phrase "augmented". The fit is again (66), with the same constants as used for example A, and is superposed in the figure.

The two phase curves are illustrated in figure 10. Now, the discrepancy between the two results is negligible (within measurement error) all the way up to 500 Hertz, the maximum frequency at which the phase was measured. Thus, we feel justified in concluding that the device under investigation is indeed a minimum-phase filter, at least over the measured frequency range up to 500 Hertz.

LIMITED FREQUENCY RANGE

It has been stated above that the measured filter appears to be minimum-phase in a particular frequency range. Strictly, this is not a valid concept; but it is necessary to allow for it in practice, where filter responses cannot possibly be measured for all frequencies. For example, suppose that the transfer function H(f) has a collection of poles and zeros in the upper-half f-plane, all fairly near the origin $f = 0$. In addition, let H(f) have a pole-zero pair far away from the origin, but symmetrically located about the real f axis, so as not to affect the gain or attenuation; see the pair near $f = f_2$ in figure 11.

Obviously, the filter in figure 11 cannot be minimum-phase, because it has a zero in the lower-half f-plane. Yet, its measured phase, for frequencies less than f_1, would be indistinguishable from that of the minimum-phase filter that does not contain that extra pair. Thus, we would reasonably conclude, upon the basis of the measurements made, that the filter is "minimum-phase for $f < f_1$." Furthermore, this is a practically useful concept because compensation of the filter in this same frequency range is certainly possible and allowable. In other words, measurement in a limited frequency range only allows us to make conclusions in that same range; in fact, the situation is slightly worse than that, because the edges of the range may also be [illegible] to question.

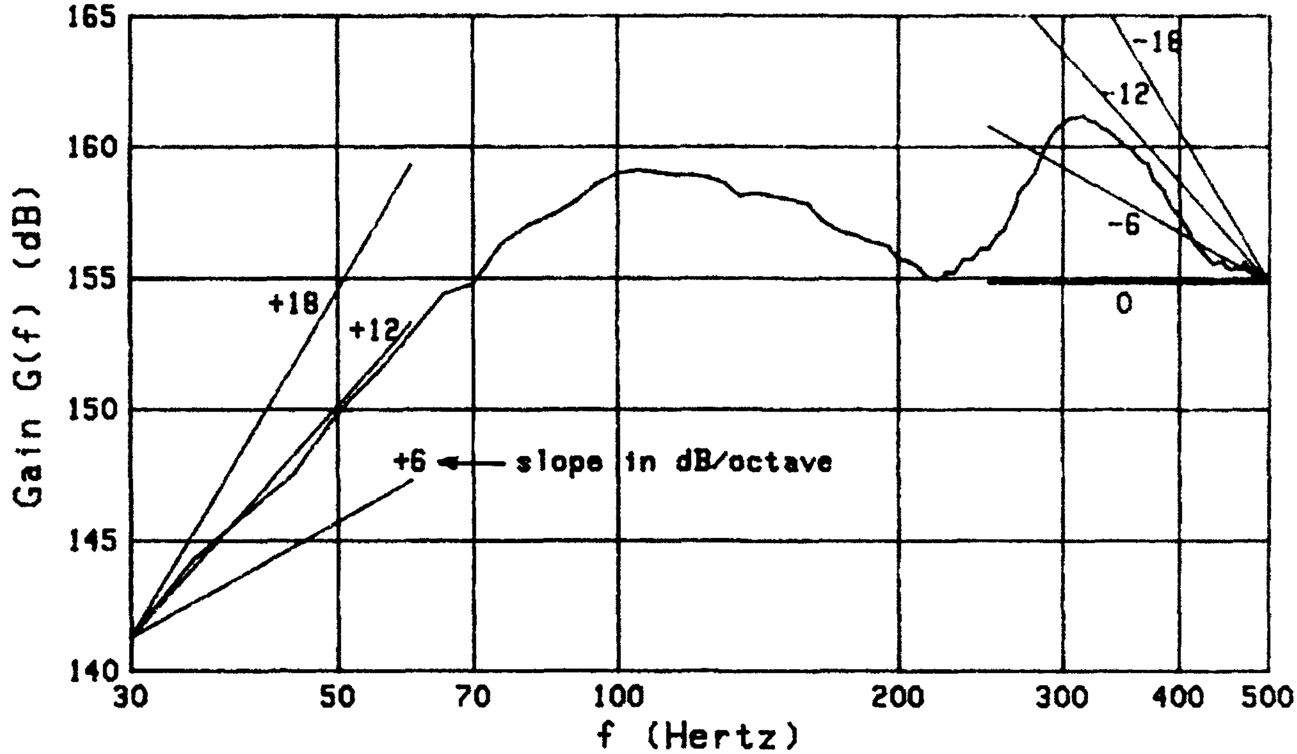

Figure 2. Measured Filter Gain

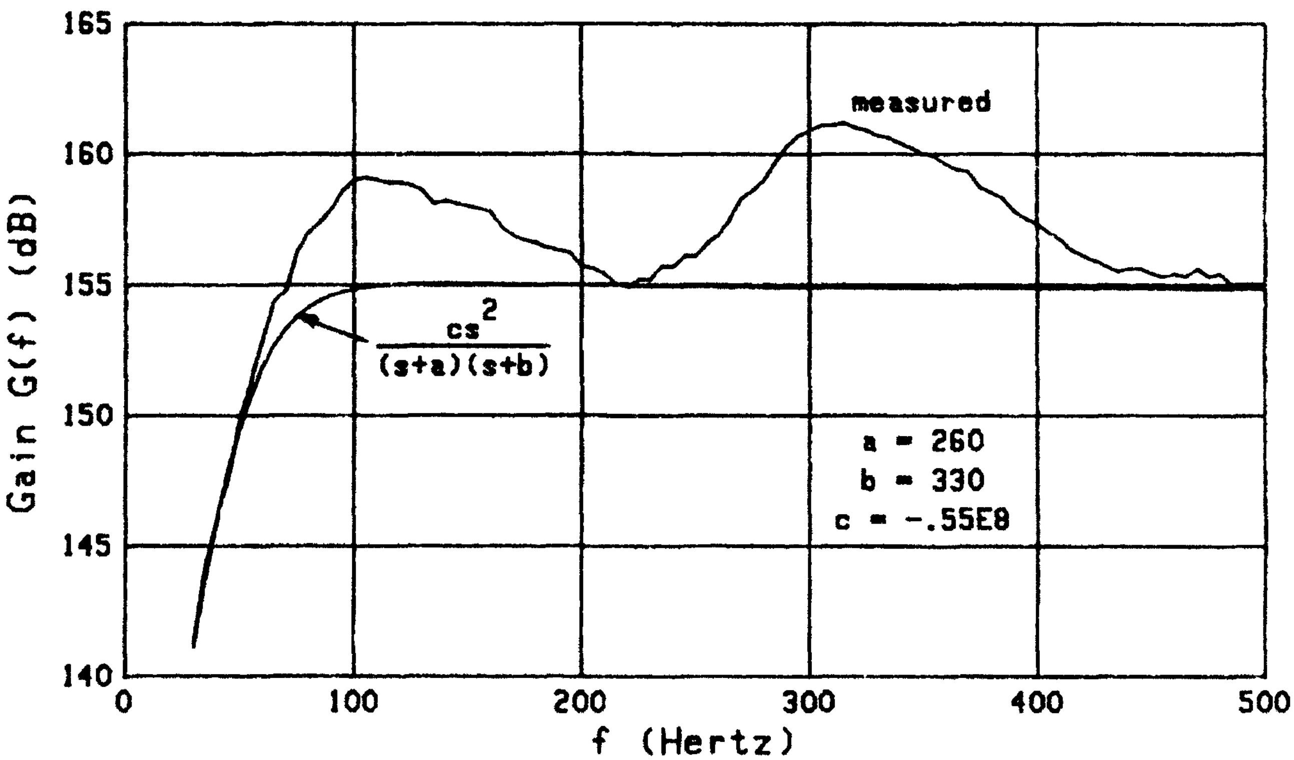

Figure 3. Fitted Gain for Example A

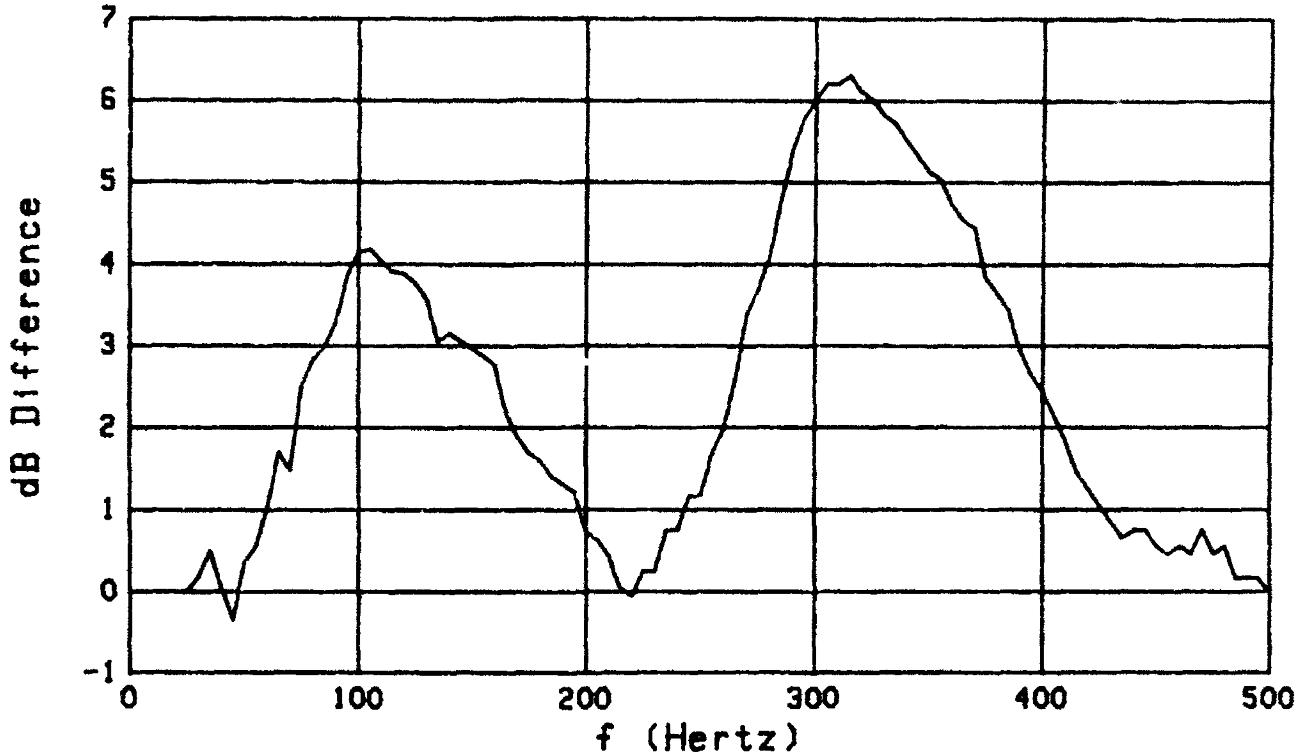

Figure 4. Decibel Difference for Example A

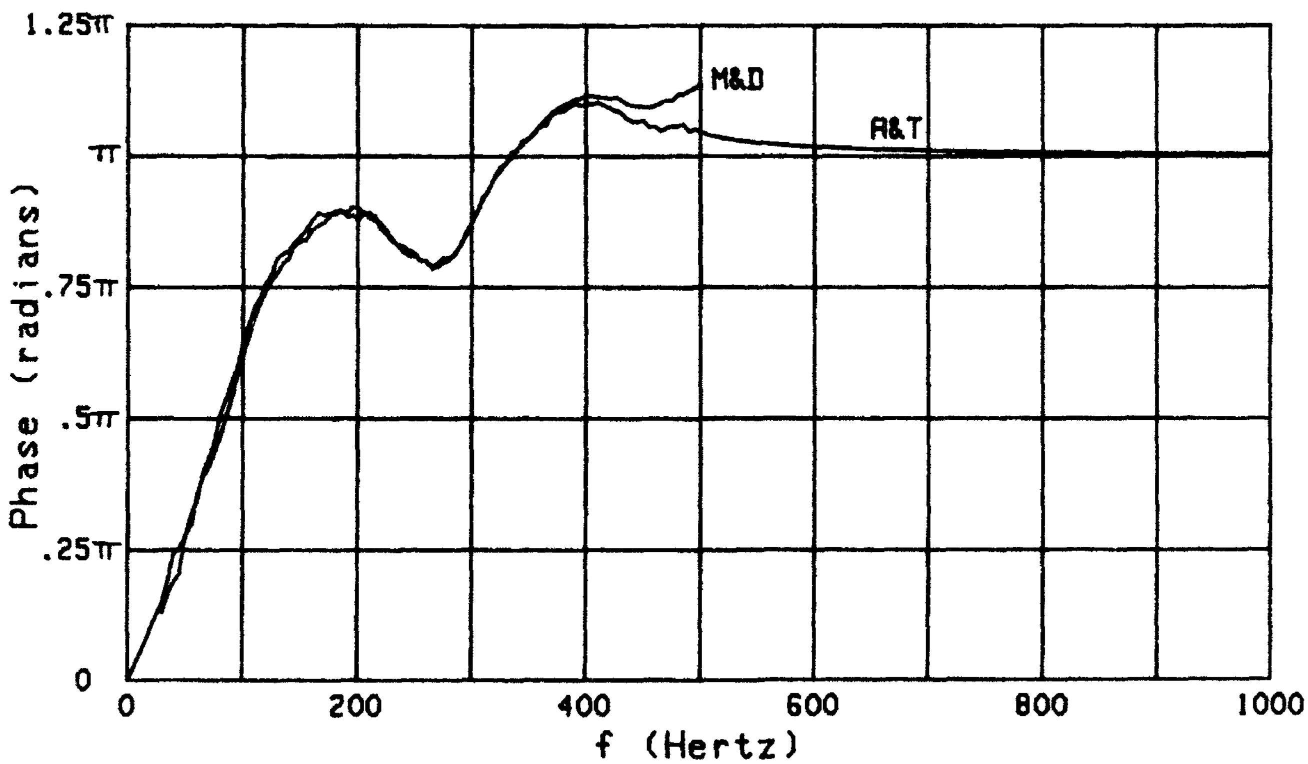

Figure 5. Measured and Transformed Phases for Example A

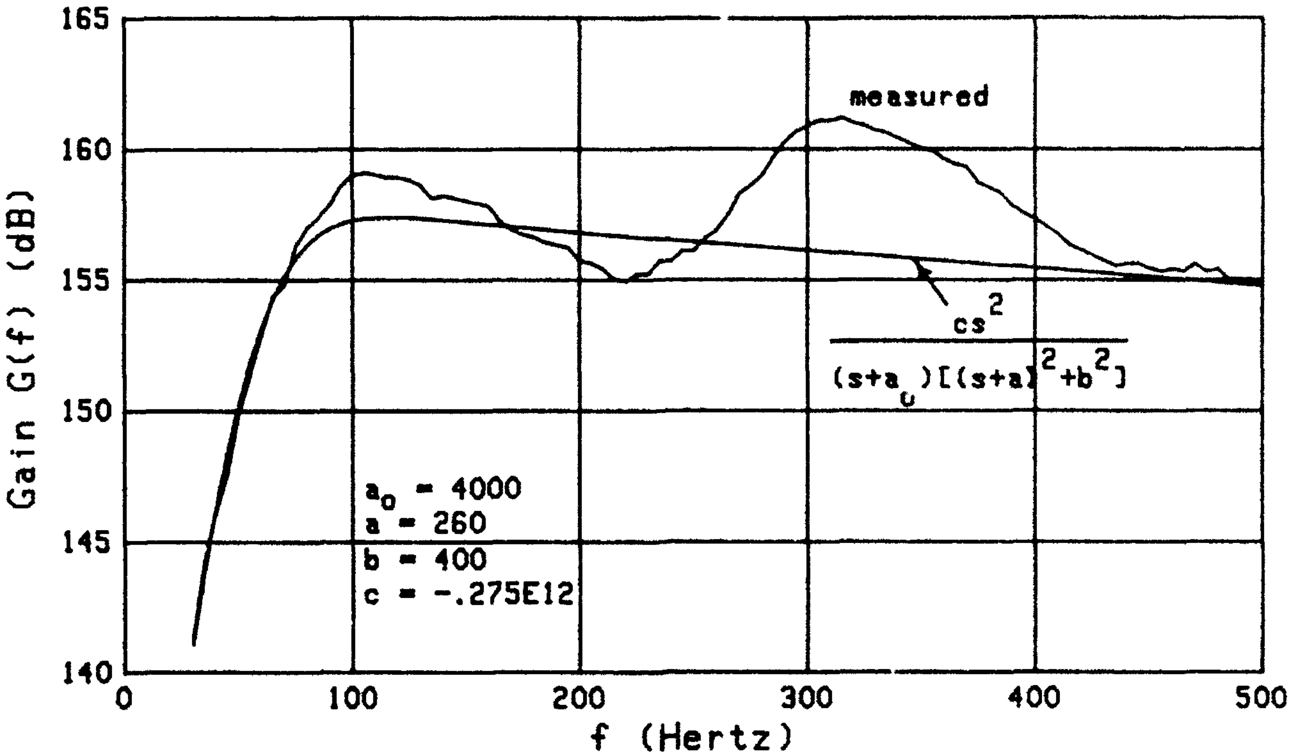

Figure 6. Fitted Gain for Example B

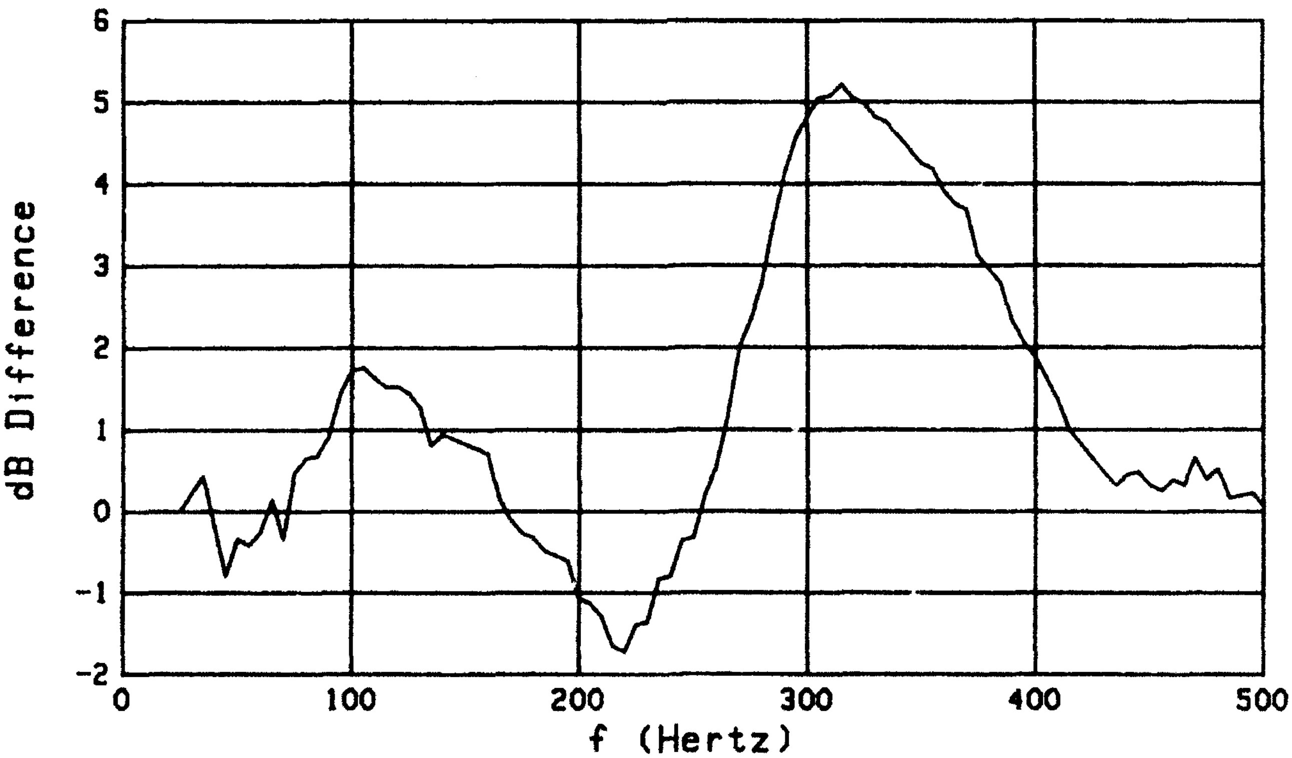

Figure 7. Decibel Difference for Example B

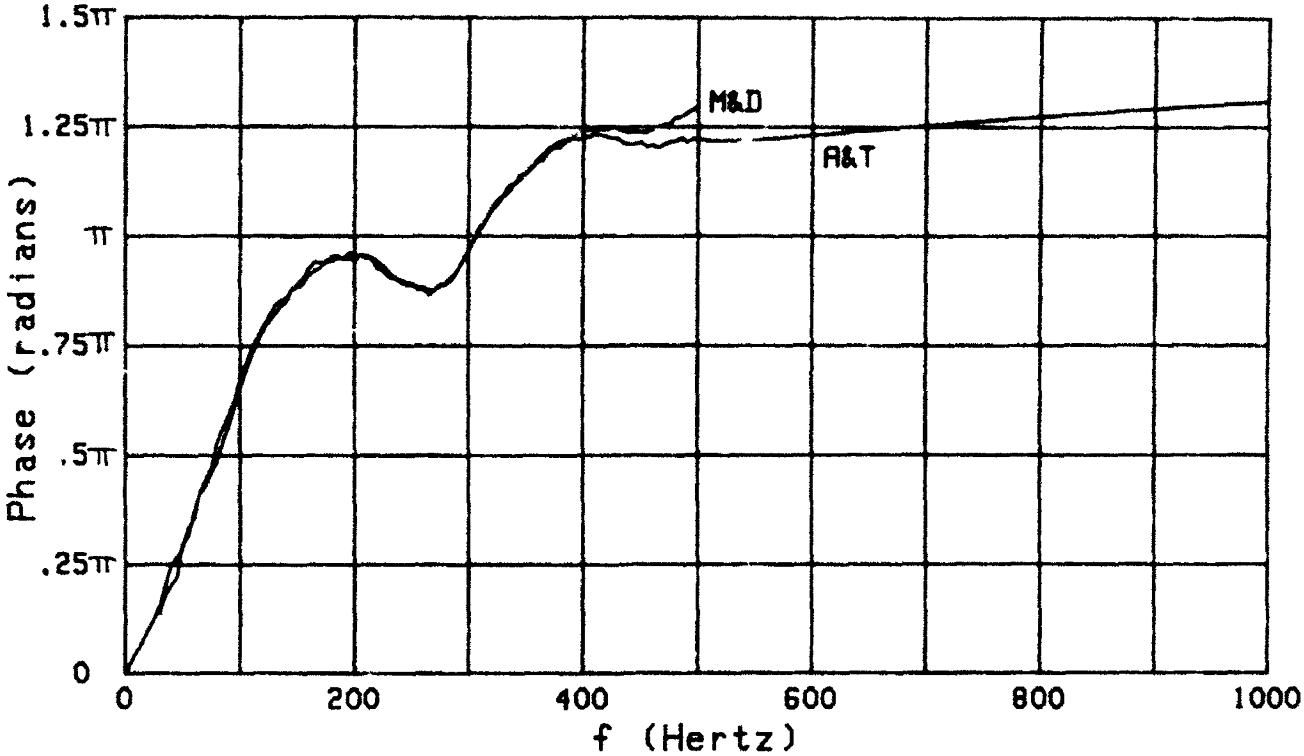

Figure 8. Measured and Transformed Phases for Example B

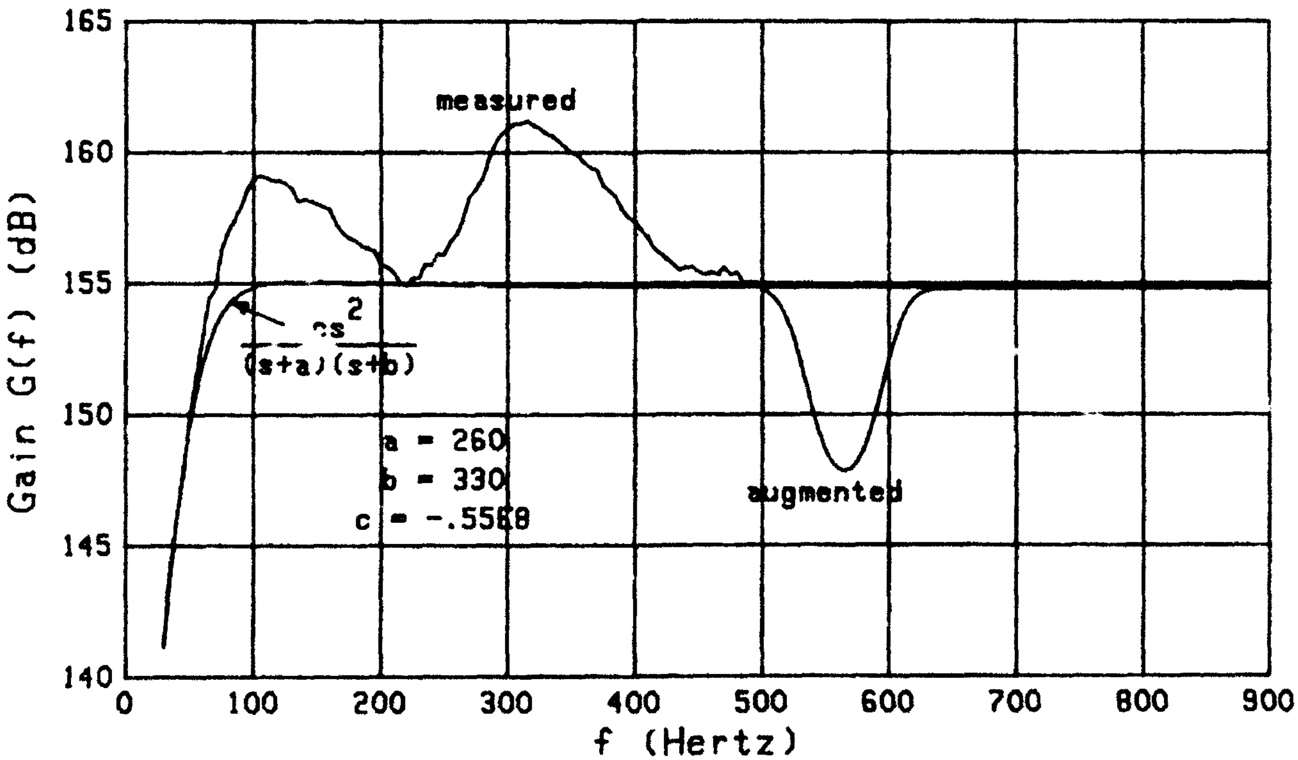

Figure 9. Fitted Gain for Example C

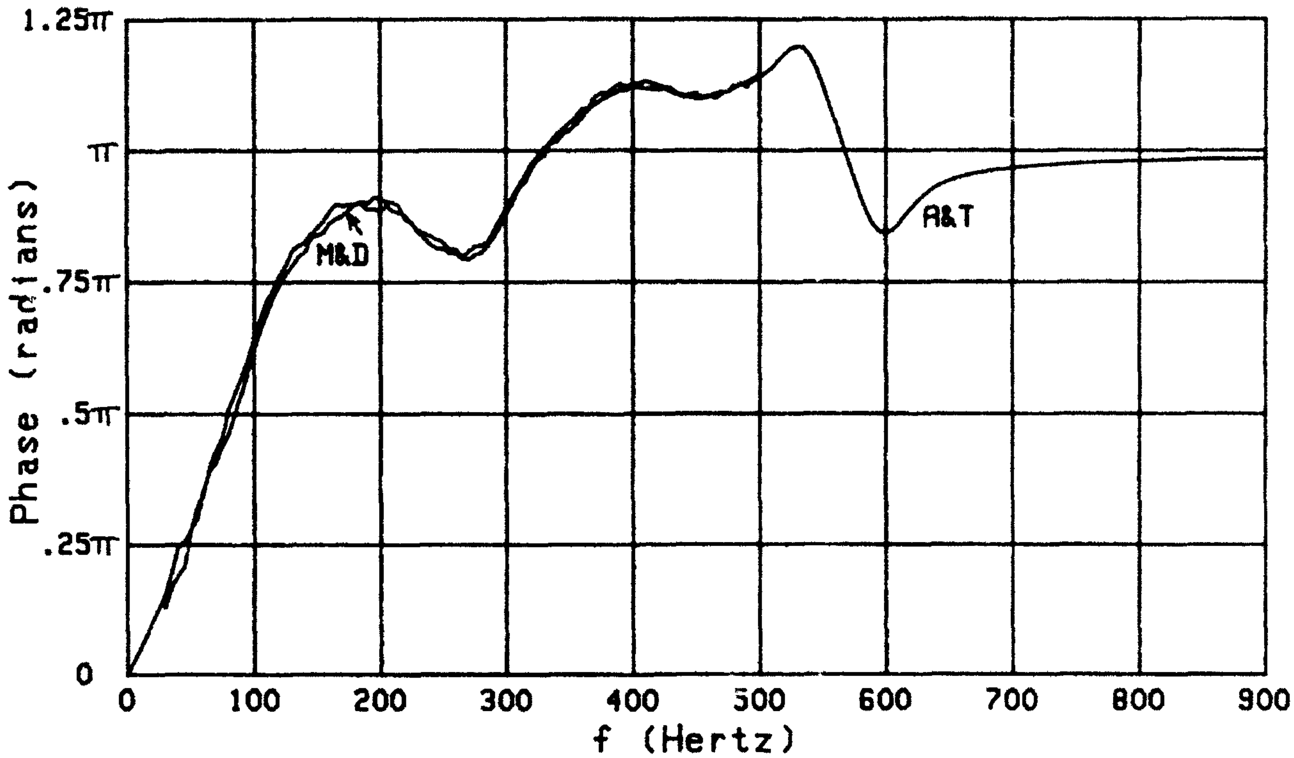

Figure 10. Measured and Transformed Phases for Example C

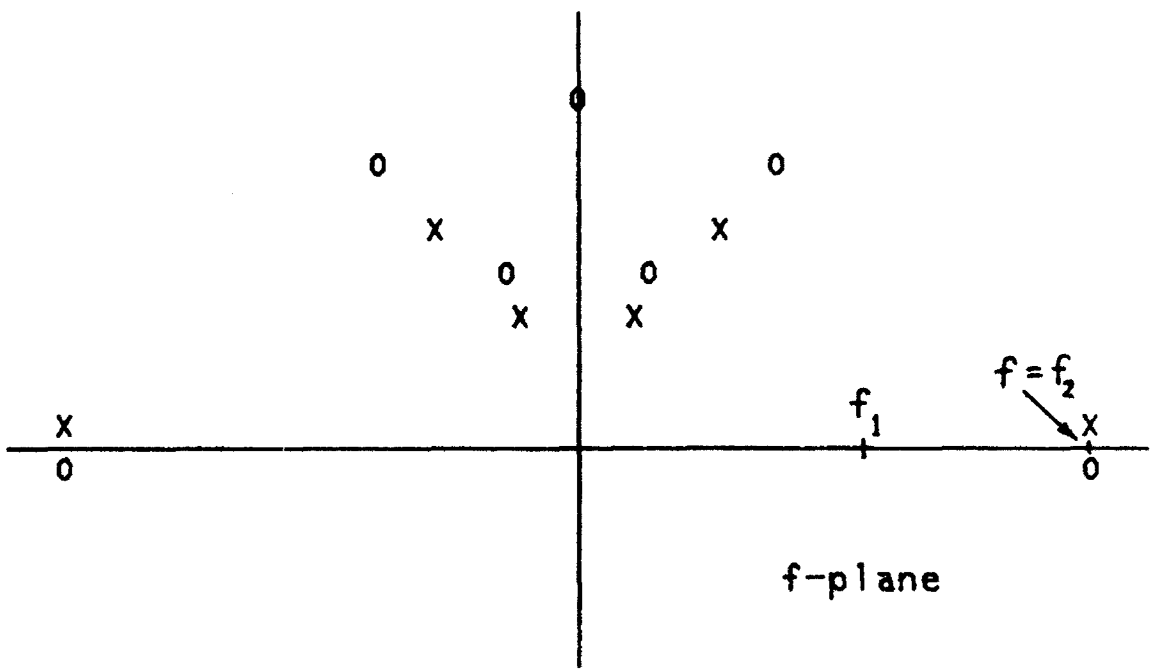

Figure 11. Pole-Zero Locations

SUMMARY

For a minimum-phase filter, the phase shift $\beta(f)$ can be found from the attenuation $\alpha(f)$ by means of two cascaded fast Fourier transforms, once the logarithmic singularities in $\alpha(f)$ have been subtracted out and handled analytically. A partial accuracy check is automatically built into the procedure, because the real part of the output should agree with the given input; the imaginary part of the output is the desired minimum-phase result. This Fourier approach yields the entire phase curve for all frequencies, not just a point-by-point output, as a Hilbert transform numerical integration would give.

In order to use this procedure, the attenuation must be measured for all frequencies, or at least for large enough and small enough frequencies that the asymptotic behavior is well developed and obvious. A plot of the attenuation (or decibel gain) on a logarithmic frequency abscissa is recommended for this purpose, because the filter magnitude characteristic should approach a straight line with a decay equal to a multiple of 6 dB/octave in the neighborhood of zero and infinite frequencies. Failure to make a complete set of measurements will lead to the need for extrapolation and the attendant errors that can occur with such a procedure, as illustrated here. Furthermore, statements about the minimum-phase behavior of a particular filter can only be made (with)in that same frequency range.

APPENDIX A. PRINCIPAL VALUE INTEGRAL EVALUATION

Through a change of variable, a principal value integral can be put in the form

$$I = ⨍_{-b}^{b} dt\, \frac{g(t)}{t} , \quad \text{where } g(0) \neq 0 . \tag{A-1}$$

Limit b can be finite or infinite. (For example, (8) fits this form when we let $g(t) = G(x-t)/\pi$.) Although (A-1) is a principal value integral, it can be expressed as (ordinary integrals)

$$I = \int_{-b}^{b} dt\, \frac{g_o(t)}{t} = 2\int_{0}^{b} dt\, \frac{g_o(t)}{t} = \int_{0}^{b} \frac{dt}{t}\, [g(t) - g(-t)] , \tag{A-2}$$

where $g_o(t)$ is the odd part of $g(t)$; see definition (5). This form can be used for numerical evaluation whether b is finite or not. If b is infinite, the integrand of the last integral in (A-2) maintains the same decay with t as original integral (A-1). This is not true of the sometimes recommended alternative form

$$I = \int_{-b}^{b} dt\, \frac{g(t) - g(0)}{t} , \tag{A-3}$$

which decays very slowly with t, although it is finite at the origin t = 0. However, another alternative that advantageously uses this subtraction device is given later in (A-11).

A simple example of (A-1)-(A-2), for b finite, is furnished by the integral

$$I = \int_{-b}^{b} dt\, \frac{\exp(t)}{t} = 2\int_{0}^{b} dt\, \frac{\sinh(t)}{t} , \tag{A-4}$$

the latter of which has a well-behaved integrand at $t = 0$.

DERIVATIVE EVALUATION

In general, the last integrand in (A-2) behaves as

$$\frac{g(t) - g(-t)}{t} \sim 2\, g'(0) \quad \text{as } t \to 0 . \tag{A-5}$$

Therefore, in order to use (A-2), it is necessary to have $g'(0)$. If all we can easily evaluate is $g(t)$, and not its derivative $g'(0)$, a good approximation is available through the following device. We know that $g'(0)$ is approximated by

$$\frac{g(\varepsilon) - g(-\varepsilon)}{2\varepsilon} \quad \text{for small } \varepsilon . \tag{A-6}$$

However, if ε is too large, this is a poor approximation, whereas if ε is too small, round-off errors cause numerical stability problems. But we know that

$$\frac{g(\varepsilon) - g(-\varepsilon)}{2\varepsilon} = g'(0) + \frac{1}{6}\, g'''(0)\, \varepsilon^2 + O(\varepsilon^4) \quad \text{as } \varepsilon \to 0 . \tag{A-7}$$

So, letting $F(\varepsilon)$ be the left-hand side of (A-7), we have, to second order,

$$\left.\begin{aligned} F(\varepsilon) &= A_o + A_1\, \varepsilon^2 \\ F(\varepsilon/2) &= A_o + A_1\, \varepsilon^2/4 \end{aligned}\right\} \text{ where } A_o \text{ and } A_1 \text{ are unknown} . \tag{A-8}$$

The desired unknown follows easily from (A-8) as

$$A_o = \frac{4\ F(\varepsilon/2)\ -\ F(\varepsilon)}{3} \cong g'(0)\ . \tag{A-9}$$

This procedure is an extrapolation to the limit; it uses $\varepsilon/2$ as the smallest argument of F.

A program for the evaluation of g'(t) at general t is furnished here in BASIC; it requires specification of a tolerance Tol in line 70 of the function subroutine FNDeriv1.

```
10  INPUT T
20  Der1=FNDeriv1(T)
30  PRINT T,Der1     !  t,g'(t)
40  END
50  !
60  DEF FNDeriv1(T) !  ~g'(t) via extrapolation
70  Tol=1.E-6       !  tolerance
80  E=.2            !  epsilon (start)
90  E=E*.5
100 V1=V2
110 V2=(FNG(T+E)-FNG(T-E))/(2.*E)
120 V=V2+(V2-V1)/3.
130 IF ABS(V2/V-1.)>Tol THEN 90
140 RETURN V
150 FNEND
160 !
170 DEF FNG(T)
180 RETURN EXP(T)   !  example exp(t)
190 FNEND
```

An application of this program to the exp(t) example in line 180, at argument t = 1.1, yielded an error of -7.8E-13.

If we instead kept terms to fourth order in (A-7), an extension to (A-8) yields approximation

$$g'(0) \cong \frac{1}{45}\left[64\ F\left(\frac{\varepsilon}{4}\right)\ -\ 20\ F\left(\frac{\varepsilon}{2}\right)\ +\ F(\varepsilon)\right]\ . \tag{A-10}$$

This procedure uses $\varepsilon/4$ as the smallest argument of F.

AN ALTERNATIVE SUBTRACTION PROCEDURE

We now express (A-1) in the form

$$I = -\!\!\!\!\!\!\int_{-b}^{b} dt\, \frac{g(t)}{t} = -\!\!\!\!\!\!\int_{-a}^{a} dt\, \frac{g(t)}{t} + \int_{R} dt\, \frac{g(t)}{t} \,, \tag{A-11}$$

where limit a is chosen for convenience and R is the union $(-b,-a) \cup (a,b)$. Then, as done in (A-3),

$$I = \int_{-a}^{a} dt\, \frac{g(t) - g(0)}{t} + \int_{R} dt\, \frac{g(t)}{t} \,. \tag{A-12}$$

These are both ordinary integrals now. The first integrand is finite at $t = 0$, with value $g'(0)$, while the second integrand maintains its original decay as $x \to \pm b$.

SECOND DERIVATIVE EVALUATION

The procedure presented in (A-5)-(A-9), for the approximate evaluation of first derivative $g'(0)$, can be extended to the second derivative $g''(0)$ as follows. We know that

$$\frac{g(\varepsilon) + g(-\varepsilon)}{2} = g(0) + \frac{1}{2}\, g''(0)\, \varepsilon^2 + O(\varepsilon^4) \quad \text{as } \varepsilon \to 0 \,. \tag{A-13}$$

Therefore,

$$\frac{g(\varepsilon) + g(-\varepsilon) - 2g(0)}{\varepsilon^2} = g''(0) + O(\varepsilon^2) \,. \tag{A-14}$$

Letting $D(\varepsilon)$ be the left-hand side of (A-14), we have, to second order,

$$\left.\begin{aligned} D(\varepsilon) &= B_o + B_1\ \varepsilon^2 \\ D(\varepsilon/2) &= B_o + B_1\ \varepsilon^2/4 \end{aligned}\right\} \text{ where } B_o \text{ and } B_1 \text{ are unknown .} \tag{A-15}$$

The desired solution is

$$B_o = \frac{4\ D(\varepsilon/2) - D(\varepsilon)}{3} \cong g''(0)\ . \tag{A-16}$$

This is an extrapolation to the limit; it uses $\varepsilon/2$ as the smallest argument of D. A program for the evaluation of g"(t) at general t is given below in BASIC; it requires specification of a tolerance Tol in line 70 of the function subroutine FNDeriv2.

```
10  INPUT T
20  Der2=FNDeriv2(T)
30  PRINT T,Der2     !  t,g"(t)
40  END
50  !
60  DEF FNDeriv2(T) !  ~g"(t) via extrapolation
70  Tol=1.E-6        !  tolerance
80  E=.2             !  epsilon (start)
90  G2=2.*FNG(T)
100 E=E*.5
110 V1=V2
120 V2=(FNG(T+E)+FNG(T-E)-G2)/(E*E)
130 V=V2+(V2-V1)/3.
140 IF ABS(V2/V-1.)>Tol THEN 100
150 RETURN V
160 FNEND
170 !
180 DEF FNG(T)
190 RETURN EXP(T)    !  example exp(t)
200 FNEND
```

An application of this program to the exp(t) example in line 190, at argument 1.1, yielded an error of 1.6E-11.

APPENDIX B. FOURIER TRANSFORM OF GENERALIZED FUNCTION

We are interested in finding the Fourier transform of the generalized function

$$\frac{\exp(-a\tau)}{\tau}\, U(\tau) \;, \qquad a > 0 \;, \tag{B-1}$$

where $U(\tau)$ is the unit step function. Letting $\omega = 2\pi f$, the integral of interest is

$$I = \int \frac{d\tau}{\tau} \exp(-a\tau)\, U(\tau)\, \exp(-i\omega\tau) =$$

$$= \int \frac{d\tau}{\tau} [\exp(-a\tau) - 1 + 1]\, U(\tau)\, \exp(-i\omega\tau) =$$

$$= - \int_0^{+\infty} \frac{d\tau}{\tau} [1 - \exp(-a\tau)]\, \exp(-i\omega\tau) + \int \frac{d\tau}{\tau} U(\tau)\, \exp(-i\omega\tau) =$$

$$= - \ln\left(\frac{a + i\omega}{i\omega}\right) - \left[i\frac{\pi}{2} \operatorname{sgn}\left(\frac{\omega}{2\pi}\right) + \ln\left|\frac{\omega}{2\pi}\right| + C'\right] = \tag{B-2}$$

$$= - \ln(a + i\omega) + \ln(i\omega) - i\frac{\pi}{2} \operatorname{sgn}(\omega) - \ln|\omega| + \ln(2\pi) - C'. \tag{B-3}$$

In (B-2), we used [4; page 334, 3.434 2] and [6; page 43, row 3, column 3, with $m = 1$]. But since

$$\ln(i\omega) = \left\{\begin{array}{ll} i\pi/2 + \ln|\omega| & \text{for } \omega > 0 \\ -i\pi/2 + \ln|\omega| & \text{for } \omega < 0 \end{array}\right\} + i2\pi n =$$

$$= i\frac{\pi}{2} \operatorname{sgn}(\omega) + \ln|\omega| + i2\pi n \;, \quad n \text{ integer} \;, \tag{B-4}$$

we can express (B-3) as

$$I = -\ln(a + i\omega) + C \ , \quad \text{where } C = \ln(2\pi) - C' + i2\pi n \ . \qquad \text{(B-5)}$$

Thus, we have the Fourier transform pair

$$\frac{\exp(-a\tau)}{\tau} U(\tau) \longleftrightarrow -\ln(a + i2\pi f) + C \ , \qquad \text{(B-6)}$$

where C is an arbitrary constant. The reason for the presence of C is that the generalized function $\frac{1}{\tau} U(\tau)$ is indeterminate within an additive arbitrary multiple of the delta function $\delta(\tau)$.

For the example in (33) of $H(f) = 1/(1 + i2\pi f)$, we have $Q(f) = \ln(1 + i2\pi f)$. Application of pair (B-6), with $a = 1$, to (39) then yields causal function

$$q(\tau) = -\frac{\exp(-\tau)}{\tau} U(\tau) \ . \qquad \text{(B-7)}$$

APPENDIX C. HILBERT TRANSFORM MANIPULATION

It was noted below (45) that the Hilbert transform of attenuation $\alpha(f)$ encounters integrals with logarithmic infinities and must be handled more carefully. This problem is treated in [3; pages 206 - 208], by dividing the attenuation by a factor that is quadratic in f, rather than linear. In current notation, that result is [3; (10-67)]

$$\beta(f) = \frac{f}{\pi} \int_{-\infty}^{+\infty} du \, \frac{\alpha(u)}{u^2 - f^2} \, . \tag{C-1}$$

If we utilize the property employed in [3; page 208, line 2], namely that attenuation $\alpha(f)$ is even, we can develop (C-1) as

$$\beta(f) = \frac{2f}{\pi} \int_{0}^{+\infty} du \, \frac{\alpha(u)}{u^2 - f^2} =$$

$$= -\frac{1}{\pi} \int_{0}^{+\infty} du \, \alpha(u) \left(\frac{1}{f - u} + \frac{1}{f + u} \right) = \tag{C-2}$$

$$= -\frac{1}{\pi} \int_{0}^{+\infty} du \, \frac{\alpha(u)}{f - u} - \frac{1}{\pi} \int_{0}^{+\infty} du \, \frac{\alpha(u)}{f + u} = \tag{C-3}$$

$$= -\frac{1}{\pi} \int_{0}^{+\infty} du \, \frac{\alpha(u)}{f - u} - \frac{1}{\pi} \int_{-\infty}^{0} dv \, \frac{\alpha(-v)}{f - v} =$$

$$= -\frac{1}{\pi} \int_{-\infty}^{+\infty} du \, \frac{\alpha(u)}{f - u} = - \underline{H}\{\alpha(f)\} \, . \tag{C-4}$$

The step leading from (C-2) to (C-3) presumes that both of the latter integrals converge separately, which need not be the case for attenuations $\alpha(f)$; this is the reason for the quadratic denominator adopted in (C-1), which guaranteed convergence of that integral.

Rather than using Hilbert transforms and having to employ the method of (C-1), we have resorted instead to the use of Fourier transforms, as outlined in (46). Of course, a similar problem arises there, as mentioned in the sequel to (51). The method of circumventing the difficulty, in the Fourier approach, is to subtract out the singularities and handle them analytically, as described in (54)-(57).

The justification of this procedure, using modified Hilbert transform (C-1) as a starting point, is as follows. Express given attenuation $\alpha(f)$ in two parts, as in (54), where residue $\alpha_2(f)$ has a convergent Hilbert transform integral

$$\frac{1}{\pi}\int_{-\infty}^{+\infty} du\, \frac{\alpha_2(u)}{f-u} = \underline{H}\{\alpha_2(f)\} \quad \text{for all } f\ . \tag{C-5}$$

The phase shift $\beta(f)$ corresponding to attenuation $\alpha(f)$ is then given by sum (56), where, following (C-1),

$$\beta_1(f) = \frac{f}{\pi}\int_{-\infty}^{+\infty} du\, \frac{\alpha_1(u)}{u^2-f^2} \tag{C-6}$$

and $\beta_2(f)$ is available as the negative of (C-5). The proof of this last claim follows immediately from the derivation in (C-1)-(C-4) if we replace $\alpha(f)$ and $\beta(f)$ everywhere by $\alpha_2(f)$ and

$\beta_2(f)$, respectively. This is legitimate because the existence of (C-5) for residual attenuation $\alpha_2(f)$ now allows the separation into two convergent integrals, as done in (C-3).

We do not actually use (C-5) or (C-6). Instead, (C-6) is accomplished by using known closed form attenuation/minimum-phase pairs for $\alpha_1(f)$ and $\beta_1(f)$, while (C-5) is replaced by the Fourier approach given in (46), with $\alpha_2(f)$ and $\beta_2(f)$ substituted for $\alpha(f)$ and $\beta(f)$, respectively. The inverse Fourier transform integral in the top line of (46), but now in terms of $\alpha_2(f)$, is convergent.

(For interest, an example of the application of (C-6) is afforded by attenuation-phase pair (51). This fact is immediately verified by use of [4; 4.295 8].)

APPENDIX D. EXAMPLES OF ATTENUATION/MINIMUM-PHASE PAIRS

In this appendix, we list a few attenuation/minimum-phase pairs that can be used in the subtraction procedure presented in (54)-(57) to eliminate the divergent integrands encountered. For convenience of notation, we employ the Laplace transform of the impulse response, namely

$$L(s) = \int_0^{+\infty} d\tau \, \exp(-s\tau) \, h(\tau) \; , \tag{D-1}$$

where we have specifically limited consideration to causal filters. The connection with the Fourier transform (1) is

$$H(f) = L(i2\pi f) \; . \tag{D-2}$$

In the following, a, b, and c are real positive constants, and $\omega = 2\pi f$.

EXAMPLE 1:

$$L(s) = \frac{c}{s + a} \; ,$$

$$\alpha(f) = \frac{1}{2} \ln(a^2 + \omega^2) - \ln(c) \; , \quad \beta(f) = \arctan(\omega/a) \; . \tag{D-3}$$

In the limit as $a \to 0+$,

$$\alpha(f) = \ln|\omega| - \ln(c) \; , \quad \beta(f) = \frac{\pi}{2} \operatorname{sgn}(\omega) \; . \tag{D-4}$$

EXAMPLE 2:

$$L(s) = \frac{c\ s}{s + a} ,$$

$$\alpha(f) = \frac{1}{2} \ln(a^2 + \omega^2) - \ln|\omega| - \ln(c) ,$$

$$\beta(f) = \arctan(\omega/a) - \frac{\pi}{2} \operatorname{sgn}(\omega) . \qquad \text{(D-5)}$$

EXAMPLE 3:

$$L(s) = \frac{c\ s}{(s + a)(s + b)} ,$$

$$\alpha(f) = \frac{1}{2} \ln(a^2 + \omega^2) + \frac{1}{2} \ln(b^2 + \omega^2) - \ln|\omega| - \ln(c) ,$$

$$\beta(f) = \arctan(\omega/a) + \arctan(\omega/b) - \frac{\pi}{2} \operatorname{sgn}(\omega) . \qquad \text{(D-6)}$$

This attenuation reaches a minimum at $\omega = (ab)^{1/2}$, at which point the phase goes through zero.

EXAMPLE 4:

$$L(s) = \frac{c}{(s + a)^2 + b^2} ,$$

$$\alpha(f) = \frac{1}{2} \ln\left[(a^2 + (\omega + b)^2\right] + \frac{1}{2} \ln\left[a^2 + (\omega - b)^2\right] - \ln(c) ,$$

$$\beta(f) = \arctan\left(\frac{\omega - b}{a}\right) + \arctan\left(\frac{\omega + b}{a}\right) . \qquad \text{(D-7)}$$

APPENDIX E. NUMERICAL EVALUATION OF (46)

We repeat here the cascaded Fourier transform operations listed in (46):

$$\underline{q}(\tau) = \underline{F}^{-1}\{\alpha(f)\} \quad , \tag{E-1}$$

$$q(\tau) = 2\; \underline{q}(\tau)\; U(\tau) \quad , \tag{E-2}$$

$$\alpha(f) + i\;\beta(f) = \underline{F}\{q(\tau)\} \quad . \tag{E-3}$$

We limit consideration to the case where attenuation $\alpha(f)$ is even, which is the typical practical situation. Also, we weight the inverse Fourier transform in (E-1) by real symmetric window $W(f)$, which is zero for $|f| > M\Delta$. We then get approximation

$$\underline{q}_a(\tau) = \int_{-\infty}^{+\infty} df\; \exp(i2\pi f\tau)\; \alpha(f)\; W(f) =$$

$$= 2\;\mathrm{Re}\int_{0}^{+\infty} df\; \exp(-i2\pi f\tau)\; \alpha(f)\; W(f) =$$

$$= 2\;\mathrm{Re}\int_{0}^{M\Delta} df\; \exp(-i2\pi f\tau)\; \alpha(f)\; W(f) =$$

$$\cong 2\;\mathrm{Re}\sum_{n=0}^{M} s_n\;\Delta\;\exp(-i2\pi n\Delta\tau)\;\alpha(n\Delta)\;W(n\Delta) = \underline{q}_b(\tau) \quad , \tag{E-4}$$

where we sample in frequency f with increment Δ. We also use some integration rule like trapezoidal or Simpson; for example, the trapezoidal rule has $s_n = 1$, except for $s_o = s_M = 1/2$.

The approximation $g_b(\tau)$, defined by the bottom line of (E-4), has period $1/\Delta$ in τ. Therefore, we compute it at the points

$$\tau = \frac{m}{N\Delta} \quad \text{for } 0 \le m \le N-1 \ , \qquad \text{(E-5)}$$

which cover a full period of $g_b(\tau)$. There follows

$$g_b\left(\frac{m}{N\Delta}\right) = 2\Delta \ \mathrm{Re} \sum_{n=0}^{M} s_n \exp(-i2\pi nm/N)\ \alpha(n\Delta)\ W(n\Delta) \ , \qquad \text{(E-6)}$$

which is an N-size fast Fourier transform of M + 1 data points. Any surplus points can be collapsed, if desired, without loss of accuracy; see [7; pages 4 - 5], for example.

Operations (E-2) and (E-3) can be combined to read

$$Q(f) = \alpha(f) + i\ \beta(f) = 2 \int_0^{+\infty} d\tau \exp(-i2\pi f\tau)\ g(\tau) \ . \qquad \text{(E-7)}$$

Because all we have available is approximation $g_b(\tau)$ from (E-4), we adopt the following approximation to Q(f), based on (E-7):

$$Q_a(f) \equiv 2 \int_0^{+\infty} d\tau \exp(-i2\pi f\tau)\ g_b(\tau) =$$

$$\cong 2 \int_0^{.5/\Delta} d\tau \exp(-i2\pi f\tau)\ g_b(\tau) = \qquad \text{(E-8)}$$

$$\cong 2 \sum_{m=0}^{N/2} w_m \frac{1}{N\Delta} \exp\left(-i2\pi f\frac{m}{N\Delta}\right) g_b\left(\frac{m}{N\Delta}\right) \equiv Q_b(f) \ , \qquad \text{(E-9)}$$

where w_m is an integration weight. The integral in (E-8) was limited to $.5/\Delta$ in τ, because approximation $g_b(\tau)$ in (E-4) is only available up to that limit without aliasing.

The period of the final approximation $Q_b(f)$ in (E-9) is $N\Delta$ in f. Therefore, we limit its computation to the values

$$Q_b(n\Delta) = \frac{2}{N\Delta} \sum_{m=0}^{N/2} w_m \exp(-i2\pi nm/N)\ g_b\left(\frac{m}{N\Delta}\right) \quad \text{for } 0 \le n \le N-1 \ . \qquad \text{(E-10)}$$

This can be accomplished as an N-size fast Fourier transform of $N/2 + 1$ data points. The final approximation to desired phase $\beta(f)$ in (E-7) is available as the imaginary part of (E-10), at frequencies $f = n\Delta$. In addition, the real part of (E-10) should be in very good agreement with specified attenuation values $\{\alpha(n\Delta)\ W(n\Delta)\}$ used in (E-6); this serves as an accuracy check on the complete procedure. Equations (E-6) and (E-10) are the final results. Strictly, (E-6) should be applied only to the residual attenuation $\alpha_2(f)$ defined in (55); then (E-10) furnishes an approximation to $\alpha_2(f) + i\ \beta_2(f)$. A program in BASIC for the Hewlett Packard 9000 computer, for the procedure given above, is presented below.

```
10 !   NUSC TR 8667, FOURIER PROCEDURE APPLIED
20 !   TO REAL EVEN FUNCTION OF FREQUENCY
30     Deltaf=5.                          !  SAMPLING INCREMENT IN FREQUENCY
40     Fmax=900.                          !  MAXIMUM FREQUENCY
50     N=16384                            !  SIZE OF FFT
60     A=260.                             !  FILTER PARAMETERS
70     B=330.                             !  FOR
80     C=-.55E8                           !  EXAMPLE C
90     COM A,B,C
100    REDIM Cos(0:N/4),X(0:N-1),Y(0:N-1)
110    DIM Cos(4096),X(16384),Y(16384),Realeven(25000),Phase(6:100)
120    DOUBLE N,M,Ns,Ms,N2,M2             !  INTEGERS
130    T=2.*PI/N
140    FOR Ns=0 TO N/4
150    Cos(Ns)=COS(T*Ns)                  !  QUARTER-COSINE TABLE
160    NEXT Ns
170    M=Fmax/Deltaf
180    REDIM Realeven(0:M)
190    CALL Input_real_even(Deltaf,Fmax,Realeven(*)) !  RESIDUAL
200    MAT X=(0.)                         !  ATTENUATION ALPHA2
210    MAT Y=(0.)
220    X(0)=.5*Realeven(0)
230    Ms=M MODULO N
240    X(Ms)=.5*Realeven(M)
250    FOR Ns=1 TO M-1
260    Ms=Ns MODULO N                     !  COLLAPSING
270    X(Ms)=X(Ms)+Realeven(Ns)
280    NEXT Ns
290    CALL Fft14(N,Cos(*),X(*),Y(*))     !  FOURIER TRANSFORM
300    N2=N/2                             !  INTO TIME DOMAIN
310      GINIT
320      PLOTTER IS "GRAPHICS"
330      GRAPHICS ON
340      WINDOW -N2,N2,-6,2
350      LINE TYPE 3
360      GRID N/8,1
370      PRINT "FOURIER TRANSFORM (TIME DOMAIN)"
380      FOR Ns=-N2 TO N2
390      Ms=Ns MODULO N
400      PLOT Ns,LGT(ABS(X(Ms))+1.E-99)   !  TIME DOMAIN FUNCTION
410      NEXT Ns
420      PENUP
430      PAUSE
440    MAT Y=(0.)
450    T=4./N                             !  2 Deltaf * 2 / (N Deltaf)
460    FOR Ms=0 TO N2
470    X(Ms)=X(Ms)*T                      !  DOUBLE FOR POSITIVE TIME
480    NEXT Ms
490    X(0)=X(0)*.5
500    X(N2)=X(N2)*.5
510    FOR Ms=N2+1 TO N-1
520    X(Ms)=0.                           !  ZERO FOR NEGATIVE TIME
530    NEXT Ms
540    CALL Fft14(N,Cos(*),X(*),Y(*))     !  FOURIER TRANSFORM
550      M2=M*2                           !  INTO FREQUENCY DOMAIN
```

```
560       GCLEAR
570       WINDOW 0,M2,-1,1
580       LINE TYPE 3
590       GRID N/16,.2
600       PRINT "ORIGINAL INPUT (FREQUENCY DOMAIN)"
610       FOR Ns=0 TO MIN(M,N2)
620       PLOT Ns,Realeven(Ns)              !  ORIGINAL INPUT
630       NEXT Ns
640       PENUP
650       PAUSE
660       LINE TYPE 1
670       FOR Ns=0 TO M2
680       PLOT Ns,X(Ns)                     !  F-T-F APPROXIMATION
690       NEXT Ns
700       PENUP
710       PAUSE
720     DATA -38.6,-48.2,-54.8,-60.4,-76.2,-82.1,-94.5,-103.8,-109.1,-117.1
730     DATA -124.1,-134.0,-143.1,-152.9,-163.1,-172.4,179.1,171.1,164.2,157.9
740     DATA 152.8,147.1,142.8,135.8,131.9,128.7,122.8,118.7,115.1,110.6
750     DATA 105.9,103.4,102.8,99.9,98.6,93.8,93.1,91.2,89.6,89.5
760     DATA 89.6,89.6,89.2,88.1,85.6,84.5,82.0,81.1,79.0,74.7
770     DATA 71.4,66.5,61.3,55.1,48.1,41.6,34.0,29.3,22.0,16.1
780     DATA 12.2,5.7,2.4,-3.1,-6.5,-11.3,-16.2,-21.2,-25.7,-29.7
790     DATA -33.4,-37.0,-40.7,-43.5,-47.0,-49.5,-51.6,-54.1,-56.2,-59.4
800     DATA -61.0,-62.4,-64.2,-66.7,-68.7,-71.4,-74.6,-78.1,-81.4,-83.8
810     DATA -88.7,-91.3,-95.0,-98.7,-103.1
820     READ Phase(*)                       !  MEASURED PHASE IN DEGREES
830     FOR Ns=22 TO 100
840     Phase(Ns)=Phase(Ns)-360.            !  UN-WRAPPING OF PHASE
850     NEXT Ns
860     MAT Phase=Phase*(-PI/180.)          !  MEASURED PHASE IN RADIANS
870       T=2.*PI*Deltaf
880       FOR Ns=0 TO N2
890       W=T*Ns
900       Phaseapp=ATN((W-B)/A)+ATN((W+B)/A) ! PHASE BETA1 OF APPROX.
910       X(Ns)=Phaseapp+Y(Ns)              !  CALCULATED PHASE IN RADIANS:
920       NEXT Ns                           !  BETA = BETA1 + BETA2
930       GCLEAR
940       WINDOW 0,180,0,PI*1.25
950       LINE TYPE 1
960       GRID 20,PI*.25
970       PRINT "PHASE (FREQUENCY DOMAIN)"
980       FOR Ns=0 TO 180
990       PLOT Ns,X(Ns)                     !  PHASE VIA FOURIER PROCEDURE
1000      NEXT Ns
1010      PENUP
1020      LINE TYPE 3
1030      FOR Ns=6 TO 100
1040      PLOT Ns,Phase(Ns)-Ns*.0448        !  MEASURED PHASE WITH
1050      NEXT Ns                           !  TIME DELAY CORRECTION
1060      PENUP                             !  OF 1.43 MILLISECONDS
1070      PAUSE
1080    END
1090    !
```

```
1100    SUB Fft14(DOUBLE N,REAL Cos(*),X(*),Y(*)) ! N<=2^14=16384; 0 SUBS
1110    DOUBLE Log2n,N1,N2,N3,N4,J,K    !  INTEGERS < 2^31 = 2,147,483,648
1120    DOUBLE I1,I2,I3,I4,I5,I6,I7,I8,I9,I10,I11,I12,I13,I14,L(0:13)
1130    IF N=1 THEN SUBEXIT
1140    IF N>2 THEN 1220
1150    A=X(0)+X(1)
1160    X(1)=X(0)-X(1)
1170    X(0)=A
1180    A=Y(0)+Y(1)
1190    Y(1)=Y(0)-Y(1)
1200    Y(0)=A
1210    SUBEXIT
1220    A=LOG(N)/LOG(2.)
1230    Log2n=A
1240    IF ABS(A-Log2n)<1.E-8 THEN 1270
1250    PRINT "N =";N;"IS NOT A POWER OF 2; DISALLOWED."
1260    PAUSE
1270    N1=N/4
1280    N2=N1+1
1290    N3=N2+1
1300    N4=N3+N1
1310    FOR I1=1 TO Log2n
1320    I2=2^(Log2n-I1)
1330    I3=2*I2
1340    I4=N/I3
1350    FOR I5=1 TO I2
1360    I6=(I5-1)*I4+1
1370    IF I6<=N2 THEN 1410
1380    A1=-Cos(N4-I6-1)
1390    A2=-Cos(I6-N1-1)
1400    GOTO 1430
1410    A1=Cos(I6-1)
1420    A2=-Cos(N3-I6-1)
1430    FOR I7=0 TO N-I3 STEP I3
1440    I8=I7+I5-1
1450    I9=I8+I2
1460    T1=X(I8)
1470    T2=X(I9)
1480    T3=Y(I8)
1490    T4=Y(I9)
1500    A3=T1-T2
1510    A4=T3-T4
1520    X(I8)=T1+T2
1530    Y(I8)=T3+T4
1540    X(I9)=A1*A3-A2*A4
1550    Y(I9)=A1*A4+A2*A3
1560    NEXT I7
1570    NEXT I5
1580    NEXT I1
```

```
1590    I1=Log2n+1
1600    FOR I2=1 TO 14
1610    L(I2-1)=1
1620    IF I2>Log2n THEN 1640
1630    L(I2-1)=2^(I1-I2)
1640    NEXT I2
1650    K=0
1660    FOR I1=1 TO L(13)
1670    FOR I2=I1 TO L(12) STEP L(13)
1680    FOR I3=I2 TO L(11) STEP L(12)
1690    FOR I4=I3 TO L(10) STEP L(11)
1700    FOR I5=I4 TO L(9) STEP L(10)
1710    FOR I6=I5 TO L(8) STEP L(9)
1720    FOR I7=I6 TO L(7) STEP L(8)
1730    FOR I8=I7 TO L(6) STEP L(7)
1740    FOR I9=I8 TO L(5) STEP L(6)
1750    FOR I10=I9 TO L(4) STEP L(5)
1760    FOR I11=I10 TO L(3) STEP L(4)
1770    FOR I12=I11 TO L(2) STEP L(3)
1780    FOR I13=I12 TO L(1) STEP L(2)
1790    FOR I14=I13 TO L(0) STEP L(1)
1800    J=I14-1
1810    IF K>J THEN 1880
1820    A=X(K)
1830    X(K)=X(J)
1840    X(J)=A
1850    A=Y(K)
1860    Y(K)=Y(J)
1870    Y(J)=A
1880    K=K+1
1890    NEXT I14
1900    NEXT I13
1910    NEXT I12
1920    NEXT I11
1930    NEXT I10
1940    NEXT I9
1950    NEXT I8
1960    NEXT I7
1970    NEXT I6
1980    NEXT I5
1990    NEXT I4
2000    NEXT I3
2010    NEXT I2
2020    NEXT I1
2030    SUBEND
2040    !
```

```
2050    SUB Input_real_even(Deltaf,Fmax,Realeven(*))
2060    DOUBLE Ns                              !  INTEGER
2070    ALLOCATE Db(6:180)                     !  30:900 HZ
2080    DATA 41.3,44.3,46.1,47.6,49.9,51.4,52.9,54.4,54.8,56.3
2090    DATA 57.0,57.4,57.9,58.6,59.0,59.1,59.0,58.9,58.9,58.8
2100    DATA 58.6,58.1,58.2,58.1,58.0,57.9,57.8,57.2,56.9,56.7
2110    DATA 56.6,56.4,56.3,56.2,55.7,55.6,55.4,55.0,54.9,55.2
2120    DATA 55.2,55.7,55.7,56.1,56.1,56.6,56.9,57.5,58.3,58.6
2130    DATA 59.0,59.7,60.3,60.7,60.9,61.1,61.1,61.2,61.0,60.9
2140    DATA 60.7,60.6,60.4,60.2,60.0,59.9,59.6,59.4,59.3,58.7
2150    DATA 58.5,58.3,57.8,57.5,57.3,57.0,56.7,56.3,56.1,55.9
2160    DATA 55.7,55.5,55.6,55.6,55.4,55.3,55.4,55.3,55.6,55.3
2170    DATA 55.4,55.0,55.0,55.0,54.8
2180    REDIM Db(6:100)
2190    READ Db(*)
2200    MAT Db=Db+(100.)                       !  MEASURED DB GAIN
2210    REDIM Db(6:180)
2220    FOR Ns=101 TO 180                      !  AUGMENTED DB GAIN
2230    F=Deltaf*Ns
2240    T1=(F-550.)*.04
2250    T2=(F-580.)*.04
2260    Db(Ns)=154.8-5.*EXP(-T1*T1)-5.*EXP(-T2*T2)
2270    NEXT Ns
2280    MAT Realeven=(0.)
2290    COM A,B,C
2300    A2=A*A
2310    B2=B*B
2320    C2=C*C
2330    D1=(A2+B2)*(A2+B2)
2340    D2=2.*(A2-B2)
2350    T=2.*PI*Deltaf
2360    FOR Ns=6 TO 180
2370    W=T*Ns
2380    W2=W*W
2390    W4=W2*W2
2400    P=C2*W4/(D1+D2*W2+W4)
2410    Attenapp=-.5*LOG(P)                    !  APPROX. ATTEN. ALPHA1
2420    Atten=Db(Ns)/(-8.686)                  !  ATTENUATION ALPHA
2430    Realeven(Ns)=Atten-Attenapp            !  RESIDUAL ATTEN. ALPHA2
2440    NEXT Ns
2450    SUBEND
```

REFERENCES

[1] N. Balabanian and W. R. LePage, "What is a Minimum-Phase Network," **Proceedings AIEE**, Communications and Electronics, vol. 75, no. 22, pages 785-787, January 1956.

[2] E. A. Guillemin, **The Mathematics of Circuit Analysis**, John Wiley & Sons, Inc., New York, NY, 1951.

[3] A. Papoulis, **The Fourier Integral and Its Applications**, McGraw-Hill Book Company, Inc., New York, NY, 1962.

[4] I. S. Gradshteyn and I. M. Ryzhik, **Table of Integrals, Series, and Products**, Academic Press, Inc., New York, NY, 1980.

[5] A. Papoulis, **Signal Analysis**, McGraw-Hill Book Company, Inc., New York, NY, 1977.

[6] M. J. Lighthill, **Introduction to Fourier Analysis and Generalised Functions**, Cambridge University Press, New York, NY, 1964.

[7] A. H. Nuttall, **Alias-Free Wigner Distribution Function and Complex Ambiguity Function for Discrete-Time Samples**, NUSC Technical Report 8533, Naval Underwater Systems Center, New London, CT, 14 April 1989.

NUSC Technical Report 8689
18 May 1990

Evaluation of Integrals and Sums Involving $[\sin(Mx)/\sin(x)]^n$

Albert H. Nuttall

ABSTRACT

The response of equispaced arrays, either linear, planar, or volumetric, to distributed spatial fields, typically encounters integrals which involve the kernel sin(Mx)/sin(x) or its square. Since this kernel oscillates rather fast with x for large M and does not decay with x, numerical integration of such functions can be very time consuming. By resorting to Parseval's theorem, such integrals can be significantly simplified, requiring only the Fourier transform of the complementary part of the integrand. This procedure is investigated and applied to several typical examples; programs for the examples are also included.

TABLE OF CONTENTS

LIST OF TABLES

LIST OF SYMBOLS

M	integer, number of elements in line array
$g(t)$	arbitrary function of t, (1)
$G(\omega)$	Fourier transform of $g(t)$, (1)
V	integral of product of $g(t)\, h^*(t)$, (2)
$H(\omega)$	Fourier transform of $h(t)$, (2)
γ	argument of sine functions, (3)
$h_1(t)$	ratio of sine functions, (3)
prime	sum with prime denotes every other term, (3)
$H_1(\omega)$	Fourier transform of $h_1(t)$, (4)
V_1	general integral (5)
$h_2(t)$	square of ratio of sine functions, (7)
$H_2(\omega)$	Fourier transform of $h_2(t)$, (8)
V_2	general integral (9)
$\phi(m)$	autocorrelation of weights, (12B)
sub r	real part, (13B)
V_{1a}	integral (18)
V_{2a}	integral (22)
V_{1b}	integral (27)
V_{2b}	integral (28)
V_{1c}	integral (33)
V_{2c}	integral (34)
Δ	increment in t, (41),(A-1)
$\delta_\Delta(t)$	impulse train, (41)
$\circledast$	convolution, (42)
$S_N(M,k)$	discrete sine ratio, (52)

INT	integer part, (55)
V_5	general integral (63)
$\psi(p)$	autocorrelation of $\phi(m)$, (61)
$g(n\Delta)$	samples of $g(t)$, (A-1)
$\underline{G}(\omega)$	approximation to $G(\omega)$, (A-1)
N	size of FFT, (A-6)
$g_c(n\Delta)$	collapsed version of $g(n\Delta)$, (A-7)
$\tilde{g}(n\Delta)$	phase modulated $g(n\Delta)$, (A-11)
$\tilde{g}_c(n\Delta)$	collapsed version of $\tilde{g}(n\Delta)$, (A-12)

EVALUATION OF INTEGRALS AND SUMS INVOLVING $[\sin(Mx)/\sin(x)]^n$

INTRODUCTION

The response of an equiweighted equispaced line array to a distributed field involves the kernel $\sin(Mx)/\sin(x)$ or its square, depending on whether the voltage or power response, respectively, is of interest [1,2]. Numerical evaluation of such integrals can be very time consuming for two reasons: this kernel oscillates quickly with x for large M, and it does not decay with x. This necessitates fine sampling in x and large integration regions, both of which can lead to a significant computational burden, especially for two-dimensional or three-dimensional arrays. The object of this report is to give an alternative numerical procedure that can be very advantageous in some cases, and, in fact, leads to closed forms for some examples.

The procedure is also applied to summations involving the same kernel. Its utility depends on the rate of decay of the complementary part of the original integrand, as compared with the Fourier transform of this component. In any event, an alternative is presented for the user to consider in any numerical investigation.

GENERAL APPROACH

For arbitrary function g(t), define its Fourier transform as

$$G(\omega) = \int dt \, \exp(-i\omega t) \, g(t) \; . \qquad (1)$$

(Integrals without limits are over the range of nonzero integrand.) Then Parseval's theorem states that the following two alternative integrals are equal:

$$V = \int dt \, g(t) \, h^*(t) = \frac{1}{2\pi} \int d\omega \, G(\omega) \, H^*(\omega) \; . \qquad (2)$$

Here, $H(\omega)$ is the Fourier transform of h(t). Now, if $H(\omega)$ takes on a noticeably simpler form than h(t), then the second integral in (2) can offer an attractive alternative to the first integral in (2). That will indeed be the case here.

CASE 1

For integer $M \geq 1$ and constant $\gamma > 0$, consider the special choice of h(t) as

$$h_1(t) = \frac{\sin(M\gamma t)}{\sin(\gamma t)} = \sum_{n=0}^{M-1} \exp[i\gamma t(2n+1-M)] =$$

$$= \sum_{m=1-M}^{M-1}{}' \exp(i\gamma tm) \ , \qquad (3)$$

where the prime on the latter sum denotes skipping every other term. Then the Fourier transform, according to (1), is

$$H_1(\omega) = 2\pi \sum_{m=1-M}^{M-1}{}' \delta(\omega - \gamma m) \ . \qquad (4)$$

Substitution of (3) and (4) in (2) yields

$$V_1 \equiv \int dt \ g(t) \ \frac{\sin(M\gamma t)}{\sin(\gamma t)} = \sum_{m=1-M}^{M-1}{}' G(\gamma m) \ . \qquad (5A)$$

This result indicates that if $G(\omega)$, the Fourier transform of g(t), can be evaluated, then the t integral in (5A) is given by a finite sum of equispaced samples of $G(\omega)$ at increment 2γ. The (complex) function g(t) in (5A) is arbitrary, except that the integral must converge. When $G(\omega)$ cannot be analytically evaluated, then proper application of a fast Fourier transform procedure to g(t) can be tailored to yield precisely the equispaced samples required for the right-hand side of (5A); this technique and a program is detailed in appendix A.

An alternative more explicit form of (5A) illustrates the calculations required:

$$V_1 = \left\{ \begin{array}{ll} \sum\limits_{n=(1-M)/2}^{(M-1)/2} G(2\gamma n) & \text{for } M \text{ odd} \\ \\ \sum\limits_{n=-M/2}^{M/2-1} G(\gamma+2\gamma n) & \text{for } M \text{ even} \end{array} \right\} . \tag{5B}$$

If function $G(\omega)$ is even in ω, then (5A) simplifies to

$$V_1 = \left\{ \begin{array}{ll} G(0) + 2 \sum\limits_{m=2}^{M-1}{}' \, G(\gamma m) & \text{for } M = 1,3,5,\ldots \\ \\ 2 \sum\limits_{m=1}^{M-1}{}' \, G(\gamma m) & \text{for } M = 2,4,6,\ldots \end{array} \right\} . \tag{6}$$

A program for (6) is given in appendix B.

CASE 2

For integer $M \geq 1$ and constant $\gamma > 0$, consider the alternative special choice of $h(t)$ as

$$h_2(t) = \left[\frac{\sin(M\gamma t)}{\sin(\gamma t)}\right]^2 = \sum_{n,k=0}^{M-1} \exp[i\gamma t(2n-2k)] = \tag{7A}$$

$$= \sum_{m=1-M}^{M-1} (M - |m|) \exp(i2\gamma tm) , \tag{7B}$$

where we used (3). There is no prime on the summation in (7B) because all terms from 1-M to M-1 are to be included. The Fourier transform of $h_2(t)$ is

$$H_2(\omega) = 2\pi \sum_{m=1-M}^{M-1} (M - |m|)\ \delta(\omega - 2\gamma m) \ . \tag{8}$$

The use of (7A) and (8) in (2) yields

$$V_2 = \int dt\ g(t)\ \left[\frac{\sin(M\gamma t)}{\sin(\gamma t)}\right]^2 = \sum_{m=1-M}^{M-1} (M - |m|)\ G(2\gamma m) \ . \tag{9}$$

Again, the integral of interest is given by a finite sum of samples of the Fourier transform of g(t), also at increment 2γ in ω. The fast Fourier transform technique and program presented in appendix A is relevant here also. If $G(\omega)$ is even in ω, then we can express (9) as

$$V_2 = M\ G(0) + 2 \sum_{m=1}^{M-1} (M - m)\ G(2\gamma m) \quad \text{for all } M \geq 1 \ . \tag{10}$$

A program for (10) is given in appendix B.

CASE 3

For arbitrary weights $\{w_m\}$ and frequencies $\{\gamma_m\}$, with

$$h_3(t) = \sum_m w_m \exp(i\gamma_m t) \ , \tag{11A}$$

then we have a generalization of (3), with

$$H_3(\omega) = 2\pi \sum_m w_m \, \delta(\omega - \gamma_m) \ . \qquad (11B)$$

(Summations without limits are over the range of nonzero summand.) Use of these expressions in general result (2) yields

$$V_3 = \int dt \; g(t) \sum_m w_m^* \exp(-i\gamma_m t) = \sum_m w_m^* \, G(\gamma_m) \ . \qquad (11C)$$

Again, the Fourier transform of g(t) is required, but now at general arguments $\{\gamma_m\}$.

CASE 4

Function $h_2(t)$ in (7) is a special case of the weighted array power response

$$h_4(t) = \left| \sum_k w_k \exp(-i2\gamma tk) \right|^2 = \sum_m \phi(m) \exp(-i2\gamma tm) \ , \qquad (12A)$$

where $\phi(m)$ is the autocorrelation of the weights:

$$\phi(m) = \sum_k w_k \, w_{k-m}^* = \phi^*(-m) \ . \qquad (12B)$$

The integral in (9) is then generalized to

$$V_4 = \int dt\ g(t)\ h_4^*(t) = \int dt\ g(t) \left| \sum_k w_k \exp(-i2\gamma tk) \right|^2 =$$

$$= \sum_m \phi(m)\ G(2\gamma m)\ , \qquad (13A)$$

upon use of (12A), where g(t) can be complex and nonsymmetric. Thus, integral V_4 requires the autocorrelation of weights $\{w_k\}$ and the Fourier transform of g(t) for its evaluation. The earlier result in (9) corresponds to weights $w_k = 1$ for $1 \leq k \leq M$.

When function g(t) is real (but possibly nonsymmetric) and the weights are real, (13A) can be simplified to

$$V_4 = \phi(0)\ G_r(0) + 2 \sum_{m \geq 1} \phi(m)\ G_r(2\gamma m)\ , \qquad (13B)$$

where $G_r(\omega)$ is the real part of Fourier transform $G(\omega)$ in (1). A program for (13B) is given in appendix B.

EXAMPLES

EXAMPLE A

The first example of interest is

$$g_a(t) = \frac{1}{(t-\mu)^2 + \beta^2} \ , \quad \beta > 0 \ . \tag{14}$$

Its Fourier transform is

$$G_a(\omega) = \frac{\pi}{\beta} \exp(-i\mu\omega-\beta|\omega|) \ , \tag{15}$$

for which the real part is

$$G_{ar}(\omega) = \frac{\pi}{\beta} \cos(\mu\omega) \exp(-\beta|\omega|) \ . \tag{16}$$

Since integral (5) is obviously real for example (14), we obtain

$$V_{1a} = \int \frac{dt}{(t-\mu)^2 + \beta^2} \frac{\sin(M\gamma t)}{\sin(\gamma t)} = \sum_{m=1-M}^{M-1}{}' G_{ar}(\gamma m) \ . \tag{17}$$

Substitution of (16) in (17) yields the closed form result

$$V_{1a} = \int \frac{dt}{(t-\mu)^2 + \beta^2} \frac{\sin(M\gamma t)}{\sin(\gamma t)} =$$

$$= \frac{2\pi}{\beta D}\left[E_{M+3}\,C_{M-1} - E_{M+1}\,C_{M+1} + \left\{\begin{matrix} C_1\,E_1\,(1-E_2) & \text{for M even} \\ \frac{1}{2}\,(1-E_4) & \text{for M odd} \end{matrix}\right\}\right] \ , \tag{18}$$

where

$$E_m = \exp(-\beta\gamma m) \ , \quad C_m = \cos(\mu\gamma m) \ , \quad D = 1 - 2\,E_2\,C_2 + E_4 \ . \tag{19}$$

A program for (18) and (19) follows; it is written in BASIC for the Hewlett Packard 9000 computer.

```
 10   INPUT M,Beta,Gamma,Mu       ! Beta > 0,  Gamma > 0
 20   B=Beta*Gamma
 30   C=Mu*Gamma
 40   E=EXP(-B*2)
 50   IF (M MODULO 2)=1 THEN 80
 60   F=COS(C)*SQR(E)*(1-E)
 70   GOTO 90
 80   F=.5-.5*E*E
 90   A=E*COS(C*(M-1))-COS(C*(M+1))
100   A=A*EXP(-B*(M+1))+F
110   V1a=A*2*PI/(Beta*(1-2*E*COS(C*2)+E*E))
120   PRINT V1a
130   END
```

When we instead substitute (14) and (16) in (9), there follows

$$V_{2a} = \int \frac{dt}{(t-\mu)^2 + \beta^2} \left[\frac{\sin(M\gamma t)}{\sin(\gamma t)}\right]^2 =$$

$$= \frac{\pi}{\beta} \sum_{m=1-M}^{M-1} (M - |m|) \cos(2\mu\gamma m) \exp(-2\beta\gamma|m|) \ . \qquad (20)$$

This finite sum can be written in compact form by use of [3; 0.113]. Namely, define here

$$E = \exp(-2\beta\gamma) \ , \quad C = \cos(2\mu\gamma) \ , \quad S = \sin(2\mu\gamma) \ ,$$

$$E_M = \exp(-2\beta\gamma M), \quad C_M = \cos(2\mu\gamma M), \quad S_M = \sin(2\mu\gamma M),$$

$$A = 1 - E^2 \ , \quad B = 1 + E^2 \ , \quad D = B - 2\,E\,C. \qquad (21)$$

Then

$$V_{2a} = \int \frac{dt}{(t-\mu)^2 + \beta^2} \left[\frac{\sin(M\gamma t)}{\sin(\gamma t)}\right]^2 =$$

$$= \frac{2\pi}{\beta D}\left[\frac{M}{2} A - \frac{E}{D}\Big((C\ B - 2\ E)(1 - E_M\ C_M) + S\ A\ E_M\ S_M\Big)\right] . \qquad (22)$$

A program for (21) and (22) follows.

```
 10  INPUT M,Beta,Gamma,Mu        ! Beta > 0,  Gamma > 0
 20  Tb=2*Beta*Gamma
 30  Tm=2*Mu*Gamma
 40  E=EXP(-Tb)
 50  A=E*E
 60  B=1+A
 70  A=1-A
 80  C=COS(Tm)
 90  D=B-2*E*C
100  Em=EXP(-Tb*M)
110  T=(C*B-2*E)*(1-Em*COS(Tm*M))
120  T=T+SIN(Tm)*A*Em*SIN(Tm*M)
130  T=.5*M*A-T*E/D
140  V2a=T*2*PI/(Beta*D)
150  PRINT V2a
160  END
```

EXAMPLE B

The next example to be considered is

$$g_b(t) = \frac{1}{(t-\mu)^2 + \beta^2}\,\frac{\sin(\alpha t)}{\alpha t} , \quad \beta > 0 , \quad \alpha > 0 . \qquad (23)$$

Since $g_b(t)$ is a product of two functions, its Fourier transform $G_b(\omega)$ is given by a convolution of the individual transforms. The Fourier transform of the first term in (23) has already been encountered in (15), and the Fourier transform of the second term in (23) is a rectangle located on interval $(-\alpha, \alpha)$ in ω. Therefore, $G_b(\omega)$ is given by convolution

$$G_b(\omega) = \frac{\pi}{2\alpha\beta} \int_{\omega-\alpha}^{\omega+\alpha} du \, \exp(-i\mu u - \beta|u|) \ . \tag{24}$$

Since $g_b(t)$ in (23) is real, we need only evaluate the real part, $G_{br}(\omega)$, of $G_b(\omega)$. With the aid of auxiliary variables

$$\begin{aligned}
C_\omega &= \cos(\mu\omega),\ S_\omega = \sin(\mu\omega),\ \underline{C}_\omega = \cosh(\beta\omega),\ \underline{S}_\omega = \sinh(\beta\omega), \\
C_\alpha &= \cos(\mu\alpha),\ S_\alpha = \sin(\mu\alpha),\ \underline{C}_\alpha = \cosh(\beta\alpha),\ \underline{S}_\alpha = \sinh(\beta\alpha), \\
B_1 &= \underline{C}_\omega\, C_\omega\, (\beta\, C_\alpha - \mu\, S_\alpha) + \underline{S}_\omega\, S_\omega\, (\mu\, C_\alpha + \beta\, S_\alpha), \\
B_2 &= \underline{S}_\alpha\, C_\alpha\, (\beta\, C_\omega - \mu\, S_\omega) + \underline{C}_\alpha\, S_\alpha\, (\mu\, C_\omega + \beta\, S_\omega),
\end{aligned} \tag{25}$$

we find that $G_{br}(\omega)$ is given by

$$G_{br}(\omega) = \frac{\pi}{\alpha\beta\left(\beta^2+\mu^2\right)} \begin{Bmatrix} \beta - \exp(-\beta\alpha)\, B_1 & \text{for } 0 \le \omega \le \alpha \\ \\ \exp(-\beta\omega)\, B_2 & \text{for } \alpha \le \omega \end{Bmatrix} . \tag{26}$$

To complete the description, we observe that $G_{br}(\omega)$ is even in ω because $g_b(t)$ is real. A program for $G_{br}(\omega)$ follows, where we have made the following identifications: $W \equiv \omega$, $A \equiv \alpha$, $B \equiv \beta$, $U \equiv \mu$.

```
10   DEF FNGbr(W,A,B,U)
20   Wa=ABS(W)
30   F=PI/(A*B*(B*B+U*U))
40   Ea=EXP(-B*A)
50   Ew=EXP(-B*Wa)
60   Ca=COS(U*A)
70   Cw=COS(U*Wa)
80   Sa=SIN(U*A)
90   Sw=SIN(U*Wa)
100  IF Wa<A THEN 150
110  Ra=1./Ea
120  T=(Ra-Ea)*Ca*(B*Cw-U*Sw)
130  B2=.5*(T+(Ra+Ea)*Sa*(U*Cw+B*Sw))
140  RETURN F*Ew*B2
150  Rw=1./Ew
160  T=(Rw+Ew)*Cw*(B*Ca-U*Sa)
170  B1=.5*(T+(Rw-Ew)*Sw*(U*Ca+B*Sa))
180  RETURN F*(B-Ea*B1)
190  FNEND
```

If we now employ (23) in (5), we obtain

$$V_{1b} = \int \frac{dt}{(t-\mu)^2 + \beta^2} \frac{\sin(\alpha t)}{\alpha t} \frac{\sin(M\gamma t)}{\sin(\gamma t)} = \sum_{m=1-M}^{M-1}{}' \, G_{br}(\gamma m) \ , \qquad (27)$$

where $G_{br}(\omega)$ is given by (25), (26), and its even property. Since there is a break in the analytic form for $G_{br}(\omega)$ at $\omega = \pm\alpha$, it is not reasonable to perform the summation in (27) in closed form; those terms in (27) for $\gamma|m| \leq \alpha$ utilize the upper line of (26), while those for $\gamma|m| \geq \alpha$ utilize the lower line of (26). However, since $G_{br}(\omega)$ is even in ω, the simplification in (6) is applicable.

Instead, when (23) is substituted in (9), there follows

$$V_{2b} = \int \frac{dt}{(t-\mu)^2 + \beta^2} \frac{\sin(\alpha t)}{\alpha t} \left[\frac{\sin(M\gamma t)}{\sin(\gamma t)}\right]^2 = \sum_{m=1-M}^{M-1} (M - |m|) \, G_{br}(2\gamma m), \qquad (28)$$

where $G_{br}(\omega)$ is given by (25) and (26). Again, the break in form of $G_{br}(\omega)$ at $\omega = \pm\alpha$ precludes a closed form result for the summation in (28); also, the simplification in (10) is immediately applicable to (28).

EXAMPLE C

The final example is

$$g_c(t) = \frac{1}{(t-\mu)^2 + \beta^2} \left[\frac{\sin(\alpha t)}{\alpha t}\right]^2 , \quad \beta > 0 , \quad \alpha > 0 . \qquad (29)$$

The Fourier transform of the second term in (29) is a triangle located on interval $(-2\alpha, 2\alpha)$ in ω. Therefore, $G_c(\omega)$ is given by convolution

$$G_c(\omega) = \frac{\pi}{2\alpha\beta} \int_{\omega-2\alpha}^{\omega+2\alpha} du \, \exp(-i\mu u-\beta|u|) \left(1 - \frac{|\omega-u|}{2\alpha}\right) . \qquad (30)$$

Because $g_c(t)$ is real, only the real part of (30) is needed. This tedious calculation has been carried through, with the following result; define auxiliary variables

$$\begin{aligned}
&R = \beta^2-\mu^2, \quad I = 2\beta\mu, \quad D = \beta^2+\mu^2, \quad E_\omega = \exp(-\beta\omega), \quad E_\alpha = \exp(-2\beta\alpha), \\
&\underline{C}_\alpha = \cosh(2\beta\alpha), \quad \underline{S}_\alpha = \sinh(2\beta\alpha), \quad C_\alpha = \cos(2\mu\alpha), \quad S_\alpha = \sin(2\mu\alpha) , \\
&\underline{C}_\omega = \cosh(\beta\omega) , \quad \underline{S}_\omega = \sinh(\beta\omega) , \quad C_\omega = \cos(\mu\omega) , \quad S_\omega = \sin(\mu\omega) , \\
&C_1 = \underline{C}_\omega C_\omega (R C_\alpha - I S_\alpha) + \underline{S}_\omega S_\omega (R S_\alpha + I C_\alpha) , \\
&C_2 = \underline{C}_\alpha C_\alpha (R C_\omega - I S_\omega) + \underline{S}_\alpha S_\alpha (R S_\omega + I C_\omega) , \\
&C = R C_\omega - I S_\omega . \qquad (31)
\end{aligned}$$

Then we find that real part

$$G_{cr}(\omega) = \frac{\pi}{2\alpha^2\beta D^2} \left\{ \begin{array}{ll} D \beta (2\alpha - \omega) - E_\omega C + E_\alpha C_1 & \text{for } 0 \le \omega \le 2\alpha \\ \\ - E_\omega C + E_\omega C_2 & \text{for } 2\alpha \le \omega \end{array} \right\} . \qquad (32)$$

Also, $G_{cr}(\omega)$ is even in ω. A program for $G_{cr}(\omega)$ is listed below, where $W \equiv \omega$, $A \equiv \alpha$, $B \equiv \beta$, $U \equiv \mu$.

```
 10  DEF FNGcr(W,A,B,U)      !  A > 0 ,  B > 0
 20  Wa=ABS(W)
 30  Tb=2.*A*B
 40  Tu=2.*A*U
 50  Bw=B*Wa
 60  Uw=U*Wa
 70  B2=B*B
 80  U2=U*U
 90  R=B2-U2
100  I=2.*B*U
110  D=B2+U2
120  Ew=EXP(-Bw)
130  Ea=EXP(-Tb)
140  Ca=COS(Tu)
150  Sa=SIN(Tu)
160  Cw=COS(Uw)
170  Sw=SIN(Uw)
180  C=R*Cw-I*Sw
190  IF Wa<2.*A THEN 250
200  Ra=1./Ea
210  C2=.5*(Ra+Ea)*Ca*C
220  C2=.5*(Ra-Ea)*Sa*(R*Sw+I*Cw)+C2
230  T=Ew*(C2-C)
240  GOTO 290
250  Rw=1./Ew
260  C1=.5*(Rw+Ew)*Cw*(R*Ca-I*Sa)
270  C1=.5*(Rw-Ew)*Sw*(R*Sa+I*Ca)+C1
280  T=D*(Tb-Bw)-Ew*C+Ea*C1
290  RETURN PI*T/(Tb*A*D*D)
300  FNEND
```

We now substitute (29) into (5) and get

$$V_{1c} = \int \frac{dt}{(t-\mu)^2 + \beta^2} \left[\frac{\sin(\alpha t)}{\alpha t}\right]^2 \frac{\sin(M\gamma t)}{\sin(\gamma t)} = \sum_{m=1-M}^{M-1}{}' \, G_{cr}(\gamma m) \quad , \quad (33)$$

where $G_{cr}(\omega)$ is given by (31), (32), and its even character. The break in form in (32) at $\omega = \pm 2\alpha$ precludes a closed form for the sum in (33). However, (6) is still applicable.

When (29) is utilized in (9), there follows

$$V_{2c} = \int \frac{dt}{(t-\mu)^2 + \beta^2} \left[\frac{\sin(\alpha t)}{\alpha t}\right]^2 \left[\frac{\sin(M\gamma t)}{\sin(\gamma t)}\right]^2 =$$

$$= \sum_{m=1-M}^{M-1} (M - |m|)\, G_{cr}(2\gamma m) \ . \qquad (34)$$

Equation (10) may also be employed here.

SPECIAL CASES

If we set M = 1 in (17), there follows

$$\int \frac{dt}{(t-\mu)^2 + \beta^2} = G_{ar}(0) = \frac{\pi}{\beta} \ , \qquad (35)$$

where we used (16). The same case in (27) yields

$$\int \frac{dt}{(t-\mu)^2 + \beta^2} \frac{\sin(\alpha t)}{\alpha t} = G_{br}(0) =$$

$$= \frac{\pi}{\alpha\beta\left(\beta^2+\mu^2\right)} \{\beta - \exp(-\beta\alpha)\ [\beta \cos(\mu\alpha) - \mu \sin(\mu\alpha)]\} \ , \qquad (36)$$

upon use of (26) and (25). Finally, from (33),

$$\int \frac{dt}{(t-\mu)^2 + \beta^2} \left[\frac{\sin(\alpha t)}{\alpha t}\right]^2 = G_{cr}(0) =$$

$$= \frac{\pi}{2\alpha^2\beta\left(\beta^2+\mu^2\right)^2} \left(2\alpha\beta(\beta^2 + \mu^2) - R + E_\alpha \,(R\, C_\alpha - I\, S_\alpha)\right) , \qquad (37)$$

using (32) and (31).

APPLICATION TO SUMS

In this section, it is more convenient to use Parseval's theorem (2) in the form

$$V = \int dt\ g(t)\ h^*(t) = \int df\ G(f)\ H^*(f)\ , \tag{38}$$

where Fourier transform

$$G(f) = \int dt\ \exp(-i2\pi ft)\ g(t)\ . \tag{39}$$

Now, we take as our candidate h(t) function,

$$h(t) = p(t)\ \Delta\delta_\Delta(t)\ , \tag{40}$$

where $\delta_\Delta(t)$ is the infinite impulse train

$$\delta_\Delta(t) = \sum_k \delta(t - k\Delta)\ . \tag{41}$$

The Fourier transform of h(t) is then

$$H(f) = P(f) \circledast \delta_{1/\Delta}(f) = \sum_k P\left(f - \frac{k}{\Delta}\right)\ , \tag{42}$$

where P(f) is the Fourier transform of p(t), $\circledast$ denotes convolution, and we have utilized the fact that the Fourier transform of impulse train $\Delta\delta_\Delta(t)$ is another impulse train, $\delta_{1/\Delta}(f)$.

Substitution of (40) and (42) in (38) yields

$$V = \Delta \sum_k g(k\Delta)\ p^*(k\Delta) = \sum_k \int df\ G(f)\ P^*\left(f - \frac{k}{\Delta}\right) . \quad (43)$$

For general p(t) and P(f), this will not be a useful relation, since the right-hand side of (43) is an infinite sum of integrals. However, we will be interested here only in the special cases of

$$p(t) = \left[\frac{\sin(M\gamma t)}{\sin(\gamma t)}\right]^n , \quad n \text{ integer} . \quad (44)$$

CASE n = 0

For n = 0, the above relations specialize to

$$p(t) = 1 , \quad P(f) = \delta(f) ,$$

$$H(f) = \sum_k \delta\left(f - \frac{k}{\Delta}\right) ,$$

$$V_o = \Delta \sum_k g(k\Delta) = \sum_k G\left(\frac{k}{\Delta}\right) . \quad (45)$$

This is a discrete version of Parseval's theorem. Although one infinite sum has been traded for another, we can now choose that alternative that has the most rapidly decaying (and/or easily computed) summand for numerical evaluation.

CASE n = 1

Now we have, via (3),

$$p(t) = \frac{\sin(M\gamma t)}{\sin(\gamma t)} = \sum_{m=1-M}^{M-1}{}' \exp(i\gamma tm) . \tag{46}$$

There follows

$$P(f) = \sum_{m=1-M}^{M-1}{}' \delta\left(f - \frac{\gamma m}{2\pi}\right) ,$$

$$H(f) = \sum_{k} \sum_{m=1-M}^{M-1}{}' \delta\left(f - \frac{k}{\Delta} - \frac{\gamma m}{2\pi}\right) ,$$

$$V_1 = \Delta \sum_{k} g(k\Delta) \frac{\sin(M\gamma\Delta k)}{\sin(\gamma\Delta k)} = \tag{47}$$

$$= \sum_{k} \sum_{m=1-M}^{M-1}{}' G\left(\frac{k}{\Delta} + \frac{\gamma m}{2\pi}\right) . \tag{48}$$

Again, we have an alternative infinite sum (48) that hopefully decays faster than the original sum (47). The $\sin(Mx)/\sin(x)$ term does not help convergence in (47) because this term never decays for large x. Although (48) is a double sum, the summation on m only contains M terms; the utility of (48) depends heavily on the asymptotic decay of G(f) for large f.

CASE n = 2

With the aid of (7), we now find

$$p(t) = \left[\frac{\sin(M\gamma t)}{\sin(\gamma t)}\right]^2 = \sum_{m=1-M}^{M-1} (M - |m|) \exp(i2\gamma tm) ,$$

$$P(f) = \sum_{m=1-M}^{M-1} (M - |m|) \, \delta\left(f - \frac{\gamma m}{\pi}\right) ,$$

$$H(f) = \sum_{k} \sum_{m=1-M}^{M-1} (M - |m|) \, \delta\left(f - \frac{k}{\Delta} - \frac{\gamma m}{\pi}\right) ,$$

$$V_2 = \Delta \sum_{k} g(k\Delta) \left[\frac{\sin(M\gamma\Delta k)}{\sin(\gamma\Delta k)}\right]^2 = \qquad (49)$$

$$= \sum_{k} \sum_{m=1-M}^{M-1} (M - |m|) \, G\left(\frac{k}{\Delta} + \frac{\gamma m}{\pi}\right) . \qquad (50)$$

EXAMPLE

Consider, as in (14) and (16),

$$g_a(t) = \frac{1}{(t-\mu)^2 + \beta^2} ,$$

$$G_{ar}(f) = \frac{\pi}{\beta} \cos(2\pi\mu f) \exp(-2\pi\beta|f|) . \qquad (51)$$

The summations in (47) and (49) are very slowly decaying, leading to difficulty in attaining accurate results. The alternatives in

(48) and (50), on the other hand, have exponential decay and can be evaluated quite accurately. The additional examples given earlier in (23) - (26) and in (29) - (32), along with the corresponding programs, lend reasonable alternatives to some otherwise lengthy numerical calculations.

SOME RELATED SUMS

Here, we collect a few closed form results for sums involving the sin(Mx)/sin(x) kernel. For ease of notation, define

$$S_N(M,k) = \frac{\sin(Mk\pi/N)}{\sin(k\pi/N)} . \tag{52}$$

Observe that

$$S_N(M,k) = \begin{Bmatrix} M & \text{for } k = 0,\ \pm 2N,\ \pm 4N, \ldots \\ M(-1)^{M-1} & \text{for } k = \pm N,\ \pm 3N, \ldots \end{Bmatrix} . \tag{53}$$

Then, we find the sum over one interval to be

$$\sum_{k=0}^{N-1} S_N(M,k) = \begin{Bmatrix} M & \text{for } M \text{ even} \\ N(1 + 2J) & \text{for } M \text{ odd} \end{Bmatrix} , \tag{54}$$

where

$$J = \mathrm{INT}\left(\frac{M-1}{2N}\right) . \tag{55}$$

The sum over a double interval is

$$\sum_{k=0}^{2N-1} S_N(M,k) = \begin{cases} 0 & \text{for } M = 0,2,4,\ldots\ldots \\ 2N & \text{for } M = 1,3,\ldots,2N-1 \end{cases} . \tag{56}$$

The correlation on the second variable of S_N is

$$\sum_{k=0}^{N-1} S_N(M,k)\ S_N(M,k+j) = N\ S_N(M,j) \quad \text{for } 0 \le M \le N \text{ and all } j. \tag{57}$$

Finally, the correlation on the first variable is

$$\sum_{k=0}^{N-1} S_N(M,k)\ S_N(M+2L,k) = M(M + 2L) +$$

$$+ \begin{cases} \underline{M}(N - \underline{M} - 2\underline{L}) & \text{for } 0 \le \underline{M} + \underline{L} \le N \\ N(3\underline{M} + 2\underline{L} - 2N) - \underline{M}(\underline{M} + 2\underline{L}) & \text{for } N < \underline{M} + \underline{L} \end{cases} , \tag{58}$$

for all M, L, N, where

$$\underline{M} = M \text{ MOD } N , \qquad \underline{L} = L \text{ MOD } N . \tag{59}$$

SUMMARY

Extensions to integrals involving $[\sin(Mx)/\sin(x)]^n$ for $n > 2$ are possible, based upon the results presented here. For example, starting from (12A) for arbitrary weights, we could consider

$$h_5(t) = h_4^2(t) = \sum_p \psi(p) \exp(-i2\gamma tp) , \tag{60}$$

where

$$\psi(p) = \sum_m \phi(m) \phi^*(m-p) \tag{61}$$

is the autocorrelation of sequence $\{\phi(m)\}$ defined in (12B). Therefore, Fourier transform

$$H_5(\omega) = 2\pi \sum_p \psi(p) \delta(\omega + 2\gamma p) , \tag{62}$$

giving rise to

$$V_5 = \int dt\ g(t)\ h_5(t) = \sum_p \psi(p)\ G(2\gamma p) . \tag{63}$$

The case of equal weights $\{w_k\}$ in (12A) now corresponds to $n = 4$ in the sine function ratio above, and $\psi(p)$ is the autocorrelation of a triangular sequence.

The evaluation of integrals and sums involving the term $[\sin(Mx)/\sin(x)]^n$ can often be simplified by the use of Parseval's theorem because this term has a Fourier transform which is a finite sum of delta functions. Major effort can then be concentrated on getting the Fourier transform of the complementary part of the integrand. This procedure has been applied here to several examples which arise in evaluation of the response of equispaced arrays to distributed spatial fields. For more complicated fields, a fast Fourier transform procedure combined with the above result leads to a very efficient method of integral evaluations; see appendix A. Applications of this procedure have been made in [5].

APPENDIX A - USE OF FAST FOURIER TRANSFORM

The summations for V_1 and V_2 in (5) and (9), respectively, require the evaluation of the Fourier transform of g(t), namely $G(\omega)$, at equispaced increment 2γ. But this latter function can be approximated by means of the trapezoidal rule according to

$$G(\omega) = \int dt \exp(-i\omega t)\, g(t) =$$

$$\cong \Delta \sum_n \exp(-i\omega\Delta n)\, g(n\Delta) \equiv \underline{G}(\omega) = \sum_n G\left(\omega - n\frac{2\pi}{\Delta}\right) , \qquad \text{(A-1)}$$

where Δ is the sampling increment in t. The latter summation in (A-1) indicates aliasing lobes separated by $2\pi/\Delta$ on the ω axis. In order to control the aliasing in (A-1), we must choose Δ small enough, say $\Delta < \Delta_o$. Then samples of aliased approximation $\underline{G}(\omega)$ in (A-1) at multiples of 2γ are given by

$$\underline{G}(2\gamma m) = \Delta \sum_n \exp(-i2\gamma\Delta mn)\, g(n\Delta) . \qquad \text{(A-2)}$$

Now since Δ is arbitrary, except for upper limit Δ_o, choose

$$\Delta = \frac{\pi}{N\gamma} , \qquad \text{(A-3)}$$

where N is an integer and 2γ is the prescribed increment in ω. In order that Δ be less than Δ_o, we must take integer

$$N > \frac{\pi}{\gamma\Delta_o} . \qquad \text{(A-4)}$$

Use of (A-3) in (A-2) gives the approximation samples

$$\underline{G}(2\gamma m) = \Delta \sum_{n} \exp(-i2\pi mn/N)\ g(n\Delta) = \tag{A-5}$$

$$= \Delta \sum_{n=0}^{N-1} \exp(-i2\pi mn/N)\ g_c(n\Delta)\ , \tag{A-6}$$

where "collapsed" sequence [4; pages 4 - 5]

$$g_c(n\Delta) \equiv \sum_{k} g(n\Delta + kN\Delta) \quad \text{for } 0 \le n \le N - 1\ . \tag{A-7}$$

The manipulation from (A-5) to (A-6) is exact; it avoids truncation error normally associated with functions $g(t)$ which decay slowly with t. The sum on k in (A-7) must be carried out (for each n) until negligible values for g are encountered for both positive as well as negative values of k.

Equation (A-6) indicates that values of $\underline{G}(2\gamma m)$ for $m = 0$ to $N - 1$ are available by an N-point fast Fourier transform when N is a power of 2. These are exactly the values of $G(\omega)$ needed for the sum in (5B) for M odd, as well as for the sum in (9) for all M. The values for negative m required in (5) and (9) are available in locations $m \bmod N$. A program for these cases is attached at the end of this appendix.

In order to get all the desired values of $\underline{G}(2\gamma m)$ required for (9), without aliasing, we also require that $N/2 > M$. (On the other hand, the requirement for (5), with M odd, is slackened to $N > M$.) Thus, the final condition on integer N is

$$N > \max\left(\frac{\pi}{\gamma\Delta_o},\ 2M\right) \quad \text{for (9)}\ . \tag{A-8}$$

For the case of (5) with M even, where the increment on ω is 2γ, but starting at $\omega = \gamma$, we return to (A-1) to find that

$$\underline{G}(\gamma + 2\gamma m) = \Delta \sum_{n} \exp(-i\gamma\Delta n - i2\gamma\Delta mn)\; g(n\Delta) \; . \qquad \text{(A-9)}$$

The same choice of Δ in (A-3) now yields

$$\underline{G}(\gamma + 2\gamma m) = \Delta \sum_{n} \exp(-i2\pi mn/N)\; \exp(-i\pi n/N)\; g(n\Delta) \; . \qquad \text{(A-10)}$$

This result is identical to (A-5) except that $g(n\Delta)$ must be replaced by

$$\exp(-i\pi n/N)\; g(n\Delta) \equiv \tilde{g}(n\Delta) \; . \qquad \text{(A-11)}$$

Calculation of the collapsed version of $\tilde{g}$ is eased by the observation that

$$\tilde{g}_c(n\Delta) \equiv \sum_{k} \tilde{g}(n\Delta + kN\Delta) =$$

$$= \sum_{k} \exp(-i\pi(n + kN)/N)\; g(n\Delta + kN\Delta) =$$

$$= \exp(-i\pi n/N) \sum_{k} (-1)^k\; g(n\Delta + kN\Delta) \quad \text{for } 0 \le n \le N - 1 \; , \qquad \text{(A-12)}$$

thereby leading exactly to

$$\underline{G}(\gamma + 2\gamma m) = \Delta \sum_{n=0}^{N-1} \exp(-i2\pi mn/N)\; \tilde{g}_c(n\Delta) \; . \qquad \text{(A-13)}$$

The leading phase factor in (A-12) only needs to be evaluated at N different values (perhaps by recurrence), and the sum in (A-12) requires differencing of "adjacent" samples of g spaced by $N\Delta$, rather than the straight summation previously adequate for (A-6) and (A-7). Condition (A-8) applies here as well.

PROGRAM FOR (5B) WITH M ODD, AND FOR (9)

```
 10  ! TR 8689, FFT EVALUATION OF (9) FOR ALL M, AND (5) FOR M ODD
 20    T1=-3000                           !  LEFT  END ARGUMENT FOR g(t)
 30    T2=3000                            !  RIGHT END ARGUMENT FOR g(t)
 40    Deltao=.05                         !  STARTING Delta, (A-4)
 50    M=7                                !  INTEGER IN (9) AND (5)
 60    Gamma=.785                         !  CONSTANT IN (9) AND (5)
 70    T=PI/(Gamma*Deltao)
 80    N=1
 90    IF N>MAX(T,2*M) THEN 120           !  (A-8)
100    N=N*2                              !  N = SIZE OF FFT
110    GOTO 90
120    Delta=PI/(N*Gamma)                 !  (A-3), INCREMENT IN t
130    DOUBLE M,N,Ns,N1,N2,Nn             !  INTEGERS
140    REDIM Cos(N/4),X(0:N-1),Y(0:N-1)
150    DIM Cos(1024),X(4096),Y(4096)
160    T=2.*PI/N
170    FOR Ns=0 TO N/4
180    Cos(Ns)=COS(T*Ns)                  !  QUARTER-COSINE TABLE
190    NEXT Ns
200    MAT X=(0.)
210    MAT Y=(0.)
220    N1=INT(T1/Delta)
230    N2=INT(T2/Delta)+1
240    FOR Ns=N1 TO N2
250    T=Delta*Ns                         !  ARGUMENT OF INTEGRAND
260    G=FNG(T)                           !  INTEGRAND g(t), REAL HERE
270    IF Ns=N1 THEN PRINT "INTEGRAND AT LEFT  END =";G
280    IF Ns=N2 THEN PRINT "INTEGRAND AT RIGHT END =";G
290    Nn=Ns MODULO N
300    X(Nn)=X(Nn)+G                      !  COLLAPSING
310    NEXT Ns
320    MAT X=X*(Delta)
330    CALL Fft14(N,Cos(*),X(*),Y(*))     !  0 SUBSCRIPT FFT
340    GINIT
350    PLOTTER IS "GRAPHICS"
360    GRAPHICS ON
```

```
370    N2=N/2
380    WINDOW -N2,N2,-16,2
390    LINE TYPE 3
400    GRID N/8,2
410    LINE TYPE 1
420    FOR Ns=-N2 TO N2
430    Nn=Ns MODULO N
440    Xn=X(Nn)
450    Yn=Y(Nn)
460    T=Xn*Xn+Yn*Yn
470    IF T>0. THEN 500
480    PENUP
490    GOTO 510
500    PLOT Ns,.5*LGT(T)                    !  MAGNITUDE OF TRANSFORM
510    NEXT Ns
520    PENUP
530    PAUSE
540    V2r=V2i=0.                           !  (9)
550    FOR Ns=1-M TO M-1
560    T=M-ABS(Ns)
570    Nn=Ns MODULO N
580    V2r=V2r+T*X(Nn)                      !  (9), REAL PART
590    V2i=V2i+T*Y(Nn)                      !  (9), IMAG PART
600    NEXT Ns
610    PRINT
620    PRINT "EDGE VALUES USED IN SUM: ";Nn;X(Nn);Y(Nn)
630    PRINT "V2r = ";V2r,"V2r/M^2 = ";V2r/M^2
640    PRINT "V2i = ";V2i,"V2i/M^2 = ";V2i/M^2
650    PAUSE
660    V1r=V1i=0.                           !  (5)
670    IF (M MODULO 2)=1 THEN 700
680    PRINT "NO GOOD FOR (5) WHEN M IS EVEN"
690    PAUSE
700    N1=(M-1)/2
710    FOR Ns=-N1 TO N1
720    Nn=Ns MODULO N
730    V1r=V1r+X(Nn)                        !  (5), REAL PART
740    V1i=V1i+Y(Nn)                        !  (5), IMAG PART
750    NEXT Ns
760    PRINT
770    PRINT "EDGE VALUES USED IN SUM: ";Nn;X(Nn);Y(Nn)
780    PRINT "V1r = ";V1r,"V1r/M = ";V1r/M
790    PRINT "V1i = ";V1i,"V1i/M = ";V1i/M
800    PRINT
810    PAUSE
820    END
830    !
840    DEF FNG(T)                           !  (29) EXAMPLE
850    Mu=.71
860    Beta=.49061
870    Alpha=.565
880    IF T=0. THEN RETURN 1./(Mu*Mu+Beta*Beta)
890    A=Alpha*T
900    S=SIN(A)/A
910    A=T-Mu
920    RETURN S*S/(A*A+Beta*Beta)
930    FNEND
940    !
```

```
950   SUB Fft14(DOUBLE N,REAL Cos(*),X(*),Y(*)) ! N<=2^14=16384; 0 SUBS
960   DOUBLE Log2n,N1,N2,N3,N4,J,K   !  INTEGERS < 2^31 = 2,147,483,648
970   DOUBLE I1,I2,I3,I4,I5,I6,I7,I8,I9,I10,I11,I12,I13,I14,L(0:13)
980   IF N=1 THEN SUBEXIT
990   IF N>2 THEN 1070
1000  A=X(0)+X(1)
1010  X(1)=X(0)-X(1)
1020  X(0)=A
1030  A=Y(0)+Y(1)
1040  Y(1)=Y(0)-Y(1)
1050  Y(0)=A
1060  SUBEXIT
1070  A=LOG(N)/LOG(2.)
1080  Log2n=A
1090  IF ABS(A-Log2n)<1.E-8 THEN 1120
1100  PRINT "N =";N;"IS NOT A POWER OF 2; DISALLOWED."
1110  PAUSE
1120  N1=N/4
1130  N2=N1+1
1140  N3=N2+1
1150  N4=N3+N1
1160  FOR I1=1 TO Log2n
1170  I2=2^(Log2n-I1)
1180  I3=2*I2
1190  I4=N/I3
1200  FOR I5=1 TO I2
1210  I6=(I5-1)*I4+1
1220  IF I6<=N2 THEN 1260
1230  A1=-Cos(N4-I6-1)
1240  A2=-Cos(I6-N1-1)
1250  GOTO 1280
1260  A1=Cos(I6-1)
1270  A2=-Cos(N3-I6-1)
1280  FOR I7=0 TO N-I3 STEP I3
1290  I8=I7+I5-1
1300  I9=I8+I2
1310  T1=X(I8)
1320  T2=X(I9)
1330  T3=Y(I8)
1340  T4=Y(I9)
1350  A3=T1-T2
1360  A4=T3-T4
1370  X(I8)=T1+T2
1380  Y(I8)=T3+T4
1390  X(I9)=A1*A3-A2*A4
1400  Y(I9)=A1*A4+A2*A3
1410  NEXT I7
1420  NEXT I5
1430  NEXT I1
```

```
1440    I1=Log2n+1
1450    FOR I2=1 TO 14
1460    L(I2-1)=1
1470    IF I2>Log2n THEN 1490
1480    L(I2-1)=2^(I1-I2)
1490    NEXT I2
1500    K=0
1510    FOR I1=1 TO L(13)
1520    FOR I2=I1 TO L(12) STEP L(13)
1530    FOR I3=I2 TO L(11) STEP L(12)
1540    FOR I4=I3 TO L(10) STEP L(11)
1550    FOR I5=I4 TO L(9) STEP L(10)
1560    FOR I6=I5 TO L(8) STEP L(9)
1570    FOR I7=I6 TO L(7) STEP L(8)
1580    FOR I8=I7 TO L(6) STEP L(7)
1590    FOR I9=I8 TO L(5) STEP L(6)
1600    FOR I10=I9 TO L(4) STEP L(5)
1610    FOR I11=I10 TO L(3) STEP L(4)
1620    FOR I12=I11 TO L(2) STEP L(3)
1630    FOR I13=I12 TO L(1) STEP L(2)
1640    FOR I14=I13 TO L(0) STEP L(1)
1650    J=I14-1
1660    IF K>J THEN 1730
1670    A=X(K)
1680    X(K)=X(J)
1690    X(J)=A
1700    A=Y(K)
1710    Y(K)=Y(J)
1720    Y(J)=A
1730    K=K+1
1740    NEXT I14
1750    NEXT I13
1760    NEXT I12
1770    NEXT I11
1780    NEXT I10
1790    NEXT I9
1800    NEXT I8
1810    NEXT I7
1820    NEXT I6
1830    NEXT I5
1840    NEXT I4
1850    NEXT I3
1860    NEXT I2
1870    NEXT I1
1880    SUBEND
```

APPENDIX B – PROGRAMS FOR (6), (10), AND (13B)

Table B-1. Program for (6)

```
 10  M=7                 !  > 0
 20  Gamma=1.31          !  > 0
 30  DOUBLE M,Ms         !  INTEGERS
 40  S=0.
 50  IF (M MODULO 2)=1 THEN 110
 60  FOR Ms=1 TO M-1 STEP 2
 70  S=S+FNG(Gamma*Ms)
 80  NEXT Ms
 90  V1=2.*S
100  GOTO 150
110  FOR Ms=2 TO M-1 STEP 2
120  S=S+FNG(Gamma*Ms)
130  NEXT Ms
140  V1=FNG(0.)+2.*S
150  PRINT M,Gamma,V1
160  END
170  !
180  DEF FNG(W)
```

Table B-2. Program for (10)

```
 10  M=6                 !  > 0
 20  Gamma=.71           !  > 0
 30  DOUBLE M,Ms         !  INTEGERS
 40  G2=2.*Gamma
 50  S=0.
 60  FOR Ms=1 TO M-1
 70  S=S+(M-Ms)*FNG(G2*Ms)
 80  NEXT Ms
 90  V2=M*FNG(0.)+2.*S
100  PRINT M,Gamma,V2
110  END
120  !
130  DEF FNG(W)
```

Table B-3. Program for (13B)

```
 10  M=9                         !  > 0
 20  Gamma=.79                   !  > 0
 30  DOUBLE M,Ms,Ks              !  INTEGERS
 40  DIM W(100)
 50  REDIM W(1:M)
 60  CALL Weights(M,W(*))        !  REAL WEIGHTS
 70  G2=2.*Gamma
 80  S=0.
 90  FOR Ms=1 TO M-1
100  Phi=0.
110  FOR Ks=Ms+1 TO M
120  Phi=Phi+W(Ks)*W(Ks-Ms)      !  CORRELATION OF WEIGHTS
130  NEXT Ks
140  S=S+Phi*FNGr(G2*Ms)
150  NEXT Ms
160  Phi=0.
170  FOR Ks=1 TO M
180  Phi=Phi+W(Ks)*W(Ks)
190  NEXT Ks
200  V4=Phi*FNGr(0.)+2.*S
210  PRINT M,Gamma,V4
220  END
230  !
240  SUB Weights(DOUBLE M,REAL W(*))
250  DOUBLE Ks                   !  INTEGER
260  T=2.*PI/M
270  FOR Ks=1 TO M
280  D=Ks-.5
290  W(Ks)=1.                    !  FLAT WEIGHTS
300  W(Ks)=.5-.5*COS(T*D)        !  HANN WEIGHTS
310  W(Ks)=.54-.46*COS(T*D)      !  HAMMING WEIGHTS
320  NEXT Ks
330  MAT W=W/SUM(W)              !  NORMALIZATION
340  SUBEND
350  !
360  DEF FNGr(W)
```

REFERENCES

[1] S. H. Ko and H. H. Schloemer, "Calculations of Turbulent Boundary Layer Pressure Fluctuations Transmitted into a Viscoelastic Layer," **Journal of the Acoustical Society of America**, volume 85, pages 1469 - 1477, 1989.

[2] S. H. Ko, "Hydrophone Array Performance in Response to Turbulent Boundary Layer Pressure Fluctuations," **Proceedings of Toyohashi International Conference on Ultrasonic Technology**, Toyohashi, Japan, April 20 - 22, 1987.

[3] I. S. Gradshteyn and I. M. Ryzhik, **Table of Integrals, Series, and Products**, Academic Press, Inc., New York, NY, 1980.

[4] A. H. Nuttall, **Alias-Free Wigner Distribution Function and Complex Ambiguity Function for Discrete-Time Samples**, NUSC Technical Report 8533, Naval Underwater Systems Center, New London, CT, 14 April 1989.

[5] S. H. Ko and A. H. Nuttall, "The Analytical Evaluation of Flush-Mounted Hydrophone Array Response to the Corcos Turbulent Wall Pressure Spectrum", to be submitted to the **Journal of the Acoustical Society of America**, June 1990.

NUSC Technical Report 8753
16 July 1990

Operating Characteristics for Weighted Energy Detector with Gaussian Signals

Albert H. Nuttall

ABSTRACT

The performance of several weighted energy detectors of Gaussian signals in noise are investigated, both by exact procedures and by five different approximation procedures. In particular, receiver operating characteristics, for false alarm probabilities ranging from 1E-10 to .1 and detection probabilities ranging from .01 to .999, are quantitatively compared. The standard Gaussian approximation is found to be severely deficient and generally optimistic for small false alarm probabilities, while two different fourth-order approximations have excellent capability over the entire range of probabilities considered.

A method of avoiding the calculation of the eigenvalues of a covariance matrix, and yet accurately predicting performance of a fading medium, is presented. It requires only sums of products of the covariance elements directly, the precise number depending on the order of the approximation.

TABLE OF CONTENTS

LIST OF ILLUSTRATIONS

LIST OF SYMBOLS

M	number of envelope-squared samples, (1)
e_m	output envelope of narrowband filter, (1)
z_m	squared-envelope output of narrowband filter, (1)
w_m	weight applied to squared-envelope z_m, (1)
x	decision variable of weighted summer, (1)
r	exponential weighting decay factor, (2), (27)
p_z	probability density function of random variable z, (3)
u	argument of probability density function, (3)
R	signal-to-noise power ratio per sample, (4)
a	signal-to-noise ratio parameter, (3), (4)
f_z	characteristic function of random variable z, (5)
ξ	argument of characteristic function, (5)
E	ensemble average, (5)
$\chi_z(k)$	k-th cumulant of random variable z, (6)
f_x	characteristic function of random variable x, (7)
$\chi_x(k)$	k-th cumulant of random variable x, (8)
W_k	sum of k-th powers of weights w_m, (8), (36)
μ_x	mean of random variable x, (9)
λ_m	m-th eigenvalue of covariance matrix, (10), (45)
σ^2	variance, (9), (10)
D	order of diversity, (10)
Q_x	exceedance distribution function of x, (14)
e_n	partial exponential, (15)
E_n	auxiliary function, (16)
T	threshold for comparison with decision variable x, (17)

P_F	false alarm probability, (17)
P_D	detection probability, (18)
B_m	coefficient in partial fraction expansion, (21), (22)
A_m	$1/(w_m a)$, (23)
f_e	approximate chi-squared characteristic function, (28)
M_e	effective number of envelope-squared samples, (28)
w_e	effective weight, (28)
Γ	gamma function, (29)
f_c	generalized chi-squared approximation, (33)
M_c	effective number of samples, (33)
t	auxiliary parameter = r^M, (40)
P	normalized covariance matrix of fading signal, (45),(46)
tr	trace of matrix, (46)
f_d	generalized chi-squared approximation, (48)
$B_m(R)$	coefficient in partial fraction expansion, (51), (52)
ρ	covariance coefficient for $P = [\rho_{mn}]$: $\rho_{mn} = \rho^{\|m-n\|}$.
f_t	fourth-order characteristic function fit, (55)
f_g	generalized non-central chi-squared fit, (58)
R_m	signal-to-noise ratio on m-th sample, (62), (63)
N	number of signal samples, (63)
$\tilde{f}$	noise-only characteristic function, (64)
B	block size, (74)
J	number of blocks occupied by signal, (75)
ROC	receiver operating characteristic
Φ	cumulative Gaussian distribution, (A-5)
$\tilde{\Phi}$	inverse Φ function, (A-9)
Λ	diagonal matrix of eigenvalues, (C-1)

OPERATING CHARACTERISTICS FOR WEIGHTED ENERGY DETECTOR WITH GAUSSIAN SIGNALS

INTRODUCTION

The operating characteristics of an equi-weighted energy detector for Gaussian signals in noise, in terms of false alarm and detection probabilities, can be characterized mathematically by a partial exponential expansion, and have previously been numerically evaluated for arbitrary numbers of samples and signal-to-noise ratios [1; (7) - (8) and figures 2 - 6]. However, when the weights employed in the energy detector are unequal, or if the signal and noise powers on each sample are unequal, these results do not apply and can be misleading, especially when the number of samples summed is not large. What is needed, in this case of arbitrary numbers of samples and unequal weights or powers, is an exact approach in terms of the characteristic function of the decision variable; this latter function is frequently available in closed form and can be employed in the fast efficient procedure presented in [2] and utilized in [3,4,5] for direct accurate evaluation of the exceedance distribution function.

At the same time, it would be very useful to have accurate approximations for the receiver operating characteristics, which apply over the full range of applicable false alarm and detection probabilities, yet are easily computed in terms of readily available functions, or circumvent some of the more difficult numerical procedures required in the exact approach. Here, we will consider four such approximations, namely Gaussian, chi-square, constant plus chi-square, and generalized noncentral chi-square, and demonstrate the range of applicability of each.

Thus, our goals here are two-fold

(1) determination of exact operating characteristics of arbitrary weighted energy detectors along with working programs, thereby allowing for investigation of other similar cases of interest to the user; and

(2) construction of accurate simple approximations to the operating characteristics, which can be extended to related difficult problems and/or circumvent complicated numerical procedures.

As a by-product, the inadequacy of some extant approximations will be delineated quantitatively; in particular, the generally optimistic results predicted by the Gaussian approximation will be shown to prevail even when the number of independent samples involved in the energy detector is very large.

CHARACTERISTIC FUNCTION

We presume that we have M channels (or samples) containing either noise-alone or signal-plus-noise, and that the random variables in each channel are statistically independent of each other. Specifically, for our interest, the output envelopes, $\{e_m\}$ for $1 \le m \le M$, of M disjoint narrowband filters are subjected to weighted square-law summation for purposes of threshold comparison and a statement about signal presence or absence on that particular observation of M outputs. The decision variable in this case is

$$x = \sum_{m=1}^{M} w_m \, e_m^2 = \sum_{m=1}^{M} w_m \, z_m \; , \tag{1}$$

where weights $\{w_m\}$ are all positive but otherwise arbitrary, and the M squared-envelope outputs $\{z_m\}$ are statistically independent and identically distributed. An example is afforded by a finite-time exponential summer where $w_m = A\, r^{m-1}$, $r \le 1$, $1 \le m \le M$.

Without loss of generality, the sum of the weights is set equal to unity,

$$\sum_{m=1}^{M} w_m = 1 \; ; \quad \text{that is,} \quad A = \frac{1-r}{1-r^M} \; . \tag{2}$$

Then, the mean of random variable x in (1) is equal to the mean of each random variable z_m, because all the $\{z_m\}$ are identically distributed. (If there are scaling differences in the variables $\{z_m\}$, these factors can be absorbed in modified scalings $\{w_m\}$, without loss of generality.) Under these assumptions, it should be observed that the performance of the weighted energy detector in (1) is independent of the ordering of the weights; thus, the weights can be arranged in any order without affecting the detection capability. Also, the absolute level of the $\{w_m\}$ cannot affect the operating characteristics of detector (1).

STATISTICS OF z_m

For Gaussian signals and noises present at the inputs to the M narrowband filters in (1), the probability density function of each filter output envelope-squared random variable z_m is

$$p_z(u) = \frac{1}{a} \exp\left(\frac{-u}{a}\right) \quad \text{for } u > 0 \; , \tag{3}$$

where parameter

$$a = \left\{ \begin{array}{ll} 1 & \text{for noise-alone} \\ 1 + R & \text{for signal-plus-noise} \end{array} \right\} . \tag{4}$$

Here, we have normalized according to the noise power; that is, the mean of random variable z_m is set equal to 1 for noise-alone. This presumption is equivalent to having knowledge of the average noise level in the absence of signal and can be accomplished in practice by monitoring the filter outputs over a sufficiently long past interval of time. Also, R is the signal-to-noise power ratio per sample at the output of each filter.

The characteristic function of each random variable z_m in (1) is given by expectation (ensemble average)

$$f_z(\xi) = E\{\exp(i\xi z)\} = \int du \exp(i\xi u)\ p_z(u) = \frac{1}{1 - i\xi a}\ , \qquad (5)$$

where we used (3). The cumulants $\{\chi_z(k)\}$ of z_m are immediately available from (5) as

$$\frac{1}{(k-1)!}\ \chi_z(k) = a^k \quad \text{for } k \geq 1\ . \qquad (6)$$

Actually, these are scaled cumulants, by the factor $1/(k-1)!$; they are more convenient and will be employed henceforth.

CHARACTERISTIC FUNCTION OF OUTPUT x

The characteristic function of summation random variable x in (1) is given by expectation

$$f_x(\xi) = E\{\exp(i\xi x)\} = \prod_{m=1}^{M} f_z(w_m\xi) = \left[\prod_{m=1}^{M}\left(1 - i\xi w_m a\right)\right]^{-1}\ , \qquad (7)$$

where we used the independence of the $\{z_m\}$ and relation (5). The (scaled) cumulants of x are available from (7) according to

$$\frac{1}{(k-1)!}\ \chi_x(k) = a^k \sum_{m=1}^{M} w_m^k \equiv a^k\ W_k \quad \text{for } k \geq 1\ . \qquad (8)$$

In particular, the mean and variance of x are, upon use of (2),

$$\mu_x = \chi_x(1) = a\ W_1 = a\ , \qquad \sigma_x^2 = \chi_x(2) = a^2\ W_2\ . \qquad (9)$$

The desired closed form for the characteristic function of x is given by (7), where the signal-to-noise ratio parameter a is given by (4). Result (7) applies for arbitrary M, weights $\{w_m\}$, and per-sample signal-to-noise ratio R.

SOME RELATED RESULTS

Characteristic functions of the form of (7) occur in numerous problems. For example, the stability of a spectral estimation technique employing overlapped FFT processing of windowed data encountered this form [6; (35) and (15)], where weights $\{w_m\}$ were proportional to the eigenvalues $\{\lambda_m\}$ of a normalized covariance function. Another example is furnished by diversity combination in a channel subject to partially-correlated signal fading; see [7; (D-14)], [8; (24)], and [9]. In particular, the exact characteristic function in [7] and [8] took the form

$$\left[\prod_{m=1}^{M}\left\{1 - i\xi\left(\sigma^2 + 2\lambda_m\right)\right\}\right]^{-D}, \qquad (10)$$

where $\{\lambda_m\}$ are the eigenvalues of a covariance matrix. Parameter D was the order of diversity in [7], but was equal to 1 in [8].

GAUSSIAN APPROXIMATION TO EXCEEDANCE DISTRIBUTION

For the general characteristic function given by (7) and (4), a Gaussian approximation to the probability density and exceedance distribution functions is given in appendix A. It is derived for arbitrary M, weights $\{w_m\}$, and signal-to-noise ratio R. However, its applicability to numerical evaluation of receiver operating characteristics, in the form of detection versus false alarm probabilities, will be shown to be rather limited in the next section.

EXCEEDANCE DISTRIBUTION FOR ALL WEIGHTS EQUAL

In this section, the weights $\{w_m\}$ in (1) and (2) are equal:

$$w_m = \frac{1}{M} \quad \text{for } 1 \le m \le M \ . \tag{11}$$

The characteristic function in (7) then becomes

$$f_x(\xi) = (1 - i\xi a/M)^{-M} \ . \tag{12}$$

This corresponds to a multiple of a chi-squared random variate with 2M degrees of freedom. The corresponding probability density function is

$$p_x(u) = \frac{u^{M-1} \exp(-uM/a)}{(M-1)! \ (a/M)^M} \quad \text{for } u > 0 \ , \tag{13}$$

while the exceedance distribution function is, for $u > 0$,

$$Q_x(u) = \int_u^\infty dt \ p_x(t) = \exp(-uM/a) \ e_{M-1}(uM/a) \equiv E_{M-1}(uM/a) \ . \tag{14}$$

Here, $e_n(x)$ is the partial exponential function [10; (6.5.11)],

$$e_n(x) = \sum_{k=0}^{n} \frac{x^k}{k!} \ , \tag{15}$$

and we have defined auxiliary function

$$E_n(x) = \exp(-x) \ e_n(x) \quad \text{for } x \ge 0 \ . \tag{16}$$

If threshold value T is used for comparison with output x of the energy detector (1), then the false alarm probability P_F is

$$P_F = Q_x(T;\ a=1) = E_{M-1}(TM) \ . \tag{17}$$

Similarly, the detection probability P_D is, from (14) and (4),

$$P_D = Q_x(T;\ a=1+R) = E_{M-1}\left(\frac{TM}{1+R}\right) \ . \tag{18}$$

When T is eliminated between (17) and (18), the operating characteristics (P_D versus P_F) can be plotted, with signal-to-noise ratio R as a parameter. Separate plots are required for different values of M, the number of envelope-squared samples.

GRAPHICAL RESULTS

The receiver operating characteristics (ROC) for

$$M = 1,\ 2,\ 4,\ 8,\ 16,\ 32,\ 64,\ 128,\ 256,\ 512,\ 1024 \tag{19}$$

are plotted in figures 1 through 1, on normal probability paper, for false alarm probabilities ranging from 1E-10 to .1 and for detection probabilities ranging from .01 to .999. Signal-to-noise ratios (in decibels) have been chosen, typically, to cover P_F,P_D possibilities from low-quality pair .01,.5 to high-quality pairs in the neighborhood of 1E-10,.99.

Superposed in figure 3 (in dashed lines) is the Gaussian approximation, for M = 4, to the exact exceedance distribution function Q_x in (14); see appendix A. Three selected values of signal-to-noise ratio R are indicated, namely R = 4, 8, and 12 dB. They are identified by a black dot where they cross the exact operating characteristic for the same signal-to-noise ratio. It is seen that the Gaussian approximation is virtually useless at this low value of M, the number of samples.

This superposition, of three representative curves afforded by the Gaussian approximation, is continued up through $M = 1024$ in figure 11. Again, agreement with the exact results is generally quite poor. Even at $M = 1024$, the required signal-to-noise ratio from the Gaussian approximation for $P_F = 1E-10$, $P_D = .3$, for example, is in error by .3 dB.

Furthermore, it should be observed that the Gaussian approximation is always optimistic in the useful range of the operating characteristics; this bias is misleading in quantitative performance predictions applied to practical detection systems. Additionally, the case in this section, namely equal weights, is the <u>most</u> favorable situation for the Gaussian approximation to apply in; any other distribution of weight values makes the effective number of weights (M_e in (A-6) and sequel) less than M, thereby deviating even further from an accurate application of the central limit theorem. The message to be conveyed here is that the performance capability of energy detectors for Gaussian signals and noises should be based on something other than the Gaussian approximation.

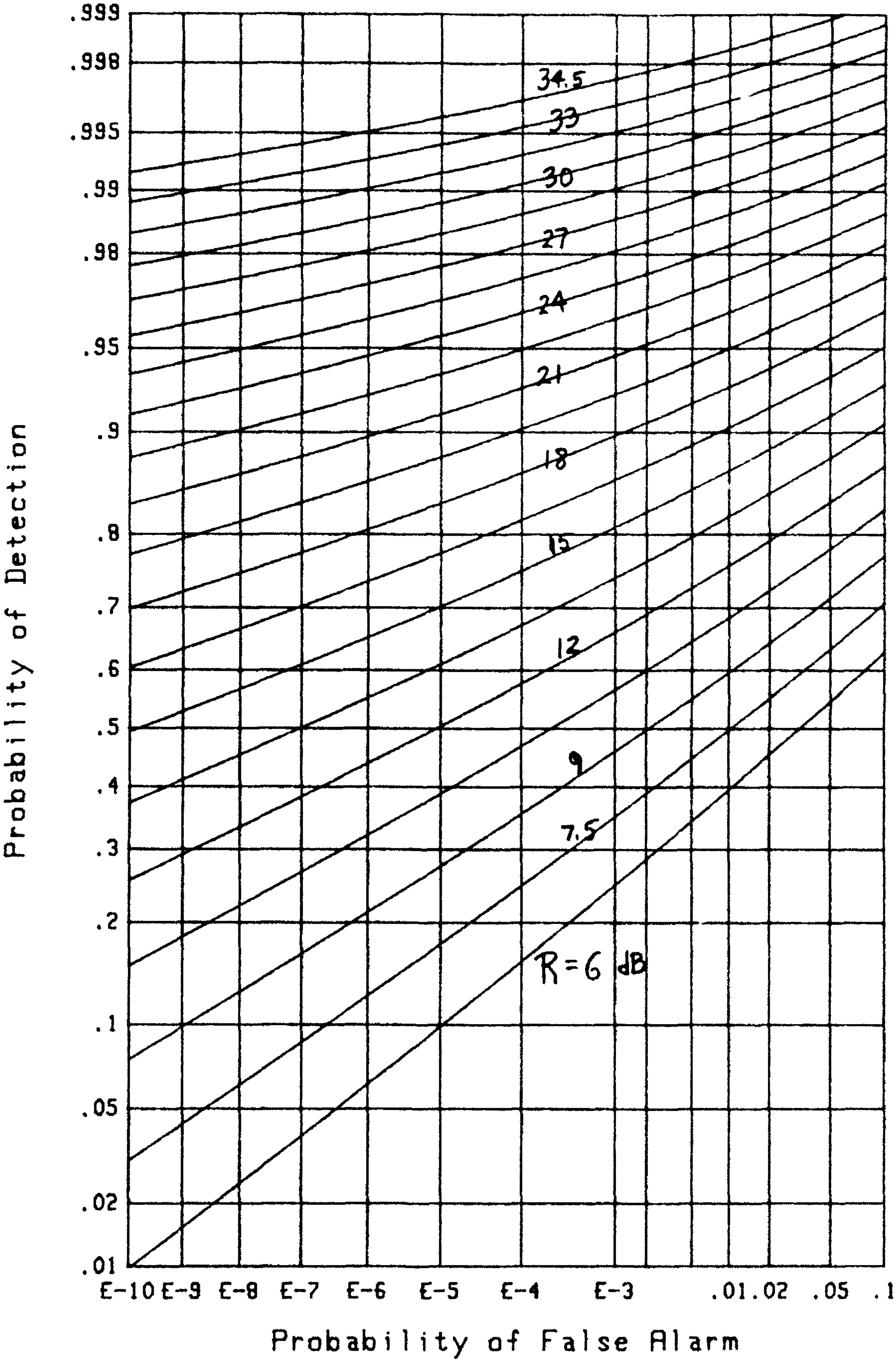

Figure 1. ROC for M=1, Equal Weights

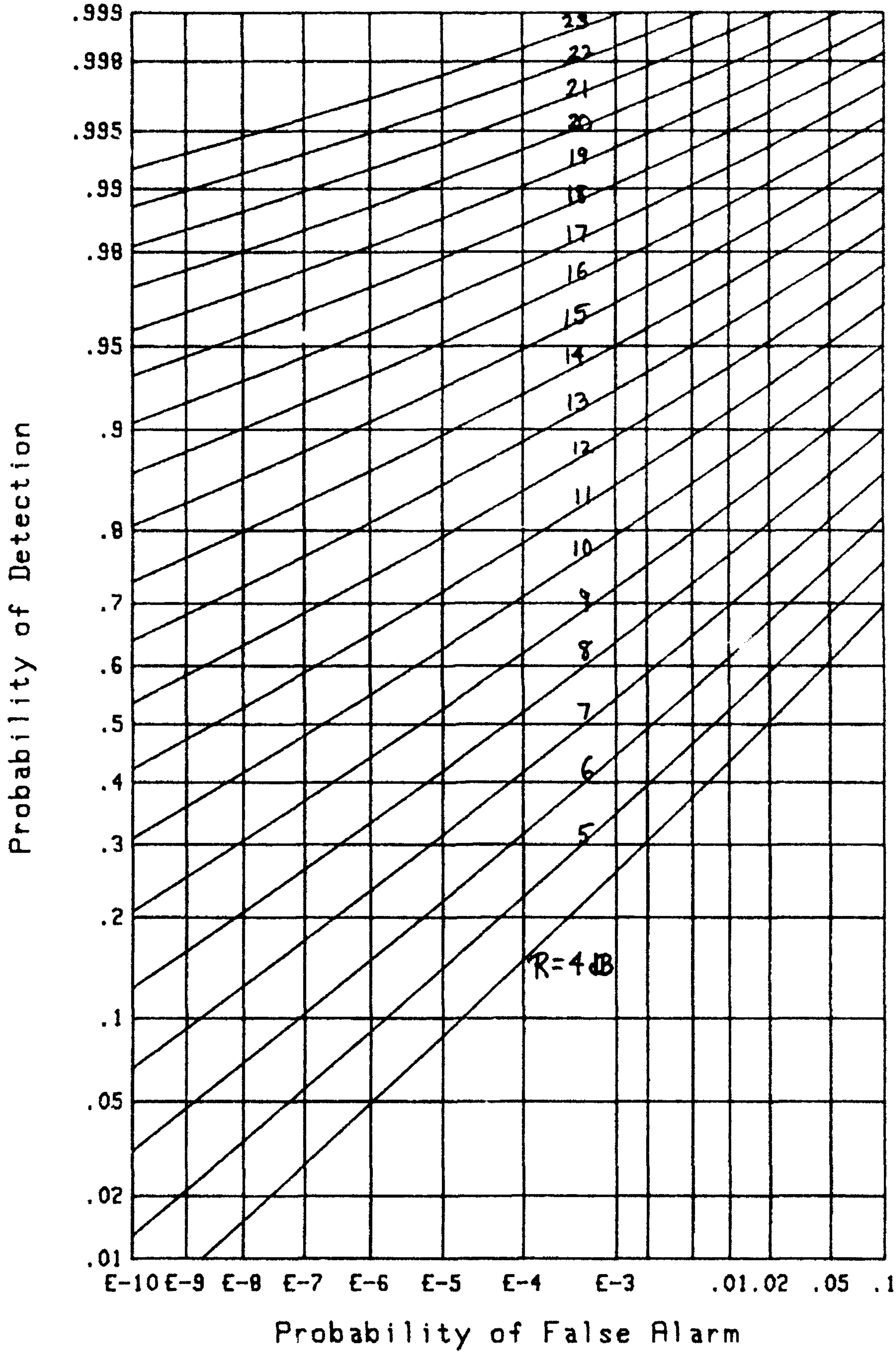

Figure 2. ROC for M=2, Equal Weights

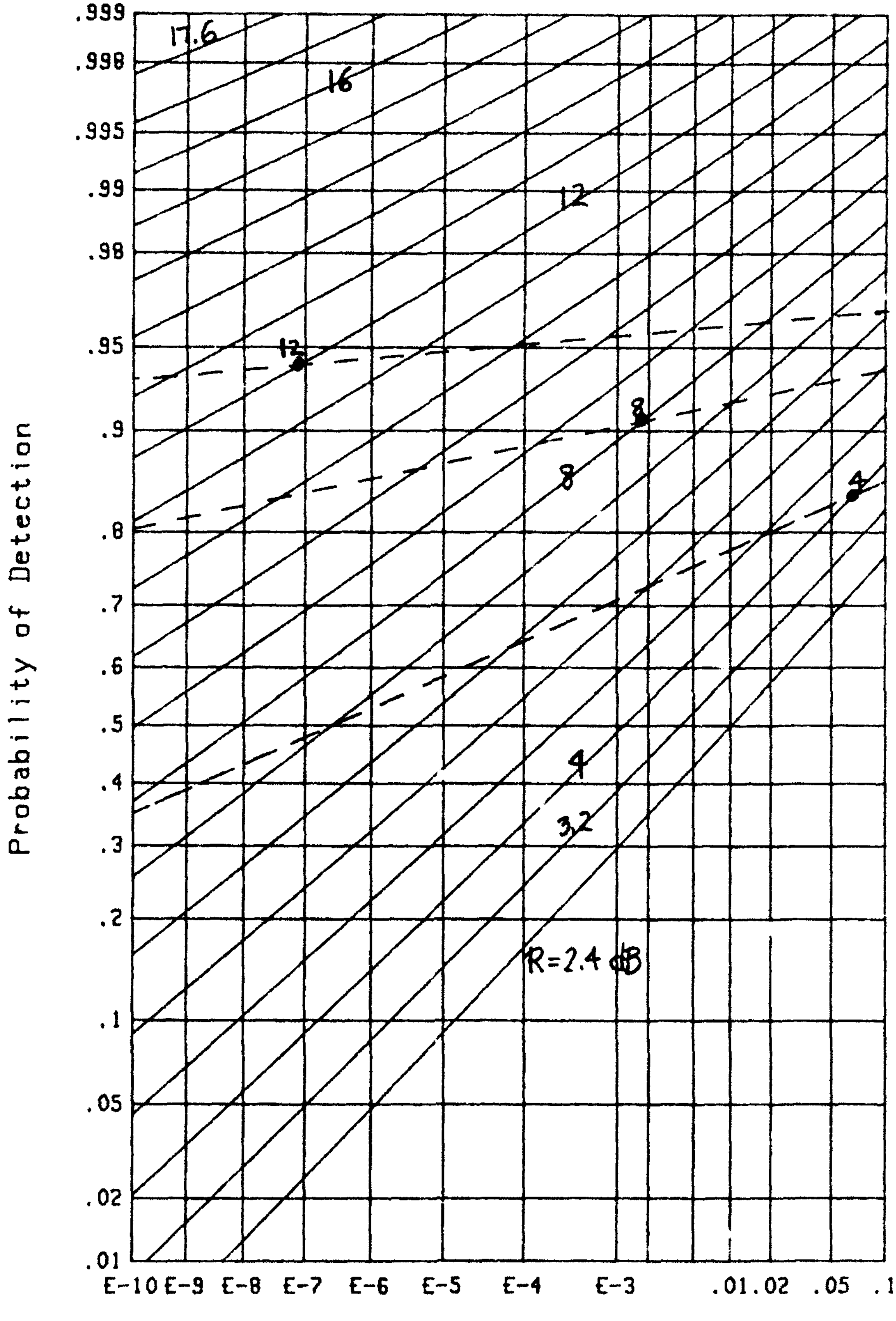

Figure 3. ROC for M=4, Equal Weights

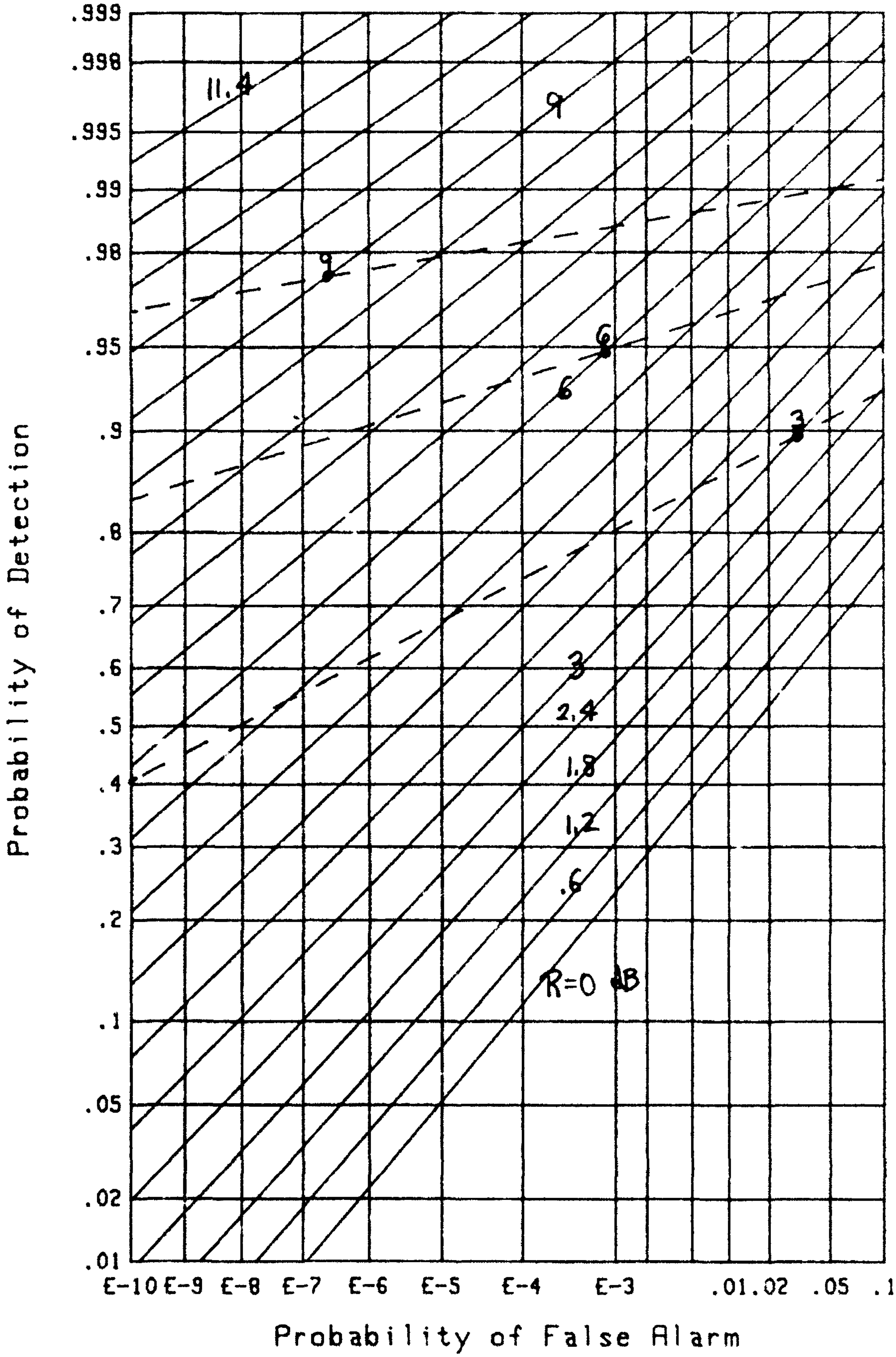

Figure 4. ROC for M=8, Equal Weights

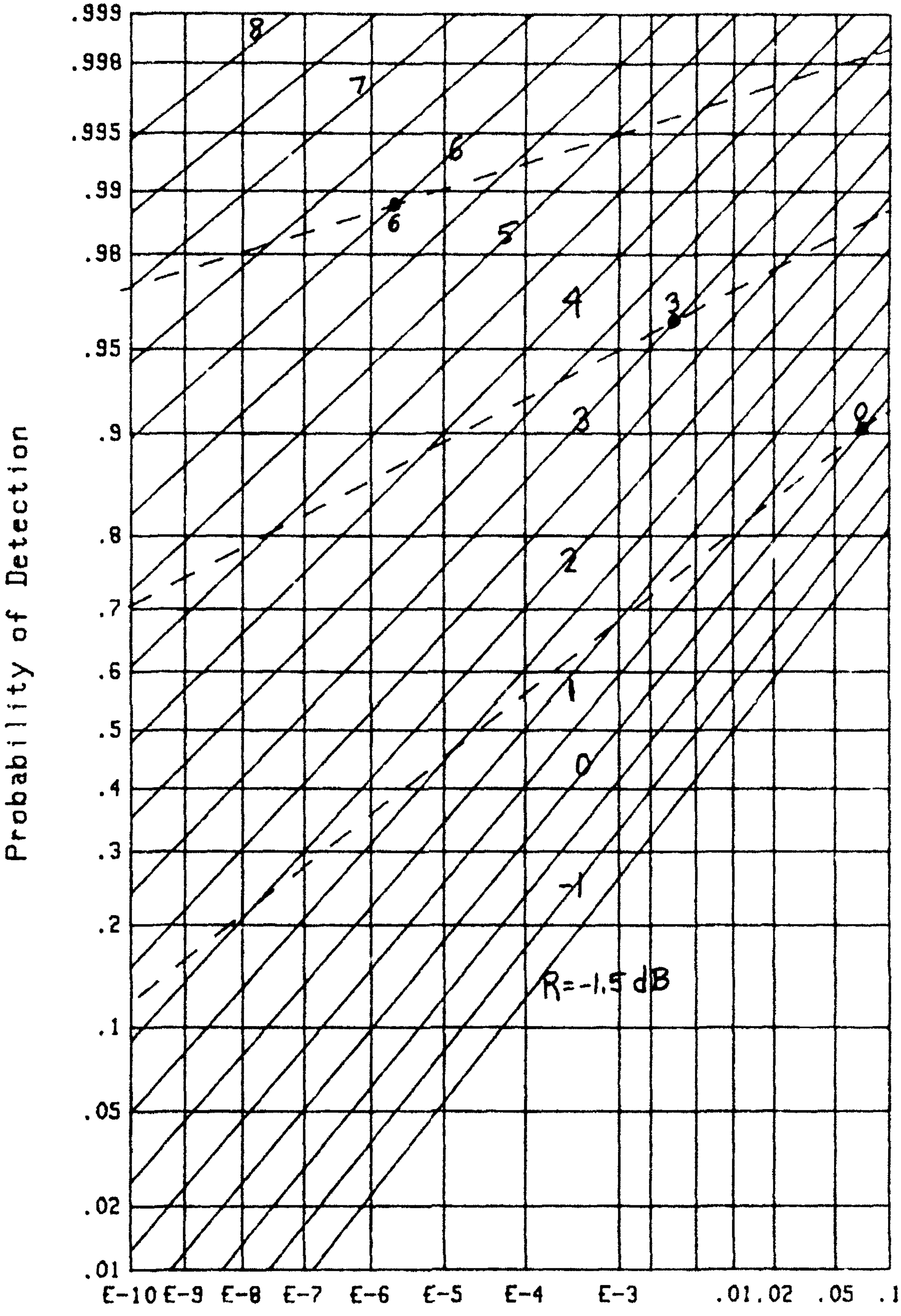

Figure 5. ROC for M=16, Equal Weights

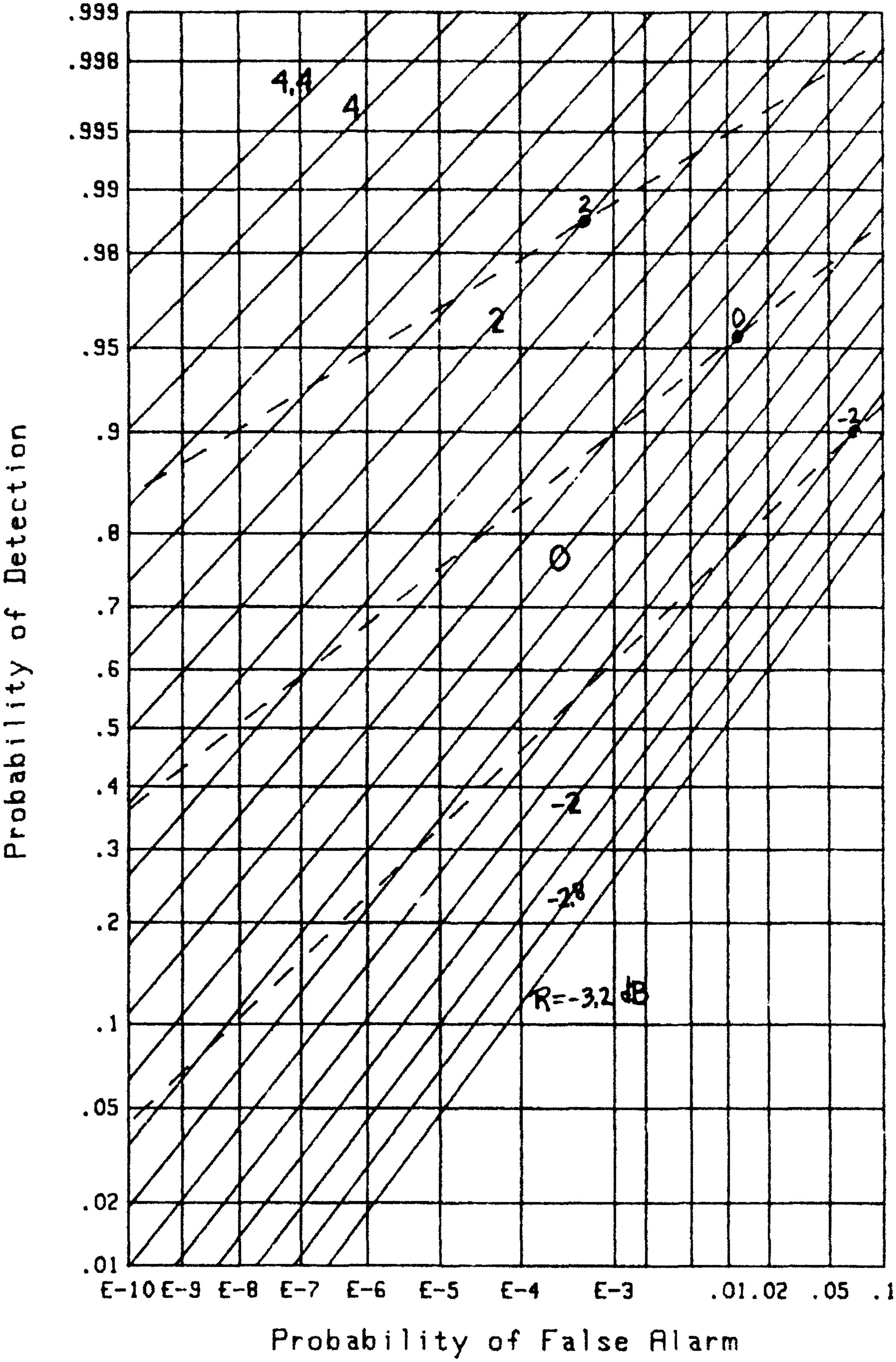

Figure 6. ROC for M=32, Equal Weights

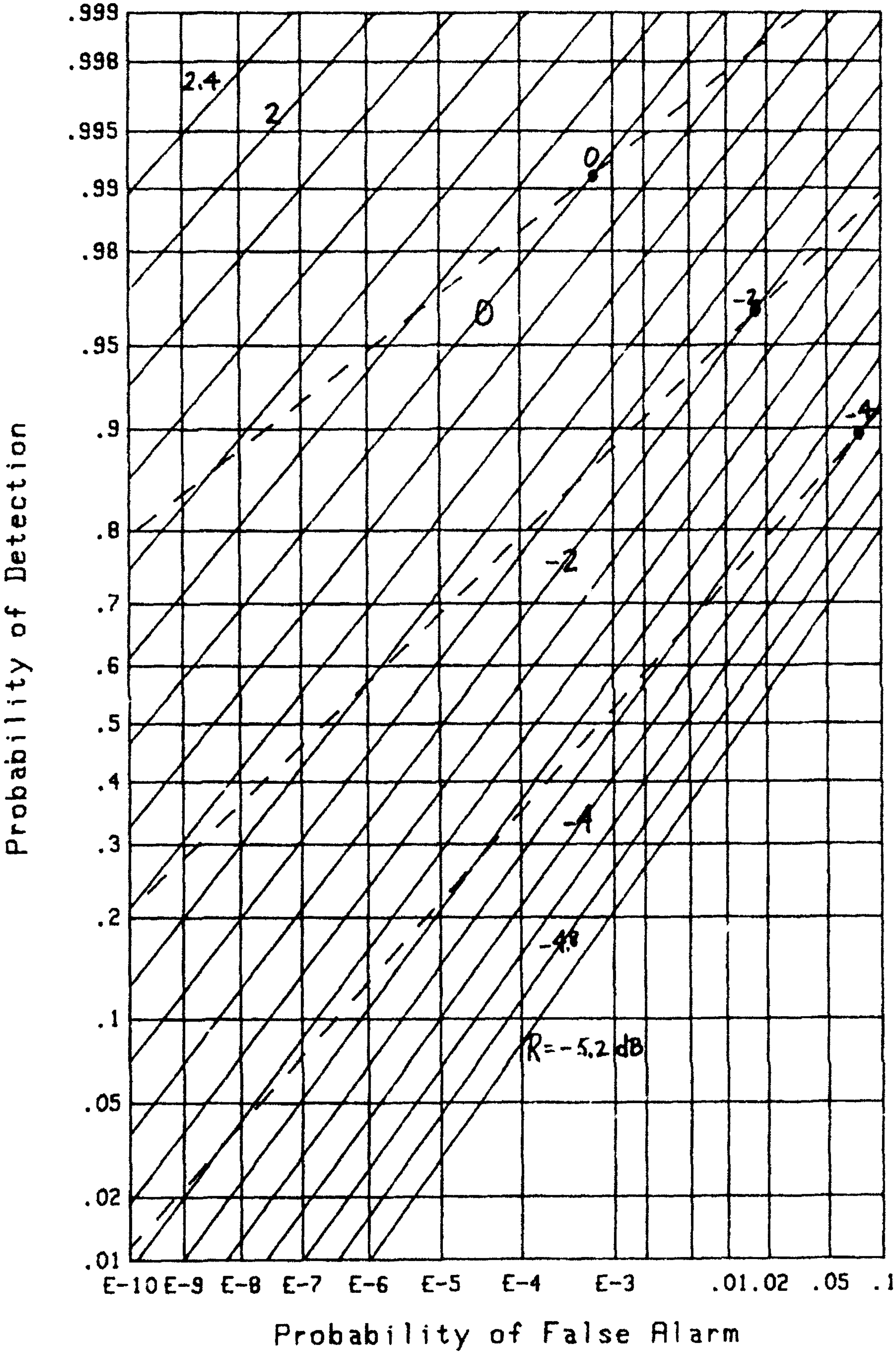

Figure 7. ROC for M=64, Equal Weights

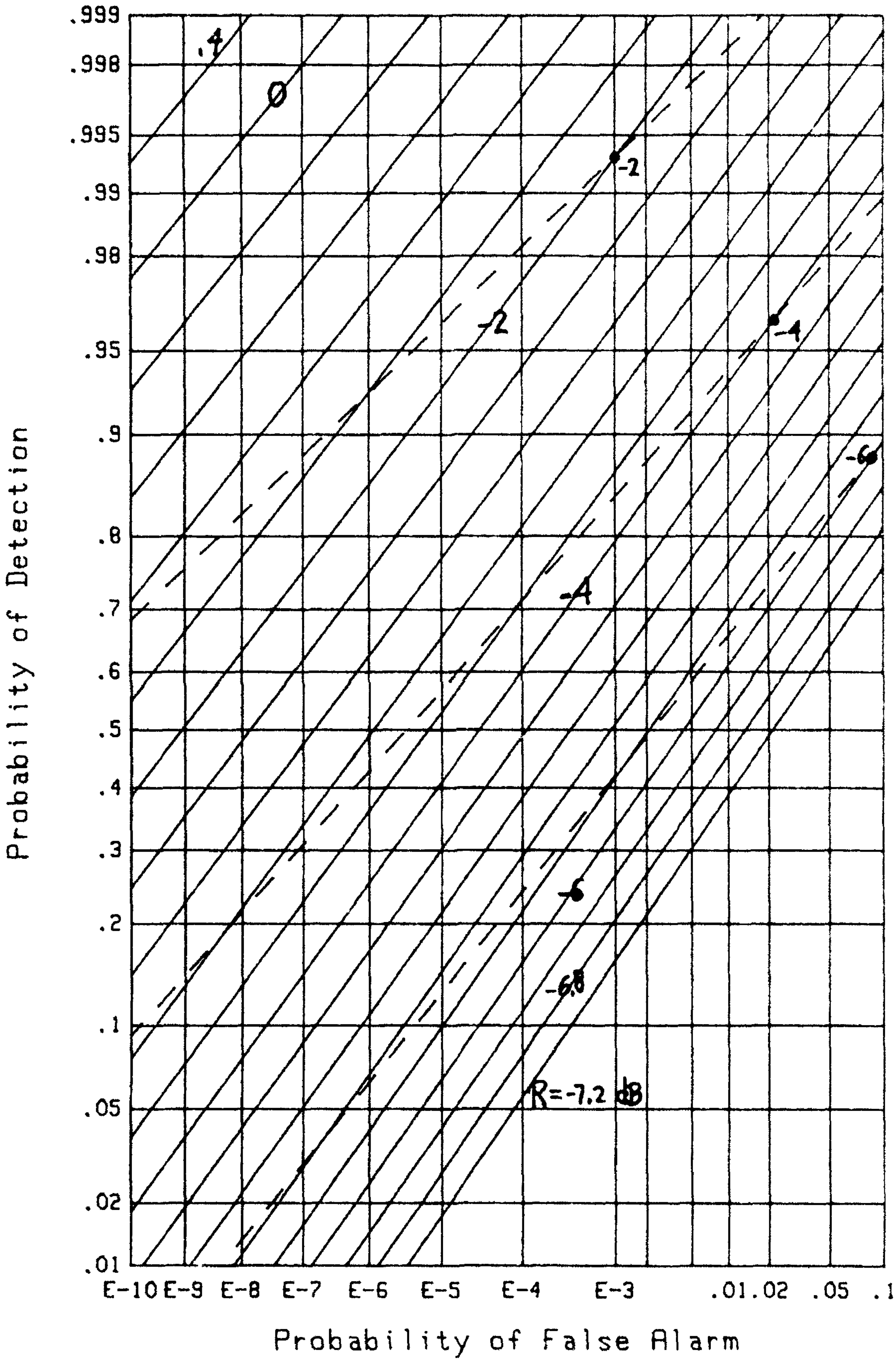

Figure 8. ROC for M=128, Equal Weights

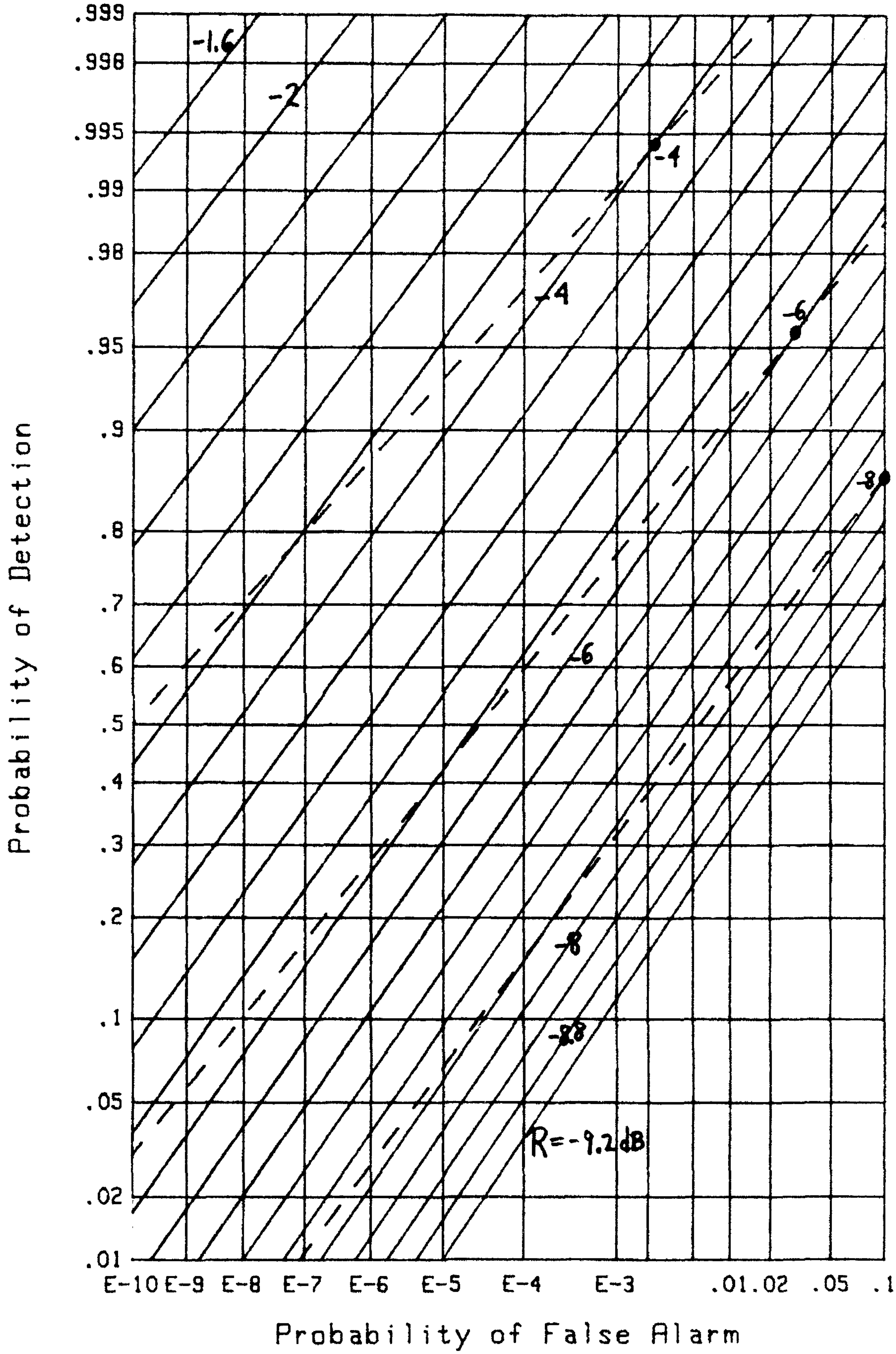

Figure 9. ROC for M=256, Equal Weights

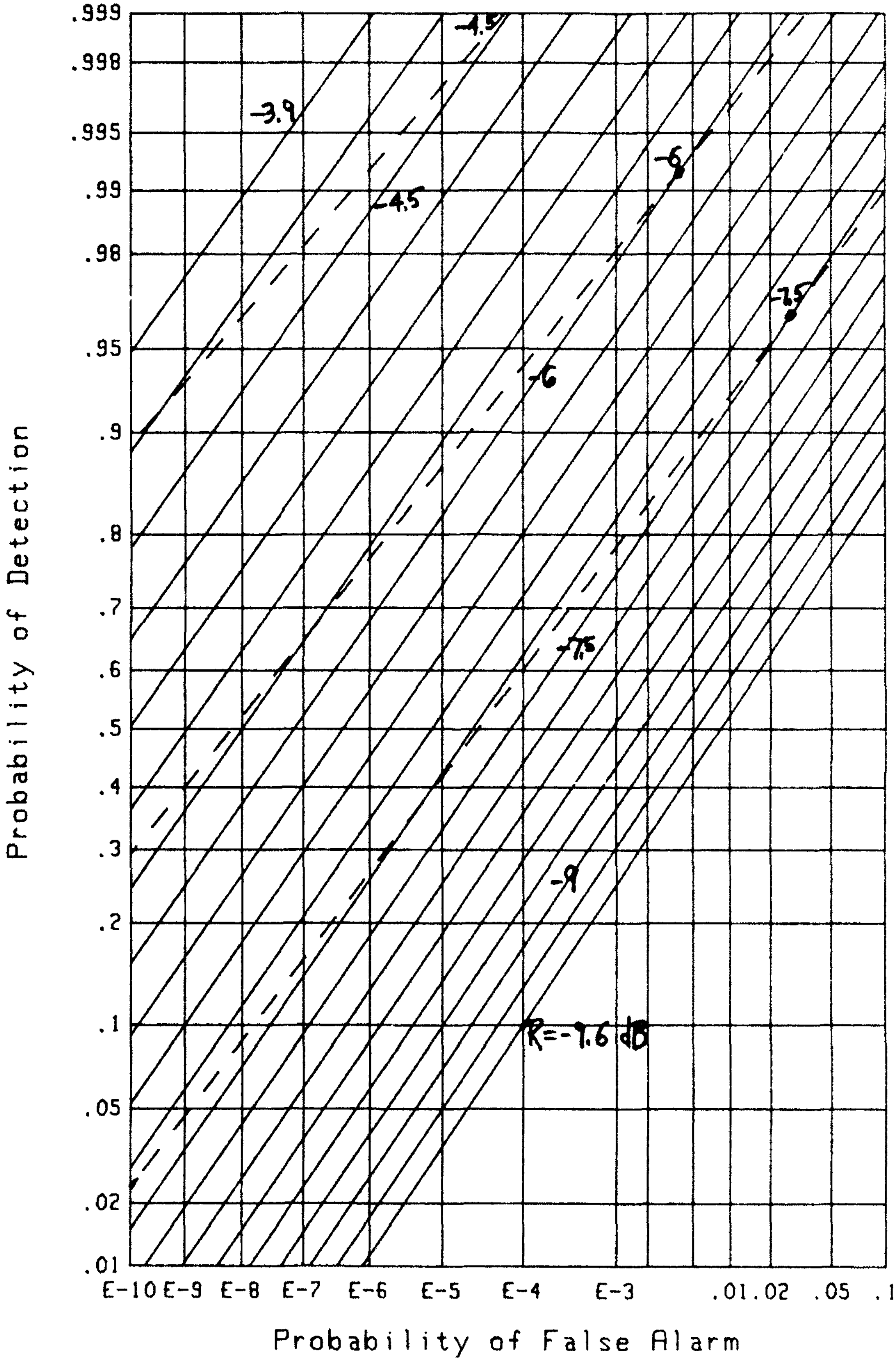

Figure 10. ROC for M=512, Equal Weights

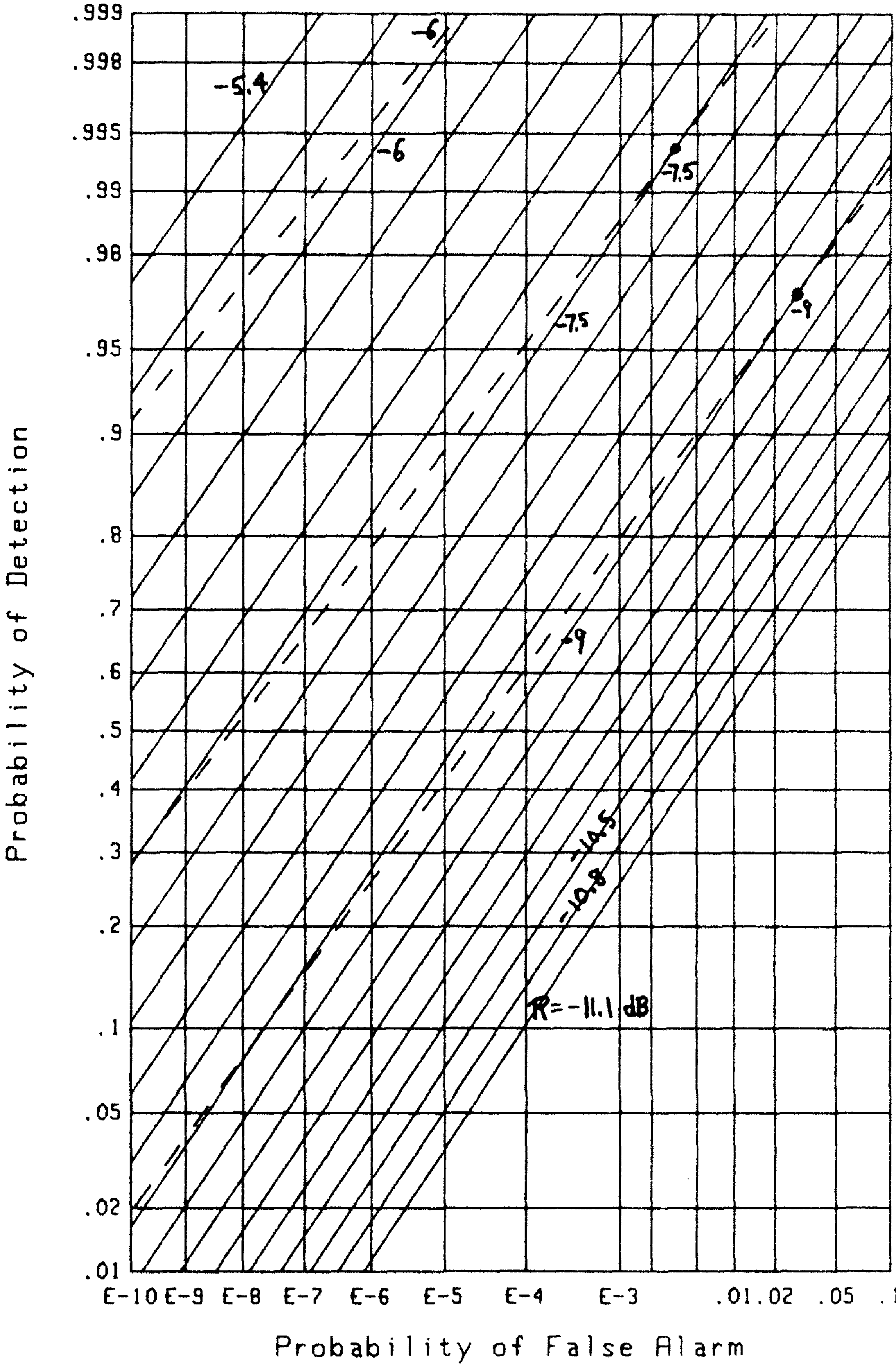

Figure 11. ROC for M=1024, Equal Weights

EXCEEDANCE DISTRIBUTION FOR ALL WEIGHTS DIFFERENT

In this section, we confine attention to the case where all the weights $\{w_m\}$ are different from each other; that is,

$$w_m \neq w_k \quad \text{if} \quad m \neq k \; ; \qquad w_m > 0 \; . \tag{20}$$

Then, we expand the characteristic function of x in (7) in a partial fraction expansion according to

$$f_x(\xi) = \left[\prod_{m=1}^{M}\left(1 - i\xi w_m a\right)\right]^{-1} = \sum_{m=1}^{M} \frac{B_m}{1 - i\xi w_m a} \; , \tag{21}$$

where coefficients

$$B_m = \frac{w_m^{M-1}}{\prod\limits_{\substack{k=1 \\ k\neq m}}^{M}\left(w_m - w_k\right)} \qquad \text{for } 1 \leq m \leq M \; , \tag{22}$$

depend only on weights $\{w_m\}$ and not on signal-to-noise ratio R.

The probability density function of x is then immediately available from (21) as

$$p_x(u) = \sum_{m=1}^{M} A_m \, B_m \exp(-A_m u) \qquad \text{for } u > 0 \; , \tag{23}$$

where $A_m = 1/(w_m a)$. The corresponding exceedance distribution is

$$Q_x(u) = \int_u^{\infty} dt \; p_x(t) = \sum_{m=1}^{M} B_m \exp(-A_m u) \quad \text{for } u > 0 \; . \tag{24}$$

If threshold T is used as the basis of comparison for output x of the weighted energy detector in (1), the false alarm and detection probabilities follow from (24), respectively, as

$$P_F = Q_x(T;\ a = 1)\ , \quad P_D = Q_x(T;\ a = 1 + R)\ . \tag{25}$$

As an example, if $M = 1$, then $w_1 = 1$, $A_1 = 1/a$, $B_1 = 1$, and (24) yields $Q_x(u) = \exp(-u/a)$ for $u > 0$. Then, (25) gives

$$P_F = \exp(-T)\ , \quad P_D = \exp\left(\frac{-T}{1+R}\right) = P_F^{\frac{1}{1+R}} = \exp\left(\frac{\ln P_F}{1+R}\right)\ . \tag{26}$$

For this special case of $M = 1$, threshold T can be eliminated and P_D expressed explicitly in terms of P_F and R.

GRAPHICAL RESULTS

The particular case of unequal weights that we shall concentrate on here is a set of exponential weights

$$w_m = A\ r^{m-1} \quad \text{for} \quad 1 \le m \le M\ , \quad r \le 1\ , \tag{27}$$

where scale factor A is selected for normalization of the weights, according to (2). Of course, the absolute level of the weights does not affect the operating characteristics.

In figure 12, the ROC for $M = 4$ and $r = .99$ is plotted, as determined from (25) and (24). Since r is close to 1 for this example, the weights (27) are all nearly equal, causing some of the coefficients $\{B_m\}$ in (22) to be rather large, in the range of $\pm.5E6$. This leads to round-off error in sum (24) for the exceedance distribution function and the possibility of useless numerical results; however, because $M = 4$ is a small number, the round-off error does not yet show up in figure 12.

When M is increased to 8 in figure 13 and r is kept at .99, coefficients $\{B_m\}$ in (22) reach values in the range of $\pm$.7E12, and round-off error begins to show up as wiggly lines in the higher detection probability values near .999. We are using a computer with 64 bits per word, which yields approximately 15 decimals of accuracy for the mantissa. Although coefficients $\{B_m\}$ can be calculated very accurately from (22), they alternate in sign and can be very large. Then Q_x in (24) requires differencing of large numbers, with an attendant possibly damaging loss of accuracy, especially tor small P_F.

When M is increased by one, to 9 in figure 14, and r is maintained at .99, round-off error is now significant at the upper edge of the ROC, although useful characteristics are still available for lower values of P_D. The reason for this problem is that all the weights are close to each other; in fact, the M-th weight is $r^{M-1} = .923$ times as large as the first weight. The largest coefficient values for $\{B_m\}$ are in the range of $\pm$.16E14.

When the weights are spread out over a wider range, larger values of M can be tolerated in sum (24), without encountering significant round-off error. For example, a set of $M = 16$ uniformly distributed random weights, over the (0,1) interval, were utilized in figure 15 without any problems. But when M was increased to 20 in figure 16, again for uniformly distributed weights, the upper edge of the ROC, for $P_D > .99$, was useless. Nevertheless, a significant portion of the ROC for lower P_D values is still acceptable.

The lesson to be drawn from these results is that the partial fraction expansion, leading to the exceedance distribution function in (24), has utility for spread out weights $\{w_m\}$ and moderately low values of M, the number of envelope-squared samples. However, it will not be a viable tool for large values of M, nor for general weight structures which may have some close or equal values. The more general approach presented in [2], in terms of an arbitrary characteristic function, has no such limitations, on the other hand, although the numerical calculations required are more extensive.

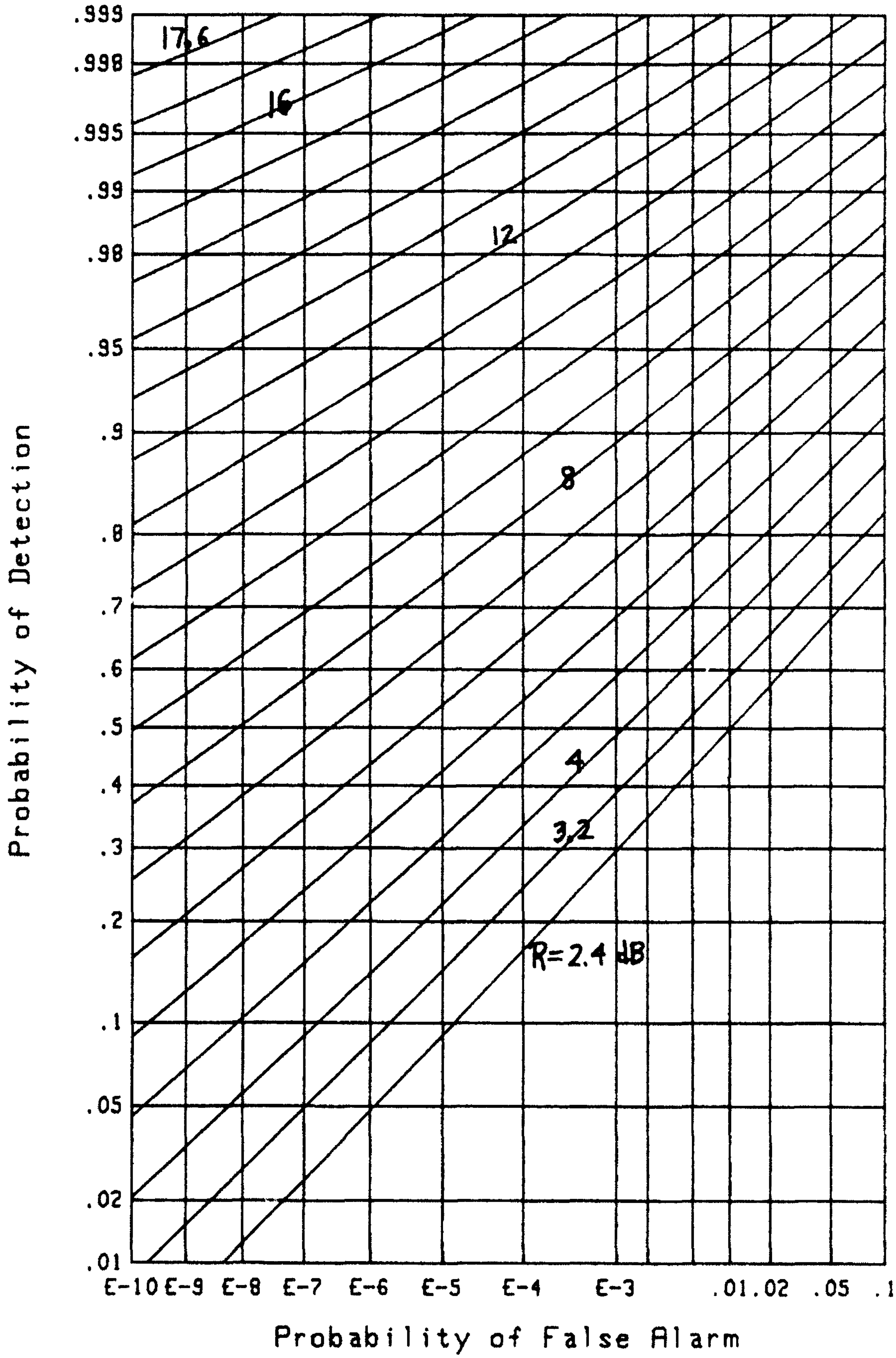

Figure 12. ROC for M=4, r=.99

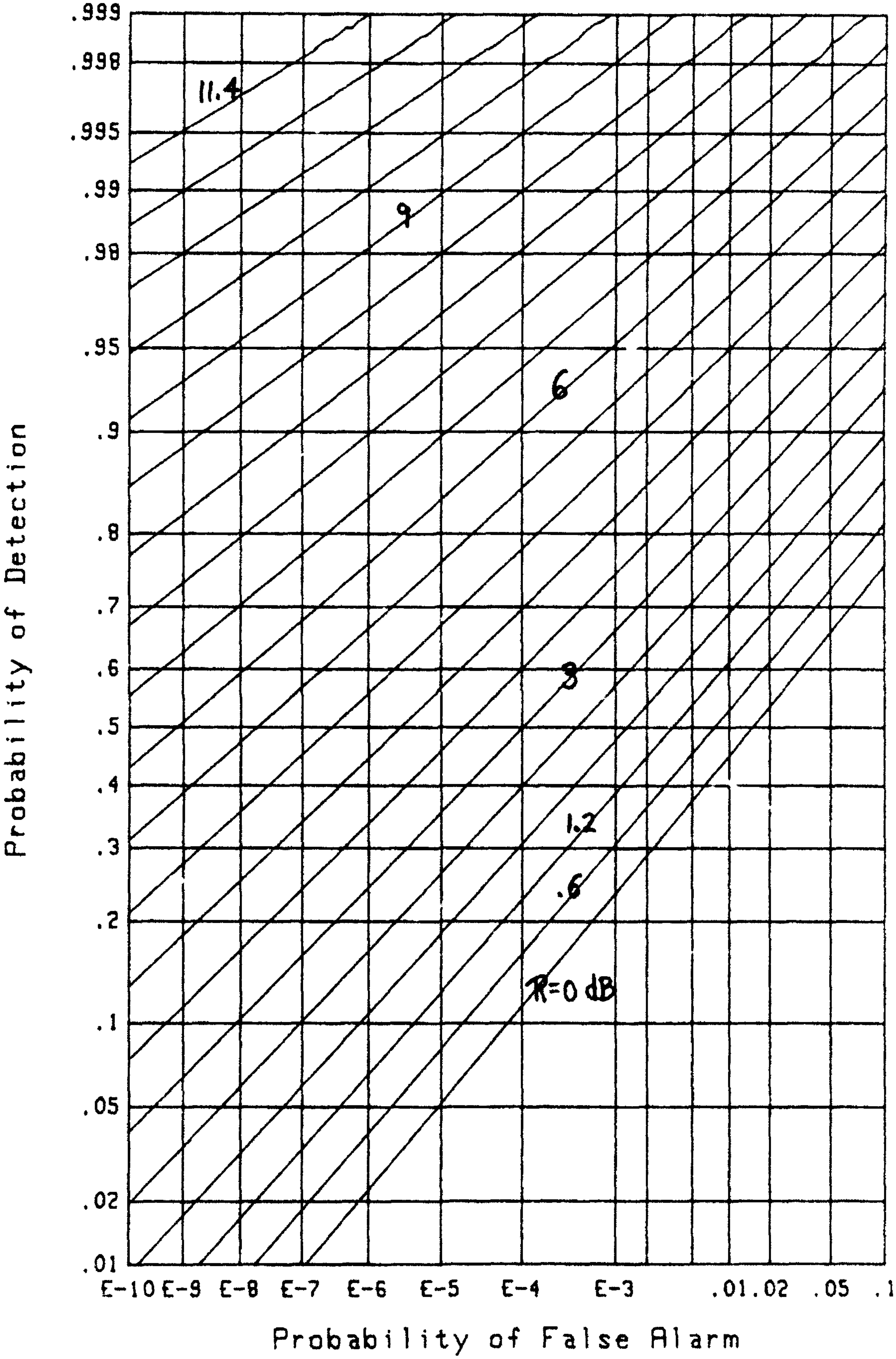

Figure 13. ROC for M=8, r=.99

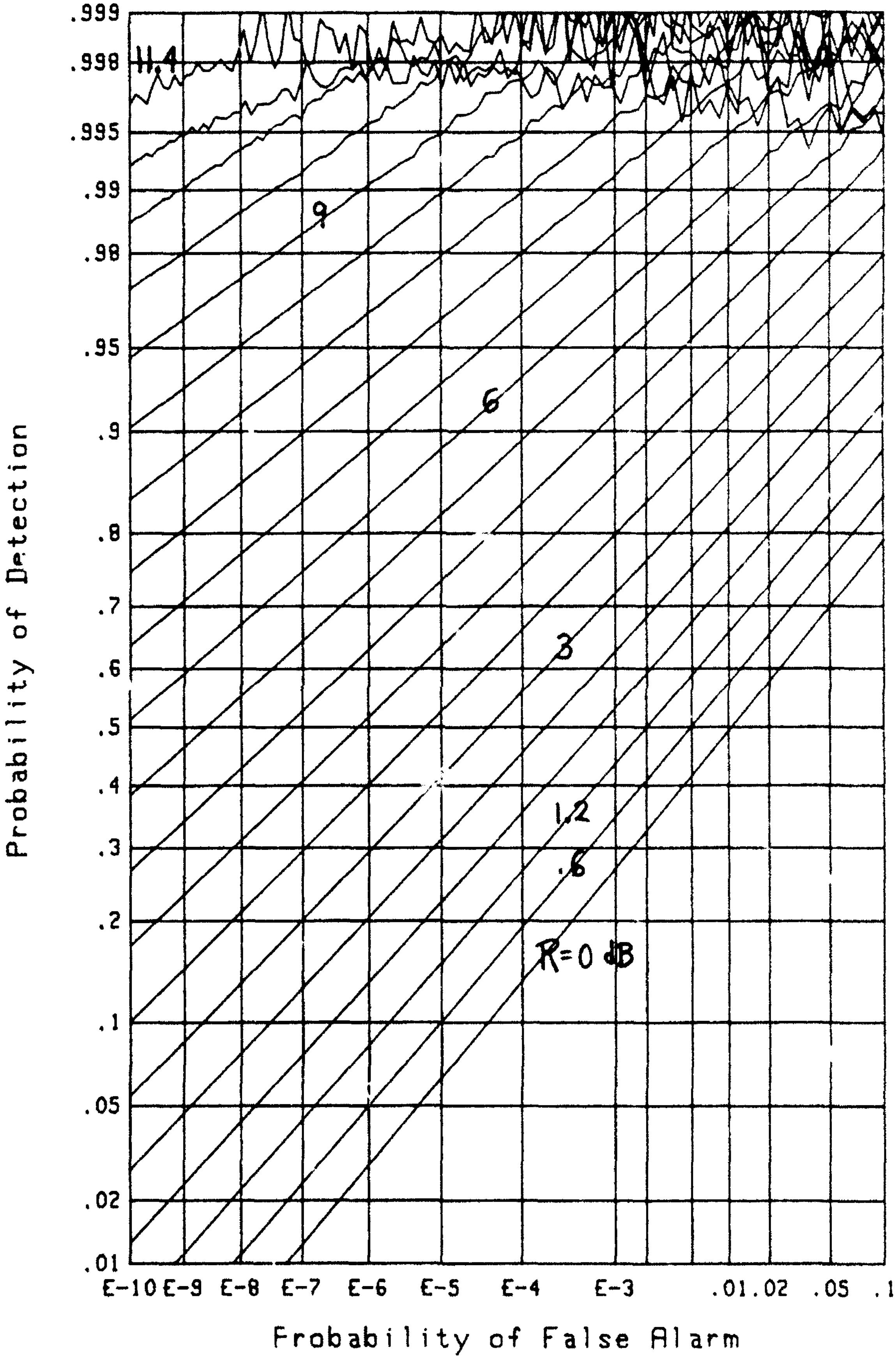

Figure 14. ROC for M=9, r=.99

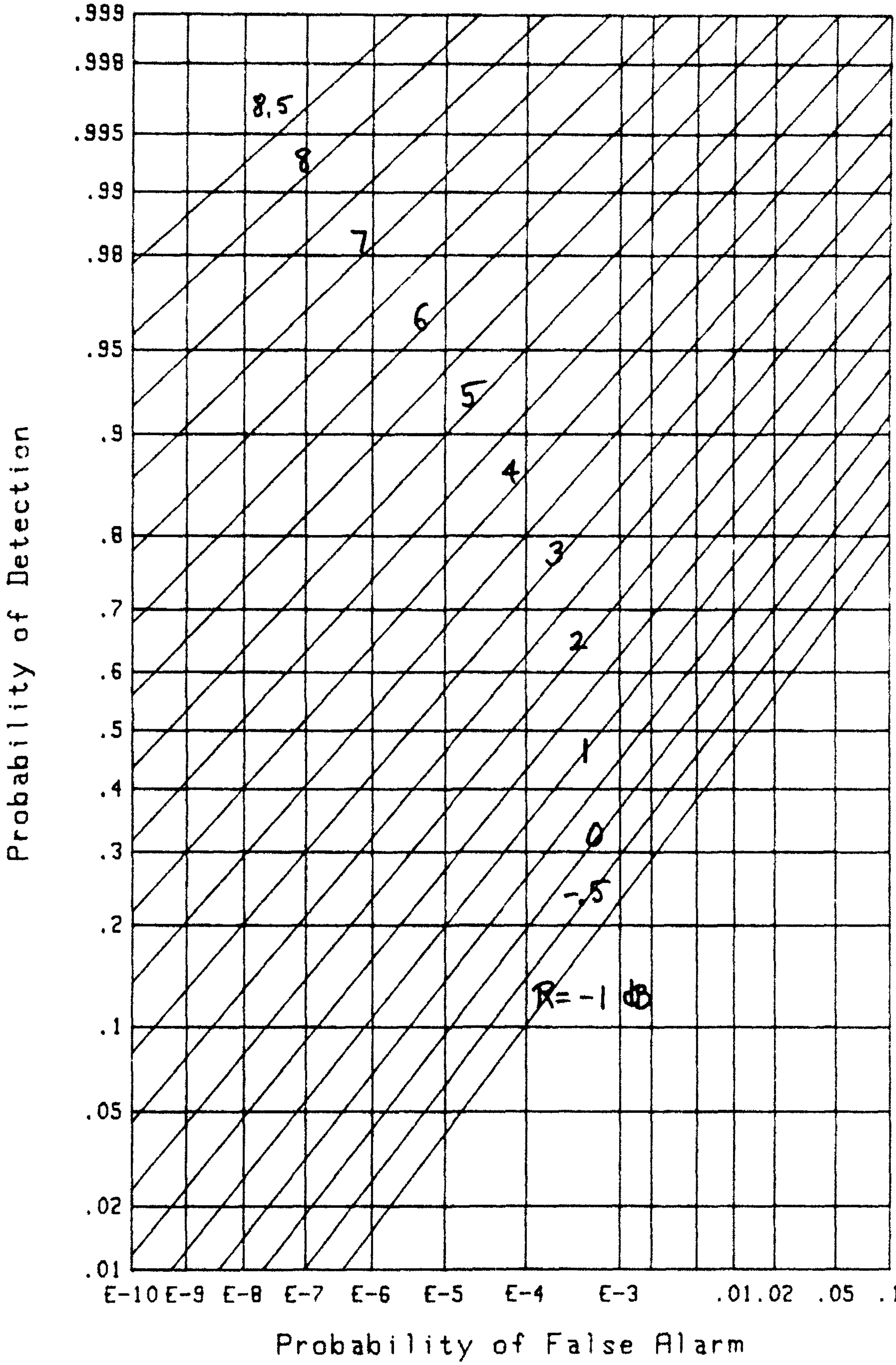

Figure 15. ROC for M=16, Random Weights

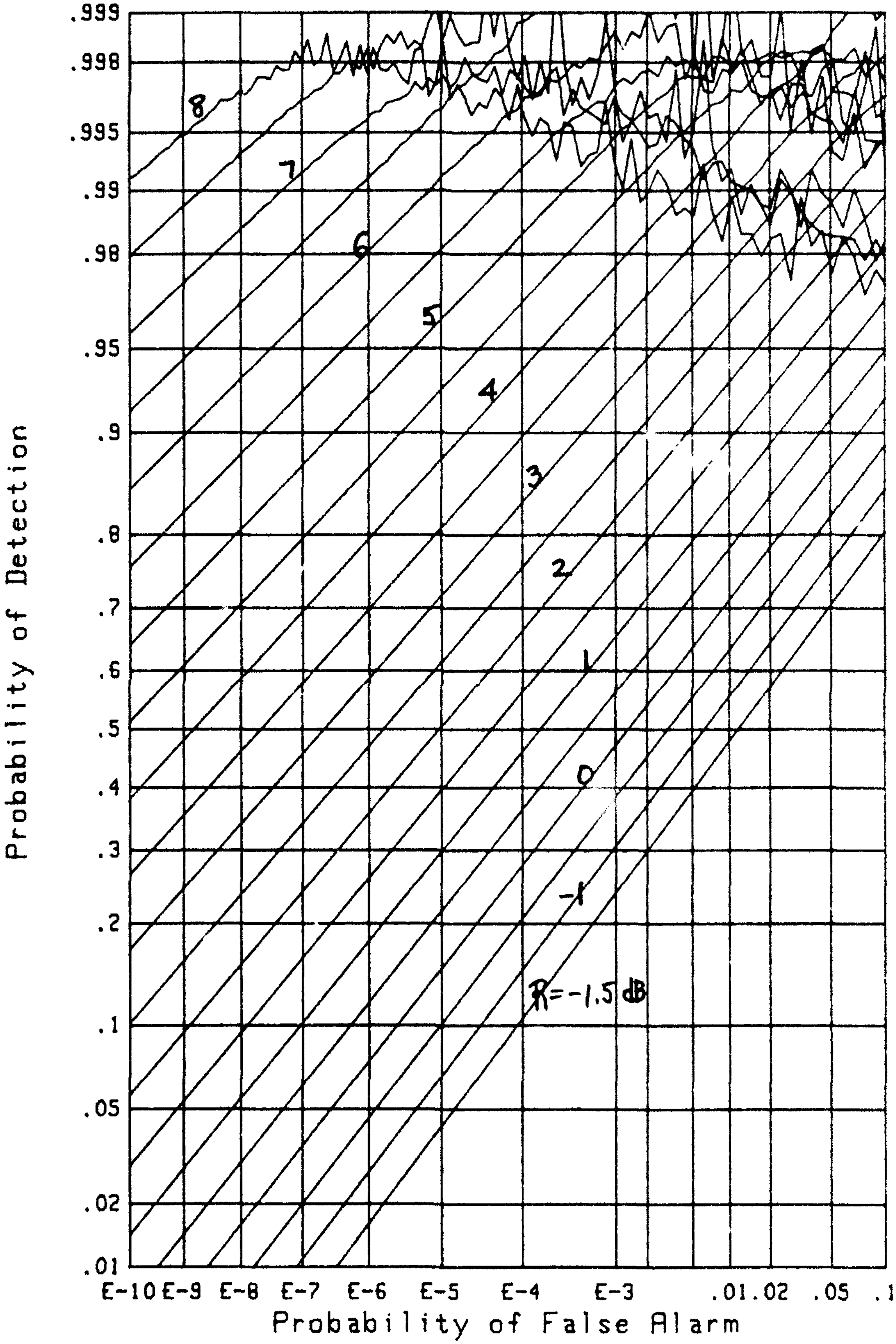

Figure 16. ROC for M=20, Random Weights

CHI-SQUARED APPROXIMATION FOR ARBITRARY WEIGHTS

The difficulty of evaluating the ROC from exact characteristic functions of the form of (7) and (10) has prompted the use of approximations that attempt to extract an effective number of independent samples from a general weight structure, and use this parameter in a simpler chi-squared fit. For example, in [6; (38) and sequel], such an approximation was fruitfully employed to study the stability of a spectral analysis technique employing equi-weighted overlapped segments. Also, in [9; (A-24) - (A-28)], a chi-squared approximation was adopted for the analysis of a diversity combiner in a partially-correlated fading channel. However, in this latter case, no quantitative measure of the error in the approximation was given.

PARAMETERS OF APPROXIMATION

Here, we will address the adequacy of the chi-squared approximation for a general exponential weight structure of the form of (27). We begin by generalizing the chi-squared characteristic function in (12) to the candidate form

$$f_e(\xi) \equiv (1 - i\xi w_e a)^{-M_e} , \tag{28}$$

where w_e is an effective weight and M_e is an effective number of envelope-squared samples, which may be noninteger. (The number of degrees of freedom in (28) is $2M_e$.) The corresponding probability density and exceedance distribution functions are

$$p_e(u) = \frac{u^{M_e-1} \exp\left(\frac{-u}{w_e a}\right)}{\Gamma(M_e)\ (w_e a)^{M_e}} \quad \text{for} \quad u > 0 \ ,$$

$$Q_e(u) = \Gamma\left(M_e, \frac{u}{w_e a}\right) \Big/ \Gamma(M_e) \quad \text{for} \quad u > 0 \ , \qquad (29)$$

respectively, where $\Gamma(\cdot,\cdot)$ is the incomplete gamma function [10; 6.5.3]. These results generalize (13) and (14). The (scaled) cumulants of this gamma distribution follow from (28) as

$$\frac{1}{(k-1)!} \chi_e(k) = M_e\ (w_e a)^k \quad \text{for } k \geq 1 \ . \qquad (30)$$

The mean and variance of this approximation are therefore $M_e\ w_e\ a$ and $M_e\ w_e^2\ a^2$, respectively.

When we equate these first two moments of the generalized chi-squared approximation (28) to the first two moments of decision variable x in (9) and (8), we find

$$w_e = \frac{W_2}{W_1} \ , \qquad M_e = \frac{W_1^2}{W_2} = \frac{\left(\sum_{m=1}^{M} w_m\right)^2}{\sum_{m=1}^{M} w_m^2} \ . \qquad (31)$$

For example, if all the weights are equal, then $M_e = M$. On the other hand, if all the weights are zero except for one, then $M_e = 1$. Both of these limiting cases obviously agree with physical intuition. Observe that w_e and M_e are independent of parameter a or R, the signal-to-noise ratio.

For the exponential weight structure in (27), the effective number of weights and the effective weight are

$$M_e = \frac{1 + r}{1 - r}\;\frac{1 - r^M}{1 + r^M}\,, \quad w_e = \frac{1}{M_e} \quad \text{for } W_1 = 1 \,. \tag{32}$$

It should be noted that as $M \to \infty$, effective number M_e saturates at value $(1 + r)/(1 - r)$, which is not infinite.

Since the incomplete gamma function in (29) is tedious to compute for M_e noninteger, performance could be bracketed by the two cases M_i, M_i+1, where M_i is the integer part of M_e. Or interpolation could be used between these two cases. Instead, we shall choose examples for which M_e is an integer; this allows us to use a form like (14), which is easily computed upon replacement of M by M_e.

GRAPHICAL RESULTS

The first example of the use of a chi-squared approximation, for the exponential weight structure in (27), is furnished by figure 17 for $M = 5$, $r = .69388907$; this particular r value is chosen to yield $M_e = 4$, as may be verified from (32). The exact results (solid lines) in this figure were obtained by the method of the previous section, namely, all weights different. The three dashed curves are yielded by the chi-squared approximation of this section, with $M_e = 4$; the latter are seen to be optimistic by almost 1 dB along the left edge of the figure.

When M is increased to 25 and r decreased to .60000182, again resulting in $M_e = 4$, figure 18 shows that the chi-squared approximation is far worse. The reason for this behavior is that

25 significantly different weights cannot be well represented by 4 equal weights in terms of evaluating the detection capability of the energy detector (1).

The series of plots in figures 19, 20, 21, 22, 23 correspond, respectively, to M_e = 8, 16, 32, 64, 128, for various combinations of M and r, as indicated on the figures. Again, the chi-squared approximation is generally optimistic in the useful range of performance. For M = 64 in figure 20, the discrepancy is almost 1 dB along the left edge. However, for large M, like 200 in figure 23, the difference is only about .25 dB along the left edge.

The results in figures 21, 22, 23 for M_e = 32, 64, 128, respectively, were not obtainable from the all-weights-different method of the previous section, due to excessively large coefficients $\{B_m\}$ in (22). Instead, it was necessary to resort to the numerical integration procedure given in [2]; the values of increment Δ_ξ and length L_ξ appropriate to each case are indicated on each figure.

A conclusion to be drawn from the results in this section is that, although the chi-squared approximation is much better than the Gaussian approximation, it is still not adequate for accurate performance predictions within a few tenths of a decibel. The chi-squared approximation is generally unacceptable for small M_e, unless r is very close to 1. And for large M_e, it is acceptable in some regions of the ROC, but not in others, especially if the extreme weight ratio, r^{M-1}, is very small.

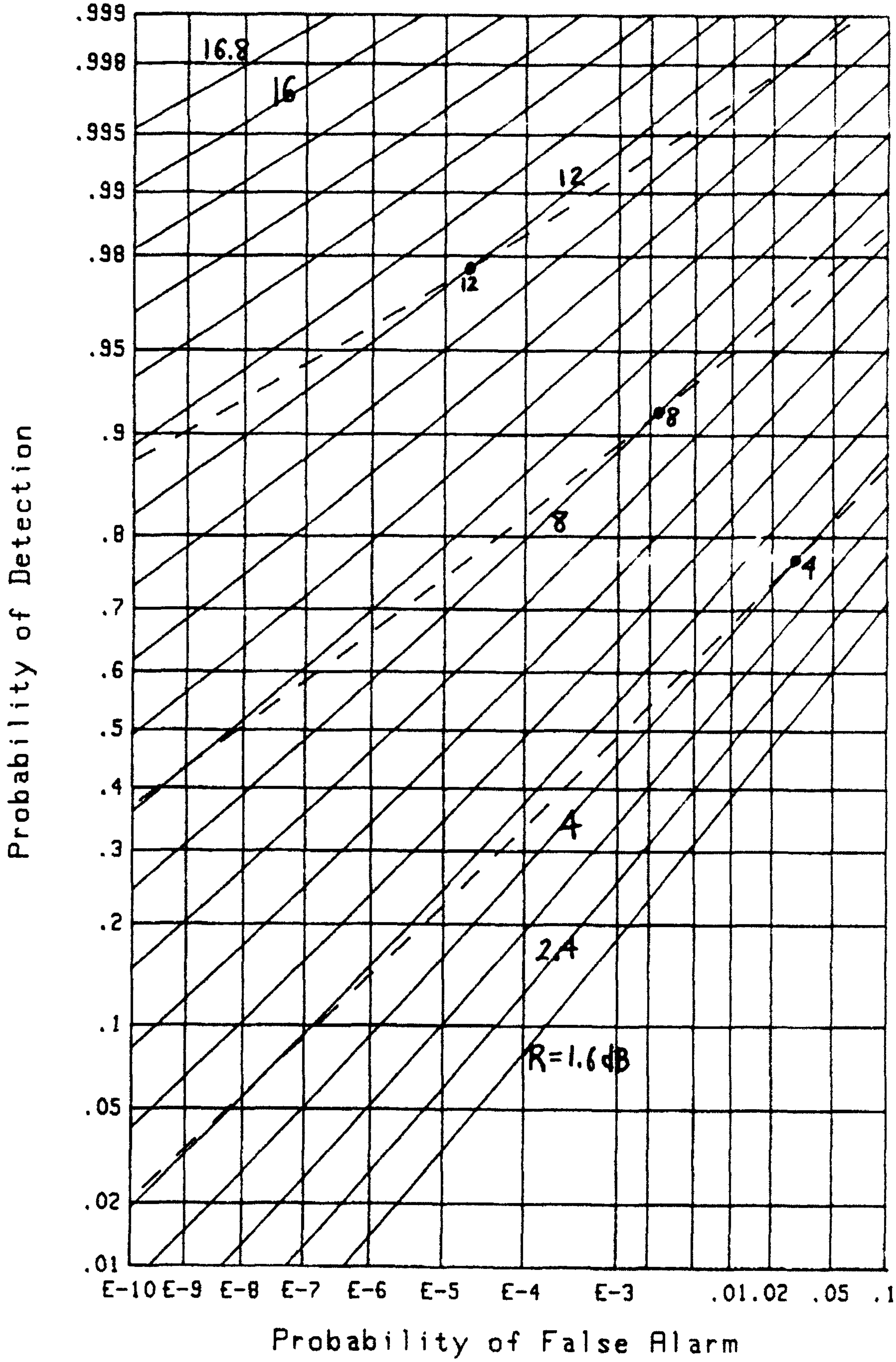

Figure 17. ROC for M=5, r=.69388907 (M_e=4)

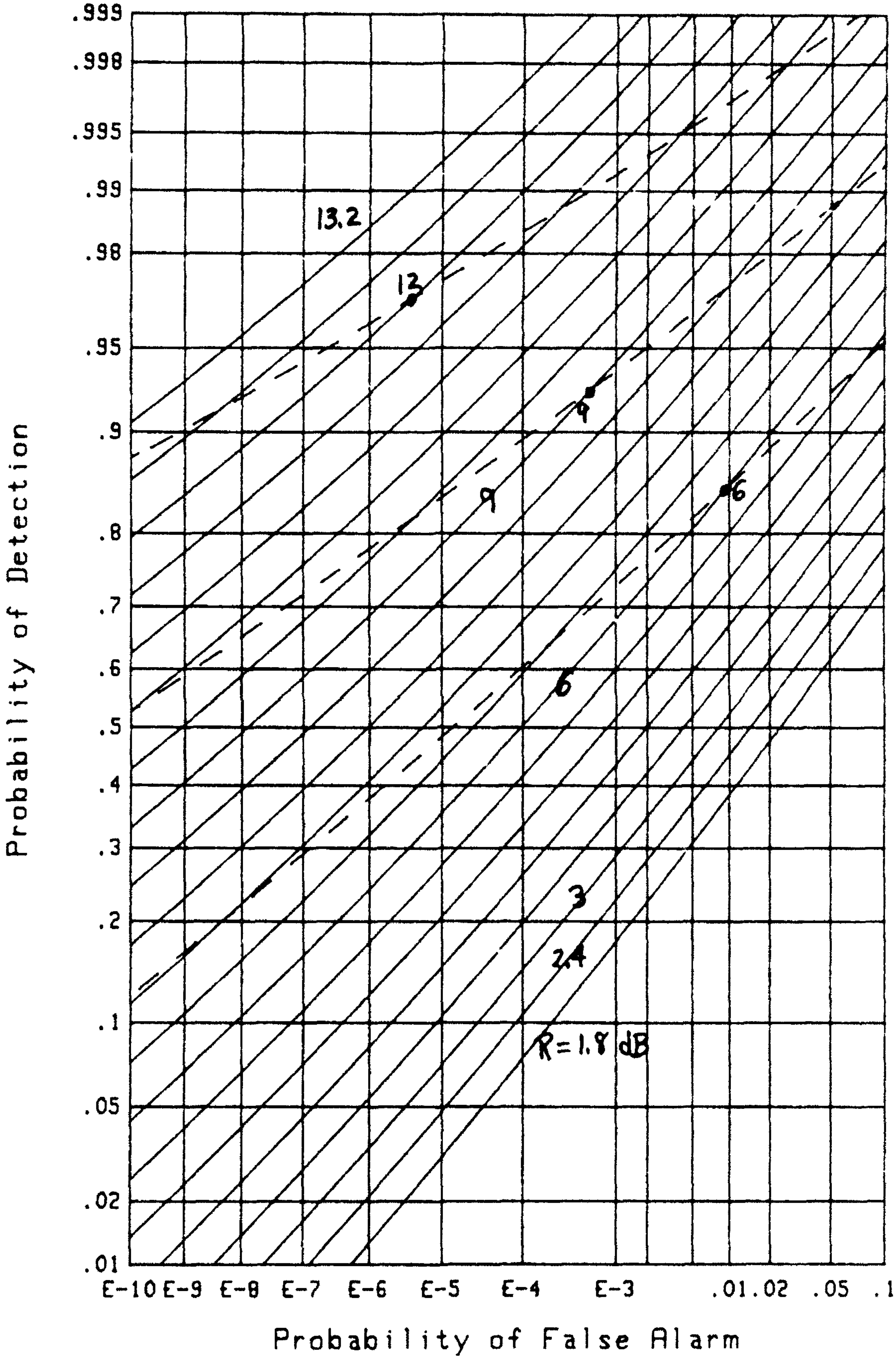

Figure 18. ROC for M=25, r=.60000182 $(M_e=4)$

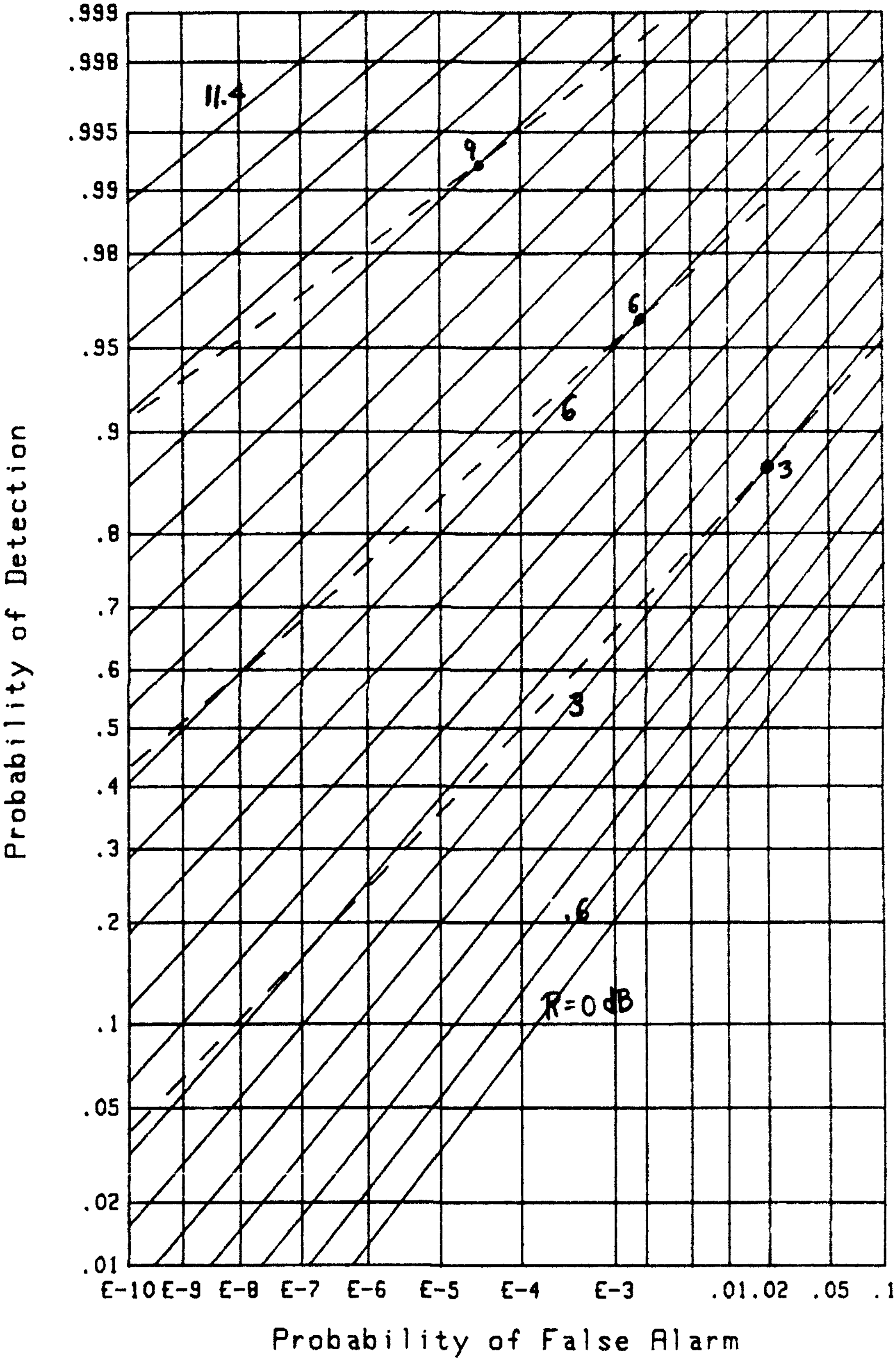

Figure 19. ROC for M=10, r=.83623826 (M_e=8)

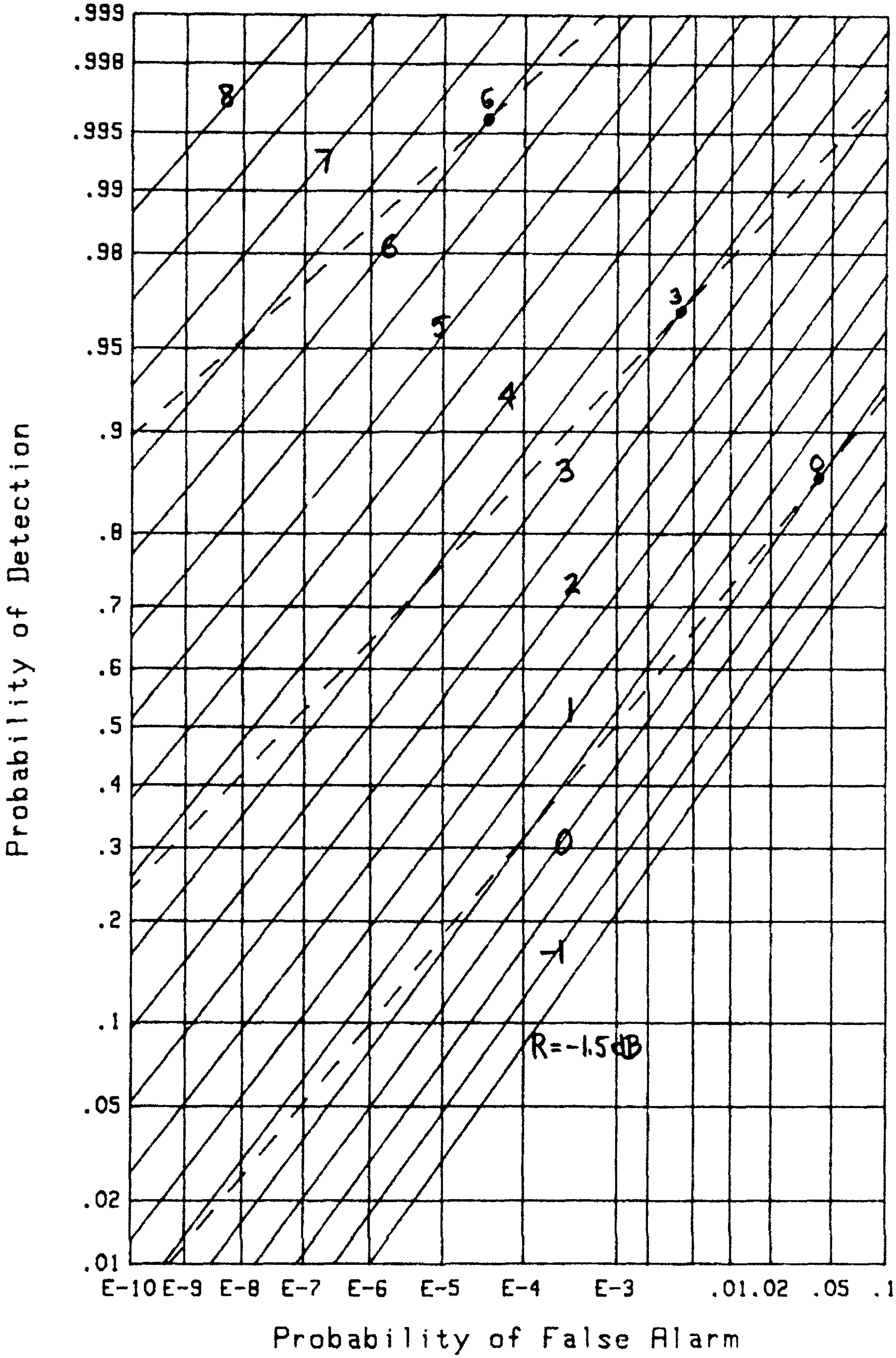

Figure 20. ROC for M=64, r=.88242683 (M_e=16)

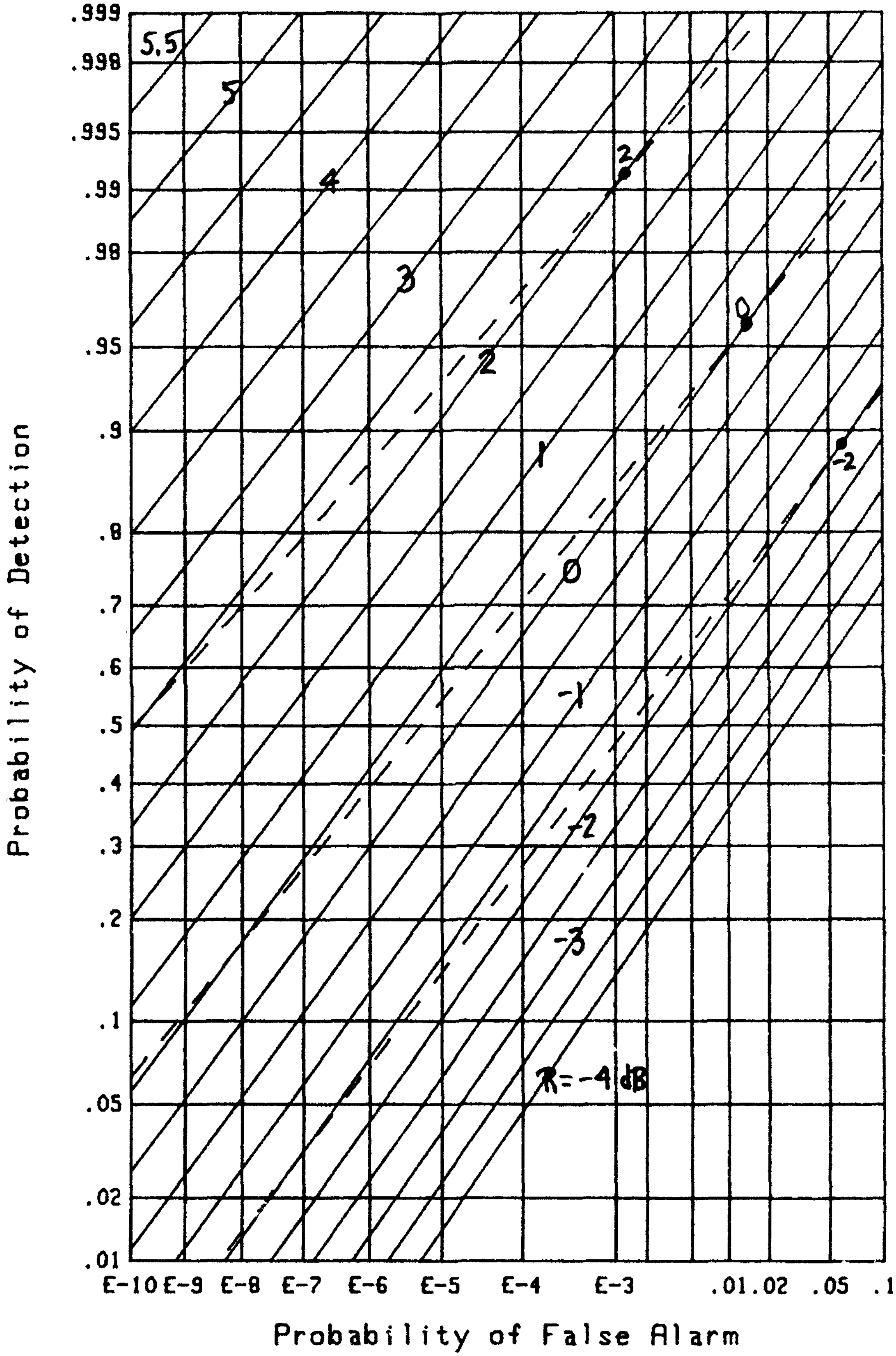

Figure 21. ROC for M=50, r=.94648071 (M_e=32)

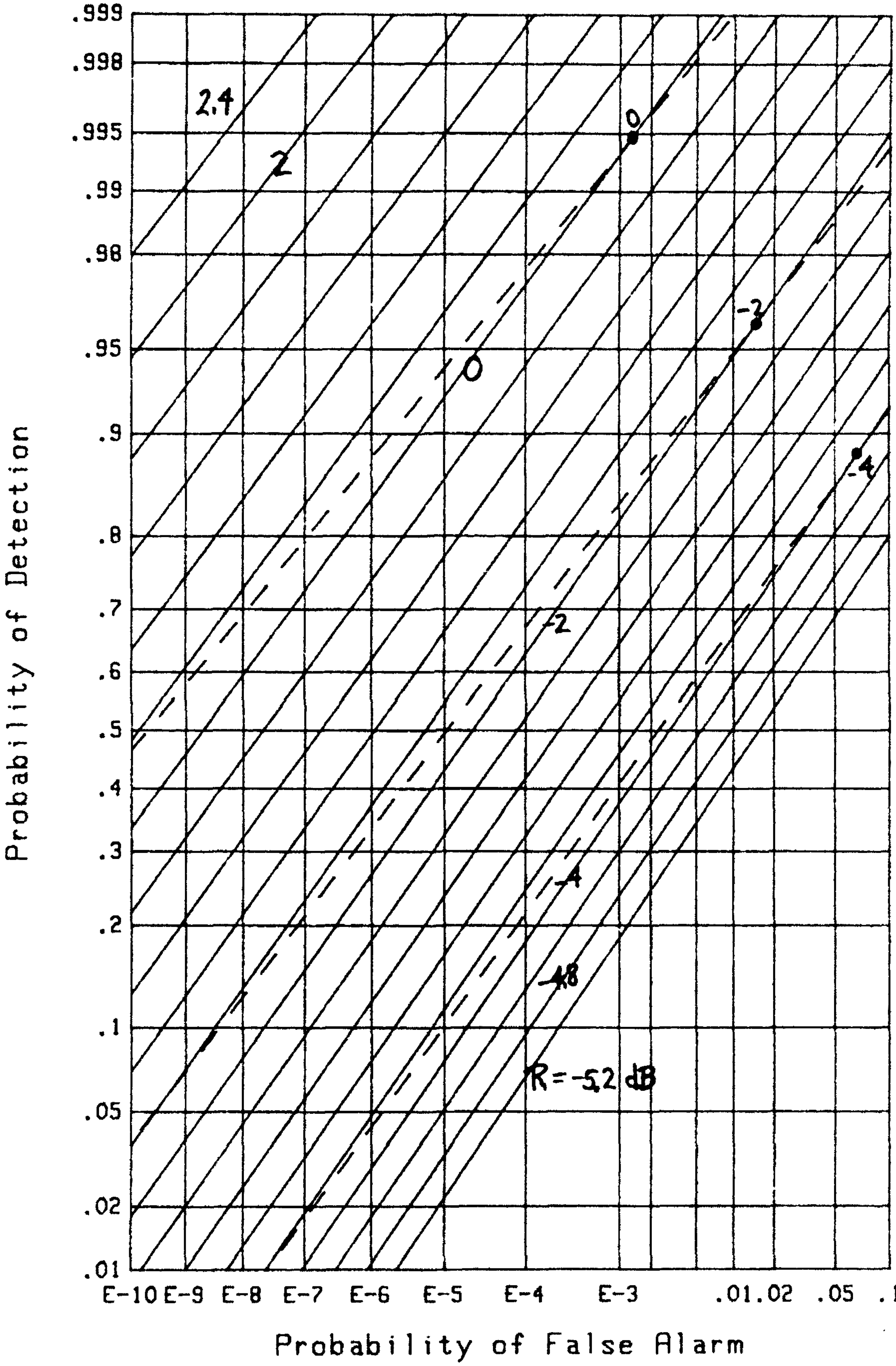

Figure 22. ROC for M=100, r=.97288022 (M_e=64)

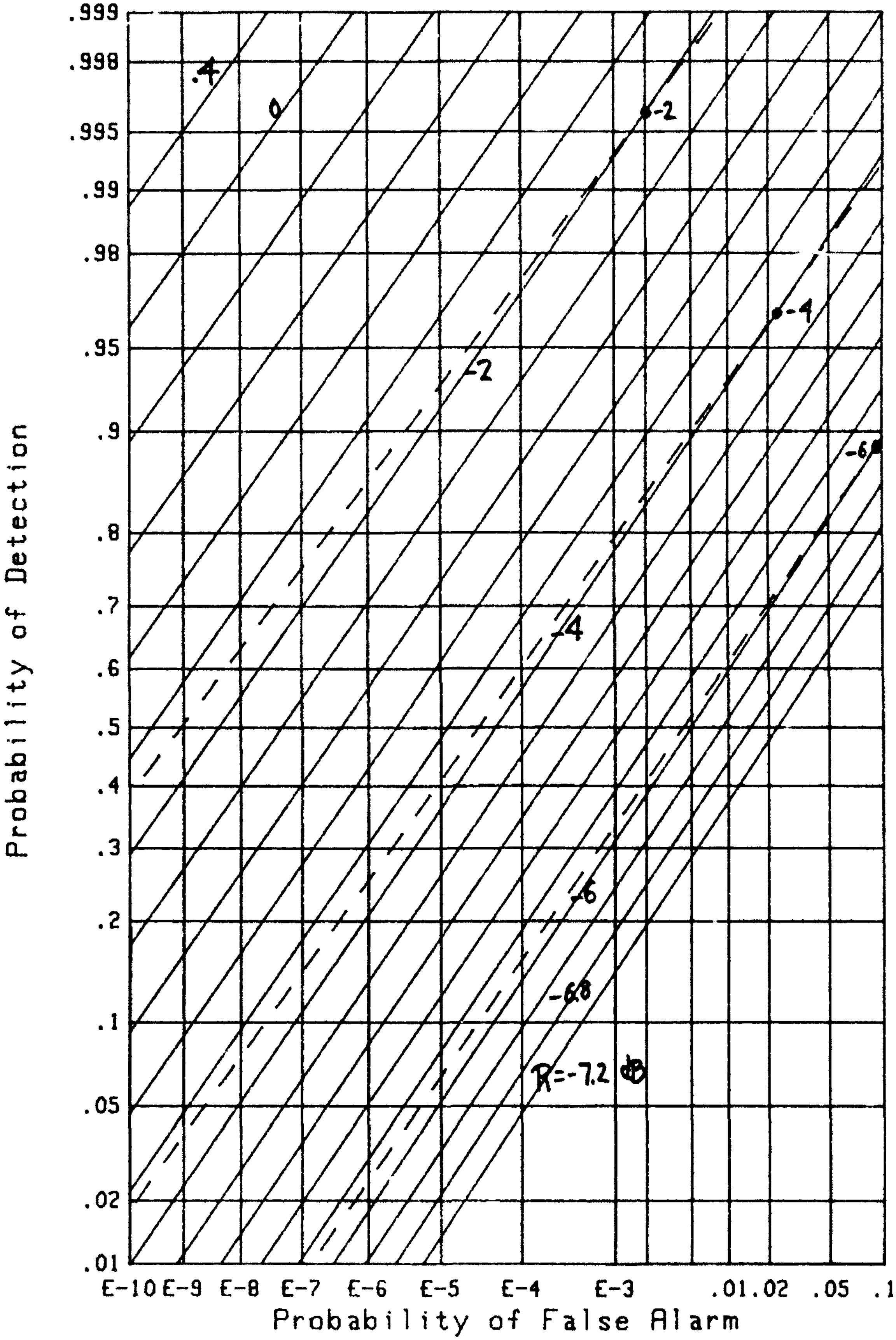

Figure 23. ROC for M=200, r=.98634790 (M_e=128)

THIRD-ORDER APPROXIMATION FOR ARBITRARY WEIGHTS

When a constant c is added to a random variable, the characteristic function is modified by multiplication by the factor $\exp(ic\xi)$. Accordingly, a further generalization of the chi-squared characteristic function in (28) is afforded by

$$f_c(\xi) \equiv \frac{\exp(i\xi b_c a)}{(1 - i\xi w_c a)^{M_c}} = \exp\left(i\xi b_c a - M_c \ln(1 - i\xi w_c a)\right) . \quad (33)$$

This form now has three parameters to choose, namely w_c, b_c, and effective number of samples M_c. This is in distinction to the chi-squared approximation (28) and the Gaussian approximation (A-2), both of which had only two free parameters to adjust. Thus, whereas we only matched the first two moments in (30) and (A-3), respectively, to those of decision variable x, we can now match the first <u>three</u> moments of x if we use characteristic function model (33).

The cumulants of characteristic function (33) are

$$\chi_c(1) = M_c\, w_c\, a + b_c\, a ,$$

$$\frac{1}{(k-1)!}\, \chi_c(k) = M_c\, (w_c\, a)^k \quad \text{for } k \geq 2 . \quad (34)$$

When the first three cumulants (or moments) of (34) are equated with the corresponding quantities of decision variable x, as given by (8), the unique solutions for the parameters of (33) are

$$M_c = \frac{W_2^3}{W_3^2} , \quad w_c = \frac{W_3}{W_2} , \quad b_c = W_1 - \frac{W_2^2}{W_3} , \quad (35)$$

where

$$W_k = \sum_{m=1}^{M} w_m^k \ . \tag{36}$$

It should be noted that the parameters in (35) are independent of parameter a or R, the signal-to-noise ratio.

The probability density function corresponding to characteristic function (33) is

$$p_c(u) = \frac{(u - b_c a)^{M_c - 1} \exp\left(\frac{- u + b_c a}{w_c a}\right)}{\Gamma\left(M_c\right) \left(w_c a\right)^{M_c}} \quad \text{for} \quad u > b_c a \ , \tag{37}$$

and zero otherwise. The exceedance (gamma) distribution function is an obvious generalization of (29), or (14) if M_c is integer; see [10; 6.5.3, 6.5.2, 6.5.13].

$$Q_c(u) = \Gamma\left(M_c, \frac{u - b_c a}{w_c a}\right) \Big/ \Gamma(M_c) = E_{M_c - 1}\left(\frac{u - b_c a}{w_c a}\right) \quad \text{for } u > b_c a \ . \tag{38}$$

For threshold value T, the false alarm and detection probabilities follow immediately as

$$P_F = E_{M_c - 1}\left(\frac{T - b_c}{w_c}\right) \ , \quad P_D = E_{M_c - 1}\left(\frac{T - b_c a}{w_c a}\right) \ , \tag{39}$$

provided that $T > b_c a$.

EXPONENTIAL WEIGHTS

We now restrict attention to the exponential weight structure

$$w_m = \frac{1 - r}{1 - t} r^{m-1} \quad \text{for} \quad 1 \le m \le M , \quad \text{with } t \equiv r^M , \tag{40}$$

where we have normalized at $W_1 = 1$. Then, from (36),

$$W_k = \left(\frac{1 - r}{1 - t}\right)^k \frac{1 - t^k}{1 - r^k} = \left(\frac{1 - r}{1 - t}\right)^{k-1} \frac{1 + t + t^2 + \cdots + t^{k-1}}{1 + r + r^2 + \cdots + r^{k-1}} . \tag{41}$$

In particular,

$$W_1 = 1 , \quad W_2 = \frac{1 - r}{1 - t} \frac{1 + t}{1 + r} , \quad W_3 = \left(\frac{1 - r}{1 - t}\right)^2 \frac{1 + t + t^2}{1 + r + r^2} . \tag{42}$$

The parameters in (35) then follow by substitution as

$$M_c = \frac{\left(1 - r^3\right)^2}{\left(1 - r^2\right)^3} \frac{\left(1 - t^2\right)^3}{\left(1 - t^3\right)^2} = \frac{1 - t}{1 - r} \left(\frac{1 + t}{1 + r}\right)^3 \left(\frac{1 + r + r^2}{1 + t + t^2}\right)^2 , \tag{43}$$

$$w_c = \frac{1 - r^2}{1 - t^2} \frac{1 + t + t^2}{1 + r + r^2} , \quad b_c = \frac{(1 - r t) (r - t)}{(1 + r)^2 \left(1 + t + t^2\right)} . \tag{44}$$

For equal weights, $w_m = 1/M$, we get the usual reduction to $W_1 = 1$, $W_2 = 1/M$, $W_3 = 1/M^2$, giving $M_c = M$, $w_c = 1/M$, $b_c = 0$. Furthermore, it is shown in appendix B that additive constant b_c in (33) and (37), as determined from (35) and (36), is never negative, for <u>any</u> nonnegative weight structure $\{w_m\}$.

GRAPHICAL RESULTS

The first example we consider here is $M = 25$, $r = .75049209$, for which (43) gives $M_c = 4$; again, the reason for the particular choice of r is made so that M_c is integer and (39) can be used. The approximation afforded by (39) is superposed (dashed lines) in figure 24 on the exact results (solid lines) obtained from (25). Increasing M to 64 and changing r to .75049170, so that M_c is maintained at 4, generates virtually the same approximation. The fit is poor and rather optimistic at the left edge of the figure, due to the small value of M_c, namely 4.

For $M = 50$ and $r = .96915298$, M_c is increased to 32 and the results are compared in figure 25. Now, the fit afforded by the constant plus chi-squared approximation is rather good over the entire range of false alarm and detection probabilities shown; in fact, the approximation is optimistic by about .1 dB on the left edge of the figure. The reason for this development is the larger value of the effective number of samples, M_c, namely 32.

Two more results, for M_c equal to 64 and 128, yield similar conclusions in figures 26 and 27, respectively. Again, the exponential weight structure was employed. However, the goodness of fit of the constant plus chi-squared approximation is not limited to this type of weights, but in fact applies to arbitrary structures. To back up this statement, an example of uniformly distributed random weights for $M = 133$ and $M_c = 77.971$ is displayed in figure 28; the overlay, which used $M_c = 78$ in approximation (39), is seen to be very good for this value of M_c.

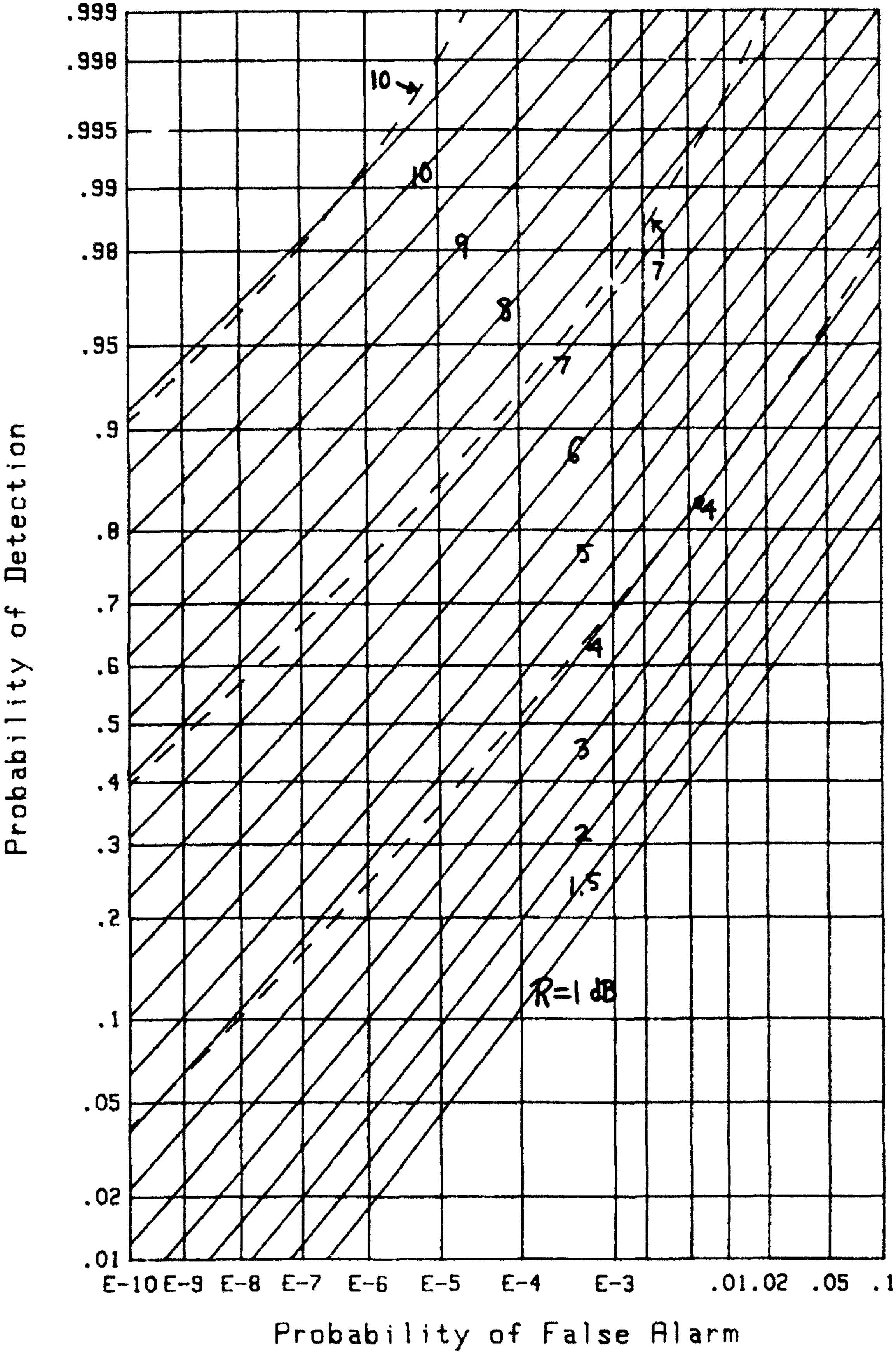

Figure 24. ROC for M=25, r=.75049209 (M_c=4)

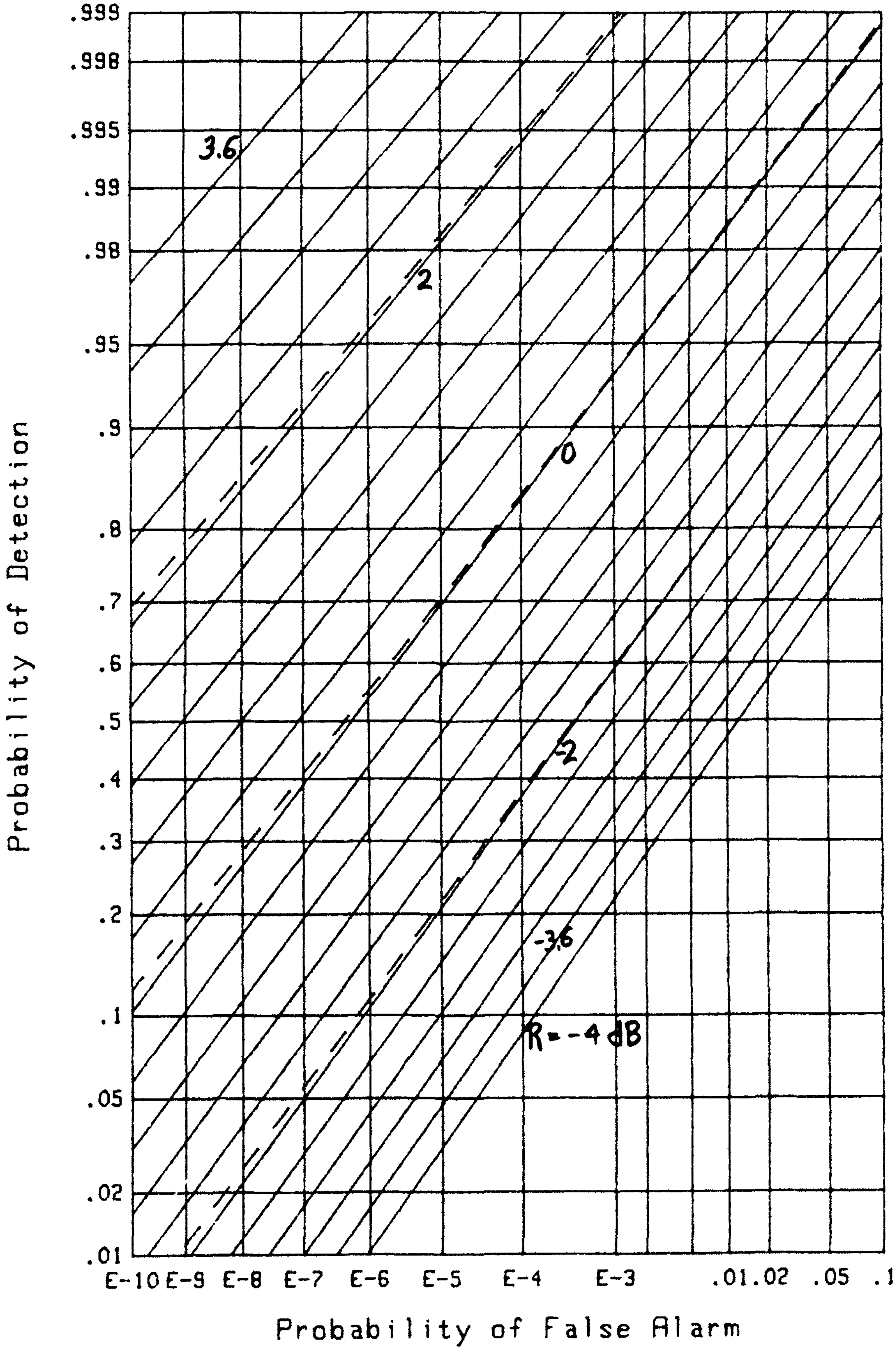

Figure 25. ROC for M=50, r=.96915298 (M_c=32)

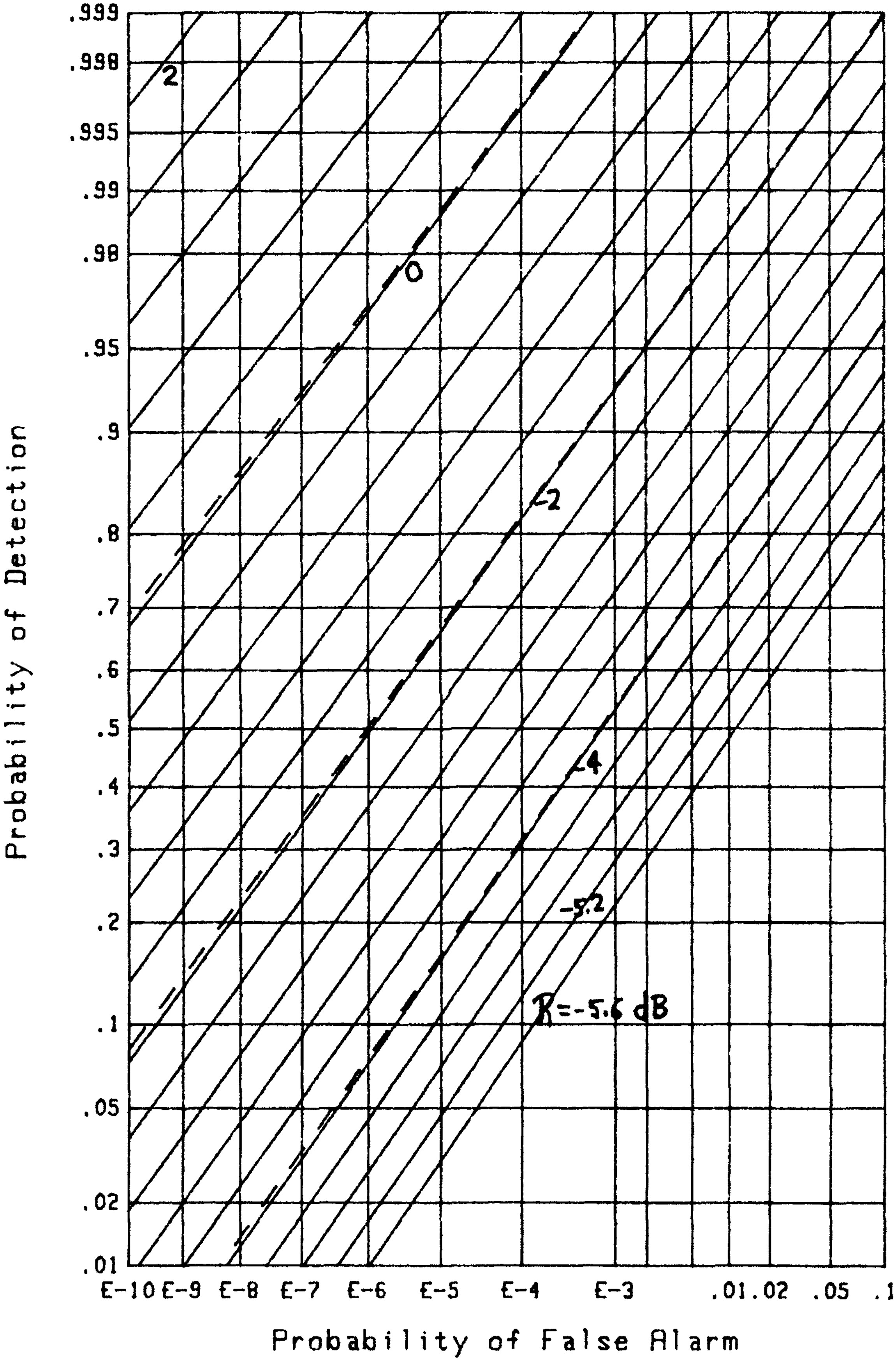

Figure 26. ROC for M=100, r=.98445999 (M_c=64)

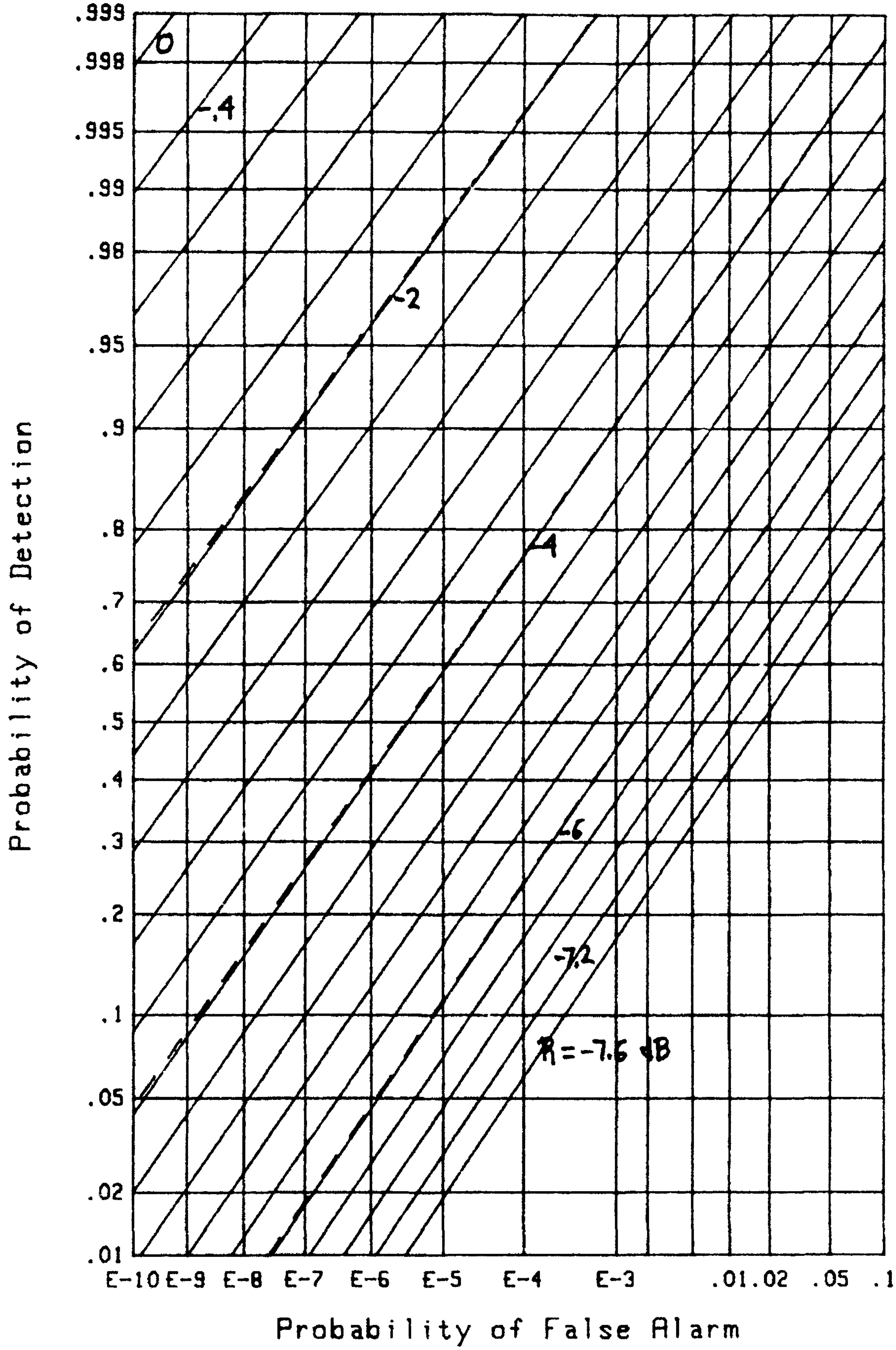

Figure 27. ROC for M=200, r=.99220012 (M_c=128)

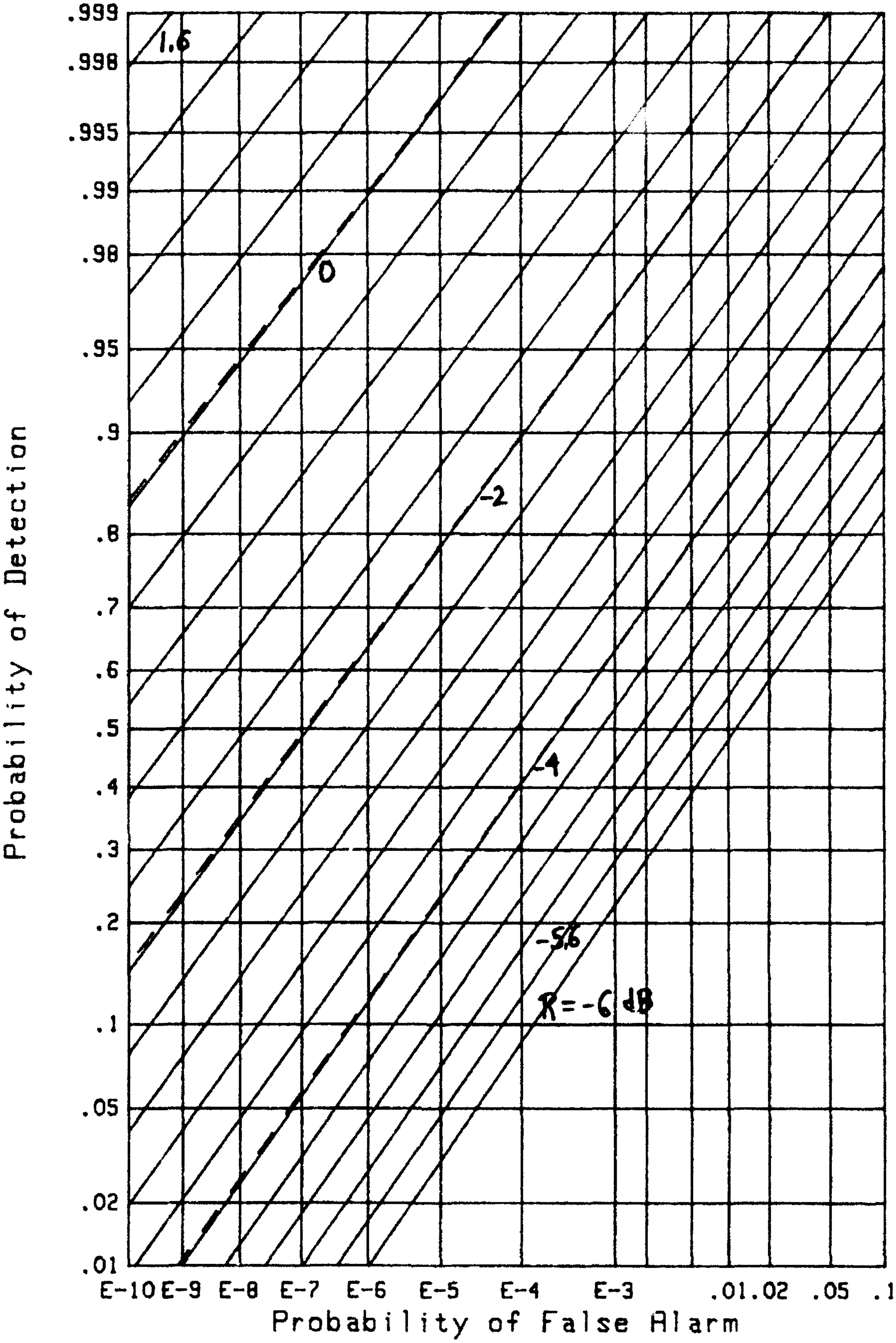

Figure 28. ROC for M=133, Random Weights (M_c=78)

APPLICATION TO EIGENVALUE PROBLEM

Earlier, in (10) and [8; (24)], a particular characteristic function was given which has occurred in a number of statistical analyses. That characteristic function, in normalized form, is

$$f_x(\xi) = \left[\prod_{m=1}^{M}\left\{1 - i\xi\left(1 + R\ \lambda_m\right)\right\}\right]^{-1} , \tag{45}$$

where R is the per-sample signal-to-noise ratio and $\{\lambda_m\}$ are the eigenvalues of the <u>normalized</u> covariance matrix P of the fading signal components. By expanding the ln of (45) in a power series in $i\xi$, the cumulants of random variable x are found to be

$$\frac{1}{(k-1)!}\ \chi_x(k) = \sum_{m=1}^{M}(1 + R\ \lambda_m)^k = \sum_{m=1}^{M}\ \sum_{n=0}^{k}\binom{k}{n}\ R^n\ \lambda_m^n =$$

$$= M + \sum_{n=1}^{k}\binom{k}{n}\ R^n\ \mathrm{tr}\left(P^n\right) \quad \text{for } k \geq 1 , \tag{46}$$

where we have used the simplifying result in appendix C regarding sums of powers of eigenvalues. In particular, there follows from (46), the first three cumulants of x in terms of $\mathrm{tr}(P^n)$:

$$\chi_x(1) = M + R\ \mathrm{tr}(P) ,$$

$$\chi_x(2) = M + 2R\ \mathrm{tr}(P) + R^2\ \mathrm{tr}(P^2) ,$$

$$\tfrac{1}{2}\chi_x(3) = M + 3R\ \mathrm{tr}(P) + 3R^2\ \mathrm{tr}(P^2) + R^3\ \mathrm{tr}(P^3) . \tag{47}$$

PARAMETERS FOR CANDIDATE APPROXIMATION

In this section, we will approximate exact characteristic function (45) by the form employing the constant plus chi-squared idea again, namely

$$f_d(\xi) \equiv \frac{\exp(i\xi b_d)}{(1 - i\xi w_d)^{M_d}} = \exp\left(i\xi b_d - M_d \ln(1 - i\xi w_d)\right) . \quad (48)$$

The cumulants are given by a form very similar to (34), and in particular, the first three (scaled) cumulants of characteristic function (48) are

$$\chi_d(1) = M_d\, w_d + b_d \,, \quad \chi_d(2) = M_d\, w_d^2 \,, \quad \tfrac{1}{2}\chi_d(3) = M_d\, w_d^3 \,. \quad (49)$$

If the first three cumulants, $\chi_d(k)$ for k=1,2,3, were specified, we could then solve (49) for the required parameters according to

$$M_d = \frac{\chi_d^3(2)}{\left(\chi_d(3)/2\right)^2} \,, \quad w_d = \frac{\chi_d(3)/2}{\chi_d(2)} \,, \quad b_d = \chi_d(1) - \frac{\chi_d^2(2)}{\chi_d(3)/2} \,. \quad (50)$$

Now, we set the cumulants of approximation (48) equal to the exact cumulants given by (47), and then solve (50) for the required parameter values. Then, approximation (48) to exact characteristic function (45) is available for numerical evaluation. If cumulants $\{\chi_x(k)\}$ for k=1,2,3 can be evaluated either analytically (via eigenvalues $\{\lambda_m\}$ in (46) or by the trace relations in (47)) or numerically (estimated via finite time averages), then the parameters in (50) can be determined and the corresponding ROC found.

EXACT PERFORMANCE OF (45)

If signal-to-noise ratio R = 0 in (45), then $f_x(\xi) = (1 - i\xi)^{-M}$ and there follows, in a manner similar to (14), $Q_x(u) = E_{M-1}(u)$ and $P_F = E_{M-1}(T)$ for threshold T.

If R > 0 and all the eigenvalues $\{\lambda_m\}$ in (45) are distinct, then, in a manner similar to (21), we can express

$$f_x(\xi) = \sum_{m=1}^{M} \frac{B_m(R)}{1 - i\xi\left(1 + R\,\lambda_m\right)} , \tag{51}$$

where coefficients

$$B_m(R) = \frac{\left(1 + R\,\lambda_m\right)^{M-1}}{R^{M-1} \prod_{\substack{k=1 \\ k \neq m}}^{M} \left(\lambda_m - \lambda_k\right)} \quad \text{for } 1 \leq m \leq M . \tag{52}$$

The exceedance distribution function is then

$$Q_x(u) = \sum_{m=1}^{M} B_m(R) \exp\left(\frac{-u}{1 + R\,\lambda_m}\right) \quad \text{for } u > 0 , \quad R > 0 , \tag{53}$$

and the detection probability is

$$P_D = \sum_{m=1}^{M} B_m(R) \exp\left(\frac{-T}{1 + R\,\lambda_m}\right) \quad \text{for } T > 0 , \quad R > 0 . \tag{54}$$

The eigenvalues $\{\lambda_m\}$ of normalized covariance matrix P are independent of signal-to-noise ratio R; however, coefficients $\{B_m(R)\}$ are dependent on R and explicitly indicated so.

GRAPHICAL RESULTS

The only example that we consider here is a covariance matrix $P = [\rho_{mn}]$, where $\rho_{mn} = \rho^{|m-n|}$. In particular, for $M = 10$ and $\rho = .5$, the M eigenvalues $\{\lambda_m\}$ of P were evaluated and the results on page 55 were used for an exact evaluation of the detection and false alarm probabilities; these are displayed as solid lines in figure 29.

Then, we returned to matrix P, ignored the knowledge of the eigenvalues, and instead employed the trace relations in (47) and appendix C to evaluate the cumulants of random variable x. These were substituted in (50) to determine the parameters of characteristic function (48), as explained in the sequel to (50). Then, the method of [2] was used to obtain the corresponding ROC.

These results are overlaid as dashed lines in figure 29, for three selected values of signal-to-noise ratio R (in decibels). The agreement for small signal-to-noise ratios is very good, and can be explained by observing that (45) approaches the chi-squared characteristic function in this case. Approximation (48) is also excellent for very small false alarm probabilities, despite the fact that the equivalent number of samples, M_d, is rather small; for example, the three curves in figure 29 for $R = 2,5,8$ dB have $M_d = 5.79, 4.83, 4.31$, respectively.

Another example for $M = 32$, $\rho = .5$ is displayed in figure 30. Here, the values of M_d for the four overlays, $R = -2,0,2,4$ dB are 24.1, 20.6, 17.6, 15.4, respectively. These larger values of M_d account for the improved fit to the exact results.

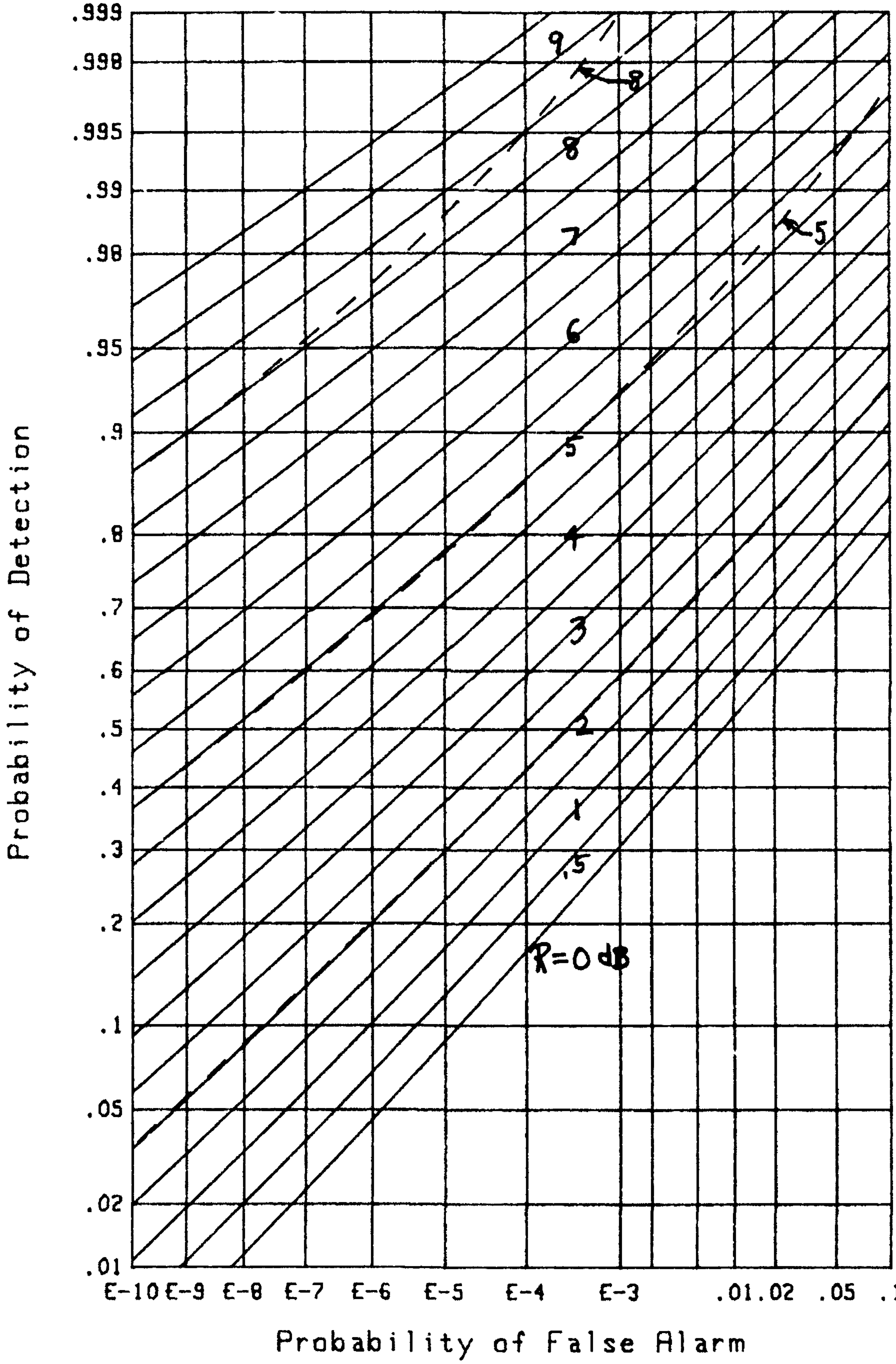

Figure 29. ROC for M=10, ρ=.5

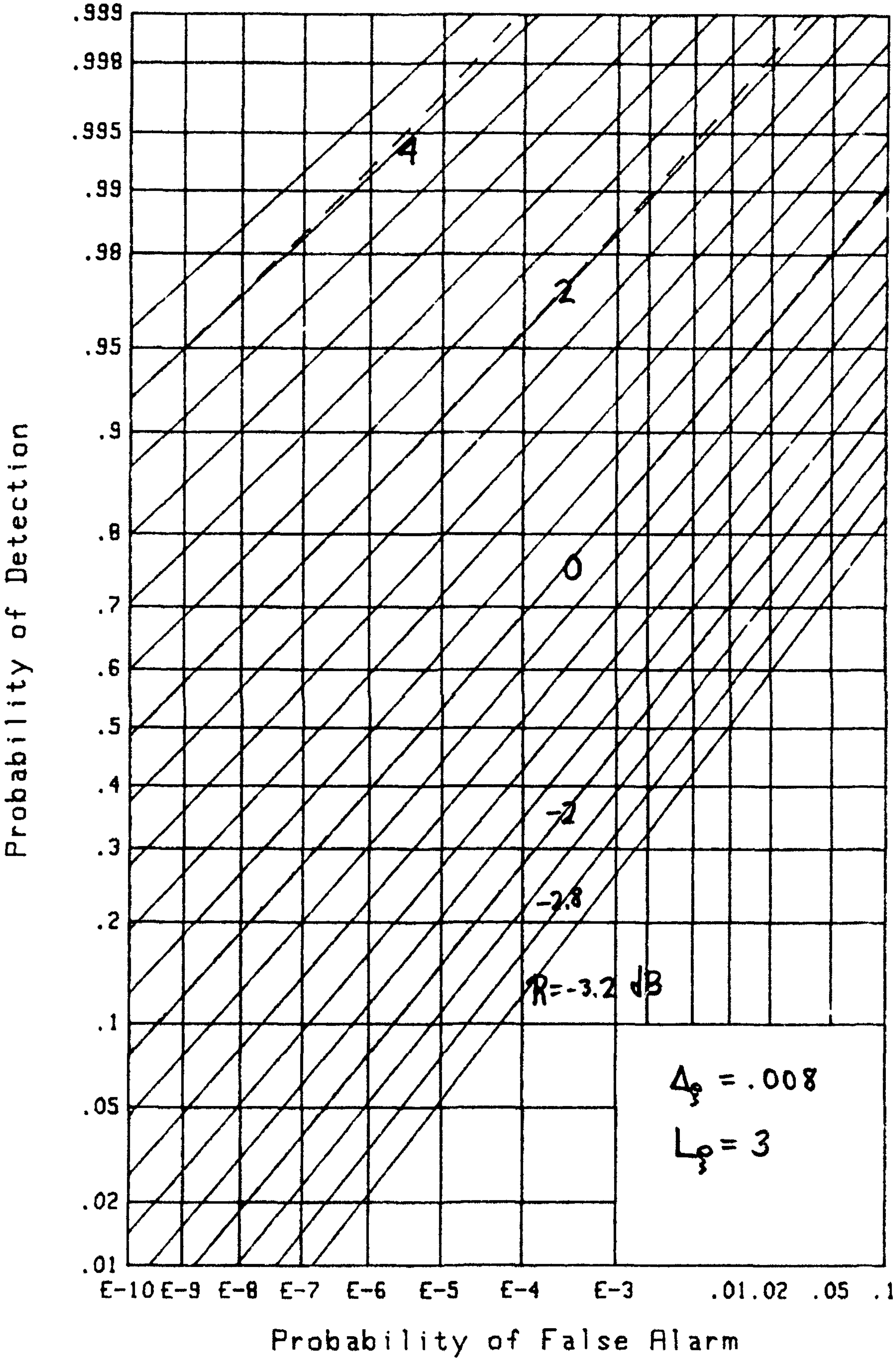

Figure 30. ROC for M=32, ρ=.5

FOURTH-ORDER APPROXIMATIONS FOR ARBITRARY WEIGHTS

In this section, we will consider a couple of fourth-order fits to a specified characteristic function and will match cumulants (or moments) through fourth-order.

GAUSSIAN PLUS CHI-SQUARED FIT

The initial fourth-order fit of interest here corresponds to the characteristic function of a (nonzero mean) Gaussian random variable plus a chi-squared variate. That is, the candidate is

$$f_f(\xi) = \frac{\exp\left(i\xi b_f - \frac{1}{2}\xi^2 c_f\right)}{\left(1 - i\xi w_f\right)^{M_f}} = \exp\left(i\xi b_f - \frac{1}{2}\xi^2 c_f - M_f \ln(1 - i\xi w_f)\right) . \tag{55}$$

The first four cumulants of characteristic function (55) are

$$\chi_f(1) = b_f + M_f w_f , \quad \chi_f(2) = c_f + M_f w_f^2 ,$$

$$\frac{1}{2}\chi_f(3) = M_f w_f^3 , \frac{1}{6}\chi_f(4) = M_f w_f^4 . \tag{56}$$

If the cumulants are specified, the parameters for characteristic function (55) can be determined explicitly as

$$M_f = \frac{\left(\chi_f(3)/2\right)^4}{\left(\chi_f(4)/6\right)^3} , \quad w_f = \frac{\chi_f(4)/6}{\chi_f(3)/2} ,$$

$$b_f = \chi_f(1) - \frac{\left(\chi_f(3)/2\right)^3}{\left(\chi_f(4)/6\right)^2} , \quad c_f = \chi_f(2) - \frac{\left(\chi_f(3)/2\right)^2}{\chi_f(4)/6} . \tag{57}$$

Numerical results will be presented in a later section.

NON-CENTRAL CHI-SQUARED FIT

The other fourth-order fit that we consider corresponds to a generalized non-central chi-squared variate, namely characteristic function

$$f_g(\xi) = \frac{\exp\left(\dfrac{i\xi b_g}{1 - i\xi c_g}\right)}{\left(1 - i\xi w_g\right)^{M_g}} = \exp\left(\frac{i\xi b_g}{1 - i\xi c_g} - M_g \ln(1 - i\xi w_g)\right) . \quad (58)$$

This is called generalized because we do not force $c_g = w_g$. The ln of (58) can be expanded in a power series in $i\xi$:

$$\ln f_g(\xi) = i\xi b_g \sum_{j=0}^{+\infty} (i\xi c_g)^j + M_g \sum_{k=1}^{+\infty} \frac{1}{k}(i\xi w_g)^k . \quad (59)$$

The first four cumulants of this characteristic function are then

$$\chi_g(1) = b_g + M_g\, w_g\ , \quad \chi_g(2) = 2\, b_g\, c_g + M_g\, w_g^2\ ,$$

$$\tfrac{1}{2}\chi_g(3) = 3\, b_g\, c_g^2 + M_g\, w_g^3\ , \quad \tfrac{1}{6}\chi_g(4) = 4\, b_g\, c_g^3 + M_g\, w_g^4\ . \quad (60)$$

The inversion of these nonlinear equations, for the parameters in terms of the cumulants, is not possible in closed form, as it was for candidate characteristic function (55). This limitation tends to discourage use of the non-central chi-squared approximation (58). However, in appendix D, an efficient numerical procedure for solving (60) for the required parameters is developed and programmed. Application of this approximation procedure is deferred to a later section.

PERFORMANCE IN STEADY STATE NOISE

Up to this point, the number of samples, M, has been finite, both for signal-present as well as signal-absent; then, the noise output of the exponential integrator, (27) or (40), has not reached steady-state. In this section, the number M of noise samples will be set equal to ∞, thereby allowing the integrator noise output to reach steady state. However, the number, N, of samples containing signal (if present) will remain finite.

This situation arises in practice, for example, when the precise arrival time of the signal is unknown. The use of surplus envelope-squared samples $\{z_m\}$, for $m > N$, does <u>not</u> improve performance, since these particular samples are always noise-only; in fact, these extra samples always degrade performance, the exact amount depending on the relative sizes of weights $\{w_m\}$ for $m > N$ compared to $m \leq N$. Here, we will give a method for quantitatively assessing the impact of these surplus noise-only samples on the operating characteristics.

CHARACTERISTIC FUNCTION

The characteristic function of the decision variable is an obvious generalization of (7) to the form

$$f_x(\xi) = \left[\prod_{m=1}^{\infty}\left(1 - i\xi w_m a_m\right)\right]^{-1} , \qquad (61)$$

where the signal-to-noise ratio parameter a_m now takes the form

$$a_m = \left\{\begin{array}{ll} 1 & \text{for noise-alone} \\ 1 + R_m & \text{for signal-plus-noise} \end{array}\right\} \text{ for } 1 \leq m \leq M = \infty . \qquad (62)$$

The particular case that will be considered at length, here, is that of a finite-duration constant-strength signal, which is accommodated mathematically by setting

$$R_m = \left\{\begin{array}{ll} R & \text{for } 1 \leq m \leq N \\ 0 & \text{for } N < m \leq M = \infty \end{array}\right\} . \qquad (63)$$

When signal-to-noise ratio R is equal to zero, that is, signal-absent, the characteristic function in (61) reduces to

$$\tilde{f}_x(\xi) \equiv \left[\prod_{m=1}^{\infty}\left(1 - i\xi w_m\right)\right]^{-1} . \qquad (64)$$

Unfortunately, even for the exponential averager,

$$w_m = (1-r)\, r^{m-1} \quad \text{for } 1 \leq m \leq M = \infty , \qquad (65)$$

the noise-only characteristic function in (64) takes a form,

$$\tilde{f}_x(\xi) = \left[\prod_{m=1}^{\infty}\left(1 - i\xi\ (1-r)\ r^{m-1}\right)\right]^{-1} , \tag{66}$$

which is not expressible in closed form; see [11; (89.18.3)]. (Likewise, the finite product cannot be simplified; see [11; (89.18.2)].) This necessitates termination of the infinite product in (66), being sure to keep the remainder below an acceptable tolerance; this issue is addressed in appendix E.

CUMULANTS

For general characteristic function (61), the cumulants are

$$\frac{1}{(k-1)!}\ \chi_x(k) = \sum_{m=1}^{\infty}(w_m\ a_m)^k \quad \text{for} \quad 1 \le k\ . \tag{67}$$

For the special case of the exponential averager (65) and the finite-duration signal (63), these cumulants reduce to

$$\frac{1}{(k-1)!}\ \chi_x(k) = \frac{(1-r)^k}{1-r^k}\left[(1+R)^k\left(1-r^{kN}\right) + r^{kN}\right] . \tag{68}$$

At the same time, characteristic function (61) becomes

$$f_x(\xi) = \left[\prod_{m=1}^{N}\left(1 - i\xi\ (1-r)\ r^{m-1}(1+R)\right)\prod_{m=N+1}^{\infty}\left(1 - i\xi\ (1-r)\ r^{m-1}\right)\right]^{-1} . \tag{69}$$

In particular, for noise-alone, then R = 0 and (68) reduces to

$$\frac{1}{(k-1)!}\,\tilde{\chi}_x(k) = \frac{(1-r)^k}{1-r^k} = \frac{(1-r)^{k-1}}{1+r+\ldots+r^{k-1}} \, . \qquad (70)$$

The three lowest-order cases are

$$\tilde{\chi}_x(1) = 1 \; , \quad \tilde{\chi}_x(2) = \frac{1-r}{1+r} \; , \quad \tfrac{1}{2}\tilde{\chi}_x(3) = \frac{(1-r)^2}{1+r+r^2} \, . \qquad (71)$$

For signal-present, R > 0, the three lowest cumulants are, from (68),

$$\chi_x(1) = 1 + R - R\,r^N \, ,$$

$$\chi_x(2) = \frac{1-r}{1+r}\left[(1+R)^2\left(1-r^{2N}\right) + r^{2N}\right] \, ,$$

$$\tfrac{1}{2}\chi_x(3) = \frac{(1-r)^2}{1+r+r^2}\left[(1+R)^3\left(1-r^{3N}\right) + r^{3N}\right] \, . \qquad (72)$$

Here, N is the number of signal components, R is the signal-to-noise ratio per sample, and r is the exponential decay factor for the weight structure (65).

In the evaluation of the signal-present characteristic function (69), the second product will have to be terminated at a finite limit $m = L$ ($\geq N$). The error due to this truncation is addressed in appendix E.

GRAPHICAL RESULTS

An example of the results in this section for $M = \infty$, $N = 32$, $r = .9$, is displayed in figure 31, as obtained via exact results (66) and (69), along with the truncation procedure of appendix E. Superposed as dashed lines are the results of using the constant plus chi-squared approximation (48), where the parameters are obtained from the cumulants, according to (50). The cumulants themselves are given by (72). The effective number of samples, M_d in (48), takes on the values 10.680, 10.676, 10.673, and 10.672 for the four signal-to-noise ratios of 0, 2, 4, and 6 dB indicated in the figure. This relatively small value of M_d is the reason for the discrepancy in figure 31 between the exact and approximate results.

Figure 32 is drawn for $M = \infty$, $N = 50$, and $r = .96915298$; compare figure 25, for which $M_c = 32$. The values of M_d for the three overlaid curves for signal-to-noise ratios equal to -2, 0, and 2 dB are 33.531, 33.030, and 32.624, respectively. These larger values, for the effective number of samples, lead to better agreement in this figure; in fact, the approximation is in error by only .15 dB along the left edge of the figure.

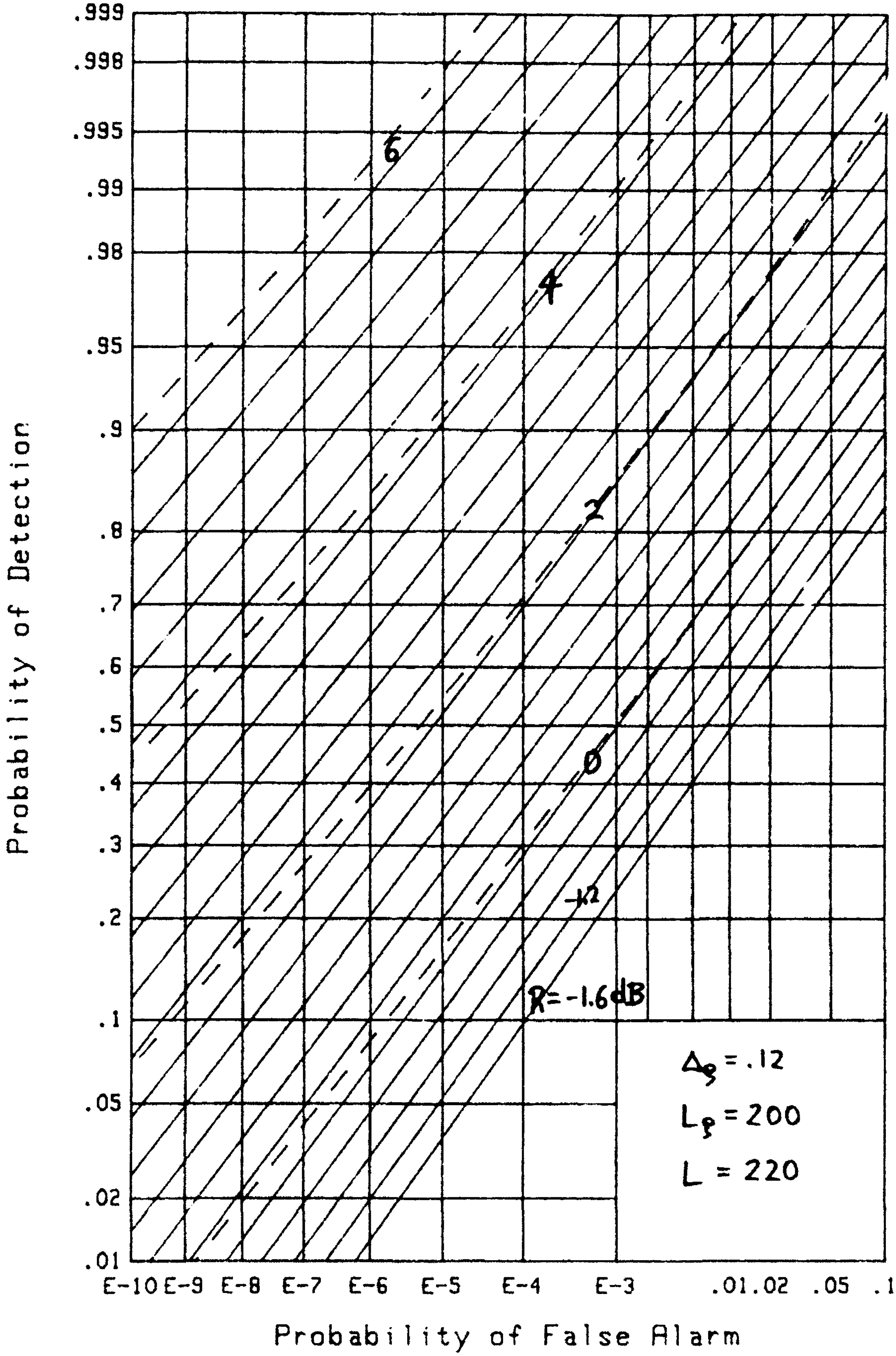

Figure 31. ROC for M=∞, N=32, r=.9

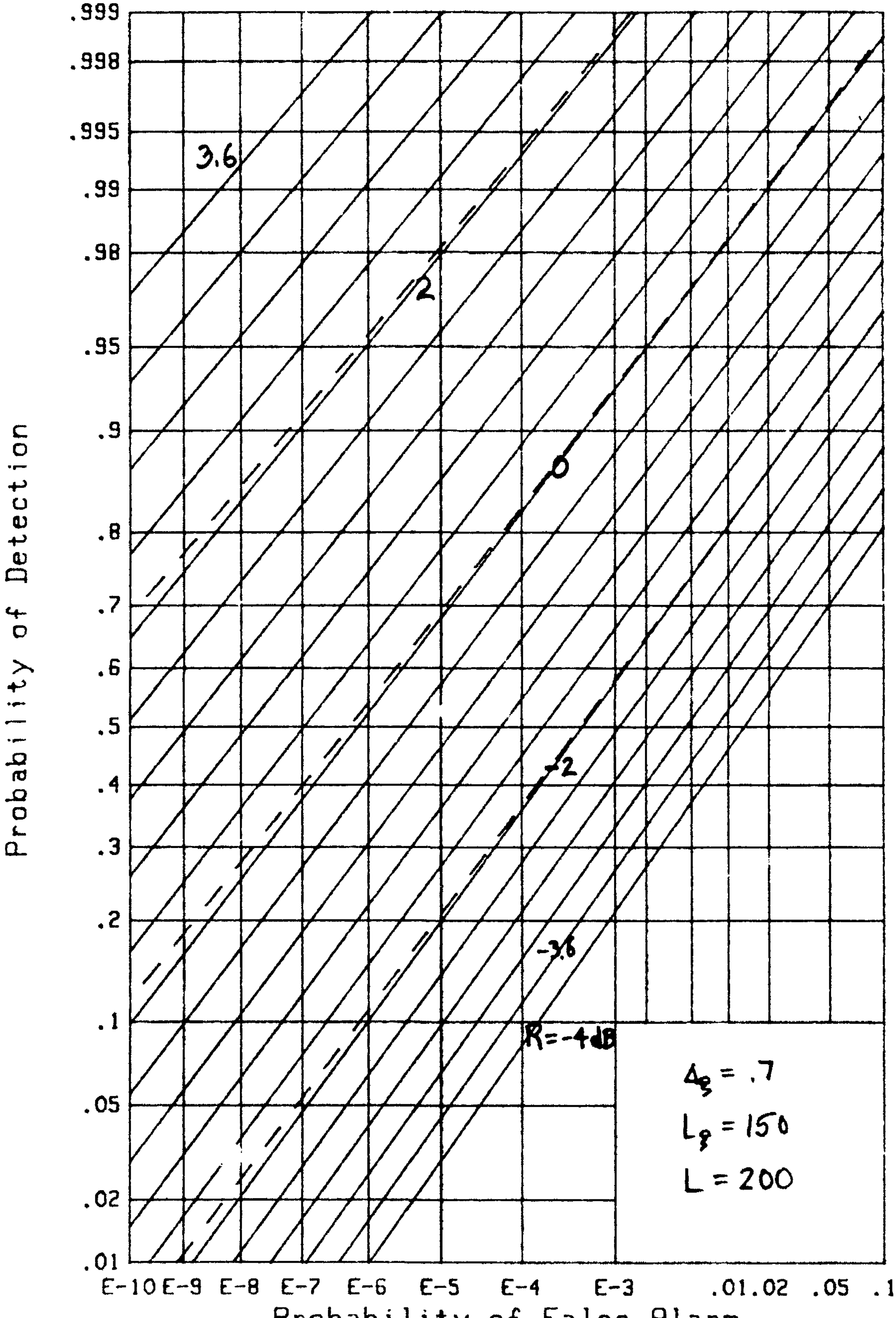

Figure 32. ROC for M=∞, N=50, r=.96915298

BLOCK EXPONENTIAL WEIGHTING

In this section, we again consider a weighted energy detector in steady state, that is, $M = \infty$. However, the averager now operates on blocks of data points which are equally weighted, but which are themselves exponentially weighted. That is, the decision variable x is now given by

$$x = \sum_{m=1}^{\infty} w_m \, z_m \, , \tag{73}$$

where the weights $\{w_m\}$ are

$$w_m = \frac{1-r}{B} \begin{Bmatrix} 1 & \text{for} & 1 \le m \le B \\ r & \text{for} & B < m \le 2B \\ r^2 & \text{for} & 2B < m \le 3B \\ \vdots & & \vdots \end{Bmatrix} . \tag{74}$$

Here, B is the block size and the weights have been normalized at $W_1 = 1$. The following diagram illustrates the block exponential weighting structure.

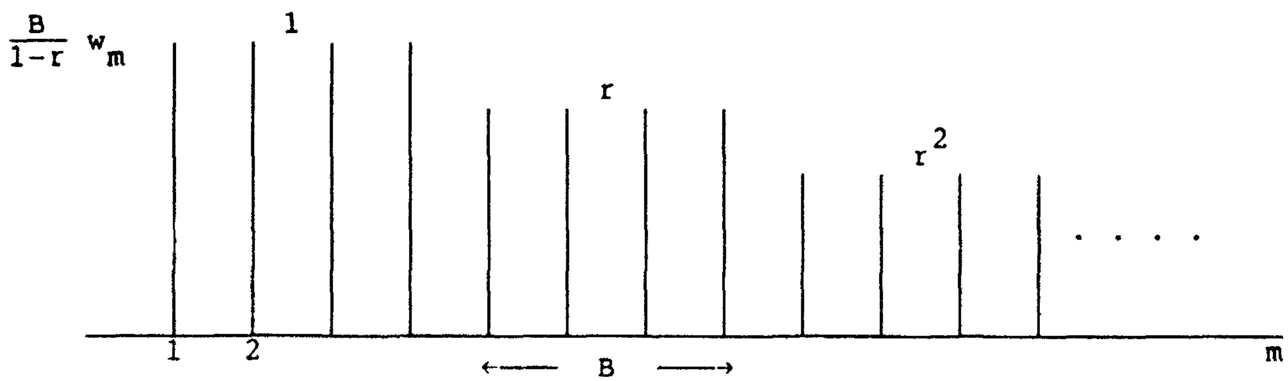

SIGNAL STATISTICS

The signal, if present, occupies the first N samples of sum (73), where

$$J \equiv \frac{N}{B} \tag{75}$$

is presumed integer; that is, J is the number of blocks occupied by signal (when present). The signal-to-noise ratio parameter is

$$a_m = \left\{ \begin{array}{ll} 1 & \text{for noise-only} \\ & \\ 1+R & \text{for signal plus noise} \end{array} \right\} \text{ for } \quad 1 \leq m \leq N \,, \tag{76A}$$

and

$$a_m = 1 \quad \text{for} \quad N \leq m < \infty \,. \tag{76B}$$

CHARACTERISTIC FUNCTION

The characteristic function of x in (73) for signal present is, using the independence of the $\{z_m\}$,

$$f_x(\xi) = \left[\prod_{m=1}^{\infty} \left(1 - i\xi w_m a_m\right) \right]^{-1} =$$

$$= \left[\prod_{j=0}^{J-1} \left(1 - i\xi \, \frac{1-r}{B} \, r^j \, (1 + R)\right) \prod_{j=J}^{\infty} \left(1 - i\xi \, \frac{1-r}{B} \, r^j\right) \right]^{-B} . \tag{77}$$

Again, an infinite product is required and the truncation procedure given in appendix E is directly relevant.

CUMULANTS

The cumulants of decision variable x follow readily from (77), upon expansion of ln $f_x(\xi)$ in a power series in $i\xi$:

$$\frac{1}{(k-1)!}\,\chi_x(k) = \frac{[(1-r)/B]^{k-1}}{1+r+\cdots+r^{k-1}}\left[(1+R)^k\left(1-r^{kJ}\right) + r^{kJ}\right] \text{ for } k \geq 1. \quad (78)$$

The four lowest-order cumulants will be used in fitting the exact characteristic function (77) by approximations (55) and (58).

GRAPHICAL RESULTS

Results for the operating characteristics for B = 4, J = 32, and r = .95 are presented in figure 33. Thus, from (75), the signal (when present) occurs on N = 128 samples. Superposed as dashed lines is the approximation afforded by third-order fit (33) and (39). The discrepancy is only .1 dB along the left edge of the figure.

Another example of block exponential weighting, for B = 4, J = 16, and r = .9, is displayed in figure 34. The dashed overlay is again the third-order approximation (33), which is optimistic by about .15 dB along the left edge of the figure.

The exact results from figure 34 are repeated in figure 35, but now the overlays are the two fourth-order approximations (55) and (58). The latter two approximations are indistinguishable from each other over the entire range of probabilities displayed. Furthermore, they differ from the exact results only by .05 dB at the left edge of the figure.

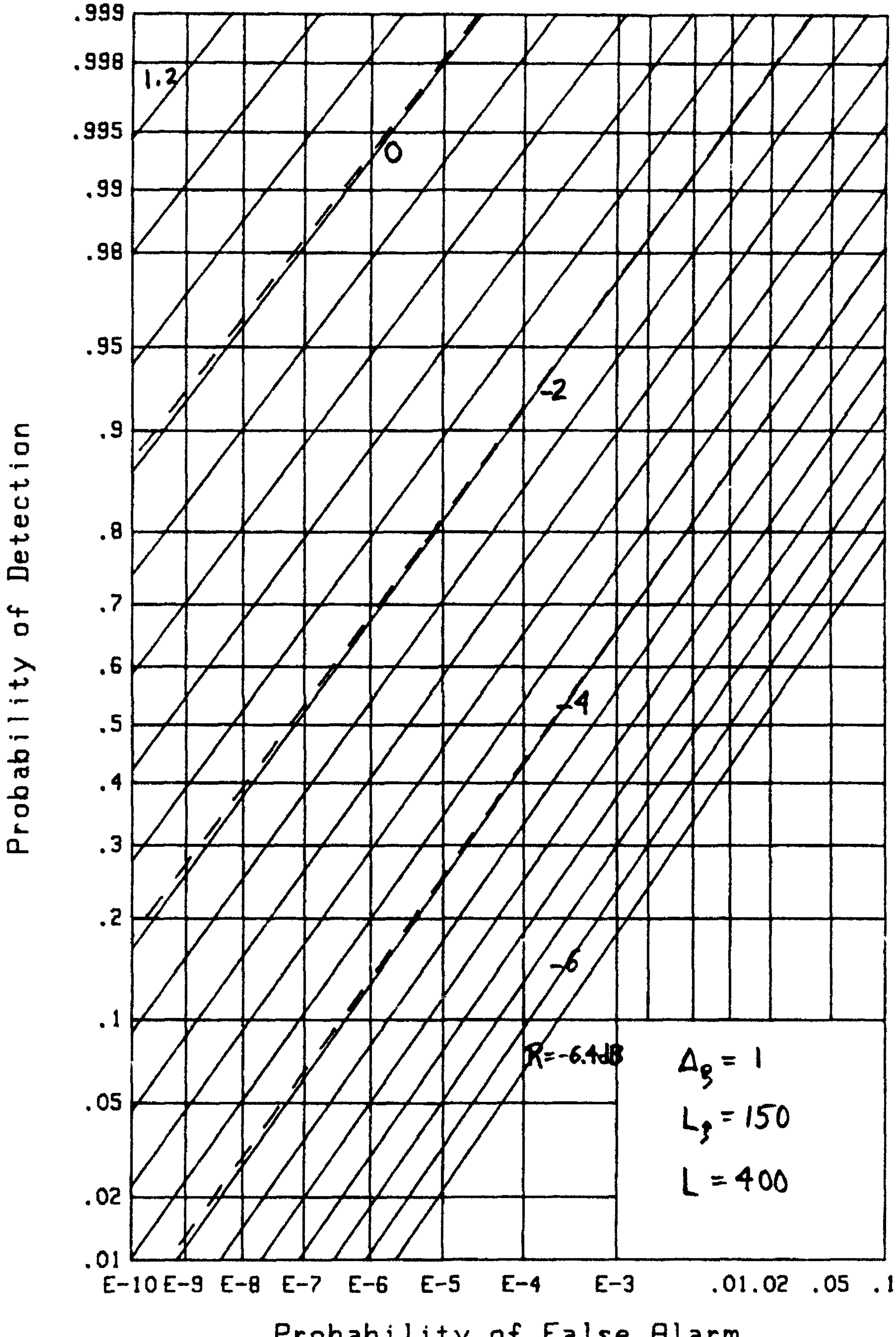

Figure 33. ROC for B=4, J=32, r=.95

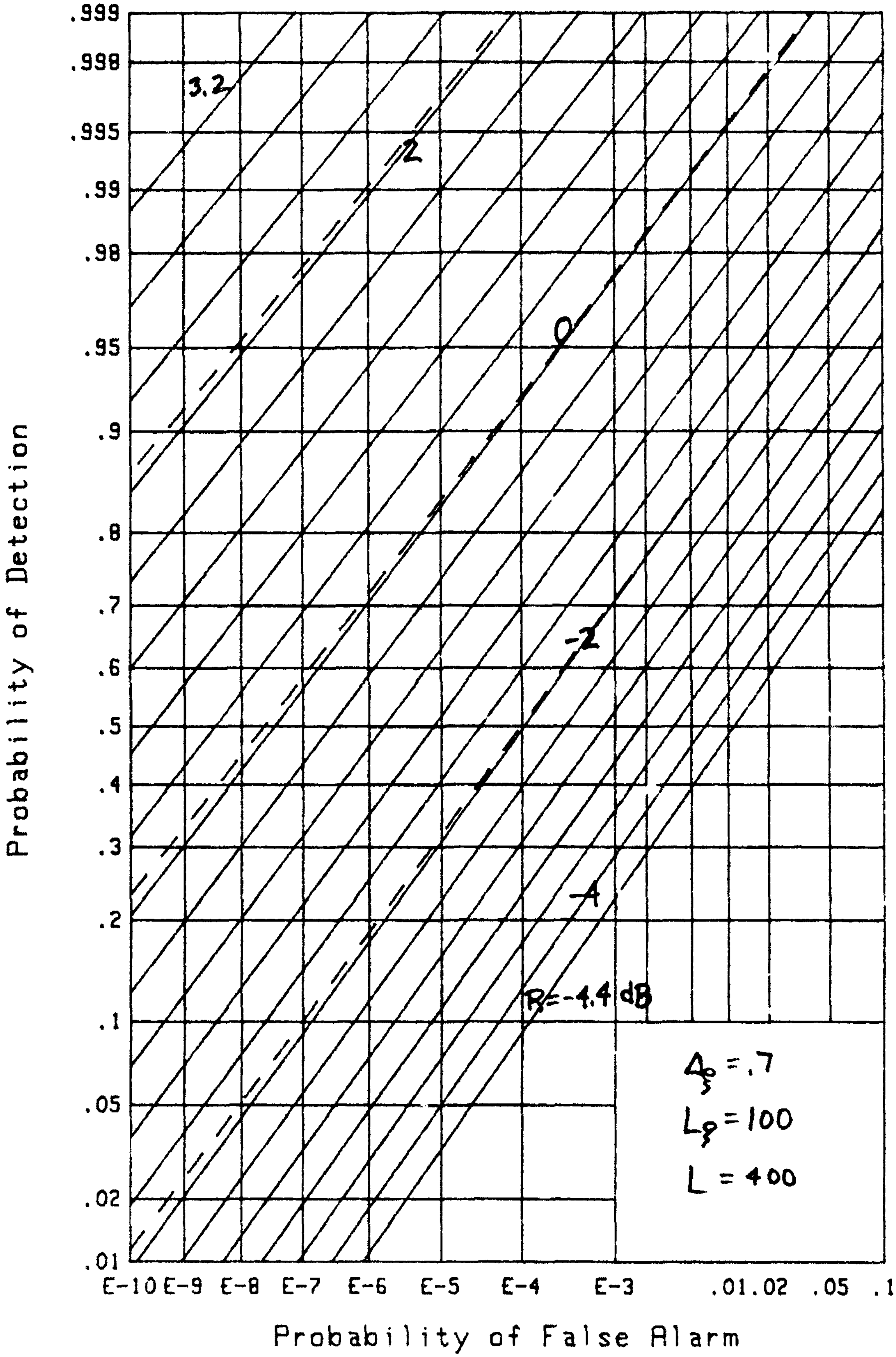

Figure 34. ROC for B=4, J=16, r=.9

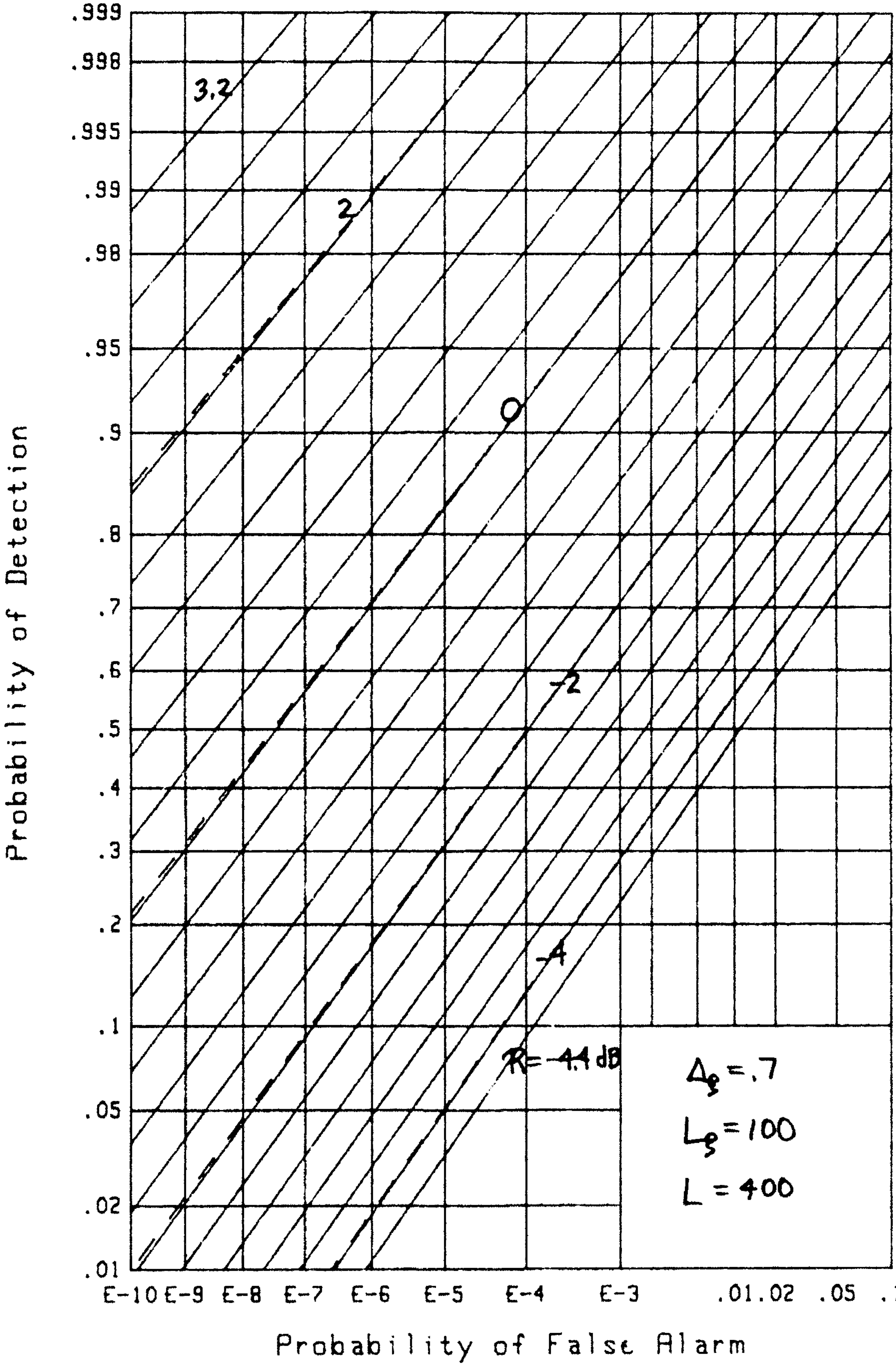

Figure 35. ROC for B=4, J=16, r=.9, fourth-order fits

SUMMARY

The receiver operating characteristics of a variety of weighted energy detectors, for Gaussian signals in noise, have been investigated exactly and compared with five different approximate procedures. The Gaussian and chi-squared approximations have been found to be generally inadequate for very small false alarm probabilities, while the generalized chi-squared (gamma) and both fourth-order fits have yielded very good results over the entire range of detection and false alarm probabilities considered. The only limitation of the latter approaches is the need to have additional cumulants (or moments), since the first two cumulants are not always entirely adequate for accurate performance predictions.

If the exact characteristic function for the decision variable of a system can be determined, either analytically or numerically, then the receiver operating characteristics can be accurately evaluated by the method of [2], as done here. However, there are occasions where it may be desirable or imperative to use an approximate characteristic function, as for example, when only a few low-order moments are known. In this fashion, we can, for example, avoid the determination of eigenvalues or avoid the evaluation of infinite products. Also, the approximate forms will frequently be faster to compute than the exact results. This report indicates the relative accuracies inherent in some of the standard approximations and some of their generalizations, which should be considered for future use.

APPENDIX A - GAUSSIAN APPROXIMATION

The characteristic function of interest was presented in (7):

$$f_x(\xi) = E\{\exp(i\xi x)\} = \prod_{m=1}^{M} f_z(w_m\xi) = \left[\prod_{m=1}^{M}\left(1 - i\xi w_m a\right)\right]^{-1}, \tag{A-1}$$

where $\{w_m\}$, for $1 \le m \le M$, are an arbitrary set of weights. The mean and variance of random variable x were given in (9).

Now, if energy detector output x in (1) were a Gaussian random variable, its probability density function would be

$$p_g(u) \equiv \frac{1}{(2\pi)^{\frac{1}{2}}\sigma_g} \exp\left(-\frac{(u-\mu_g)^2}{2\sigma_g^2}\right) \quad \text{for all } u , \tag{A-2}$$

where, from (9) and (4), we set

$$\mu_g = \left\{\begin{matrix} 1 \\ \text{or} \\ 1 + R \end{matrix}\right\}, \qquad \sigma_g^2 = \left\{\begin{matrix} W_2 \\ \text{or} \\ (1+R)^2\, W_2 \end{matrix}\right\}. \tag{A-3}$$

The exceedance distribution function corresponding to (A-2) is

$$Q_g(u) = \int_u^{\infty} dt\; p_g(t) = \Phi\left(\frac{\mu_g - u}{\sigma_g}\right) \quad \text{for all } u , \tag{A-4}$$

where

$$\Phi(t) \equiv \int_{-\infty}^{t} dv\; (2\pi)^{-\frac{1}{2}} \exp(-v^2/2) \tag{A-5}$$

is the normalized Gaussian cumulative distribution function.

At this point, it is convenient to define an effective number of samples, M_e, for an arbitrary set of weights $\{w_m\}$ as in (31)

$$M_e = \frac{\left(\sum_{m=1}^{M} w_m\right)^2}{\sum_{m=1}^{M} w_m^2} = \frac{W_1^2}{W_2} = \frac{1}{W_2} \; . \tag{A-6}$$

Here, we used (8) and (2).

If threshold T is utilized for a comparison with energy detector output x for a decision on signal presence or absence, then the approximate false alarm probability follows from (A-4):

$$P_F = Q_g(T;\ R=0) = \Phi\left(M_e^{\frac{1}{2}}(1-T)\right) \; , \tag{A-7}$$

with the help of (A-3) and (A-6). Similarly, the approximate detection probability is

$$P_D = Q_g(T;\ R\neq 0) = \Phi\left(M_e^{\frac{1}{2}}\left(1 - \frac{T}{1+R}\right)\right) \; . \tag{A-8}$$

Equations (A-7) and (A-8) produce the Gaussian approximation to the operating characteristics of the energy detector (1), described by characteristic function (A-1). They depend only on the single parameter M_e defined in (A-6), in addition to the per-sample signal-to-noise ratio R. That is, M and $\{w_m\}$ are all collapsed into the single parameter, effective number M_e.

An immediate obvious problem with (A-8) is that the limit of detection probability P_D, as $R \to \infty$, is not 1; in fact, it is $\Phi\left(M_e^{\frac{1}{2}}\right) < 1$. This drawback serves as a warning about the adequacy of the Gaussian approximation.

For the approximations in (A-7) and (A-8), we can explicitly solve for P_D in terms of P_F, as follows. Let $\underset{\sim}{\Phi}$ be the inverse function to Φ; see [10; 26.2.23]. Then (A-7) can be solved for threshold T according to

$$T = 1 - M_e^{-\frac{1}{2}} \underset{\sim}{\Phi}(P_F) \ . \qquad \text{(A-9)}$$

Substitution of this result into (A-8) yields

$$P_D = \Phi\left(\frac{M_e^{\frac{1}{2}} R + \underset{\sim}{\Phi}(P_F)}{1 + R}\right) \ . \qquad \text{(A-10)}$$

It now follows immediately from (A-10) that, for specified P_F and P_D, the required signal-to-noise ratio R is

$$R = \frac{D - F}{M_e^{\frac{1}{2}} - D} \ , \qquad \text{(A-11)}$$

where

$$F \equiv \underset{\sim}{\Phi}(P_F) \ , \quad D \equiv \underset{\sim}{\Phi}(P_D) \ . \qquad \text{(A-12)}$$

The result in (A-11) is a generalization of [1; (C-8) and (11)] to the case of arbitrary weights $\{w_m\}$. It is immediately obvious from the denominator of (A-11) that the desired P_D must be smaller than $\Phi\left(M_e^{\frac{1}{2}}\right)$.

APPENDIX B - POSITIVITY OF PARAMETER b_c

Here, we will show that the parameter b_c in (35) is never negative, regardless of the weight structure $\{w_m\}$, provided that $w_m \geq 0$. The Cauchy-Schwartz inequality states that

$$\left(\sum_{m=1}^{M} a_m \, b_m \right)^2 \leq \sum_{m=1}^{M} a_m^2 \sum_{m=1}^{M} b_m^2 \tag{B-1}$$

for any real quantities $\{a_m\}$ and $\{b_m\}$. If we let $a_m = w_m{}^{3/2}$ and $b_m = w_m{}^{1/2}$, then (B-1) yields

$$\left(\sum_{m=1}^{M} w_m^2 \right)^2 \leq \sum_{m=1}^{M} w_m^3 \sum_{m=1}^{M} w_m \; , \tag{B-2}$$

that is, $W_2^2 \leq W_3 \, W_1$, where

$$W_k = \sum_{m=1}^{M} w_m^k \; . \tag{B-3}$$

Therefore

$$b_c = W_1 - \frac{W_2^2}{W_3} \geq 0 \; . \tag{B-4}$$

In addition, there follows

$$M_c \, w_c = \frac{W_2^2}{W_3} \leq W_1 \; . \tag{B-5}$$

APPENDIX C - TRACE RELATIONS FOR EIGENVALUES

Suppose MxM matrix $P = [\rho_{mn}]$ has eigenvalues $\{\lambda_m\}$, $1 \le m \le M$. Let Λ be the diagonal matrix of eigenvalues $\{\lambda_m\}$ and let Q be the normalized modal matrix of eigenvectors of P; see [12; section 1.13]. Then we can express matrix P in the form

$$P = Q \, \Lambda \, Q^T \, , \tag{C-1}$$

from which there follows the k-th power

$$P^k = Q \, \Lambda^k \, Q^T \, . \tag{C-2}$$

We now use the trace relation

$$\mathrm{tr}(A \, B \, C) = \mathrm{tr}(B \, C \, A) \, , \tag{C-3}$$

to evaluate the trace of P^k:

$$\mathrm{tr}\left(P^k\right) = \mathrm{tr}\left(Q \, \Lambda^k \, Q^T\right) = \mathrm{tr}\left(\Lambda^k \, Q^T \, Q\right) = \mathrm{tr}\left(\Lambda^k\right) = \sum_{m=1}^{M} \lambda_m^k \, . \tag{C-4}$$

That is, the sum of the k-th powers of eigenvalues $\{\lambda_m\}$ can be obtained from the trace of matrix P^k, without ever having to evaluate the eigenvalues at all. In particular,

$$\sum_{m=1}^{M} \lambda_m = \mathrm{tr}(P) = \sum_{m=1}^{M} \rho_{mm} \, , \tag{C-5}$$

$$\sum_{m=1}^{M} \lambda_m^2 = \mathrm{tr}\left(P^2\right) = \sum_{m,n=1}^{M} \rho_{mn} \, \rho_{nm} \, , \tag{C-6}$$

$$\sum_{m=1}^{M} \lambda_m^3 = tr\left(P^3\right) = \sum_{m,n,k=1}^{M} \rho_{mn}\ \rho_{nk}\ \rho_{km} \ . \tag{C-7}$$

In order to compute the sums of the three lowest powers of the eigenvalues of matrix P, we simply have to compute the three sums on the elements of matrix P, as indicated in (C-5) through (C-7). In fact, there is no need to compute matrices P^2 or P^3 either. Thus, a seemingly difficult numerical chore is replaced by straightforward simple summations of products of matrix elements, yielding a very significant savings in complexity and time.

APPENDIX D - INVERSION OF EQUATION (60)

For notational efficiency, we suppress all the g subscripts in (60), let $y_k = \chi(k)/(k-1)!$, and set $p = M\,w$. The nonlinear equations then take the form

$$y_1 = b + p \;, \quad y_2 = 2\,b\,c + p\,w \;,$$
$$y_3 = 3\,b\,c^2 + p\,w^2 \;, \quad y_4 = 4\,b\,c^3 + p\,w^3 \;. \qquad \text{(D-1)}$$

We solve the first two equations for p and b, getting

$$p = \frac{y_2 - 2\,y_1\,c}{w - 2\,c} \;, \quad b = \frac{y_1\,w - y_2}{w - 2\,c} \;. \qquad \text{(D-2)}$$

These quantities are now substituted in the third and fourth equations in (D-1), resulting in the highly nonlinear pair of coupled equations for c and w:

$$c^2\,3\,(y_1\,w - y_2) + c\,2\,(y_3 - y_1\,w^2) + w\,(y_2\,w - y_3) = 0 \;, \qquad \text{(D-3)}$$
$$c^3\,4\,(y_1\,w - y_2) + c\,2\,(y_4 - y_1\,w^3) + w\,(y_2\,w^2 - y_4) = 0 \;. \qquad \text{(D-4)}$$

The procedure we have adopted for solving these latter two equations is to start with an initial guess for w as in (57), namely

$$w = \frac{\chi(4)/6}{\chi(3)/2} = \frac{y_4}{y_3} \;; \qquad \text{(D-5)}$$

then solve quadratic (D-3) for c; substitute this result into (D-4) and compute the left-hand side; now vary w until the left-hand side equals zero. Repeat these operations until c and w stabilize. Equation (D-2) can now be used to get final values of p and b. This is the numerical procedure used in the main text.

APPENDIX E - TERMINATION OF INFINITE PRODUCT

If we terminate the infinite product for the characteristic functions in (66) or (69) at limit value $m = L$ ($\geq N$), then the neglected remainder product in the denominator is

$$\text{Rem} = \prod_{m=L+1}^{\infty}\left(1 - i\xi\,(1-r)\,r^{m-1}\right) = 1 - i\xi r^{L} - \xi^{2}\,\frac{r^{2L+1}}{1+r} + O\left(r^{3L}\right). \quad \text{(E-1)}$$

This relation enables a choice of L to control the neglected remainder. For example, $\xi = 200$, $L = 220$, $r = .9$ leads to Rem = 1 - i1.7E-8 - 1.4E-16. Thus, the ξ^2 term and above can be safely ignored. One final product in the denominator of (66), by the factor $1 - i\xi r^{L}$, will account for Rem and suffice for complete accuracy, up to computer round-off error in the characteristic function evaluation. For larger values of r, it is necessary to increase the limit L; for example, $\xi = 150$, $L = 700$, $r = .96915298$ yields Rem = 1 - i4.5E-8 - 1E-15.

If we terminate the infinite product for the characteristic function in (77) at limit value $j = L$ ($\geq J-1$), the neglected remainder product in the denominator is

$$\text{Rem} = \left[\prod_{j=L+1}^{\infty}\left(1 - i\xi\,\frac{1-r}{B}\,r^{j}\right)\right]^{B} \sim \left(1 - \frac{i\xi}{B}\,r^{L+1}\right)^{B} \sim 1 - i\xi\,r^{L+1}. \quad \text{(E-2)}$$

This is substantially the same as (E-1), where terms of the order of r^{2L} have been neglected.

REFERENCES

[1] A. H. Nuttall and A. F. Magaraci, **Signal-to-Noise Ratios Required for Short-Term Narrowband Detection of Gaussian Processes**, NUSC Technical Report 4417, Naval Underwater Systems Center, New London, CT, 20 October 1972.

[2] A. H. Nuttall, **Accurate Efficient Evaluation of Cumulative or Exceedance Probability Distributions Directly From Characteristic Functions**, NUSC Technical Report 7023, Naval Underwater Systems Center, New London, CT, 1 October 1983.

[3] A. H. Nuttall, **Exact Performance of General Second-Order Processors for Gaussian Inputs**, NUSC Technical Report 7035, Naval Underwater Systems Center, New London, CT, 15 October 1983.

[4] A. H. Nuttall and B. Dedreux, **Exact Operating Characteristics for Linear Sum of Envelopes of Narrowband Gaussian Process and Sinewave**, NUSC Technical Report 7117, Naval Underwater Systems Center, New London, CT, 11 January 1984.

[5] A. H. Nuttall, **Operating Characteristics of Cross-Correlator With or Without Sample Mean Removal**, NUSC Technical Report 7045, Naval Underwater Systems Center, New London, CT, 14 August 1984.

[6] A. H. Nuttall, **Probability Distribution of Spectral Estimates Obtained via Overlapped FFT Processing of Windowed Data**, NUSC Technical Report 5529, Naval Underwater Systems Center, New London, CT, 3 December 1976.

[7] A. H. Nuttall, **Operating Characteristics for Detection of a Fading Signal with K Dependent Fades and D-fold Diversity in M Alternative Locations**, NUSC Technical Report 5739, Naval Underwater Systems Center, New London, CT, 25 October 1977.

[8] I. Kanter, "Exact Detection Probability for Partially Correlated Rayleigh Targets", **IEEE Transactions on Aerospace and Electronics Systems**, volume AES-22, number 2, pages 184 - 195, March 1986.

[9] A. H. Nuttall and E. S. Eby, **Signal-to-Noise Ratio Requirements for Detection of Multiple Pulses Subject to Partially Correlated Fading With Chi-Squared Statistics of Various Degrees of Freedom**, NUSC Technical Report 7707, Naval Underwater Systems Center, New London, CT, 2 June 1986.

[10] **Handbook of Mathematical Functions**, U. S. Department of Commerce, National Bureau of Standards, Applied Mathematics Series Number 55, U. S. Government Printing Office, Washington, DC, June 1964.

[11] E. R. Hansen, **A Table of Series and Products**, Prentice-Hall, Inc., Englewood Cliffs, NJ, 1975.

[12] F. B. Hildebrand, **Methods of Applied Mathematics**, Prentice-Hall, Inc., New York, NY, 1954.

NUSC Technical Report 8759
6 August 1990

Two-Dimensional Convolutions, Correlations, and Fourier Transforms of Combinations of Wigner Distribution Functions and Complex Ambiguity Functions

Albert H. Nuttall

ABSTRACT

A number of new two-dimensional Fourier transforms of combinations of cross Wigner distribution functions, W, of convolution form or correlation form are derived. In addition, similar relations are obtained for combinations of cross complex ambiguity functions, χ. Their great generality subsumes most of the already known available properties, such as: the volume constraint of magnitude-squared ambiguity functions; the positivity of the convolution of two Wigner distribution functions; and Moyal's theorem. An example is displayed below:

$$\iint d\nu' d\tau' \exp(+i2\pi\nu' t - i2\pi f\tau') \, \chi_{ab}(\nu+\tfrac{1}{2}\nu', \tau+\tfrac{1}{2}\tau') \, \chi^*_{cd}(\nu-\tfrac{1}{2}\nu', \tau-\tfrac{1}{2}\tau')$$

$$= \iint dt' df' \exp(-i2\pi\nu t' + i2\pi f'\tau) \, W_{ab}(t+\tfrac{1}{2}t', f+\tfrac{1}{2}f') \, W^*_{cd}(t-\tfrac{1}{2}t', f-\tfrac{1}{2}f')$$

$$= W_{ac}(t+\tfrac{1}{2}\tau, f+\tfrac{1}{2}\nu) \, W^*_{bd}(t-\tfrac{1}{2}\tau, f-\tfrac{1}{2}\nu) \; .$$

Extensions to contracted time and frequency arguments are made, as well as to mixed products involving a Wigner distribution function and a complex ambiguity function. Additional relationships connecting the temporal correlation function and the spectral correlation function complete a symmetric set of very general relationships.

TABLE OF CONTENTS

LIST OF ILLUSTRATIONS

LIST OF ABBREVIATIONS

TCF	temporal correlation function, (49)
SCF	spectral correlation function, (51)
CAF	complex ambiguity function, (53), (72)
WDF	Wigner distribution function, (55), (73)

LIST OF SYMBOLS

t	time, (1)
$g(t)$	arbitrary complex function of time, (1)
f	frequency, (1)
$G(f)$	Fourier transform of g(t), $g(t) \leftrightarrow G(f)$, (1)
h,H	Fourier transform pair, (4)
ν	frequency shift or separation, (4), (27), (51)
α,β,μ,γ	real constants, (4)
x,X	Fourier transform pair, (10), (11)
ψ_{xx}	auto-correlation of x, (11)
C_{xy}	convolution of x and y, (16)

ψ_{xy}	cross-correlation of x and y, (21)
R, W, χ, Φ	general two-dimensional functions, figure 1, (27)-(34)
τ	time delay or separation, (27), (49)
I	two-dimensional convolution and Fourier transform, (39)
J	two-dimensional correlation and Fourier transform, (43)
R_{ab}	cross temporal correlation function (TCF), (49)
Φ_{ab}	cross spectral correlation function (SCF), (51)
χ_{ab}	cross complex ambiguity function (CAF), (53), (72)
W_{ab}	cross Wigner distribution function (WDF), (55), (73)
$\underset{\sim}{W}_{ab}$	scaled and contracted WDF, (61)
ψ_{ab}	cross-correlation of a(t) and b(t), (64)
Ψ_{ab}	cross-spectrum of a(t) and b(t), (65)
$\underline{a}(t)$	mirror-image function of a(t), (69)
χ_{AB}	definition of CAF in frequency domain, (72)
W_{AB}	definition of WDF in frequency domain, (73)
$\zeta_n(t)$	n-th orthonormal Hermite function, (107)
W_{km}	cross WDF between ζ_k and ζ_m, (109)
α	contraction factor, (C-1)
$\underset{\sim}{a}(t)$	contracted waveform, (C-1)
K	more general two-dimensional transform, (C-3)
p	contraction parameter, (C-5)
W_{ab}	generalized WDF, (C-5)

TWO-DIMENSIONAL CONVOLUTIONS, CORRELATIONS, AND FOURIER TRANSFORMS OF COMBINATIONS OF WIGNER DISTRIBUTION FUNCTIONS AND COMPLEX AMBIGUITY FUNCTIONS

INTRODUCTION

Over the years, a number of properties of integrals of products of complex ambiguity functions (CAFs) or products of Wigner distribution functions (WDFs) have been derived, such as: the volume constraint of magnitude-squared ambiguity functions [1; page 308], the positivity of the convolution of any two WDFs [2; (106)], and Moyal's theorem involving the volume under the square of a WDF [3]. Now, it appears that these are very special cases of a general class of two-dimensional Fourier transforms of combinations of CAFs and WDFs with delayed or time-reversed arguments.

We begin by deriving a general one-dimensional transform relation involving two arbitrary complex waveforms and their Fourier transforms. An application of this relation to energy density spectra yields three alternative expressions for the output correlation of a filtered time function. This general transform relation is also the basic tool for setting up the two-dimensional transforms that are the subject of succeeding sections. The extreme generality of the two-dimensional relations allows for a large number of special cases; some of these are pointed out, but undoubtedly there are additional ones not listed here.

When we begin our two-dimensional transform investigation, we do not immediately specialize to WDFs or CAFs. Rather, we first consider a set of four general functions, each of two variables, all of which are related to each other by Fourier transforms. We show that two-dimensional Fourier transforms of products of pairs of these general functions are all equal to a common value, although that value cannot be expressed in any simple closed form. These relations are derived for convolution type operations as well as for correlation operations.

When we make a specialization of these results to waveforms, relatively simple closed form results, in terms of products of WDFs and CAFs, are obtained for these two-dimensional transforms. And when the arguments of these relations are further specialized in value (such as zero), some of the currently known relations involving CAFs and WDFs result.

Extensions of these results to time contracted or expanded arguments are made in the appendices. Again, specializations to waveforms yield closed form results, in terms of products of WDFs and/or CAFs.

ONE-DIMENSIONAL TRANSFORM RELATIONS

Function g(t) is an arbitrary complex function of real argument t, which will be thought of as time. Its Fourier transform will be denoted by complex function G(f), where

$$G(f) = \int dt \, \exp(-i2\pi ft) \, g(t) \; . \tag{1}$$

Integrals without limits are along the real axis and over the range of nonzero integrand. Argument f is a real cyclic frequency, not a radian frequency. The inverse Fourier transform relation to (1) is

$$g(t) = \int df \, \exp(+i2\pi ft) \, G(f) \; . \tag{2}$$

The Fourier transform pair in (1) and (2) will be denoted by

$$g(t) \leftrightarrow G(f) \; . \tag{3}$$

Similarly, h(t) and H(f) will be a Fourier transform pair.

TRANSFORM OF PRODUCT OF WAVEFORMS

The variables $\nu,\alpha,\beta,\mu,\gamma$ are all real in the following. A generalization of Parseval's theorem is then possible, namely

$$\int dt' \, \exp(-i2\pi\nu t') \, g(\alpha t+\beta t') \, h^*(\mu t+\gamma t') = \exp\left(i2\pi\nu t\frac{\alpha\gamma+\beta\mu}{2\beta\gamma}\right) \times$$

$$\times \int d\nu' \, \exp\left(i2\pi\nu' t(\alpha\gamma-\beta\mu)\right) \, G\left(\gamma\left(\nu'+\frac{\nu}{2\beta\gamma}\right)\right) \, H^*\left(\beta\left(\nu'-\frac{\nu}{2\beta\gamma}\right)\right) \; , \tag{4}$$

where it is presumed that $\beta \neq 0$ and $\gamma \neq 0$. This result may be derived by substituting for g according to (2), interchanging integrals, and using (1) for Fourier transform pair $h(t) \Leftrightarrow H(f)$. A more symmetric form for relation (4) is available, if desired:

$$\int dt' \exp(-i2\pi\nu t')\; g\left(\beta\left(t'+\frac{t}{2\beta\gamma}\right)\right)\; h^*\left(\gamma\left(t'-\frac{t}{2\beta\gamma}\right)\right) =$$

$$= \int d\nu' \exp(+i2\pi\nu' t)\; G\left(\gamma\left(\nu'+\frac{\nu}{2\beta\gamma}\right)\right)\; H^*\left(\beta\left(\nu'-\frac{\nu}{2\beta\gamma}\right)\right) . \qquad (5)$$

SPECIAL CASES

By specializing the parameter values in (4), several interesting and useful results can be obtained. For example, if we take $\gamma = \beta$, $\mu = -\alpha$, then we obtain a combined one-dimensional Fourier transform and correlation:

$$\int dt' \exp(-i2\pi\nu t')\; g(\beta t'+\alpha t)\; h^*(\beta t'-\alpha t) =$$

$$= \int d\nu' \exp\left(i2\pi\nu' t 2\alpha\beta\right)\; G\left(\beta\nu'+\frac{\nu}{2\beta}\right)\; H^*\left(\beta\nu'-\frac{\nu}{2\beta}\right) . \qquad (6)$$

On the other hand, if we take $\gamma = -\beta$, $\mu = \alpha$ in (4), there follows a combined one-dimensional Fourier transform and convolution:

$$\int dt' \exp(-i2\pi\nu t')\; g(\alpha t+\beta t')\; h^*(\alpha t-\beta t') =$$

$$= \int d\nu' \exp\left(i2\pi\nu' t 2\alpha\beta\right)\; G\left(\frac{\nu}{2\beta}+\beta\nu'\right)\; H^*\left(\frac{\nu}{2\beta}-\beta\nu'\right) . \qquad (7)$$

Further specialization to the specific numerical values $\gamma = \beta = 1$, $-\mu = \alpha = \frac{1}{2}$, in (6) yields

$$\int dt' \exp(-i2\pi\nu t')\, g(t'+\tfrac{1}{2}t)\, h^*(t'-\tfrac{1}{2}t) =$$

$$= \int d\nu' \exp(+i2\pi\nu' t)\, G(\nu'+\tfrac{1}{2}\nu)\, H^*(\nu'-\tfrac{1}{2}\nu) \ . \qquad (8)$$

Alternatively, the choice $-\gamma = \beta = \frac{1}{2}$, $\mu = \alpha = 1$ in (7) yields

$$\int dt' \exp(-i2\pi\nu t')\, g(t+\tfrac{1}{2}t')\, h^*(t-\tfrac{1}{2}t') =$$

$$= \int d\nu' \exp(+i2\pi\nu' t)\, G(\nu+\tfrac{1}{2}\nu')\, H^*(\nu-\tfrac{1}{2}\nu') \ . \qquad (9)$$

APPLICATION TO ENERGY DENSITY SPECTRA

Case 1. Suppose that we choose

$$G(\nu) = |X(\nu)|^2 \ , \quad H(\nu) = |Y(\nu)|^2 \ , \qquad (10)$$

which are the energy density spectra of waveforms x(t) and y(t), respectively. Then $g(t) = \psi_{xx}(t)$ and $h(t) = \psi_{yy}(t)$, where $\psi_{xx}(t)$ is the auto-correlation function of complex waveform x(t):

$$\psi_{xx}(t) = \int du\, x(t + u)\, x^*(u) \ . \qquad (11)$$

The use of (10) and (11) in (8) yields

$$I_1(t,\nu) \equiv \int d\nu' \exp(+i2\pi\nu' t) \; |X(\nu'+\tfrac{1}{2}\nu)|^2 \; |Y(\nu'-\tfrac{1}{2}\nu)|^2 =$$

$$= \int dt' \exp(-i2\pi\nu t') \; \psi_{xx}(t'+\tfrac{1}{2}t) \; \psi^*_{yy}(t'-\tfrac{1}{2}t) \; . \qquad (12)$$

The last term in (12) is identical to $\psi_{yy}(\frac{1}{2}t-t')$.

The special case of $\nu = 0$ in (12) reduces to

$$I_1(t,0) = \int d\nu' \exp(+i2\pi\nu' t) \; |X(\nu')|^2 \; |Y(\nu')|^2 =$$

$$= \int dt' \; \psi_{xx}(t'+\tfrac{1}{2}t) \; \psi^*_{yy}(t'-\tfrac{1}{2}t) \; . \qquad (13)$$

The additional restriction to $t = 0$ becomes

$$I_1(0,0) = \int d\nu' \; |X(\nu')|^2 \; |Y(\nu')|^2 =$$

$$= \int dt' \; \psi_{xx}(t') \; \psi^*_{yy}(t') \; . \qquad (14)$$

Case 2. Here, instead, make the identifications

$$G(\nu) = X(\nu) \; Y(\nu) = H(\nu) \; . \qquad (15)$$

Then

$$g(t) = C_{xy}(t) \equiv \int du \; x(u) \; y(t-u) = h(t) \; , \qquad (16)$$

which is the convolution of $x(t)$ and $y(t)$. Substitution of (15) and (16) in (8) gives

$$I_2(t,\nu) \equiv \int d\nu' \exp(+i2\pi\nu' t)\ X(\nu'+\tfrac{1}{2}\nu)\ Y(\nu'+\tfrac{1}{2}\nu)\ X^*(\nu'-\tfrac{1}{2}\nu)\ Y^*(\nu'-\tfrac{1}{2}\nu)$$

$$= \int dt' \exp(-i2\pi\nu t')\ C_{xy}(t'+\tfrac{1}{2}t)\ C^*_{xy}(t'-\tfrac{1}{2}t)\ . \tag{17}$$

Setting ν to zero yields

$$I_2(t,0) = \int d\nu' \exp(+i2\pi\nu' t)\ |X(\nu')|^2\ |Y(\nu')|^2 =$$

$$= \int dt'\ C_{xy}(t'+\tfrac{1}{2}t)\ C^*_{xy}(t'-\tfrac{1}{2}t)\ . \tag{18}$$

Finally, also setting t equal to zero,

$$I_2(0,0) = \int d\nu'\ |X(\nu')|^2\ |Y(\nu')|^2 = \int dt'\ |C_{xy}(t')|^2\ . \tag{19}$$

<u>Case 3.</u> Now identify

$$G(\nu) = X(\nu)\ Y^*(\nu) = H(\nu)\ . \tag{20}$$

Then

$$g(t) = \psi_{xy}(t) \equiv \int du\ x(u+t)\ y^*(u) = h(t)\ , \tag{21}$$

which is the cross-correlation of x(t) and y(t). The use of (20) and (21) in (8) leads to

$$I_3(t,\nu) \equiv \int d\nu' \exp(+i2\pi\nu' t)\ X(\nu'+\tfrac{1}{2}\nu)\ Y^*(\nu'+\tfrac{1}{2}\nu)\ X^*(\nu'-\tfrac{1}{2}\nu)\ Y(\nu'-\tfrac{1}{2}\nu)$$

$$= \int dt' \exp(-i2\pi\nu t')\ \psi_{xy}(t'+\tfrac{1}{2}t)\ \psi^*_{xy}(t'-\tfrac{1}{2}t)\ . \tag{22}$$

The result of setting ν to zero is

$$I_3(t,0) = \int d\nu' \exp(+i2\pi\nu' t) \, |X(\nu')|^2 \, |Y(\nu')|^2 =$$

$$= \int dt' \, \psi_{xy}(t'+\tfrac{1}{2}t) \, \psi_{xy}^*(t'-\tfrac{1}{2}t) \ . \qquad (23)$$

When t is also set equal to zero, (23) reduces to

$$I_3(0,0) = \int d\nu' \, |X(\nu')|^2 \, |Y(\nu')|^2 = \int dt' \, |\psi_{xy}(t')|^2 \ . \qquad (24)$$

It should be observed that the upper lines of (13), (18), and (23) are identical to each other; that is,

$$I_1(t,0) = I_2(t,0) = I_3(t,0) \ . \qquad (25)$$

Therefore, the lower lines of (13), (18), and (23) furnish three equal alternative expressions involving autocorrelations, convolutions, or cross-correlations, respectively.

There are many other possibilities for identifications of G and H in (8), besides (10), (15), and (20). For example, we could take

$$G(\nu) = |X(\nu)|^2 \, Y(\nu) \ , \quad H(\nu) = Y(\nu) \ . \qquad (26)$$

However, it may be shown that this choice leads identically to result (13) when ν is set to zero; so not all selections yield new relations. Additional convolution type relations may be obtained if (9) is used instead of (8).

GENERAL TWO-DIMENSIONAL TRANSFORM RELATIONS

In this section, we will consider a set of four general functions, each of two variables, which are related to each other by Fourier transforms. These four functions are indicated in figure 1, where a two-headed arrow denotes a Fourier transform relationship. These functions are, for the moment, <u>arbitrary</u> complex functions of two variables; they are <u>not</u> necessarily Wigner distribution functions or complex ambiguity functions.

$$\begin{tikzcd} R(t,\tau) \arrow[r, leftrightarrow] \arrow[d, leftrightarrow] & \chi(\nu,\tau) \arrow[d, leftrightarrow] \\ W(t,f) \arrow[r, leftrightarrow] & \Phi(\nu,f) \end{tikzcd}$$

Figure 1. General Two-Dimensional Functions

The paired transform variables, here and for the rest of the report, are $t \leftrightarrow \nu$ and $\tau \leftrightarrow f$. The detailed Fourier transform interrelationships between the four functions in figure 1 are

$$\chi(\nu,\tau) = \int dt \, \exp(-i2\pi\nu t) \, R(t,\tau) \, , \tag{27}$$

$$R(t,\tau) = \int d\nu \, \exp(+i2\pi\nu t) \, \chi(\nu,\tau) \, , \tag{28}$$

$$W(t,f) = \int d\tau \, \exp(-i2\pi f\tau) \, R(t,\tau) \, , \tag{29}$$

$$R(t,\tau) = \int df \, \exp(+i2\pi f\tau) \, W(t,f) \, , \tag{30}$$

$$\Phi(\nu,f) = \int dt \, \exp(-i2\pi\nu t) \, W(t,f) \, , \tag{31}$$

$$W(t,f) = \int d\nu \, \exp(+i2\pi\nu t) \, \Phi(\nu,f) \, , \tag{32}$$

$$\Phi(\nu,f) = \int d\tau \, \exp(-i2\pi f\tau) \, \chi(\nu,\tau) \, , \tag{33}$$

$$\chi(\nu,\tau) = \int df \, \exp(+i2\pi f\tau) \, \Phi(\nu,f) \, . \tag{34}$$

A double Fourier transform relationship exists between R and Φ, as well as between W and χ.

TWO-DIMENSIONAL CONVOLUTIONS

We repeat (9) here, but with a change of variables $t \to \tau$ and $\nu \to f$:

$$\int d\tau' \, \exp(-i2\pi f\tau') \, g(\tau+\tfrac{1}{2}\tau') \, h^*(\tau-\tfrac{1}{2}\tau') =$$

$$= \int df' \, \exp(+i2\pi f'\tau) \, G(f+\tfrac{1}{2}f') \, H^*(f-\tfrac{1}{2}f') \, . \tag{35}$$

Let χ_1 and χ_2 be two different functions of the type indicated in figure 1, and consider (35) with the assignments

$$g(\tau) = \chi_1(\nu_a,\tau) \, , \quad h(\tau) = \chi_2(\nu_b,\tau) \, . \tag{36}$$

The corresponding Fourier transform pairs for (36) are

$$G(f) = \Phi_1(\nu_a,f) \, , \quad H(f) = \Phi_2(\nu_b,f) \, , \tag{37}$$

upon use of (33). There follows, from (35),

$$\int d\tau' \exp(-i2\pi f\tau')\ \chi_1(\nu_a,\tau+\tfrac{1}{2}\tau')\ \chi_2^*(\nu_b,\tau-\tfrac{1}{2}\tau') =$$

$$= \int df' \exp(+i2\pi f'\tau)\ \Phi_1(\nu_a,f+\tfrac{1}{2}f')\ \Phi_2^*(\nu_b,f-\tfrac{1}{2}f')\ . \tag{38}$$

See appendix A for the most general result of this form.

If we now let $\nu_a = \nu+\frac{1}{2}\nu'$ and $\nu_b = \nu-\frac{1}{2}\nu'$ in (38), then an additional Fourier transform on ν' yields the middle two lines in (39) below. More generally, in a similar fashion to that used above, we find that the combined two-dimensional convolution and Fourier transform can be expressed in four equivalent forms:

$$I(\nu,f,t,\tau) \equiv \tag{39}$$

$$= \iint dt'd\tau' \exp(-i2\pi\nu t'-i2\pi f\tau')\ R_1(t+\tfrac{1}{2}t',\tau+\tfrac{1}{2}\tau')\ R_2^*(t-\tfrac{1}{2}t',\tau-\tfrac{1}{2}\tau') =$$

$$= \iint d\nu'd\tau' \exp(+i2\pi\nu' t-i2\pi f\tau')\ \chi_1(\nu+\tfrac{1}{2}\nu',\tau+\tfrac{1}{2}\tau')\ \chi_2^*(\nu-\tfrac{1}{2}\nu',\tau-\tfrac{1}{2}\tau') =$$

$$= \iint d\nu'df' \exp(+i2\pi\nu' t+i2\pi f'\tau)\ \Phi_1(\nu+\tfrac{1}{2}\nu',f+\tfrac{1}{2}f')\ \Phi_2^*(\nu-\tfrac{1}{2}\nu',f-\tfrac{1}{2}f') =$$

$$= \iint dt'df' \exp(-i2\pi\nu t'+i2\pi f'\tau)\ W_1(t+\tfrac{1}{2}t',f+\tfrac{1}{2}f')\ W_2^*(t-\tfrac{1}{2}t',f-\tfrac{1}{2}f')\ .$$

Alternative forms of (39) are available; for example, the last line can be written in the more typical convolution form

$$\iint dt'df' \exp(-i2\pi\nu t'+i2\pi f'\tau)\ W_1(t',f')\ W_2^*(t-t',f-f') =$$

$$= \frac{1}{4} \exp(-i\pi\nu t+i\pi f\tau)\ I(\tfrac{1}{2}\nu,\tfrac{1}{2}f,\tfrac{1}{2}t,\tfrac{1}{2}\tau)\ . \tag{40}$$

TWO-DIMENSIONAL CORRELATIONS

Here, we use (8) with identifications

$$g(t) = R_1(t,\tau_a) \ , \quad h(t) = R_2(t,\tau_b) \ ,$$
$$G(\nu) = \chi_1(\nu,\tau_a) \ , \quad H(\nu) = \chi_2(\nu,\tau_b) \ . \qquad (41)$$

Then there follows immediately

$$\int dt' \, \exp(-i2\pi\nu t') \, R_1(t'+\tfrac{1}{2}t,\tau_a) \, R_2^*(t'-\tfrac{1}{2}t,\tau_b) =$$
$$= \int d\nu' \, \exp(+i2\pi\nu' t) \, \chi_1(\nu'+\tfrac{1}{2}\nu,\tau_a) \, \chi_2^*(\nu'-\tfrac{1}{2}\nu,\tau_b) \ . \qquad (42)$$

Now let $\tau_a = \tau'+\frac{1}{2}\tau$ and $\tau_b = \tau'-\frac{1}{2}\tau$, and Fourier transform on τ'. The result is the first two relations, given below, of four equivalent forms of the combined two-dimensional correlation and Fourier transform

$$J(\nu,f,t,\tau) \equiv \qquad (43)$$
$$= \iint dt'd\tau' \, \exp(-i2\pi\nu t'-i2\pi f\tau') \, R_1(t'+\tfrac{1}{2}t,\tau'+\tfrac{1}{2}\tau) \, R_2^*(t'-\tfrac{1}{2}t,\tau'-\tfrac{1}{2}\tau) =$$
$$= \iint d\nu'd\tau' \, \exp(+i2\pi\nu' t-i2\pi f\tau') \, \chi_1(\nu'+\tfrac{1}{2}\nu,\tau'+\tfrac{1}{2}\tau) \, \chi_2^*(\nu'-\tfrac{1}{2}\nu,\tau'-\tfrac{1}{2}\tau) =$$
$$= \iint d\nu'df' \, \exp(+i2\pi\nu' t+i2\pi f'\tau) \, \Phi_1(\nu'+\tfrac{1}{2}\nu,f'+\tfrac{1}{2}f) \, \Phi_2^*(\nu'-\tfrac{1}{2}\nu,f'-\tfrac{1}{2}f) =$$
$$= \iint dt'df' \, \exp(-i2\pi\nu t'+i2\pi f'\tau) \, W_1(t'+\tfrac{1}{2}t,f'+\tfrac{1}{2}f) \, W_2^*(t'-\tfrac{1}{2}t,f'-\tfrac{1}{2}f) \ .$$

Alternative forms to (43) are possible; for example, the last line can be expressed in the more typical correlation form

$$\iint dt'df' \exp(-i2\pi\nu t'+i2\pi f'\tau)\ W_1(t',f')\ W_2^*(t'-t,f'-f) =$$

$$= \exp(-i\pi\nu t+i\pi f\tau)\ J(\nu,f,t,\tau)\ . \qquad (44)$$

MIXED RELATIONS

The results in (39) and (43) all involve two $W(t,f)$ functions, or two $\chi(\nu,\tau)$ functions, etc. However, it is possible to obtain relations which involve, for example, one $W(t,f)$ function and one $\chi(\nu,\tau)$ function. As an illustrative example, consider (9) with $g(t) = W_1(t,f_a)$ and $h(t) = \chi_2(f_b,t)$. Then, from figure 1, $G(\nu) = \Phi_1(\nu,f_a)$ and $H(\nu) = \Phi_2(f_b,\nu)$, giving

$$\int dt' \exp(-i2\pi\nu t')\ W_1(t+\tfrac{1}{2}t',f_a)\ \chi_2^*(f_b,t-\tfrac{1}{2}t') =$$

$$= \int d\nu' \exp(+i2\pi\nu' t)\ \Phi_1(\nu+\tfrac{1}{2}\nu',f_a)\ \Phi_2^*(f_b,\nu-\tfrac{1}{2}\nu')\ . \qquad (45)$$

If we now let $f_a = f+\frac{1}{2}f'$ and $f_b = f-\frac{1}{2}f'$, and perform a Fourier transform on f', there follows immediately

$$\iint dt'df' \exp(-i2\pi\nu t'+i2\pi f'\tau)\ W_1(t+\tfrac{1}{2}t',f+\tfrac{1}{2}f')\ \chi_2^*(f-\tfrac{1}{2}f',t-\tfrac{1}{2}t') =$$

$$(46)$$

$$= \iint d\nu'df' \exp(+i2\pi\nu' t+i2\pi f'\tau)\ \Phi_1(\nu+\tfrac{1}{2}\nu',f+\tfrac{1}{2}f')\ \Phi_2^*(f-\tfrac{1}{2}f',\nu-\tfrac{1}{2}\nu')\ .$$

Thus, a combined two-dimensional convolution and Fourier transform of a $W(t,f)$ function and a $\chi(\nu,\tau)$ function can be expressed in terms of two $\Phi(\nu,f)$ functions. (Strictly, some of the arguments are reversed, as seen in (46).)

If, instead, we use (8) with g(t) and h(t) assigned as above, then we obtain

$$\int dt' \exp(-i2\pi\nu t')\ W_1(t'+\tfrac{1}{2}t, f_a)\ \chi_2^*(f_b, t'-\tfrac{1}{2}t) =$$

$$= \int d\nu' \exp(+i2\pi\nu' t)\ \Phi_1(\nu'+\tfrac{1}{2}\nu, f_a)\ \Phi_2^*(f_b, \nu'-\tfrac{1}{2}\nu) \ . \qquad (47)$$

Letting $f_a = f'+\tfrac{1}{2}f$, $f_b = f'-\tfrac{1}{2}f$, and performing an additional Fourier transform on f', there follows

$$\iint dt'df' \exp(-i2\pi\nu t'+i2\pi f'\tau)\ W_1(t'+\tfrac{1}{2}t, f'+\tfrac{1}{2}f)\ \chi_2^*(f'-\tfrac{1}{2}f, t'-\tfrac{1}{2}t) =$$

$$(48)$$

$$= \iint d\nu' df' \exp(+i2\pi\nu' t+i2\pi f'\tau)\ \Phi_1(\nu'+\tfrac{1}{2}\nu, f'+\tfrac{1}{2}f)\ \Phi_2^*(f'-\tfrac{1}{2}f, \nu'-\tfrac{1}{2}\nu) \ .$$

Here, a combined two-dimensional correlation and Fourier transform of a $W(t,f)$ function and a $\chi(\nu,\tau)$ function can be expressed in terms of two $\Phi(\nu,f)$ functions. (Again, some arguments are reversed or replaced. However, the first argument in a χ function is always a frequency variable, while the second argument is always a time variable; similar restrictions hold for the remaining functions R, W, Φ in figure 1.)

SPECIALIZATION TO WAVEFORMS

In the previous section, the functions R, W, χ, Φ were arbitrary, except that they were related by Fourier transforms according to figure 1. Here, we will specialize their forms, thereby enabling more explicit relations for their two-dimensional convolutions and correlations.

For arbitrary complex waveforms a(t), b(t), c(t), d(t), let

$$R_1(t,\tau) = a(t+\tfrac{1}{2}\tau)\; b^*(t-\tfrac{1}{2}\tau) \equiv R_{ab}(t,\tau) \;, \tag{49}$$

$$R_2(t,\tau) = c(t+\tfrac{1}{2}\tau)\; d^*(t-\tfrac{1}{2}\tau) \equiv R_{cd}(t,\tau) \;. \tag{50}$$

These are known as (cross) temporal correlation functions (TCFs). Thus, $R_{ab}(t,\tau)$ is the "instantaneous" cross-correlation between waveforms a and b, corresponding to center time t and separation (or delay) time τ. Then, from (31) and (29), or [4; (35)], there follows

$$\Phi_1(\nu,f) = \Phi_{ab}(\nu,f) = \iint dt\, d\tau\, \exp(-i2\pi\nu t - i2\pi f\tau)\; R_{ab}(t,\tau) =$$
$$= A(f+\tfrac{1}{2}\nu)\; B^*(f-\tfrac{1}{2}\nu) \;, \tag{51}$$

$$\Phi_2(\nu,f) = \Phi_{cd}(\nu,f) = C(f+\tfrac{1}{2}\nu)\; D^*(f-\tfrac{1}{2}\nu) \;. \tag{52}$$

These functions are known as (cross) spectral correlation functions (SCFs). (In [4], the notation $A(\nu,f)$ was used for this function; however, A(f) will be used here for the Fourier transform of waveform a(t).) The SCF corresponds to center frequency f and separation (or shift) frequency ν.

The Fourier transform relationships in figure 1 and equations (27) - (34) still hold true, but now are specialized to the waveform cases above. Specifically, figure 2 illustrates the four two-dimensional functions for waveforms a(t) and b(t), where now $W_1 = W_{ab}$ is a cross Wigner distribution function (WDF) and $X_1 = X_{ab}$ is a cross complex ambiguity function (CAF).

$$\begin{tikzcd}
\text{TCF} \quad R_{ab}(t,\tau) \arrow[r, leftrightarrow] \arrow[d, leftrightarrow] & X_{ab}(\nu,\tau) \quad \text{CAF} \arrow[d, leftrightarrow] \\
\text{WDF} \quad W_{ab}(t,f) \arrow[r, leftrightarrow] & \Phi_{ab}(\nu,f) \quad \text{SCF}
\end{tikzcd}$$

Figure 2. Two-Dimensional Functions for Waveforms

The detailed Fourier transform interrelationships are now

$$X_{ab}(\nu,\tau) = \int dt \, \exp(-i2\pi\nu t) \, R_{ab}(t,\tau) \, , \tag{53}$$

$$R_{ab}(t,\tau) = \int d\nu \, \exp(+i2\pi\nu t) \, X_{ab}(\nu,\tau) \, , \tag{54}$$

$$W_{ab}(t,f) = \int d\tau \, \exp(-i2\pi f\tau) \, R_{ab}(t,\tau) \, , \tag{55}$$

$$R_{ab}(t,\tau) = \int df \, \exp(+i2\pi f\tau) \, W_{ab}(t,f) \, , \tag{56}$$

$$\Phi_{ab}(\nu,f) = \int dt \, \exp(-i2\pi\nu t) \, W_{ab}(t,f) \, , \tag{57}$$

$$W_{ab}(t,f) = \int d\nu \, \exp(+i2\pi\nu t) \, \Phi_{ab}(\nu,f) \, , \tag{58}$$

$$\Phi_{ab}(\nu,f) = \int d\tau \; \exp(-i2\pi f\tau) \; X_{ab}(\nu,\tau) \; , \tag{59}$$

$$X_{ab}(\nu,\tau) = \int df \; \exp(+i2\pi f\tau) \; \Phi_{ab}(\nu,f) \; . \tag{60}$$

The function $W_{aa}(t,f)$, for example, is an auto WDF, since it involves only one waveform, $a(t)$. We will frequently drop the terminology auto and cross, when possible without confusion, and let the notation indicate the particular case.

It will be found advantageous for future purposes to define a scaled and contracted WDF according to

$$\underset{\sim}{W}_{ab}(t,f) = \frac{1}{2} W_{ab}(\tfrac{1}{2}t,\tfrac{1}{2}f) \; . \tag{61}$$

GENERAL CROSS PROPERTIES

Due to the restriction of form taken on by the TCF in (49) and the SCF in (51), the four functions in figure 2 obey some symmetry rules; they are

$$\begin{aligned} R_{ab}(t,-\tau) &= R^{*}_{ba}(t,\tau) \; , \\ \Phi_{ab}(-\nu,f) &= \Phi^{*}_{ba}(\nu,f) \; , \\ X_{ab}(-\nu,-\tau) &= X^{*}_{ba}(\nu,\tau) \; , \\ W_{ab}(t,f) &= W^{*}_{ba}(t,f) \; . \end{aligned} \tag{62}$$

AUTO PROPERTIES

When waveform $b(t) = a(t)$, some specializations follow:

$$R_{aa}(t,-\tau) = R^*_{aa}(t,\tau) \ ,$$

$$\Phi_{aa}(-\nu,f) = \Phi^*_{aa}(\nu,f) \ ,$$

$$\chi_{aa}(-\nu,-\tau) = \chi^*_{aa}(\nu,\tau) \ ,$$

$$W_{aa}(t,f) = \text{real for all } t,\ f,\ a(t), \tag{63}$$

with the only significant specialization being the realness of WDF $W_{aa}(t,f)$. Waveform $a(t)$ can still be complex.

SOME SPECIAL CASES

The ordinary cross-correlation of two waveforms $a(t)$ and $b(t)$ is a special case of a CAF:

$$\psi_{ab}(\tau) \equiv \int dt\ a(t)\ b^*(t-\tau) = \chi_{ab}(0,\tau) \ . \tag{64}$$

The ordinary cross-spectrum is then a special case of an SCF:

$$\Psi_{ab}(f) \equiv \int d\tau\ \exp(-i2\pi f\tau)\ \psi_{ab}(\tau) = \Phi_{ab}(0,f) = A(f)\ B^*(f) \ . \tag{65}$$

The autospectrum is then simply

$$\Psi_{aa}(f) = \Phi_{aa}(0,f) = |A(f)|^2 \ , \tag{66}$$

which is always nonnegative.

The ordinary convolution of two waveforms $a(t)$ and $b(t)$ is a special case of a WDF:

$$\int d\tau\ a(\tau)\ b^*(t-\tau) = \tfrac{1}{2}W_{ab}(\tfrac{1}{2}t,0) = \underset{\sim}{W}_{ab}(t,0) \ . \tag{67}$$

REAL WAVEFORM a(t)

In addition, if waveform a(t) is real, the following (auto) properties hold true:

$$R_{aa}(t,-\tau) = R_{aa}(t,\tau) \quad \text{and } R_{aa} \text{ is real} ,$$

$$\Phi_{aa}(\nu,-f) = \Phi_{aa}(\nu,f) ,$$

$$X_{aa}(\nu,-\tau) = X_{aa}(\nu,\tau) ,$$

$$W_{aa}(t,-f) = W_{aa}(t,f) . \qquad (68)$$

The situation for a real waveform a(t) is summarized in figure 3 below.

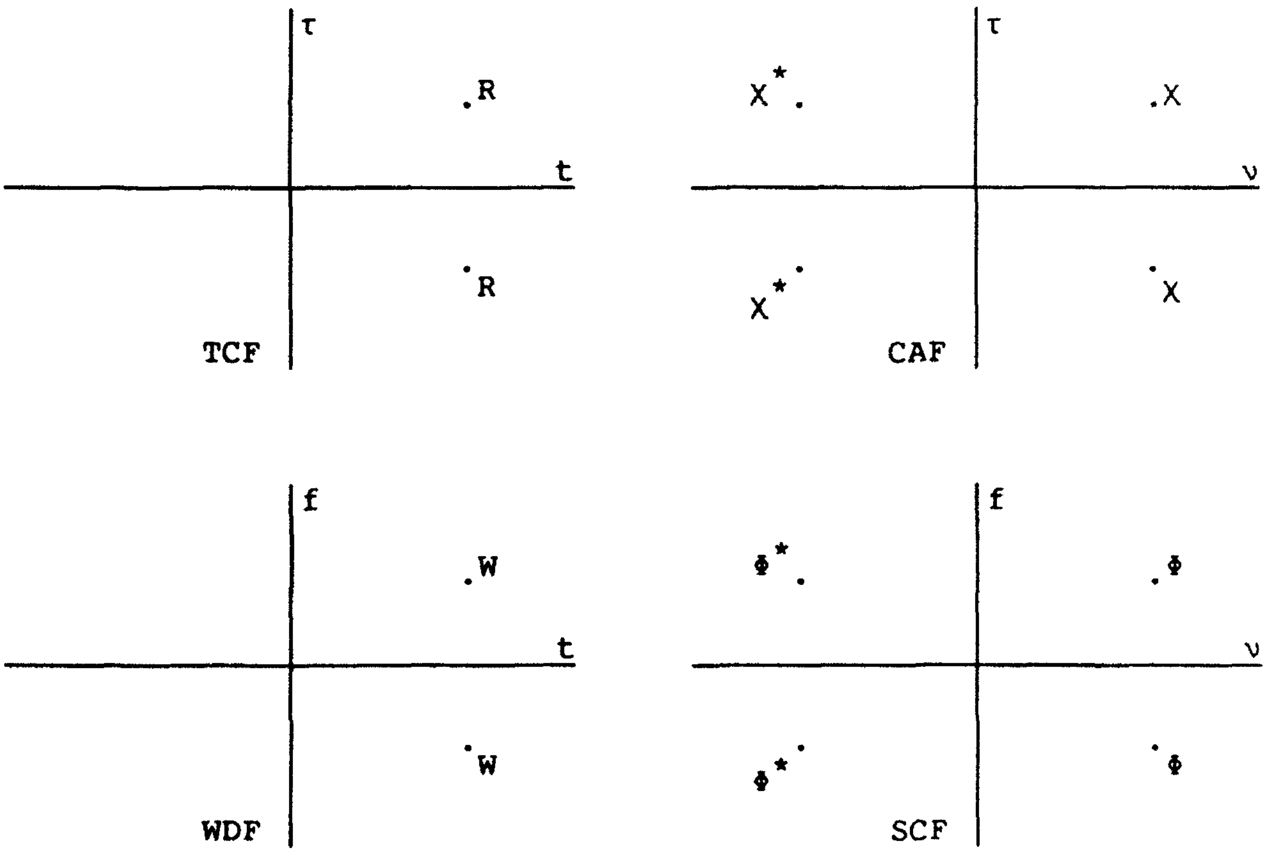

Figure 3. Symmetry Properties for Real Waveform a(t)

MIRROR-IMAGE RELATIONS

For general complex waveforms a(t) and b(t), define mirror-image functions

$$\underline{a}(t) = a(-t) \ , \quad \underline{b}(t) = b(-t) \ . \tag{69}$$

Then it follows directly that the voltage density spectrum of mirror-image $\underline{a}(t)$ is

$$\underline{A}(f) \equiv \int dt \, \exp(-i2\pi ft) \, \underline{a}(t) = A(-f) \ , \tag{70}$$

which is the mirror-image of A(f). Also, there follows

$$\begin{aligned} R_{ab}(-t,-\tau) &= R_{\underline{ab}}(t,\tau) \ , \\ \Phi_{ab}(-\nu,-f) &= \Phi_{\underline{ab}}(\nu,f) \ , \\ X_{ab}(-\nu,-\tau) &= X_{\underline{ab}}(\nu,\tau) \ , \\ W_{ab}(-t,-f) &= W_{\underline{ab}}(t,f) \ . \end{aligned} \tag{71}$$

Thus, the mirror-image property for A(f) carries over into all the two-dimensional domains, such as the WDF and CAF, as well. There is no significant simplification for b(t) = a(t), except for the realness of $W_{aa}(t,f)$, as before.

Use of mirror-image definition (69) allows for an interesting connection between WDFs and CAFs. First, substituting (49) into (53) and (55), we have cross CAF

$$\chi_{ab}(\nu,\tau) = \int dt\ \exp(-i2\pi\nu t)\ a(t+\tfrac{1}{2}\tau)\ b^*(t-\tfrac{1}{2}\tau) =$$

$$= \int df\ \exp(+i2\pi f\tau)\ A(f+\tfrac{1}{2}\nu)\ B^*(f-\tfrac{1}{2}\nu) \equiv \chi_{AB}(\nu,\tau) \qquad (72)$$

and cross WDF

$$W_{ab}(t,f) = \int d\tau\ \exp(-i2\pi f\tau)\ a(t+\tfrac{1}{2}\tau)\ b^*(t-\tfrac{1}{2}\tau) =$$

$$= \int d\nu\ \exp(+i2\pi\nu t)\ A(f+\tfrac{1}{2}\nu)\ B^*(f-\tfrac{1}{2}\nu) \equiv W_{AB}(t,f)\ . \qquad (73)$$

Reference to (69) now immediately reveals that

$$W_{ab}(t,f) = 2\chi_{a\underline{b}}(2f,2t) \qquad (74)$$

or

$$\chi_{ab}(\nu,\tau) = \tfrac{1}{2}W_{a\underline{b}}(\tfrac{1}{2}\tau,\tfrac{1}{2}\nu) = \underset{\sim}{W}_{a\underline{b}}(\tau,\nu)\ . \qquad (75)$$

Here, we also used (61). That is, the WDF of two waveforms a and b is proportional to the CAF of waveforms a and $\underline{b}$, the mirror-image of b.

Finally, since

$$B^*(f) \Leftrightarrow b^*(-t) = \underline{b}^*(t)\ , \qquad (76)$$

then, using (72),

$$\chi_{AB^*}(\nu,\tau) = \int df\ \exp(i2\pi f\tau)\ A(f+\tfrac{1}{2}\nu)\ B(f-\tfrac{1}{2}\nu) =$$

$$= \chi_{a\underline{b}^*}(\nu,\tau) = \tfrac{1}{2}W_{ab^*}(\tfrac{1}{2}\tau,\tfrac{1}{2}\nu) = \underset{\sim}{W}_{ab^*}(\tau,\nu)\ . \qquad (77)$$

TWO-DIMENSIONAL TRANSFORM RELATIONS FOR WAVEFORMS

In an earlier section, general two-dimensional transform relations were derived between sets of four functions related by Fourier transforms; see figure 1 and (39) and (43). Here, we will utilize the particular forms considered in the previous section for waveforms (see figure 2) and will derive closed forms for I and J in (39) and (43), respectively.

TWO-DIMENSIONAL CONVOLUTIONS

If we substitute (49) and (50) in the top relation in (39), there follows

$$I(\nu,f,t,\tau) = \iint dt'd\tau' \exp(-i2\pi\nu t'-i2\pi f\tau') \, a(t+\tfrac{1}{2}t'+\tfrac{1}{2}\tau+\tfrac{1}{4}\tau') \times$$

$$\times \, b^*(t+\tfrac{1}{2}t'-\tfrac{1}{2}\tau-\tfrac{1}{4}\tau') \times c^*(t-\tfrac{1}{2}t'+\tfrac{1}{2}\tau-\tfrac{1}{4}\tau') \, d(t-\tfrac{1}{2}t'-\tfrac{1}{2}\tau+\tfrac{1}{4}\tau') \, . \quad (78)$$

Now let

$$u = \tfrac{1}{2}t'+\tfrac{1}{4}\tau', \; v = \tfrac{1}{2}t'-\tfrac{1}{4}\tau'; \quad u+v = t', \; 2(u-v) = \tau'. \quad (79)$$

Since the Jacobian of this transformation is 4, (78) becomes

$$I(\nu,f,t,\tau) = 4\iint du\,dv \exp\Big(-i2\pi\nu(u+v)-i2\pi f2(u-v)\Big) \times$$

$$\times \, a(t+\tfrac{1}{2}\tau+u) \, b^*(t-\tfrac{1}{2}\tau+v) \, c^*(t+\tfrac{1}{2}\tau-u) \, d(t-\tfrac{1}{2}\tau-v) =$$

$$= \int du' \exp(-i2\pi u'(f+\tfrac{1}{2}\nu)) \, a(t+\tfrac{1}{2}\tau+\tfrac{1}{2}u') \, c^*(t+\tfrac{1}{2}\tau-\tfrac{1}{2}u') \times$$

$$\times \int dv' \exp(+i2\pi v'(f-\tfrac{1}{2}\nu)) \, b^*(t-\tfrac{1}{2}\tau+\tfrac{1}{2}v') \, d(t-\tfrac{1}{2}\tau-\tfrac{1}{2}v') =$$

$$= W_{ac}(t+\tfrac{1}{2}\tau, f+\tfrac{1}{2}\nu)\ W^*_{bd}(t-\tfrac{1}{2}\tau, f-\tfrac{1}{2}\nu)\ . \tag{80}$$

That is, all the following quantities are equal:

$$I(\nu,f,t,\tau) =$$

$$= \iint dt'd\tau'\ \exp(-i2\pi\nu t'-i2\pi f\tau')\ R_{ab}(t+\tfrac{1}{2}t', \tau+\tfrac{1}{2}\tau')\ R^*_{cd}(t-\tfrac{1}{2}t', \tau-\tfrac{1}{2}\tau') =$$

$$= \iint d\nu'd\tau'\ \exp(+i2\pi\nu' t-i2\pi f\tau')\ \chi_{ab}(\nu+\tfrac{1}{2}\nu', \tau+\tfrac{1}{2}\tau')\ \chi^*_{cd}(\nu-\tfrac{1}{2}\nu', \tau-\tfrac{1}{2}\tau') =$$

$$= \iint d\nu'df'\ \exp(+i2\pi\nu' t+i2\pi f'\tau)\ \Phi_{ab}(\nu+\tfrac{1}{2}\nu', f+\tfrac{1}{2}f')\ \Phi^*_{cd}(\nu-\tfrac{1}{2}\nu', f-\tfrac{1}{2}f') =$$

$$= \iint dt'df'\ \exp(-i2\pi\nu t'+i2\pi f'\tau)\ W_{ab}(t+\tfrac{1}{2}t', f+\tfrac{1}{2}f')\ W^*_{cd}(t-\tfrac{1}{2}t', f-\tfrac{1}{2}f') =$$

$$= W_{ac}(t+\tfrac{1}{2}\tau, f+\tfrac{1}{2}\nu)\ W^*_{bd}(t-\tfrac{1}{2}\tau, f-\tfrac{1}{2}\nu)\ . \tag{81}$$

All four double-integrals in (81) can be expressed as a product of the same two one-dimensional integrals, which are cross WDFs. This reduction is only possible when the two-dimensional functions, like W_{ab} and χ_{ab}, are WDFs and CAFs, respectively. The transformations in (81) are combined two-dimensional Fourier transforms and convolutions of TCFs, CAFs, SCFs, or WDFs.

By use of (74), an alternative expression for the end result in (81) is

$$I(\nu,f,t,\tau) = 4\ \chi_{a\underline{c}}(2f+\nu, 2t+\tau)\ \chi^*_{b\underline{d}}(2f-\nu, 2t-\tau)\ , \tag{82}$$

in terms of mirror-image functions; see (69). Also, a more typical convolution form for (81), for example, is (using (61))

$$\iint du\, dv\, \exp(-i2\pi\nu u+i2\pi\nu\tau)\, W_{ab}(u,v)\, W^*_{cd}(t-u,f-v) =$$

$$= \exp(-i\pi\nu t+i\pi f\tau)\, \underset{\sim}{W}_{ac}(t+\tfrac{1}{2}\tau,f+\tfrac{1}{2}\nu)\, \underset{\sim}{W}^*_{bd}(t-\tfrac{1}{2}\tau,f-\tfrac{1}{2}\nu)\ . \qquad (83)$$

TWO-DIMENSIONAL CORRELATIONS

In an identical fashion to that used above, result (43) becomes

$$J(\nu,f,t,\tau) =$$

$$= \iint dt'd\tau'\, \exp(-i2\pi\nu t'-i2\pi f\tau')\, R_{ab}(t'+\tfrac{1}{2}t,\tau'+\tfrac{1}{2}\tau)\, R^*_{cd}(t'-\tfrac{1}{2}t,\tau'-\tfrac{1}{2}\tau) =$$

$$= \iint d\nu'd\tau'\, \exp(+i2\pi\nu' t-i2\pi f\tau')\, \chi_{ab}(\nu'+\tfrac{1}{2}\nu,\tau'+\tfrac{1}{2}\tau)\, \chi^*_{cd}(\nu'-\tfrac{1}{2}\nu,\tau'-\tfrac{1}{2}\tau) =$$

$$= \iint d\nu'df'\, \exp(+i2\pi\nu' t+i2\pi f'\tau)\, \Phi_{ab}(\nu'+\tfrac{1}{2}\nu,f'+\tfrac{1}{2}f)\, \Phi^*_{cd}(\nu'-\tfrac{1}{2}\nu,f'-\tfrac{1}{2}f) =$$

$$= \iint dt'df'\, \exp(-i2\pi\nu t'+i2\pi f'\tau)\, W_{ab}(t'+\tfrac{1}{2}t,f'+\tfrac{1}{2}f)\, W^*_{cd}(t'-\tfrac{1}{2}t,f'-\tfrac{1}{2}f) =$$

$$= \chi_{ac}(f+\tfrac{1}{2}\nu,t+\tfrac{1}{2}\tau)\, \chi^*_{bd}(f-\tfrac{1}{2}\nu,t-\tfrac{1}{2}\tau)\ . \qquad (84)$$

All these double integrals in (84) are equal to a product of two cross CAFs. Again, this only holds for the special forms of the two-dimensional functions, like W_{ab} and χ_{ab}, which are WDFs and CAFs, respectively. The transformations in (84) are combined two-dimensional Fourier transforms and correlations of TCFs, CAFs, SCFs, or WDFs.

By use of (75), an alternative expression for the end result in (84) is

$$J(\nu,f,t,\tau) = \underset{\sim}{W}_{a\underline{c}}(t+\tfrac{1}{2}\tau,f+\tfrac{1}{2}\nu)\ \underset{\sim}{W}^{*}_{b\underline{d}}(t-\tfrac{1}{2}\tau,f-\tfrac{1}{2}\nu)\ , \tag{85}$$

in terms of mirror-image functions. Also, a more typical correlation form for (84) is, for example,

$$\iint du\ dv\ \exp(-i2\pi\nu u+i2\pi v\tau)\ W_{ab}(u,v)\ W^{*}_{cd}(u-t,v-f) =$$

$$= \exp(-i\pi\nu t+i\pi f\tau)\ \chi_{ac}(f+\tfrac{1}{2}\nu,t+\tfrac{1}{2}\tau)\ \chi^{*}_{bd}(f-\tfrac{1}{2}\nu,t-\tfrac{1}{2}\tau)\ . \tag{86}$$

A MIXED RELATION

As an example in this category, if we take (46) with

$$W_1(t,f) = W_{ab}(t,f)\ ,\qquad \chi_2(\nu,\tau) = \chi_{cd}(2\nu,2\tau)\ , \tag{87}$$

then

$$\Phi_1(\nu,f) = \Phi_{ab}(\nu,f) = A(f+\tfrac{1}{2}\nu)\ B^{*}(f-\tfrac{1}{2}\nu)\ ,$$

$$\Phi_2(\nu,f) = \frac{1}{2}\ \Phi_{cd}(2\nu,\tfrac{1}{2}f) = \frac{1}{2}\ C(\tfrac{1}{2}f+\nu)\ D^{*}(\tfrac{1}{2}f-\nu)\ . \tag{88}$$

Substitution of these results in (46) yields

$$\iint dt'df'\ \exp(-i2\pi\nu t'+i2\pi f'\tau)\ W_{ab}(t+\tfrac{1}{2}t',f+\tfrac{1}{2}f')\ \chi^{*}_{cd}(2f-f',2t-t') =$$

$$= W_{ac}(t+\tfrac{1}{2}\tau,f+\tfrac{1}{2}\nu)\ \chi^{*}_{bd}(2f-\nu,2t-\tau)\ . \tag{89}$$

This mixed relation is a two-dimensional Fourier transform and convolution, involving a WDF and a CAF, expressible in closed form as a product of another WDF and CAF.

SPECIAL CASES

The two-dimensional transform results in (81) and (84) in the previous section involve four arguments, namely ν, f, t, τ, and four functions, $a(t)$, $b(t)$, $c(t)$, $d(t)$. Their extreme generality allows for numerous special cases upon selection of the arguments and/or the functions. We consider some of these possibilities, but are aware that this list could be considerably augmented.

Case 1. As an example of the generality of these results, consider in (84) the particular selection

$$\nu = f = t = \tau = 0, \quad c(t) = a(t), \quad d(t) = b(t). \tag{90}$$

There follows immediately the "volume constraint"

$$\iint d\nu' d\tau' \left| \chi_{ab}(\nu',\tau') \right|^2 = \iint dt' df' \left| W_{ab}(t',f') \right|^2 =$$

$$= \chi_{aa}(0,0)\, \chi_{bb}(0,0) = \int dt\, |a(t)|^2 \int dt\, |b(t)|^2 . \tag{91}$$

Case 2. In (84), take $\nu = \tau = 0$, $b(t) = a(t)$, $d(t) = c(t)$. Then there follows, upon use of (85),

$$\iint d\nu' d\tau' \exp(+i2\pi\nu' t - i2\pi f\tau')\, \chi_{aa}(\nu',\tau')\, \chi^*_{cc}(\nu',\tau') =$$

$$= \iint dt' df'\, W_{aa}(t'+\tfrac{1}{2}t, f'+\tfrac{1}{2}f)\, W_{cc}(t'-\tfrac{1}{2}t, f'-\tfrac{1}{2}f) =$$

$$= \left| \chi_{ac}(f,t) \right|^2 = \left| \underset{\sim}{W}_{ac}(t,f) \right|^2 , \tag{92}$$

which is nonnegative real for all f, t, a(t), c(t). Thus, the two-dimensional correlation of two auto WDFs is nonnegative.

An alternative form of (92) is

$$\iint du\, dv\; W_{aa}(u,v)\; W_{cc}(u-t,v-f) = \left|X_{ac}(f,t)\right|^2 . \tag{93}$$

Further specialization to t = f = 0 yields

$$\iint du\, dv\; W_{aa}(u,v)\; W_{cc}(u,v) = \left|X_{ac}(0,0)\right|^2 = \left|\int dt\; a(t)\; c^*(t)\right|^2, \tag{94}$$

which yields Moyal's result [3] for c(t) = a(t), namely

$$\iint dt\, df\; W_{aa}^2(t,f) = \left[\int dt\; |a(t)|^2\right]^2 . \tag{95}$$

<u>Case 3.</u> In (81), take $\nu = \tau = 0$, b(t) = a(t), d(t) = c(t). We then get the "smoothing result"

$$\iint dt'df'\; W_{aa}(t+\tfrac{1}{2}t',f+\tfrac{1}{2}f')\; W_{cc}(t-\tfrac{1}{2}t',f-\tfrac{1}{2}f') =$$

$$= \left|W_{ac}(t,f)\right|^2 = \left|\int d\tau'\; \exp(-i2\pi f\tau')\; a(t+\tfrac{1}{2}\tau')\; c^*(t-\tfrac{1}{2}\tau')\right|^2 \geq 0 \tag{96}$$

for all t, f, a(t), c(t). An alternative form is

$$\iint du\, dv\; W_{aa}(u,v)\; W_{cc}(t-u,f-v) = \left|\tfrac{1}{2}W_{ac}(\tfrac{1}{2}t,\tfrac{1}{2}f)\right|^2 = \left|\underset{\sim}{W}_{ac}(t,f)\right|^2 =$$

$$= \left|\int d\tau'\; \exp(-i2\pi f\tau')\; a(\tau')\; c^*(t-\tau')\right|^2 . \tag{97}$$

That is, the two-dimensional convolution of two auto WDFs is never negative (just as for the correlation in (92)).

Case 4. Using (62), the same basic end result is obtained from (81) for the following double integral involving CAFs:

$$\iint d\nu' d\tau' \exp(+i2\pi\nu' t - i2\pi f\tau')\ \chi_{aa}(\tfrac{1}{2}\nu', \tfrac{1}{2}\tau')\ \chi_{cc}(\tfrac{1}{2}\nu', \tfrac{1}{2}\tau') =$$

$$= \left| W_{ac}(t,f) \right|^2 . \qquad (98)$$

This right-hand side is nonnegative real for all t, f, a(t), c(t). An alternative form is, upon use of (61),

$$\iint d\nu\, d\tau\, \exp(+i2\pi\nu t - i2\pi f\tau)\ \chi_{aa}(\nu,\tau)\ \chi_{cc}(\nu,\tau) = \left| \underset{\sim}{W}_{ac}(t,f) \right|^2 . \qquad (99)$$

Case 5. Consider (81) with c(t) = a(t), d(t) = b(t). Then the right-hand side of (81) is always real. For example, we have

$$\iint d\nu' d\tau' \exp(+i2\pi\nu' t - i2\pi f\tau')\ \chi_{ab}(\nu+\tfrac{1}{2}\nu', \tau+\tfrac{1}{2}\tau')\ \chi^*_{ab}(\nu-\tfrac{1}{2}\nu', \tau-\tfrac{1}{2}\tau') =$$

$$= \iint dt' df' \exp(-i2\pi\nu t' + i2\pi f'\tau)\ W_{ab}(t+\tfrac{1}{2}t', f+\tfrac{1}{2}f')\ W^*_{ab}(t-\tfrac{1}{2}t', f-\tfrac{1}{2}f') =$$

$$= W_{aa}(t+\tfrac{1}{2}\tau, f+\tfrac{1}{2}\nu)\ W_{bb}(t-\tfrac{1}{2}\tau, f-\tfrac{1}{2}\nu) . \qquad (100)$$

This is real for all t, τ, f, ν, a(t), b(t), although it could go negative.

Case 6. From (81), with $\nu = \tau = 0$, there follows

$$\iint dt' df'\ W_{ab}(t+\tfrac{1}{2}t', f+\tfrac{1}{2}f')\ W^*_{cd}(t-\tfrac{1}{2}t', f-\tfrac{1}{2}f') =$$

$$= W_{ac}(t,f)\ W^*_{bd}(t,f) , \qquad (101)$$

or, with the help of (61) and (75), alternative form

$$\iint du\, dv\, W_{ab}(u,v)\, W^*_{cd}(t-u,f-v) =$$

$$= \underset{\sim}{W}_{ac}(t,f)\, \underset{\sim}{W}^*_{bd}(t,f) = \chi_{a\underline{c}}(f,t)\, \chi^*_{b\underline{d}}(f,t) \, . \qquad (102)$$

Furthermore, if we set $c(t) = a(t)$, $d(t) = b(t)$, we obtain

$$\iint du\, dv\, W_{ab}(u,v)\, W^*_{ab}(t-u,f-v) =$$

$$= \underset{\sim}{W}_{aa}(t,f)\, \underset{\sim}{W}_{bb}(t,f) = \chi_{a\underline{a}}(f,t)\, \chi^*_{b\underline{b}}(f,t) \, . \qquad (103)$$

Thus, the two-dimensional convolution of a complex cross WDF with itself is always real, but could go negative.

<u>Case 7.</u> From (83) and (84), with $\nu = \tau = 0$, there follows

$$\iint dt'df'\, W_{ab}(t'+\tfrac{1}{2}t, f'+\tfrac{1}{2}f)\, W^*_{cd}(t'-\tfrac{1}{2}t, f'-\tfrac{1}{2}t) =$$

$$= \iint du\, dv\, W_{ab}(u,v)\, W^*_{cd}(u-t,v-f) =$$

$$= \iint d\nu' d\tau'\, \exp(+i2\pi\nu' t - i2\pi f\tau')\, \chi_{ab}(\nu',\tau')\, \chi^*_{cd}(\nu',\tau') =$$

$$= \chi_{ac}(f,t)\, \chi^*_{bd}(f,t) = \underset{\sim}{W}_{a\underline{c}}(t,f)\, \underset{\sim}{W}^*_{b\underline{d}}(t,f) \, . \qquad (104)$$

The two-dimensional correlation of two cross WDFs is a product of two cross CAFs.

Case 8. If we now set c(t) = a(t) and d(t) = b(t) in (104), we obtain

$$\iint du\, dv\, W_{ab}(u,v)\, W^{*}_{ab}(u-t,v-f) =$$

$$= \iint d\nu' d\tau' \exp(+i2\pi\nu' t - i2\pi f\tau') \left|\chi_{ab}(\nu',\tau')\right|^2 =$$

$$= \chi_{aa}(f,t)\, \chi^{*}_{bb}(f,t) = \underset{\sim}{W}_{\underline{aa}}(t,f)\, \underset{\sim}{W}^{*}_{\underline{bb}}(t,f) \ . \qquad (105)$$

The two-dimensional correlation of a cross WDF with itself is a product of two auto CAFs.

Case 9. From (84), with t = f = 0, c(t) = a(t), d(t) = b(t), and with the help of (63), we find

$$\iint dt' df' \exp(-i2\pi\nu t' + i2\pi f'\tau) \left|W_{ab}(t',f')\right|^2 =$$

$$= \chi_{aa}(\tfrac{1}{2}\nu,\tfrac{1}{2}\tau)\, \chi_{bb}(\tfrac{1}{2}\nu,\tfrac{1}{2}\tau) \ . \qquad (106)$$

This is a generalization of (91).

APPLICATION TO HERMITE FUNCTIONS

This material is heavily based on [5; appendix A, (A-36) and the sequel]. Let $\zeta_n(t)$ be the n-th orthonormal Hermite function with linear frequency-modulation, as given in [5; (A-36)]. Also let waveforms

$$a(t) = \zeta_k(\mu t),\ b(t) = \zeta_j(\gamma t),\ c(t) = \zeta_m(\mu t),\ d(t) = \zeta_n(\gamma t). \quad (107)$$

The particular cross WDFs

$$W_{ab}(t,f) = \int d\tau\ \exp(-i2\pi f\tau)\ \zeta_k(\mu t+\tfrac{1}{2}\mu\tau)\ \zeta_j^*(\gamma t-\tfrac{1}{2}\gamma\tau)\ ,$$

$$W_{cd}(t,f) = \int d\tau\ \exp(-i2\pi f\tau)\ \zeta_m(\mu t+\tfrac{1}{2}\mu\tau)\ \zeta_n^*(\gamma t-\tfrac{1}{2}\gamma\tau)\ , \quad (108)$$

cannot be expressed in closed form. However, the cross WDFs

$$W_{ac}(t,f) = \int d\tau\ \exp(-i2\pi f\tau)\ \zeta_k(\mu t+\tfrac{1}{2}\mu\tau)\ \zeta_m^*(\mu t-\tfrac{1}{2}\mu\tau) =$$

$$= \frac{1}{\mu}\ W_{km}(\mu t, f/\mu) \quad (109)$$

and

$$W_{bd}(t,f) = \frac{1}{\gamma}\ W_{jn}(\gamma t, f/\gamma) \quad (110)$$

can be simply expressed, in the notation of [5; (A-40) and (A-41)]. Thus, the very complicated two-dimensional convolution and Fourier transform in (81), of W_{ab} and W_{cd}, can be written in a closed form involving the product of two generalized Laguerre functions. Numerous specializations are possible.

SUMMARY

Some very general two-dimensional Fourier transforms of convolution and correlation form have been derived for various combinations of WDFs and CAFs. In particular, closed forms for the convolution form are given in (81), while results for the correlation form are given in (84). Numerous special cases may be obtained from these results, of which a brief list has been presented in (90) - (106).

Some extensions to more general arguments have been derived in appendices A and B. In particular, appendix A treats the case where a product of CAFs is of interest, while the case of a product of WDFs is considered in appendix B. The possibility of a combined convolution and correlation has also been considered in appendix A.

For signals reflected off moving targets, it is necessary to define a generalized WDF, allowing for contracted arguments. This possibility has been considered in appendix C, where a two-dimensional Fourier transform and convolution has been evaluated in terms of the generalized WDF.

The results of this report should enable rapid evaluation of integrals of products of WDFs and/or CAFs with a wide variety of arguments and including exponential terms with linear arguments. They also significantly extend a number of special cases already known in the literature.

APPENDIX A - PRODUCTS OF CAFs

In this appendix, we will further generalize the results in (81) and (84), for products of two CAFs, to allow for more general arguments. However, we begin by considering general two-dimensional functions as in figure 1. In particular, let

$$g(\tau) = \chi_1(\nu_a,\tau) \;, \quad h(\tau) = \chi_2(\nu_b,\tau) \;, \tag{A-1}$$

in (4). Then

$$G(f) = \Phi_1(\nu_a,f) \;, \quad H(f) = \Phi_2(\nu_b,f) \;, \tag{A-2}$$

giving

$$\int d\tau' \; \exp(-i2\pi f\tau') \; \chi_1(\nu_a,\beta\tau'+\alpha\tau) \; \chi_2^*(\nu_b,\gamma\tau'+\mu\tau) = \exp\left(i2\pi f\tau\frac{\alpha\gamma+\beta\mu}{2\beta\gamma}\right) \times$$

$$\times \int df' \; \exp\left(i2\pi f'\tau(\alpha\gamma-\beta\mu)\right) \; \Phi_1\left(\nu_a,\gamma\left(f'+\frac{f}{2\beta\gamma}\right)\right) \; \Phi_2^*\left(\nu_b,\beta\left(f'-\frac{f}{2\beta\gamma}\right)\right) =$$

$$= \frac{1}{|\alpha\gamma-\beta\mu|} \exp\left(i2\pi f\tau\frac{\alpha\gamma+\beta\mu}{2\beta\gamma}\right) \int df' \; \exp(i2\pi f'\tau) \times$$

$$\times \; \Phi_1\left(\nu_a, \frac{\gamma f'}{\alpha\gamma-\beta\mu} + \frac{f}{2\beta}\right) \; \Phi_2^*\left(\nu_b, \frac{\beta f'}{\alpha\gamma-\beta\mu} - \frac{f}{2\gamma}\right) \;. \tag{A-3}$$

Now, let $\nu_a=\boldsymbol{\beta}\nu'+\boldsymbol{\alpha}\nu$, $\nu_b=\boldsymbol{\gamma}\nu'+\boldsymbol{\mu}\nu$, where the boldface constants are unrelated to their counterparts; that is, $\boldsymbol{\beta}$ need not equal β, with the same true of $\boldsymbol{\alpha},\boldsymbol{\mu},\boldsymbol{\gamma}$. Then Fourier transform (A-3) on ν' to obtain

$$\iint d\nu' d\tau' \ \exp(+i2\pi\nu' t - i2\pi f\tau') \ \chi_1(\beta\nu'+\alpha\nu, \beta\tau'+\alpha\tau) \ \chi_2^*(\gamma\nu'+\mu\nu, \gamma\tau'+\mu\tau) =$$

$$= \frac{1}{|\alpha\gamma-\beta\mu|} \exp\left(i2\pi f\tau \frac{\alpha\gamma+\beta\mu}{2\beta\gamma}\right) \iint d\nu' df' \ \exp(+i2\pi\nu' t + i2\pi f'\tau) \ \times$$

$$\times \ \Phi_1\left(\beta\nu'+\alpha\nu, \ \frac{\gamma f'}{\alpha\gamma-\beta\mu} + \frac{f}{2\beta}\right) \ \Phi_2^*\left(\gamma\nu'+\mu\nu, \ \frac{\beta f'}{\alpha\gamma-\beta\mu} - \frac{f}{2\gamma}\right) \ . \qquad \text{(A-4)}$$

In general, we cannot proceed any further on this double integral of a product of general two-dimensional functions χ_1 and χ_2.

Now let R_1 and R_2 be TCFs; that is,

$$R_1(t,\tau) = a(t+\tfrac{1}{2}\tau) \ b^*(t-\tfrac{1}{2}\tau) = R_{ab}(t,\tau) \ ,$$

$$R_2(t,\tau) = c(t+\tfrac{1}{2}\tau) \ d^*(t-\tfrac{1}{2}\tau) = R_{cd}(t,\tau) \ . \qquad \text{(A-5)}$$

Then Φ_1 and Φ_2 become SCFs:

$$\Phi_1(\nu,f) = \Phi_{ab}(\nu,f) = A(f+\tfrac{1}{2}\nu) \ B^*(f-\tfrac{1}{2}\nu) \ ,$$

$$\Phi_2(\nu,f) = \Phi_{cd}(\nu,f) = C(f+\tfrac{1}{2}\nu) \ D^*(f-\tfrac{1}{2}\nu) \ . \qquad \text{(A-6)}$$

As a first case, let $\gamma=\beta$ and $\gamma=\beta$. Then (A-4) becomes

$$\iint d\nu' d\tau' \exp(i2\pi\nu' t - i2\pi f\tau') \ \chi_{ab}(\beta\nu'+\alpha\nu, \beta\tau'+\alpha\tau) \ \chi_{cd}^*(\beta\nu'+\mu\nu, \beta\tau'+\mu\tau) =$$

$$= \frac{1}{|\beta(\alpha-\mu)|} \exp\left(i2\pi f\tau \frac{\alpha+\mu}{2\beta}\right) \iint d\nu' df' \ \exp(+i2\pi\nu' t + i2\pi f'\tau) \ \times$$

$$\times \ A\left(\frac{f'}{\alpha-\mu} + \tfrac{1}{2}\frac{f}{\beta} + \tfrac{1}{2}\beta\nu' + \tfrac{1}{2}\alpha\nu\right) \ B^*\left(\frac{f'}{\alpha-\mu} + \tfrac{1}{2}\frac{f}{\beta} - \tfrac{1}{2}\beta\nu' - \tfrac{1}{2}\alpha\nu\right) \ \times$$

$$\times \ C^*\left(\frac{f'}{\alpha-\mu} - \tfrac{1}{2}\frac{f}{\beta} + \tfrac{1}{2}\beta\nu' + \tfrac{1}{2}\mu\nu\right) \ D\left(\frac{f'}{\alpha-\mu} - \tfrac{1}{2}\frac{f}{\beta} - \tfrac{1}{2}\beta\nu' - \tfrac{1}{2}\mu\nu\right) =$$

$$= |\beta\boldsymbol{\beta}|^{-1} \exp\left(+i2\pi f\tau\frac{\alpha+\boldsymbol{\mu}}{2\beta} - i2\pi\nu t\frac{\boldsymbol{\alpha}+\mu}{2\boldsymbol{\beta}}\right) \times$$

$$\times\ \chi_{ac}\left(\frac{f}{\beta} + \tfrac{1}{2}\nu(\boldsymbol{\alpha}-\mu), \frac{t}{\boldsymbol{\beta}} + \tfrac{1}{2}\tau(\alpha-\mu)\right)\ \chi^*_{bd}\left(\frac{f}{\boldsymbol{\beta}} - \tfrac{1}{2}\nu(\boldsymbol{\alpha}-\mu), \frac{t}{\boldsymbol{\beta}} - \tfrac{1}{2}\tau(\alpha-\mu)\right). \quad \text{(A-7)}$$

Thus, this very general two-dimensional correlation and Fourier transform of cross CAFs can be expressed as a product of two different cross CAFs. For $\beta=\boldsymbol{\beta}=1$, $\alpha=\boldsymbol{\alpha}=\frac{1}{2}$, $\mu=\boldsymbol{\mu}=-\frac{1}{2}$, this result reduces to (84).

As a second case, let $\gamma=-\beta$ and $\boldsymbol{\gamma}=-\boldsymbol{\beta}$. Then (A-4) becomes

$$\iint d\nu' d\tau' \exp(i2\pi\nu' t - i2\pi f\tau')\ \chi_{ab}(\alpha\nu+\beta\nu', \alpha\tau+\beta\tau')\ \chi^*_{cd}(\boldsymbol{\mu}\nu-\boldsymbol{\beta}\nu', \boldsymbol{\mu}\tau-\boldsymbol{\beta}\tau') =$$

$$= \frac{1}{|\beta(\alpha+\mu)|} \exp\left(i2\pi f\tau\frac{\alpha-\mu}{2\beta}\right) \iint d\nu' df' \exp(+i2\pi\nu' t + i2\pi f'\tau) \times$$

$$\times\ A\left(\frac{f'}{\alpha+\mu} + \tfrac{1}{2}\frac{f}{\beta} + \tfrac{1}{2}\beta\nu' + \tfrac{1}{2}\alpha\nu\right)\ B^*\left(\frac{f'}{\alpha+\mu} + \tfrac{1}{2}\frac{f}{\beta} - \tfrac{1}{2}\beta\nu' - \tfrac{1}{2}\alpha\nu\right) \times$$

$$\times\ C^*\left(\frac{-f'}{\alpha+\mu} + \tfrac{1}{2}\frac{f}{\beta} - \tfrac{1}{2}\beta\nu' + \tfrac{1}{2}\mu\nu\right)\ D\left(\frac{-f'}{\alpha+\mu} + \tfrac{1}{2}\frac{f}{\beta} + \tfrac{1}{2}\beta\nu' - \tfrac{1}{2}\mu\nu\right) =$$

$$= |\beta\boldsymbol{\beta}|^{-1} \exp\left(+i2\pi f\tau\frac{\alpha-\mu}{2\beta} - i2\pi\nu t\frac{\boldsymbol{\alpha}-\boldsymbol{\mu}}{2\boldsymbol{\beta}}\right) \times$$

$$\times\ \underset{\sim}{W}_{ac}\left(\frac{t}{\beta} + \tfrac{1}{2}\tau(\alpha+\mu), \frac{f}{\beta} + \tfrac{1}{2}\nu(\alpha+\mu)\right)\ \underset{\sim}{W}^*_{bd}\left(\frac{t}{\boldsymbol{\beta}} - \tfrac{1}{2}\tau(\alpha+\mu), \frac{f}{\boldsymbol{\beta}} - \tfrac{1}{2}\nu(\boldsymbol{\alpha}+\mu)\right), \quad \text{(A-8)}$$

where we used (61). Thus, this very general two-dimensional convolution and Fourier transform of cross CAFs can be expressed as a product of two different cross WDFs. For $\beta=\boldsymbol{\beta}=\frac{1}{2}$, $\alpha=\boldsymbol{\alpha}=1$, $\mu=\boldsymbol{\mu}=1$, this result reduces to (81).

As a third case, let $\gamma=\beta$, $\gamma=-\boldsymbol{\beta}$. There follows a two-dimensional relation involving both a convolution and a correlation:

$$\iint d\nu' d\tau' \exp(i2\pi\nu' t-i2\pi f\tau')\ \chi_{ab}(\beta\nu'+\boldsymbol{\alpha}\nu,\beta\tau'+\alpha\tau)\ \chi^*_{cd}(-\boldsymbol{\beta}\nu'+\boldsymbol{\mu}\nu,\beta\tau'+\mu\tau)$$

$$= |\beta\boldsymbol{\beta}|^{-1}\exp\left(+i2\pi f\tau\frac{\alpha+\mu}{2\beta}-i2\pi\nu t\frac{\boldsymbol{\alpha}-\boldsymbol{\mu}}{2\boldsymbol{\beta}}\right)\times$$

$$\times\ \underset{\sim}{W}_{ad*}\left(\frac{t}{\boldsymbol{\beta}}+\tfrac{1}{2}\tau(\alpha-\mu),\frac{f}{\beta}+\tfrac{1}{2}\nu(\boldsymbol{\alpha}+\boldsymbol{\mu})\right)\ \underset{\sim}{W}^*_{bc*}\left(\frac{t}{\boldsymbol{\beta}}-\tfrac{1}{2}\tau(\alpha-\mu),\frac{f}{\beta}-\tfrac{1}{2}\nu(\boldsymbol{\alpha}+\boldsymbol{\mu})\right), \quad \text{(A-9)}$$

where $\underset{\sim}{W}(t,f) = \frac{1}{2}W(\tfrac{1}{2}t,\tfrac{1}{2}f)$ again. Observe the conjugates on subscripts d and c of the scaled WDFs $\underset{\sim}{W}$.

For $\beta=\boldsymbol{\beta}=\tfrac{1}{2}$, $\alpha=\boldsymbol{\alpha}=1$, $\mu=\boldsymbol{\mu}=1$, this relation becomes

$$\iint d\nu' d\tau'\ \exp(i2\pi\nu' t-i2\pi f\tau')\ \chi_{ab}(\nu+\tfrac{1}{2}\nu',\tau+\tfrac{1}{2}\tau')\ \chi^*_{cd}(\nu-\tfrac{1}{2}\nu',\tau+\tfrac{1}{2}\tau') =$$

$$= 4\ \exp(i4\pi f\tau)\ \underset{\sim}{W}_{ad*}(2t,2f+\nu)\ \underset{\sim}{W}^*_{bc*}(2t,2f-\nu) =$$

$$= \exp(i4\pi f\tau)\ W_{ad*}(t,f+\tfrac{1}{2}\nu)\ W^*_{bc*}(t,f-\tfrac{1}{2}\nu)\ . \quad \text{(A-10)}$$

APPENDIX B - PRODUCTS OF WDFs

In this appendix, we will also generalize the results in (81) and (84), but now for products of two WDFs, to allow for more general arguments. Again, we begin by considering general two-dimensional functions as in figure 1. In particular, let

$$g(t) = W_1(t,f_a) \ , \quad h(t) = W_2(t,f_b) \ , \tag{B-1}$$

in (4). Then

$$G(\nu) = \Phi_1(\nu,f_a) \ , \quad H(\nu) = \Phi_2(\nu,f_b) \ , \tag{B-2}$$

giving

$$\int dt' \exp(-i2\pi\nu t') \, W_1(\beta t'+\alpha t,f_a) \, W_2^*(\gamma t'+\mu t,f_b) = \exp\left(i2\pi\nu t\frac{\alpha\gamma+\beta\mu}{2\beta\gamma}\right) \times$$

$$\times \int d\nu' \exp\left(i2\pi\nu' t(\alpha\gamma-\beta\mu)\right) \, \Phi_1\left(\gamma\nu'+\frac{\nu}{2\beta},f_a\right) \, \Phi_2^*\left(\beta\nu'-\frac{\nu}{2\gamma},f_b\right). \tag{B-3}$$

Now, let $f_a=\boldsymbol{\beta}f'+\boldsymbol{\alpha}f$, $f_b=\boldsymbol{\gamma}f'+\boldsymbol{\mu}f$, where the boldface constants are unrelated to their counterparts; that is, $\boldsymbol{\beta}$ need not equal β, with the same true of $\boldsymbol{\alpha},\boldsymbol{\mu},\boldsymbol{\gamma}$. Then Fourier transform (B-3) on f', to obtain

$$\iint dt'df' \exp(-i2\pi\nu t'+i2\pi f'\tau) \, W_1(\beta t'+\alpha t,\boldsymbol{\beta}f'+\boldsymbol{\alpha}f) \, W_2^*(\gamma t'+\mu t,\boldsymbol{\gamma}f'+\boldsymbol{\mu}f)=$$

$$= \exp\left(i2\pi\nu t\frac{\alpha\gamma+\beta\mu}{2\beta\gamma}\right) \iint d\nu'df' \exp\left(+i2\pi\nu' t(\alpha\gamma-\beta\mu)+i2\pi f'\tau\right) \times$$

$$\times \, \Phi_1\left(\gamma\nu'+\frac{\nu}{2\beta},\boldsymbol{\beta}f'+\boldsymbol{\alpha}f\right) \, \Phi_2^*\left(\beta\nu'-\frac{\nu}{2\gamma},\boldsymbol{\gamma}f'+\boldsymbol{\mu}f\right) \ . \tag{B-4}$$

In general, we cannot proceed any further on this double integral of a product of general two-dimensional functions W_1 and W_2.

Now let R_1 and R_2 be TCFs; that is,

$$R_1(t,\tau) = a(t+\tfrac{1}{2}\tau)\, b^*(t-\tfrac{1}{2}\tau) = R_{ab}(t,\tau) \;,$$

$$R_2(t,\tau) = c(t+\tfrac{1}{2}\tau)\, d^*(t-\tfrac{1}{2}\tau) = R_{cd}(t,\tau) \;. \qquad \text{(B-5)}$$

Then Φ_1 and Φ_2 become SCFs:

$$\Phi_1(\nu,f) = \Phi_{ab}(\nu,f) = A(f+\tfrac{1}{2}\nu)\, B^*(f-\tfrac{1}{2}\nu) \;,$$

$$\Phi_2(\nu,f) = \Phi_{cd}(\nu,f) = C(f+\tfrac{1}{2}\nu)\, D^*(f-\tfrac{1}{2}\nu) \;. \qquad \text{(B-6)}$$

Substitution in (B-4) yields

$$\iint dt'df' \exp(-i2\pi\nu t'+i2\pi f'\tau)\; W_{ab}(\beta t'+\alpha t,\beta f'+\alpha f)\; W^*_{cd}(\gamma t'+\mu t,\gamma f'+\mu f)$$

$$= \exp\left(i2\pi\nu t\frac{\alpha\gamma+\beta\mu}{2\beta\gamma}\right) \iint d\nu'df' \;\exp\left(+i2\pi\nu' t(\alpha\gamma-\beta\mu)+i2\pi f'\tau\right) \times$$

$$\times\; A\left(\beta f'+\alpha f+\tfrac{1}{2}\gamma\nu'+\tfrac{1}{4}\nu/\beta\right)\; B^*\left(\beta f'+\alpha f-\tfrac{1}{2}\gamma\nu'-\tfrac{1}{4}\nu/\beta\right) \times$$

$$\times\; C^*\left(\gamma f'+\mu f+\tfrac{1}{2}\beta\nu'-\tfrac{1}{4}\nu/\gamma\right)\; D\left(\gamma f'+\mu f-\tfrac{1}{2}\beta\nu'+\tfrac{1}{4}\nu/\gamma\right) \;. \qquad \text{(B-7)}$$

As a first case, let $\gamma=\beta$ and $\gamma=\beta$. Then (B-7) becomes

$$\iint dt'df' \exp(-i2\pi\nu t'+i2\pi f'\tau)\; W_{ab}(\beta t'+\alpha t,\beta f'+\alpha f)\; W^{*}_{cd}(\beta t'+\mu t,\beta f'+\mu f)$$

$$= \exp\left(i2\pi\nu t\frac{\alpha+\mu}{2\beta}\right) \iint d\nu' df' \; \exp\left(+i2\pi\nu' t\beta(\alpha-\mu)+i2\pi f'\tau\right) \times$$

$$\times\; A\left(\beta f'+\alpha f+\tfrac{1}{2}\beta\nu'+\tfrac{1}{4}\nu/\beta\right)\; B^{*}\left(\beta f'+\alpha f-\tfrac{1}{2}\beta\nu'-\tfrac{1}{4}\nu/\beta\right) \times$$

$$\times\; C^{*}\left(\beta f'+\mu f+\tfrac{1}{2}\beta\nu'-\tfrac{1}{4}\nu/\beta\right)\; D\left(\beta f'+\mu f-\tfrac{1}{2}\beta\nu'+\tfrac{1}{4}\nu/\beta\right) =$$

$$= |\beta\beta|^{-1} \exp\left(+i2\pi\nu t\frac{\alpha+\mu}{2\beta} - i2\pi f\tau\frac{\alpha+\mu}{2\beta}\right) \times$$

$$\times\; \chi_{ac}\left(f(\alpha-\mu)+\frac{\nu}{2\beta},\, t(\alpha-\mu)+\frac{\tau}{2\beta}\right)\; \chi^{*}_{bd}\left(f(\alpha-\mu)-\frac{\nu}{2\beta},\, t(\alpha-\mu)-\frac{\tau}{2\beta}\right) . \quad \text{(B-8)}$$

Thus, the very general two-dimensional correlation and Fourier transform of cross WDFs can be expressed as a product of two different cross CAFs. For $\beta=\beta=1$, $\alpha=\alpha=\frac{1}{2}$, $\mu=\mu=-\frac{1}{2}$, this result reduces to (84).

As a second case, let $\gamma=-\beta$ and $\gamma=-\beta$. Then (B-7) becomes

$$\iint dt'df' \exp(-i2\pi\nu t'+i2\pi f'\tau)\; W_{ab}(\alpha t+\beta t',\alpha f+\beta f')\; W^{*}_{cd}(\mu t-\beta t',\mu f-\beta f')$$

$$= \exp\left(i2\pi\nu t\frac{\alpha-\mu}{2\beta}\right) \iint d\nu' df' \; \exp\left(-i2\pi\nu' t\beta(\alpha+\mu)+i2\pi f'\tau\right) \times$$

$$\times\; A\left(\beta f'+\alpha f-\tfrac{1}{2}\beta\nu'+\tfrac{1}{4}\nu/\beta\right)\; B^{*}\left(\beta f'+\alpha f+\tfrac{1}{2}\beta\nu'-\tfrac{1}{4}\nu/\beta\right) \times$$

$$\times\; C^{*}\left(-\beta f'+\mu f+\tfrac{1}{2}\beta\nu'+\tfrac{1}{4}\nu/\beta\right)\; D\left(-\beta f'+\mu f-\tfrac{1}{2}\beta\nu'-\tfrac{1}{4}\nu/\beta\right) =$$

$$= |\beta\boldsymbol{\beta}|^{-1} \exp\left(+i2\pi\nu t\frac{\alpha-\mu}{2\beta} - i2\pi f\tau\frac{\boldsymbol{\alpha}-\boldsymbol{\mu}}{2\boldsymbol{\beta}}\right) \times$$

$$\times\ \underset{\sim}{W}_{ac}\left(t(\alpha+\mu)+\frac{\tau}{2\boldsymbol{\beta}},\, f(\boldsymbol{\alpha}+\boldsymbol{\mu})+\frac{\nu}{2\beta}\right) \underset{\sim}{W}^{*}_{bd}\left(t(\alpha+\mu)-\frac{\tau}{2\boldsymbol{\beta}},\, f(\boldsymbol{\alpha}+\boldsymbol{\mu})-\frac{\nu}{2\beta}\right), \quad \text{(B-9)}$$

using (61). Thus, the very general two-dimensional convolution and Fourier transform of cross WDFs can be expressed as a product of two different cross WDFs. For $\beta=\boldsymbol{\beta}=\frac{1}{2}$, $\alpha=\boldsymbol{\alpha}=1$, $\mu=\boldsymbol{\mu}=1$, this result reduces to (81).

For $\tau = 0$, $\nu = 0$, $b(t) = a(t)$, $d(t) = c(t)$, (B-9) reduces to

$$\iint dt'df'\ W_{aa}(\alpha t+\beta t', \boldsymbol{\alpha} f+\boldsymbol{\beta} f')\ W_{cc}(\mu t-\beta t', \boldsymbol{\mu} f-\boldsymbol{\beta} f') =$$

$$= |\beta\boldsymbol{\beta}|^{-1} \left|\underset{\sim}{W}_{ac}\left(t(\alpha+\mu),\ f(\boldsymbol{\alpha}+\boldsymbol{\mu})\right)\right|^{2}, \quad \text{(B-10)}$$

which is nonnegative for all parameter values and waveforms a(t) and c(t). This is a generalization of (96).

APPENDIX C - A GENERALIZED WDF

When a signal is reflected from a moving target, the effect is to contract (or expand) the time scale of the echo, rather than cause a frequency shift. This requires us to consider a more general version of a WDF. To begin, if waveforms

$$\underset{\sim}{a}(t) \equiv a(\alpha t) \ , \quad \underset{\sim}{b}(t) \equiv b(\alpha t) \ , \quad \alpha > 0 \ , \tag{C-1}$$

then their cross WDF is

$$W_{\underset{\sim}{a}\underset{\sim}{b}}(t,f) = \frac{1}{\alpha} W_{ab}(\alpha t, f/\alpha) \ . \tag{C-2}$$

Thus, we have need to consider integrals of the form

$$K \equiv \iint dt'df' \exp(-i2\pi\nu t' + i2\pi f'\tau) \, W_{ab}(t',f') \, W^{*}_{cd}(t-\alpha t', f-f'/\alpha) . \tag{C-3}$$

This form is general enough to accommodate integrand

$$W_{ab}(\beta t', \beta f') \, W^{*}_{cd}(t-\alpha t', f-f'/\alpha) \tag{C-4}$$

by a change of variable.

To accomplish evaluation of (C-3), we must define a generalized WDF as

$$W_{ab}(t,f;p) \equiv \int d\tau \exp(-i2\pi f\tau) \, a(t+p\tau) \, b^{*}(t-(1-p)\tau) \ . \tag{C-5}$$

Then we have the usual WDF as a special case, namely

$$W_{ab}(t,f;\tfrac{1}{2}) = W_{ab}(t,f) \ . \tag{C-6}$$

Also, (C-5) enables us to evaluate the following more general integral according to

$$\int dt' \exp(-i2\pi ft')\, a(t')\, b^*(t-\alpha t') =$$

$$= p \exp(-i2\pi ftp)\, W_{ab}(pt,pf;p) \;; \quad p = \frac{1}{1+\alpha} \,. \tag{C-7}$$

Now we are in a position to reconsider integral K defined above in (C-3):

$$K = \iint dt'df' \exp(-i2\pi\nu t'+i2\pi f'\tau) \int du \exp(-i2\pi f'u)\, a(t'+\tfrac{1}{2}u) \times$$

$$\times\, b^*(t'-\tfrac{1}{2}u) \int dv \exp[i2\pi(f-f'/\alpha)v]\, c^*(t-\alpha t'+\tfrac{1}{2}v)\, d(t-\alpha t'-\tfrac{1}{2}v) . \tag{C-8}$$

The integral on f' yields $\delta(\tau-u-v/\alpha)$. Integration on u then yields

$$K = \iint dt'dv \exp(-i2\pi\nu t'+i2\pi fv)\, a(t'+\tfrac{1}{2}\tau-\tfrac{1}{2}v/\alpha) \times$$

$$\times\, b^*(t'-\tfrac{1}{2}\tau+\tfrac{1}{2}v/\alpha)\, c^*(t-\alpha t'+\tfrac{1}{2}v)\, d(t-\alpha t'-\tfrac{1}{2}v) \,. \tag{C-9}$$

Now let

$$x = t'+\tfrac{1}{2}\tau-\tfrac{1}{2}v/\alpha \,, \quad y = t'-\tfrac{1}{2}\tau+\tfrac{1}{2}v/\alpha \,;$$

$$t' = \frac{1}{2}(x+y) \,, \quad v = \alpha(y-x+\tau) \,. \tag{C-10}$$

The Jacobian of this two-dimensional transformation is α, leading to

$$K = \alpha \iint dx\, dy\, \exp[-i\pi\nu(x+y)+i2\pi f\alpha(y-x+\tau)] \times$$

$$\times\, a(x)\, b^*(y)\, c^*(t+\tfrac{1}{2}\alpha\tau-\alpha x)\, d(t-\tfrac{1}{2}\alpha\tau-\alpha y) =$$

$$= \alpha \exp(i2\pi\alpha f\tau) \int dx\, \exp[-i2\pi(\alpha f+\tfrac{1}{2}\nu)x]\, a(x)\, c^*(t+\tfrac{1}{2}\alpha\tau-\alpha x) \times$$

$$\times \int dy\, \exp[i2\pi(\alpha f-\tfrac{1}{2}\nu)y]\, b^*(y)\, d(t-\tfrac{1}{2}\alpha\tau-\alpha y) =$$

$$= \frac{\alpha}{(1+\alpha)^2} \exp\left(i2\pi\frac{\alpha f\tau-\nu t}{1+\alpha}\right) W_{ac}\left(\frac{t+\frac{1}{2}\alpha\tau}{1+\alpha}, \frac{\alpha f+\frac{1}{2}\nu}{1+\alpha}; \frac{1}{1+\alpha}\right) \times$$

$$\times\, W_{bd}^*\left(\frac{t-\frac{1}{2}\alpha\tau}{1+\alpha}, \frac{\alpha f-\frac{1}{2}\nu}{1+\alpha}; \frac{1}{1+\alpha}\right) , \qquad \text{(C-11)}$$

by use of (C-7). For $\alpha = 1$, this reduces to alternative form (83), upon use of (C-6) and (61).

REFERENCES

[1] H. L. Van Trees, **Detection, Estimation, and Modulation Theory, Part III, Radar-Sonar Signal Processing and Gaussian Signals in Noise**, John Wiley & Sons, Inc., New York, NY, 1971.

[2] A. H. Nuttall, **Wigner Distribution Function: Relation to Short-Term Spectral Estimation, Smoothing, and Performance in Noise**, NUSC Technical Report 8225, Naval Underwater Systems Center, New London, CT, 16 February 1988.

[3] J. E. Moyal, "Quantum Mechanics as a Statistical Theory", **Proceedings Cambridge Philosophical Society**, volume 45, pages 99 - 132, 1949.

[4] A. H. Nuttall, **Alias-Free Wigner Distribution Function and Complex Ambiguity Function for Discrete-Time Samples**, NUSC Technical Report 8533, Naval Underwater Systems Center, New London, CT, 14 April 1989.

[5] A. H. Nuttall, **The Wigner Distribution Function With Minimum Spread**, NUSC Technical Report 8317, Naval Underwater Systems Center, New London, CT, 1 June 1988.

NUSC Technical Report 8785
9 October 1990

Alias-Free Smoothed Wigner Distribution Function for Discrete-Time Samples

Albert H. Nuttall

ABSTRACT

An alias-free Wigner distribution function (WDF), for a time waveform s(t) limited to total frequency extent F, is available if the time sampling increment Δ is less than 1/F. Furthermore, the WDF can be efficiently numerically evaluated via fast Fourier transform (FFT) procedures if the FFT size N is greater than $2T/\Delta$, where T is the effective duration of s(t).

However, in order to suppress the undesired inherent oscillating interference terms in the WDF, it is necessary to smooth the WDF, or equivalently, weight the complex ambiguity function. This smoothing operation cannot be accomplished without a penalty in terms of sampling increment Δ and FFT size N. In particular, if the smearings in the time and frequency domains of the WDF are 2/B and 2/D, respectively, the new tighter requirements are

$$\Delta < \left(F + \frac{2}{D}\right)^{-1} , \quad N > \frac{2T}{\Delta} + \frac{4}{B\Delta} ,$$

in order to realize an unaliased smoothed WDF and to be able to track its variations in time and frequency. The impact of these more stringent bounds, which depends on the particular waveform s(t) of interest and the degree of smoothing utilized, must be anticipated and investigated for each case; if either bound is violated, an aliased smoothed WDF will result.

TABLE OF CONTENTS

LIST OF ILLUSTRATIONS

LIST OF ABBREVIATIONS

FFT	fast Fourier transform
WDF	Wigner distribution function
CAF	complex ambiguity function
TCF	temporal correlation function
SCF	spectral correlation function
TFR	time-frequency representation
GTFR	generalized time-frequency representation

LIST OF SYMBOLS

t	time, (1)
f	frequency, (1)
$s(t)$	waveform of interest, (1)
$S(f)$	spectrum of $s(t)$, (1)
T	total time extent of $s(t)$, (2)
F	total frequency extent of $S(f)$, (3)
τ	time delay or separation, (4)
ν	frequency shift or separation, (5)
$R(t,\tau)$	temporal correlation function, (4)
$\Phi(\nu,f)$	spectral correlation function, (5)
$W(t,f)$	Wigner distribution function, (6)
$\chi(\nu,\tau)$	complex ambiguity function, (7)
$\tilde{v}(\nu,\tau)$	weighting or kernel, (8)
$\tilde{V}(\nu,f)$	bispectral function, (9)
$v(t,\tau)$	bitemporal function, (10)
$V(t,f)$	smoothing function, (11)
B	$1/B$ is positive extent of $V(t,f)$ in t, figures 2 and 4
D	$1/D$ is positive extent of $V(t,f)$ in f, figures 2 and 4
$\chi(\nu,\tau)$	modified complex ambiguity function, (16)
$\Phi(\nu,f)$	modified spectral correlation function, (17)
$R(t,\tau)$	modified temporal correlation function, (18)
$W(t,f)$	modified Wigner distribution function, (19)
$\oplus$	convolution, under (19)
r	tilt parameter, (23) and figure 4
q	$(1-r^2)^{\frac{1}{2}}$, (24)

A_{tf}	effective area of $V(t,f)$, figure 4
$A_{\nu\tau}$	effective area of $\tilde{v}(\nu,\tau)$, figure 4
σ	parameter of Choi-Williams kernel, (25)
Δ	time increment in sampling $s(t)$, (31)
$\overline{S}(f)$	spectrum calculated from samples $\{s(k\Delta)\}$, (31)
N	FFT size, (33)
Δ_f	frequency increment, (33)
sub a	approximation, (34), (43), (48)
$\delta_{\underset{\sim}{b}}$	infinite impulse train of period b, (35)
Δ_ν	increment in ν, (39)
Δ_τ	increment in τ, (40)
Δ_t	increment in t, (52)

ALIAS-FREE SMOOTHED WIGNER DISTRIBUTION FUNCTION FOR DISCRETE-TIME SAMPLES

INTRODUCTION

The utility of the Wigner distribution function (WDF) for detailed time-frequency analysis of waveforms has been summarized very well in a recent article by Cohen [1]; this material will be assumed to be known by the reader. As for actual numerical calculation, the problem of obtaining an alias-free WDF and complex ambiguity function (CAF), from discrete-time samples, was solved in a recent report by Nuttall [2]. Specifically, an upper bound on the time sampling increment and a lower bound on the fast Fourier transform (FFT) size were determined that allowed for evaluation of the original continuous WDF and CAF at a discrete set of points with sufficient detail and coverage to avoid any significant loss of information. Furthermore, a detailed prescription for the required data processing of the available discrete-time samples, in terms of FFTs, was given.

However, the presence of large oscillating interference terms, which are inherent to the WDF, requires that some smoothed version of the WDF be made available from discrete data. This problem was addressed recently by Harms [3], and a procedure was delineated for its realization in terms of FFTs. However, the additional data processing required for the smoothed WDF cannot be realized without some extra effort or penalty; in fact, new more stringent bounds on the sampling increment and FFT sizes must be met in order to retain the alias-free character of the resultant smoothed WDF. These bounds were derived by Nuttall and furnished to Harms who listed them in [3; section 4 (see ... reference 11)].

In this current report, we will present the detailed derivations that lead to these bounds. In the process, interpretations of the smoothed temporal correlation function (TCF) and smoothed spectral correlation function (SCF) are required and furnished. Allowance for a very general form of ambiguity weighting (multiplication) or Wigner smoothing (convolution), including tilts in the appropriate time-frequency planes, is made and accounted for. The specific data processing and FFT operations are presented in complete detail.

CONTINUOUS TIME-FREQUENCY REPRESENTATIONS

In this section, waveform $s(t)$ is considered to be available for continuous time t. We will point out some basic properties of the various time-frequency representations (TFRs) of the waveform, which will be required later when we address the discrete-time case; some of this material was given in [2; especially appendix A].

WAVEFORM CHARACTERISTICS

Complex waveform $s(t)$ has voltage density spectrum

$$S(f) = \int dt \exp(-i2\pi ft)\, s(t) \,, \tag{1}$$

where f is cyclic frequency and integrals without limits are conducted over the range of nonzero integrand. It will be presumed that the waveform is essentially time limited and frequency limited; that is,

$$|s(t)| \cong 0 \quad \text{for } |t| > T/2 \tag{2}$$

and

$$|S(f)| \cong 0 \quad \text{for } |f| > F/2 \,. \tag{3}$$

Thus, the total time extent of $s(t)$ is T seconds while the total frequency extent of $S(f)$ is F Hertz. The <u>effective</u> extent of $s(t)$, say where $|s(t)|$ is within $1/e$ of its peak, is smaller than T; similarly, the effective extent of $S(f)$ is smaller than F.

This distinction between the essential (total) extent and the effective extent is kept below. The time-bandwidth product TF must be larger than 1 and can be much larger than 1 for some waveforms with detailed amplitude- and/or frequency-modulation.

The fact that s(t) is centered at t = 0 results in no loss of generality because we can delay or advance a given waveform to this location. Similarly, a centered spectrum S(f) is easily achieved by frequency shifting. We allow for complex s(t), thereby accommodating analytic or complex envelope waveforms.

TIME-FREQUENCY REPRESENTATIONS

The temporal correlation function (TCF) of s(t) is defined as

$$R(t,\tau) = s(t+\tfrac{1}{2}\tau)\, s^*(t-\tfrac{1}{2}\tau) \ . \tag{4}$$

Reference to (2) immediately reveals that $R(t,\tau)$ is essentially confined to $|t| < T/2$, $|\tau| < T$. The quantity τ is the time delay or separation variable.

The spectral correlation function (SCF) is the double Fourier transform of $R(t,\tau)$ and is given by

$$\Phi(\nu,f) = \iint dt\, d\tau\, \exp(-i2\pi\nu t - i2\pi f\tau)\, R(t,\tau) =$$

$$= S(f+\tfrac{1}{2}\nu)\, S^*(f-\tfrac{1}{2}\nu) \ . \tag{5}$$

Use of (3) then demonstrates that $\Phi(\nu,f)$ is essentially limited to $|\nu| < F$, $|f| < F/2$. The quantity ν is the frequency shift or separation variable.

The Wigner distribution function (WDF) is then given by either of the following transforms

$$W(t,f) = \int d\tau \exp(-i2\pi f\tau)\ R(t,\tau) = \tag{6a}$$

$$= \int d\nu \exp(+i2\pi\nu t)\ \Phi(\nu,f)\ . \tag{6b}$$

From (6a), we can conclude that $W(t,f)$ is confined to $|t| < T/2$, while from (6b), the frequency extent is essentially $|f| < F/2$.

Finally, the complex ambiguity function (CAF) is available from either of the following transforms

$$\chi(\nu,\tau) = \int dt \exp(-i2\pi\nu t)\ R(t,\tau) = \tag{7a}$$

$$= \int df \exp(+i2\pi f\tau)\ \Phi(\nu,f)\ . \tag{7b}$$

Therefore, the region of essential contribution of $\chi(\nu,\tau)$ is $|\nu| < F$, $|\tau| < T$, from (7b) and (7a), respectively.

The extents of all four of these two-dimensional time-frequency representations are summarized in figure 1. In fact, for Gaussian waveform $s(t) = a \exp(-\frac{1}{2}t^2/\sigma^2)$, the choices $T = 4\sigma$ and $F = 2/(\pi\sigma)$, for example, give these exact results in figure 1, at the $\exp(-4) = .018$ level. Horizontal movement in this figure is accomplished by means of a Fourier transform between variables t and ν; vertical movement utilizes a Fourier transform relationship between τ and f. Relations (6) and (7), along with their inverse Fourier transforms, constitute the totality of these one-dimensional transforms.

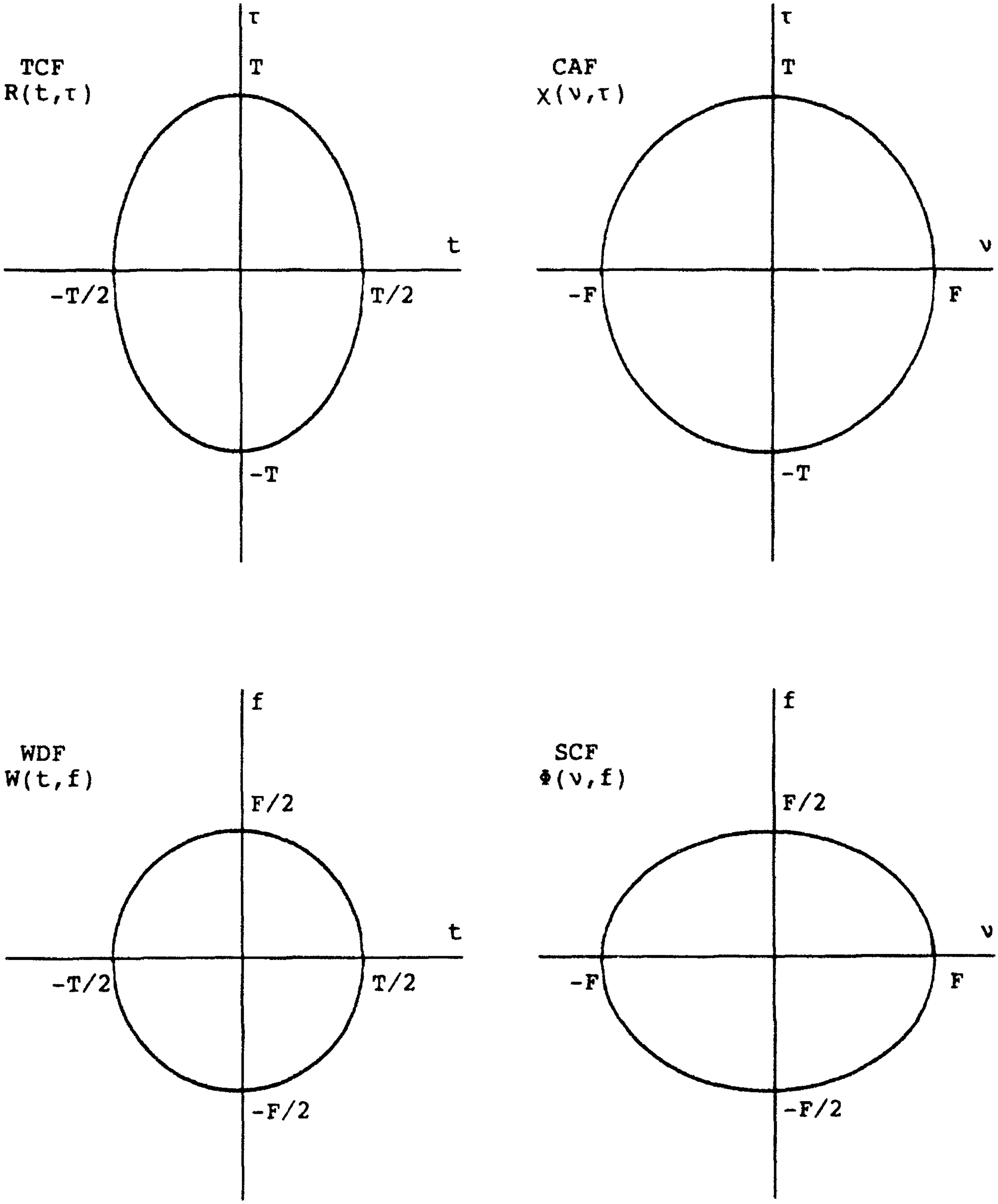

Figure 1. Extents of the Time-Frequency Representations

GENERALIZED TIME-FREQUENCY REPRESENTATIONS

Since there are four two-dimensional domains of interest in the TFRs depicted in figure 1, it is necessary to consider the effects of weighting and smoothing in all of them.

TWO-DIMENSIONAL SMOOTHING OPERATIONS

Consider ν,τ weighting (or kernel) $\tilde{v}(\nu,\tau)$ applied multiplicatively to CAF $\chi(\nu,\tau)$ to yield modified (weighted) CAF

$$\chi(\nu,\tau) = \chi(\nu,\tau)\ \tilde{v}(\nu,\tau)\ . \tag{8}$$

The three equivalent descriptors to weighting $\tilde{v}(\nu,\tau)$, in the remaining domains, are given by Fourier transform relations

$$\tilde{V}(\nu,f) = \int d\tau\ \exp(-i2\pi f\tau)\ \tilde{v}(\nu,\tau)\ , \tag{9}$$

$$v(t,\tau) = \int d\nu\ \exp(+i2\pi\nu t)\ \tilde{v}(\nu,\tau)\ , \tag{10}$$

$$\begin{aligned} V(t,f) &= \int d\tau\ \exp(-i2\pi f\tau)\ v(t,\tau) = \\ &= \int d\nu\ \exp(+i2\pi\nu t)\ \tilde{V}(\nu,f) = \\ &= \iint d\nu\ d\tau\ \exp(+i2\pi\nu t - i2\pi f\tau)\ \tilde{v}(\nu,\tau)\ . \end{aligned} \tag{11}$$

The last function, $V(t,f)$ in (11), will be called the smoothing function, for reasons to be seen below. The notational convention adopted here is that a Fourier transform from t to ν is indicated by a tilda, while a Fourier transform from τ to f is indicated by a capital.

GAUSSIAN EXAMPLE

Probably the simplest example of a unimodal two-dimensional smoothing operation in all four domains is furnished by the following Gaussian example, where B and D are arbitrary:

$$\tilde{v}(\nu,\tau) = \exp(-\pi\nu^2/B^2-\pi\tau^2/D^2) \quad , \tag{12}$$

$$\tilde{V}(\nu,f) = D \exp(-\pi\nu^2/B^2-\pi D^2f^2) \quad , \tag{13}$$

$$v(t,\tau) = B \exp(-\pi B^2t^2-\pi\tau^2/D^2) \quad , \tag{14}$$

$$V(t,f) = BD \exp(-\pi B^2t^2-\pi D^2f^2) \quad . \tag{15}$$

The effective areas of these four two-dimensional functions, at the 1/e contour level relative to each peak, are BD, B/D, D/B, and 1/(BD), respectively. It is seen from (12) that B and D are the essential (positive) extents of weighting $\tilde{v}(\nu,\tau)$ in the ν and τ directions, respectively. That is, $\tilde{v}(B,0) = \tilde{v}(0,D) = \exp(-\pi) = .043 << 1 = \tilde{v}(0,0)$. Similarly, from (15), 1/B and 1/D are the essential (positive) extents of smoothing function V(t,f) in the t and f dimensions, respectively. These properties are illustrated in figure 2, where each contour depicted is at level $\exp(-\pi) = .043$, relative to its peak. Shortly, we will generalize this smoothing function example to allow for tilts in the ν,τ and t,f planes, thereby enabling better smoothing capability to be applied to the WDF, without loss of significant information.

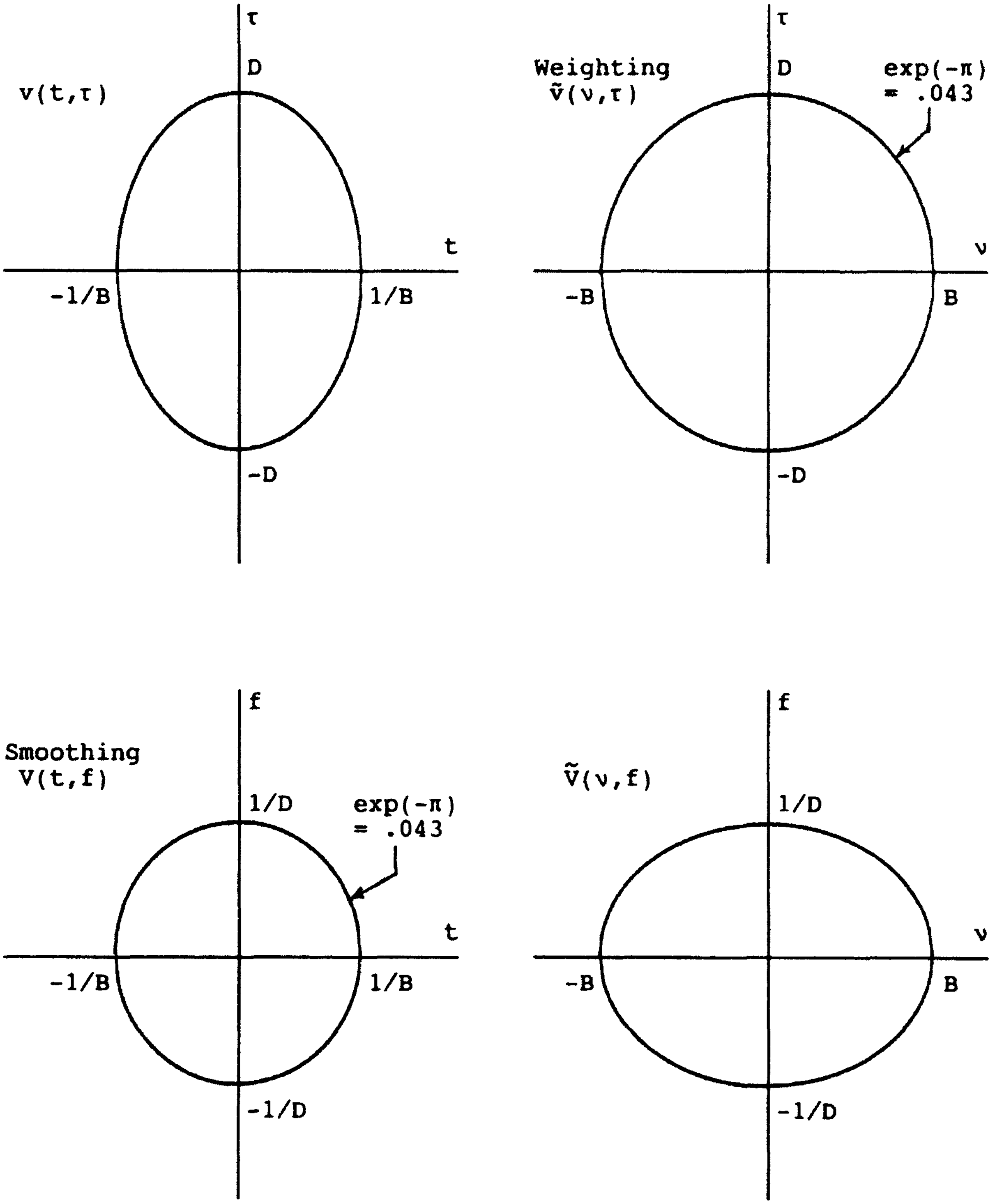

Figure 2. Two-Dimensional Smoothing Functions

MODIFIED TIME-FREQUENCY REPRESENTATIONS

The effects of each of the general smoothing functions in (8) - (11) on the four two-dimensional TFRs (4) - (7) of the previous section are now investigated; see also [4; appendix F]. The resultant generalized time-frequency representations (GTFRs) are indicated on the left-hand sides by bold type:

$$\boldsymbol{\chi}(\nu,\tau) \equiv \chi(\nu,\tau)\ \tilde{v}(\nu,\tau) \ , \tag{16}$$

$$\boldsymbol{\Phi}(\nu,f) \equiv \int d\tau\ \exp(-i2\pi f\tau)\ \boldsymbol{\chi}(\nu,\tau) = \Phi(\nu,f) \overset{f}{\circledast} \tilde{V}(\nu,f) \ , \tag{17}$$

$$\mathbf{R}(t,\tau) \equiv \int d\nu\ \exp(+i2\pi\nu t)\ \boldsymbol{\chi}(\nu,\tau) = R(t,\tau) \overset{t}{\circledast} v(t,\tau) \ , \tag{18}$$

$$\mathbf{W}(t,f) \equiv \int d\tau\ \exp(-i2\pi f\tau)\ \mathbf{R}(t,\tau) = W(t,f) \overset{tf}{\circledast} V(t,f) \ . \tag{19}$$

Here, $\overset{x}{\circledast}$ denotes convolution on x, with all other variables held fixed; thus, for example, (17) is $\int df'\ \Phi(\nu,f-f')\ \tilde{V}(\nu,f')$.

The interpretations of (16) - (19) are as follows: the CAF is simply multiplied by weighting $\tilde{v}(\nu,\tau)$; the SCF is smeared in frequency f according to $\tilde{V}(\nu,f)$; the TCF is smeared in time t according to $v(t,\tau)$; and the WDF is smeared in both t and f according to smoothing function $V(t,f)$. It is this latter two-dimensional smoothing (convolution) operation in t,f space that suppresses or eliminates the undesired oscillating components that are present in the original WDF, at the expense, of course, of spreading out localized energy components of the waveform.

The extents of the GTFRs are sketched in figure 3; these results are based upon (16) - (19), in combination with figures 1 and 2. Because $\chi(\nu,\tau)$ is the result of multiplication (16), its extents in ν,τ are the minima of the two contributing functions. On the other hand, the f extent of $\Phi(\nu,f)$ is increased by 1/D, which is the positive extent of $\tilde{V}(\nu,f)$ in f. Similarly, the t extent of $R(t,\tau)$ is lengthened by 1/B, owing to the smoothing action of $v(t,\tau)$. In both of these latter cases, the length of the untransformed variable (ν for $\Phi(\nu,f)$ and τ for $R(t,\tau)$) is unchanged. Finally, $W(t,f)$ is lengthened by 1/B and 1/D in the t and f dimensions, respectively, owing to the double convolution with smoothing function $V(t,f)$.

Since the smoothing function $V(t,f)$ in figure 2 has essentially reached zero by the time $|t| = 1/B$ and $|f| = 1/D$, the <u>effective</u> extents in t and f are approximately $|t| < 1/(2B)$ and $|f| < 1/(2D)$. That is, $V(t,f)$ is approximately 1/B by 1/D wide in the t,f plane, for an effective area of 1/(BD); see the line under (15). If this area 1/(BD) is .5 or greater, then we can expect that smoothed WDF $W(t,f)$ will be everywhere positive [4; (F-7) - (F-19)].

On the other hand, if effective area 1/(BD) is significantly less than .5, then smoothing function $V(t,f)$ is rather impulsive-like and little averaging will occur as a result of double convolution (19). Thus, it appears that BD, at least for the simple Gaussian example in (12) - (15) and figure 2, should be chosen of the order of 3 to 4. Then, the effective area of weighting $\tilde{v}(\nu,\tau)$ in (12) and figure 2 is BD, which is of the

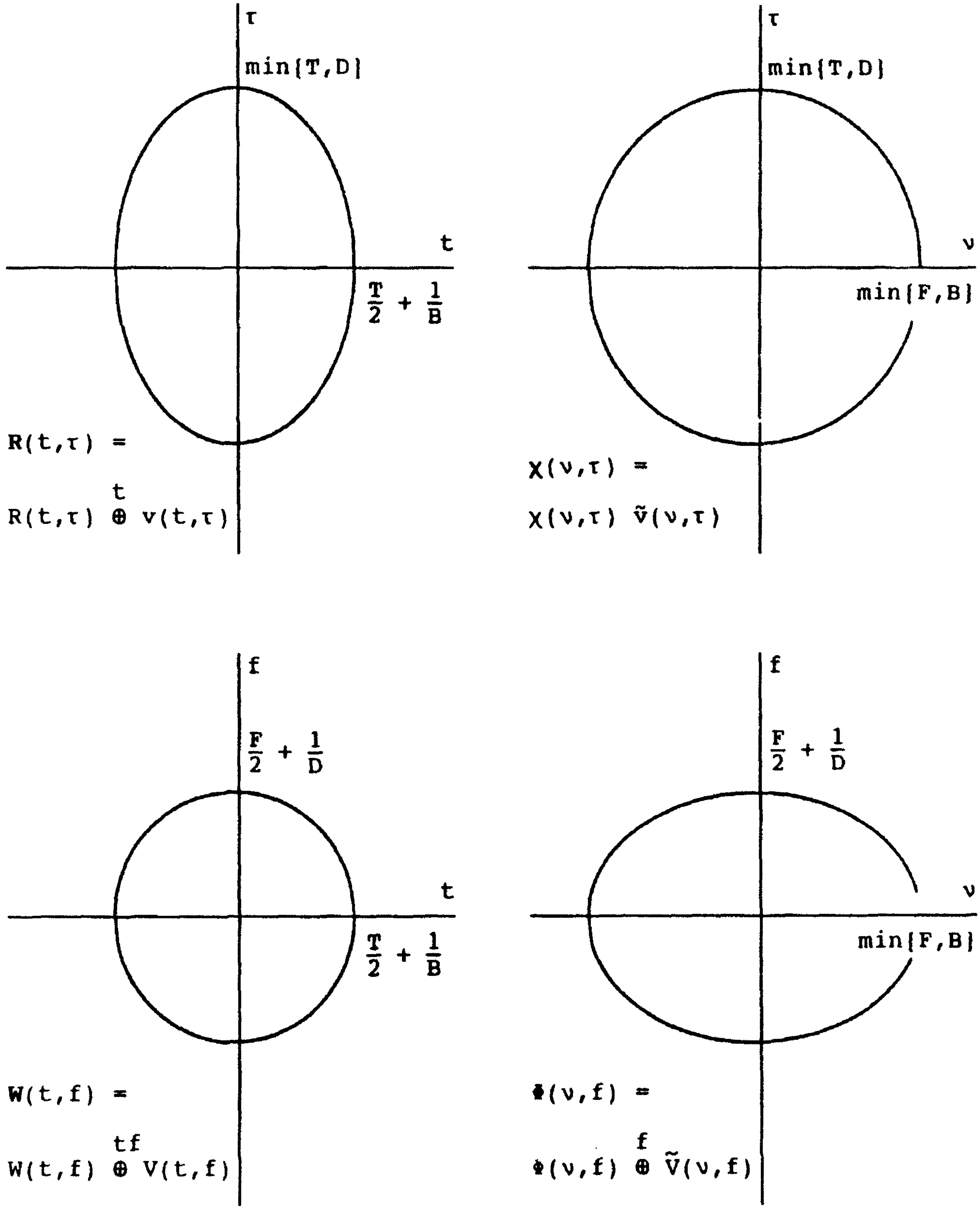

Figure 3. Generalized Time-Frequency Representations

order of 3 to 4. This area is significantly smaller than the effective extent of CAF $\chi(\nu,\tau)$ in figure 1, which covers an area of the order of FT, which is generally much larger than 1. Therefore, we can anticipate significant modifications in the weighted CAF $\chi(\nu,\tau)$, and, hence, in the smoothed WDF $\mathbf{W}(t,f)$, in the majority of the t,f plane; in fact, $\mathbf{W}(t,f)$ will have some regions with negative lobes if BD ~ 3 to 4. Except to say that we expect that B < F and D < T, there is little quantitative connection between these parameters, in general.

TILTED GAUSSIAN EXAMPLE

When waveform s(t) contains some linear frequency modulation, the simple Gaussian smoothing functions in (12) - (15) and figure 2 are inadequate. The CAF and WDF of s(t) have contours in their respective planes that are similar to tilted ellipses; see, for example, [4; pages 35 - 39]. It is then necessary to realize a weighting function $\tilde{v}(\nu,\tau)$ and a smoothing function V(t,f), which also have the capability of moving their contours to approximately match those of typical CAFs and WDFs.

A very useful set of smoothing functions is furnished by the tilted Gaussian mountain, with B and D arbitrary [4; appendices F and D]:

$$\tilde{v}(\nu,\tau) = \exp\left[-\pi\left(\frac{\nu^2}{B^2} + \frac{\tau^2}{D^2} + 2r\,\frac{\nu}{B}\,\frac{\tau}{D}\right)\right] , \tag{20}$$

$$\tilde{V}(\nu,f) = D\,\exp\left[-\pi\left(\left(1-r^2\right)\frac{\nu^2}{B^2} + D^2 f^2 - i2r\,\frac{\nu}{B}\,Df\right)\right] , \tag{21}$$

$$v(t,\tau) = B \exp\left[-\pi\left(B^2t^2 + \left(1-r^2\right)\frac{\tau^2}{D^2} + i2r\ Bt\ \frac{\tau}{D}\right)\right] , \qquad (22)$$

$$V(t,f) = \frac{BD}{\left(1-r^2\right)^{\frac{1}{2}}} \exp\left[-\frac{\pi}{1-r^2}\left(B^2t^2 + D^2f^2 + 2r\ Bt\ Df\right)\right] . \qquad (23)$$

For $r = 0$, these reduce to (12) - (15). Plots of weighting function $\tilde{v}(\nu,\tau)$ and smoothing function $V(t,f)$ are displayed in figure 4 for $r < 0$; the contours drawn are at the $\exp(-\pi) = .043$ level relative to the peak value of each function. Dimensionless tilt parameter r satisfies $|r| < 1$; also, we define $q = (1-r^2)^{\frac{1}{2}}$.

The smoothing function $V(t,f)$ again has essential extent $2/B$ by $2/D$ in the t,f plane; that is, $V(t,f)$ is substantially zero for $|t| > 1/B$ or $|f| > 1/D$. However, the effective area A_{tf} (inside the $1/e$ relative contour level) of $V(t,f)$ is now $q/(BD)$, which can be considerably less than $1/(BD)$ for $|r|$ near 1, that is, when $q << 1$. Weighting function $\tilde{v}(\nu,\tau)$ now has essential extent $2B/q$ by $2D/q$ in the ν,τ plane; its effective area $A_{\nu\tau}$ is BD/q, which is the reciprocal of that for smoothing function $V(t,f)$: $A_{\nu\tau} = 1/A_{tf}$. Values of A_{tf} of the order of 1/3 to 1/4 are desired for smoothing purposes; then, $A_{\nu\tau} \sim 3$ to 4.

Although effective area A_{tf} can be considerably less than $1/(BD)$, the smearing caused by double convolution (19) still leads to a smoothed WDF $\mathbf{W}(t,f)$ which occupies the same region indicated in figure 3. The extents of the four GTFRs are exactly the same as figure 3, except that the limits on ν and τ are now

$$\min\{F,B/q\} \quad \text{and} \quad \min\{T,D/q\}, \text{ respectively;} \quad q = (1-r^2)^{\frac{1}{2}} . \qquad (24)$$

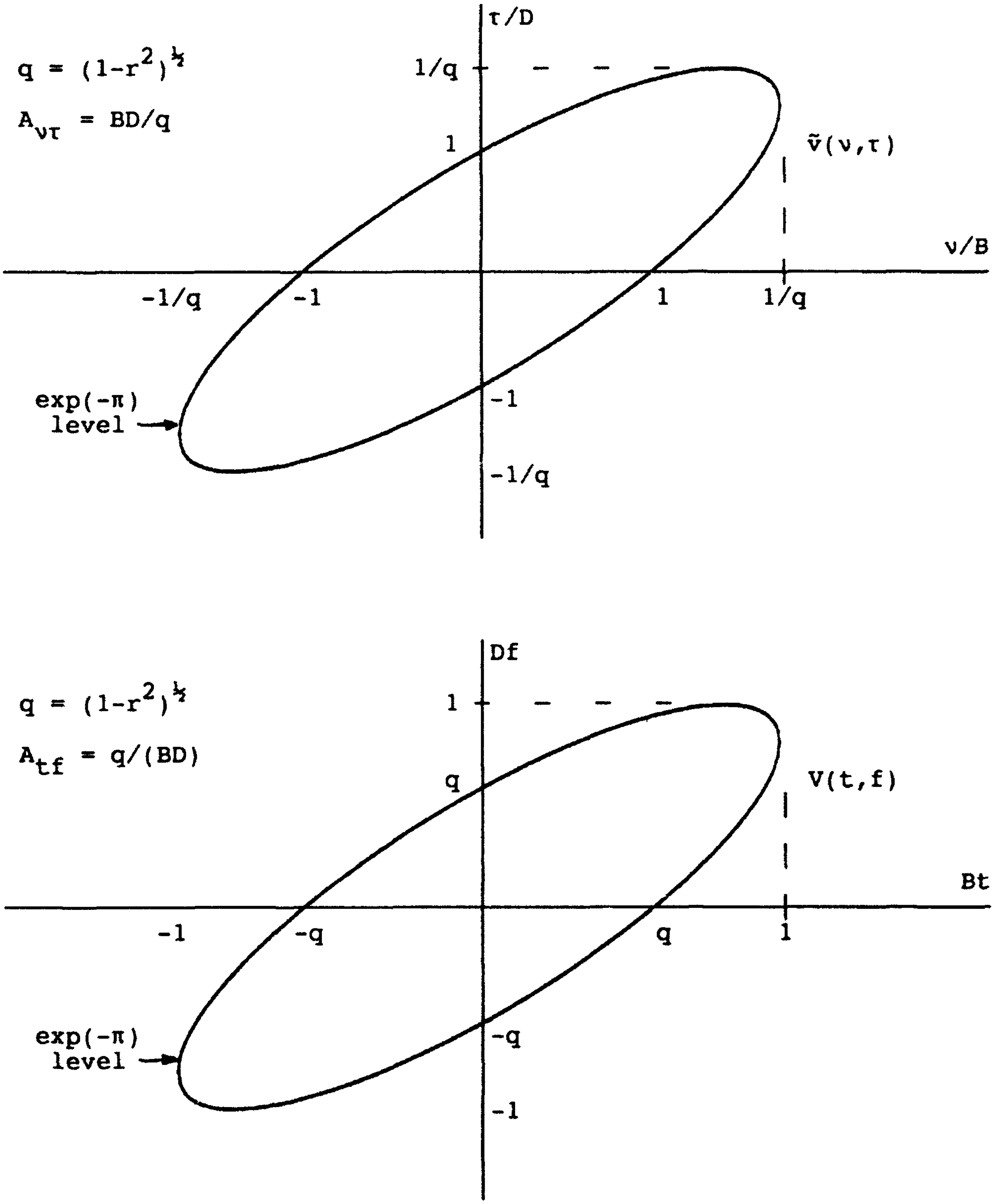

Figure 4. Tilted Smoothing Functions

CHOI-WILLIAMS KERNEL

Another example of the smoothing operations in (8) - (11) is furnished by [5]:

$$\tilde{v}(\nu,\tau) = \exp(-\nu^2\tau^2/\sigma^2) \;, \qquad \sigma > 0 \;, \tag{25}$$

$$v(t,\tau) = \left\{\begin{array}{ll} \pi^{\frac{1}{2}}\sigma/|\tau| \; \exp(-\pi^2\sigma^2t^2/\tau^2) & \text{for } \tau \neq 0 \\ \delta(t) & \text{for } \tau = 0 \end{array}\right\} , \tag{26}$$

$$\tilde{V}(\nu,f) = \left\{\begin{array}{ll} \pi^{\frac{1}{2}}\sigma/|\nu| \; \exp(-\pi^2\sigma^2f^2/\nu^2) & \text{for } \nu \neq 0 \\ \delta(f) & \text{for } \nu = 0 \end{array}\right\} , \tag{27}$$

$$V(t,f) = 2\pi^{\frac{1}{2}}\sigma \int_{0+}^{+\infty} \frac{d\nu}{\nu} \cos(2\pi\nu t) \exp(-\pi^2\sigma^2f^2/\nu^2) = \tag{28a}$$

$$= 2\pi^{\frac{1}{2}}\sigma \int_{0+}^{+\infty} \frac{d\tau}{\tau} \cos(2\pi f\tau) \exp(-\pi^2\sigma^2t^2/\tau^2) \;, \tag{28b}$$

provided that $t \neq 0$ and $f \neq 0$. Integral (28a) is convergent at $\nu = 0+$ only if $f \neq 0$ and is convergent at $\nu = +\infty$ only if $t \neq 0$. Similarly, (28b) converges at $\tau = 0+$ only if $t \neq 0$ and converges at $\tau = +\infty$ only if $f \neq 0$. Also, (28) yields $V(0,f) = \infty$ for all finite f, and $V(t,0) = \infty$ for all finite t. This smoothing function $V(t,f)$ in (28) has an integrable singularity all along both coordinate axes since $\tilde{v}(0,0) = \iint dt df \; V(t,f) = 1$ is finite. Probably, $V(t,f)$ has a logarithmic singularity as $tf \to 0$. Letting $\tau = |t|x$ in (28b), $V(t,f)$ is seen to be a function only of $|tf|$.

Because of these singularities, the actual numerical calculation of the GTFR $\mathbf{W}(t,f)$, by means of double convolution (19), appears very unattractive; rather, the Fourier transform in (19) is the recommended procedure. The delta functions in the bottom lines of (26) and (27) mean that

$$\mathbf{R}(t,0) = R(t,0) \quad \text{and} \quad \mathbf{\Phi}(0,f) = \Phi(0,f) \ . \tag{29}$$

These results follow directly from (18) and (17), respectively. Therefore, when computing GTFR $\mathbf{R}(t,\tau)$ by means of the Fourier transform in (18), the slice for $\tau = 0$ need not be done at all, but rather (29) should be employed. That is,

$$\mathbf{R}(t,\tau) = \left\{ \begin{array}{lr} \int d\nu \ \exp(i2\pi\nu t) \ \chi(\nu,\tau) \ \exp(-\nu^2\tau^2/\sigma^2) & \text{for } \tau \neq 0 \\ R(t,0) = |s(t)|^2 & \text{for } \tau = 0 \end{array} \right\} . \tag{30}$$

Finally, GTFR $\mathbf{W}(t,f)$ is obtained by Fourier transform (19). Numerous other possibilities for kernel $\tilde{v}(\nu,\tau)$ are listed in [1].

PRODUCT KERNELS

The weighting in (25) is an example of a product kernel, that is, the weighting takes the form

$$\tilde{v}(\nu,\tau) = g(\nu\tau) \ , \quad g(0) = 1 \ . \tag{30a}$$

In order that smoothing function $V(t,f)$ be real for all t,f, it is necessary that $\tilde{v}^*(-\nu,-\tau) = \tilde{v}(\nu,\tau)$ for all ν,τ, which in turn requires that $g(x)$ be real for all arguments x. Now define

$$G(y) = \int dx \exp(-i2\pi xy)\, g(x) \ . \tag{30b}$$

Then $G(-y) = G^*(y)$ for all y.

With the help of these functions and properties, we find that the rest of the two-dimensional smoothing functions are given by

$$\tilde{V}(\nu,f) = \begin{Bmatrix} \frac{1}{|\nu|}\, G\left(\frac{f}{\nu}\right) & \text{for } \nu \neq 0 \\ \delta(f) & \text{for } \nu = 0 \end{Bmatrix} , \tag{30c}$$

$$v(t,\tau) = \begin{Bmatrix} \frac{1}{|\tau|}\, G^*\left(\frac{t}{\tau}\right) & \text{for } \tau \neq 0 \\ \delta(t) & \text{for } \tau = 0 \end{Bmatrix} , \tag{30d}$$

$$V(t,f) = 2 \operatorname{Re} \int_0^\infty \frac{dy}{y} \exp(i2\pi tfy)\, G\left(\frac{1}{y}\right) \ . \tag{30e}$$

This last result shows that the smoothing function $V(t,f)$ for a product kernel is always a function of the product tf, and is never a function of t or f separately.

The last integral on y converges at $y = 0$ if $G(\infty) = 0$. Alternatively, it converges at $y = 0$ for $G(\infty) \neq 0$ if $tf \neq 0$. And the integral converges at $y = \infty$ if $tf \neq 0$.

On the other hand, if $tf = 0$, then the last integral on y above is infinite if $G(0) \neq 0$; that is, $V(t,f) = \infty$ for $tf = 0$, which corresponds to both coordinate axes $t = 0$ and $f = 0$. The example in (25) is of this nature and corresponds to the special case of $g(x) = \exp(-x^2/\sigma^2)$ and $G(y) = \pi^{\frac{1}{2}}\sigma \exp(-\pi^2 y^2 \sigma^2)$, for which $G(0) = \pi^{\frac{1}{2}}\sigma \neq 0$.

DISCRETE-TIME CONSIDERATIONS

Up to this point, it has been assumed that $s(t)$ is available for continuous time t. Now, we address the case where the only knowledge of $s(t)$ is through samples taken at multiples of time increment Δ. The proper treatment of these samples $\{s(k\Delta)\}$, in order to obtain an unaliased WDF $W(t,f)$, was determined in [2]; namely, it was found necessary to take $\Delta < 1/F$, where bandwidth F is specified in (3). Also, when an efficient FFT procedure for evaluating discrete spectral values of $S(f)$ was employed, it was found necessary to choose FFT size $N > 2T/\Delta$, where duration T is specified in (2). The following extension is aimed at obtaining an unaliased version of smoothed WDF $\mathbf{W}(t,f)$ defined in (19). The reader must be familiar with the procedures presented in [2].

EVALUATION OF MODIFIED CAF $\chi(\nu,\tau)$

As in [2; (69)], define

$$\overline{S}(f) = \left\{ \begin{array}{ll} \Delta \sum\limits_k \exp(-i2\pi f\Delta k)\; s(k\Delta) & \text{for } |f| < (2\Delta)^{-1} \\ 0 & \text{otherwise} \end{array} \right\} , \qquad (31)$$

where the sum on k is over all nonzero summand values. Then since $\Delta < 1/F$, we have $\overline{S}(f) = S(f)$ for all f; furthermore, $\overline{S}(f)$ can be computed at any f values of interest, directly from the available samples $\{s(k\Delta)\}$. Therefore, from (16), (7b), and (5), the modified continuous CAF is

$$\chi(\nu,\tau) = \tilde{v}(\nu,\tau) \int df \exp(i2\pi f\tau)\ \Phi(\nu,f) = \tag{32a}$$

$$= \tilde{v}(\nu,\tau) \int df \exp(i2\pi f\tau)\ \overline{S}(f+\tfrac{1}{2}\nu)\ \overline{S}^*(f-\tfrac{1}{2}\nu)\ . \tag{32b}$$

Now, in practice, $\overline{S}(f)$ must be computed at a discrete set of points; in particular, when we choose frequency increment $\Delta_f = 1/(N\Delta)$, where N is arbitrary, we obtain from (31)

$$\overline{S}\left(\frac{n}{N\Delta}\right) = \Delta \sum_k \exp(-i2\pi nk/N)\ s(k\Delta) \quad \text{for } |n| < \frac{N}{2}\ . \tag{33}$$

There is no need to consider n beyond the $\pm N/2$ range, because the argument f of $\overline{S}(f)$ then covers the $\pm 1/(2\Delta)$ frequency range, which is greater than the $\pm F/2$ range of S(f) in (3). We adopt, as our approximation to desired function (32), the trapezoidal form

$$\chi_a(\nu,\tau) \equiv \tilde{v}(\nu,\tau)\ \frac{1}{N\Delta} \sum_j \exp\left(i2\pi\frac{j}{N\Delta}\tau\right)\ \overline{S}\left(\frac{j}{N\Delta} + \frac{\nu}{2}\right)\ \overline{S}^*\left(\frac{j}{N\Delta} - \frac{\nu}{2}\right)$$
$$\text{for all } \nu,\tau\ . \tag{34}$$

Now let infinite impulse train

$$\delta_b(x) \equiv \sum_k \delta(x - kb)\ . \tag{35}$$

Then, using $\Delta_f = 1/(N\Delta)$, (34) can be expressed and developed as

$$\chi_a(\nu,\tau) = \tilde{v}(\nu,\tau) \int df \exp(i2\pi f\tau)\ \Phi(\nu,f)\ \Delta_f\ \delta_{\Delta_f}(f) =$$

$$= \tilde{v}(\nu,\tau)\ \left[\chi(\nu,\tau) \overset{\tau}{\circledast} \sum_j \delta(\tau - jN\Delta)\right] =$$

$$= \tilde{v}(\nu,\tau) \sum_j \chi(\nu,\tau - jN\Delta) \quad \text{for all } \nu,\tau\ . \tag{36}$$

The sum on j in (36) represents sets of aliasing lobes spaced by multiples of $N\Delta$ on the τ axis. From figure 1, since the τ extent of $\chi(\nu,\tau)$ is $\pm T$, the first aliasing lobe in (36) for $j = 1$ extends down to $\tau = N\Delta - T$. In order that this lobe not overlap the desired main lobe, $j = 0$, we must have $T < N\Delta - T$, or

$$N > \frac{2T}{\Delta}\,, \quad \Delta_f = \frac{1}{N\Delta} < \frac{1}{2T}\,. \tag{37}$$

This last constraint on Δ_f is consistent with the fact that the τ extents of $R(t,\tau)$ and $\chi(\nu,\tau)$ are $\pm T$; see figure 1 and [2; page A-4].

Equation (37) states that the size of the FFT in (33) must be at least equal to twice the number of waveform samples taken at increment Δ in duration T of $s(t)$. When this selection is made, (36) and (16) yield

$$\chi_a(\nu,\tau) = \tilde{v}(\nu,\tau)\;\chi(\nu,\tau) = \chi(\nu,\tau) \quad \text{for } |\tau| < N\Delta/2\,, \quad \text{all } \nu\,. \tag{38}$$

That is, approximate GTFR $\chi_a(\nu,\tau)$, defined by the sum in (34), is equal to the desired GTFR $\chi(\nu,\tau)$ within a strip in the ν,τ plane.

Now, in order to convert (34) to a form where we can use the spectrum calculations (33), we limit ν to the values $2n/(N\Delta)$:

$$\chi\left(\frac{2n}{N\Delta},\tau\right) = \tilde{v}\left(\frac{2n}{N\Delta},\tau\right)\frac{1}{N\Delta}\sum_j \exp\left(i2\pi\frac{j}{N\Delta}\tau\right)\,\overline{S}\left(\frac{j+n}{N\Delta}\right)\,\overline{S}^*\left(\frac{j-n}{N\Delta}\right)$$

$$\text{for } |\tau| < \frac{N\Delta}{2}\,, \quad \text{all } n\,. \tag{39}$$

We have dropped the subscript a on $\chi(\nu,\tau)$, by virtue of (38). The ν increment in (39) is $\Delta_\nu = 2/(N\Delta)$, which is less than $1/T$

according to (37); this increment is fine enough to track variations of $\chi(\nu,\tau)$ in ν, since the t extent of the TFRs in figure 2 is $\pm T/2$.

Finally, in order to manipulate (39) into an FFT form, we restrict the τ-value calculations to the set

$$\chi\left(\frac{2n}{N\Delta},m\Delta\right) = \tilde{v}\left(\frac{2n}{N\Delta},m\Delta\right) \frac{1}{N\Delta} \sum_j \exp(i2\pi jm/N)\ \overline{S}\left(\frac{j+n}{N\Delta}\right)\ \overline{S}^*\left(\frac{j-n}{N\Delta}\right)$$

$$\text{for } |m| < \frac{N}{2}, \quad \text{all } n . \qquad (40)$$

Actually, since the $|\nu|$ extent of $\chi(\nu,\tau)$ is $\min\{F,B/q\}$ according to (24), we only need to consider

$$\frac{2|n|}{N\Delta} < \min\{F,B/q\} , \quad \text{that is, } |n| < \frac{N}{2} \min\{F\Delta,B\Delta/q\} . \qquad (40a)$$

But, since we always have $F\Delta < 1$, then $|n| < N/2$ will always suffice. Thus, m and n in (40) can be limited to $\pm N/2$. Also, when $|j\pm n|$ in (40) exceeds $N/2$, use $\overline{S} = 0$ in (40), according to (31) and (33).

So far, we have shown that if $\Delta < 1/F$ and $N > 2T/\Delta$, then an unaliased version of GTFR $\chi(\nu,\tau)$ is available and that this version can be efficiently computed by (40). These conditions are the same as those derived in [2; appendix D]. The multiplication of $\chi(\nu,\tau)$ by weighting $\tilde{v}(\nu,\tau)$ in (16) or (32) to obtain $\chi(\nu,\tau)$ has no effect on <u>aliasing</u> in the ν,τ plane; this is an obvious result in retrospect. However, since GTFR $\chi(\nu,\tau)$ in (38) is the product of $\chi(\nu,\tau)$ and $\tilde{v}(\nu,\tau)$, it varies <u>faster</u> with ν and τ and must be sampled more finely. This effect is now addressed.

The τ increment in (40) is $\Delta_\tau = \Delta$. But since the f extent, E_f, of GTFR $\Phi(\nu,f)$ in (32a), according to figure 3, is $\pm E_f$, where $E_f = F/2 + 1/D$, we must take $\Delta_\tau < 1/(2E_f)$, that is,

$$\Delta < \frac{1}{F + \frac{2}{D}} \quad \left(< \frac{1}{F}\right) . \tag{41}$$

Also, the ν increment in (40) is $\Delta_\nu = 2/(N\Delta)$. But since the t extent, E_t, of GTFR $R(t,\tau)$, according to figure 3, is $\pm E_t$, where $E_t = T/2 + 1/B$, we must take $\Delta_\nu < 1/(2E_t)$, that is,

$$N > \frac{2T}{\Delta} + \frac{4}{B\Delta} \quad \left(> \frac{2T}{\Delta}\right) . \tag{42}$$

These two more-stringent conditions in (41) and (42) are consistent with the observation, above, that $\chi(\nu,\tau)$ in (38) is the product of two functions. From this point on, we presume that (41) and (42) are satisfied.

EVALUATION OF MODIFIED SCF $\Phi(\nu,f)$

The modified SCF $\Phi(\nu,f)$ is given by (17) as the Fourier transform of $\chi(\nu,\tau)$. Since $\chi(\nu,\tau)$ will only be available at increment $\Delta_\tau = \Delta$, as given by (40), we adopt as our approximation the trapezoidal form

$$\Phi_a(\nu,f) \equiv \Delta \sum_m \exp(-i2\pi fm\Delta)\ \chi(\nu,m\Delta) =$$

$$= \int d\tau\ \exp(-i2\pi f\tau)\ \chi(\nu,\tau)\ \Delta\ \delta_\Delta(\tau) =$$

$$= \Phi(\nu,f) \overset{f}{\circledast} \delta_{1/\Delta}(f) = \sum_m \Phi\left(\nu, f - \frac{m}{\Delta}\right) \quad \text{for all } \nu, f\ . \qquad (43)$$

The first aliasing lobe for $m = 1$ is centered at $f = 1/\Delta$.

The f extent of GTFR $\Phi(\nu,f)$ is $\pm(F/2 + 1/D)$, as seen in figure 3. In order that aliasing be insignificant in (43), we must have $F/2 + 1/D < 1/(2\Delta)$; that is, time sampling increment Δ must satisfy constraint (41), as before. This is tighter than the original constraint $\Delta < 1/F$, which was sufficient for reconstruction of $s(t)$ and the unmodified TFRs such as $\chi(\nu,\tau)$ and $W(t,f)$. If we anticipate doing some smoothing of the TFRs, sampling with a time increment Δ satisfying (41) must be undertaken in order to avoid aliasing of $\Phi(\nu,f)$ in f. In this case, we have

$$\Phi_a(\nu,f) = \Phi(\nu,f) \quad \text{for } |f| < 1/(2\Delta)\ ,\ \text{all } \nu\ . \qquad (44)$$

As for the actual evaluation of GTFR $\Phi(\nu,\tau)$, we use (43) and (44) to get

$$\Phi\left(\nu,\frac{j}{N\Delta}\right) = \Delta \sum_m \exp(-i2\pi jm/N)\ \chi(\nu,m\Delta) \quad \text{for } |j| < \frac{N}{2}\text{ , all } \nu\ . \tag{45}$$

Finally, in order to use the available quantities in (40), we restrict the calculation to the values

$$\Phi\left(\frac{2n}{N\Delta},\frac{j}{N\Delta}\right) = \Delta \sum_m \exp(-i2\pi jm/N)\ \chi\left(\frac{2n}{N\Delta},m\Delta\right)$$

$$\text{for } |n| < \frac{N}{2}\text{ , } |j| < \frac{N}{2}\ . \tag{46}$$

This procedure in (46) yields unaliased samples of the GTFR $\Phi(\nu,\tau)$ when (41) is satisfied. It utilizes FFT operations, applied to the GTFR $\chi(\nu,\tau)$, which is available by the FFT prescription in (40). The ranges of integers n and j in (46) are sufficient to cover the ranges $\pm 1/\Delta$ and $\pm 1/(2\Delta)$ in ν and f, respectively. But since $1/\Delta > F + 2/D$ by (41), the ranges $\pm(F + 2/D)$ and $\pm(F/2 + 1/D)$ in ν and f, respectively, are adequate to fully cover the extent of GTFR $\Phi(\nu,f)$; see figure 3.

The frequency increment $\Delta_f = 1/(N\Delta)$ in (46) is fine enough to track variations of $\Phi(\nu,f)$ in f, since $1/(N\Delta) < 1/(2T)$ according to (42), while the τ extent of the GTFRs in figure 3 is always less than $\pm T$.

Also, the increment $\Delta_\nu = 2/(N\Delta)$ in (46) is fine enough to track variations of $\Phi(\nu,f)$ in ν, since $2/(N\Delta) < 1/(T + 2/B)$ according to (42), while the t extent of the GTFRs in figure 3 is always less than $\pm(T/2 + 1/B)$.

EVALUATION OF MODIFIED WDF W(t,f)

The modified WDF W(t,f) was given by (19) as the Fourier transform of $R(t,\tau)$. However, in analogy to the two alternatives in (6), there is also the form

$$W(t,f) = \int d\nu \, \exp(i2\pi\nu t) \, \Phi(\nu,f) \; . \qquad (47)$$

Since $\Phi(\nu,f)$ will only be available at increment $\Delta_\nu = 2/(N\Delta)$, as given by (46), we utilize the following trapezoidal approximation to (47):

$$W_a(t,f) \equiv \frac{2}{N\Delta} \sum_n \exp\left(i2\pi\frac{2n}{N\Delta}t\right) \Phi\left(\frac{2n}{N\Delta},f\right) =$$

$$= \int d\nu \, \exp(i2\pi\nu t) \, \Phi(\nu,f) \, \Delta_\nu \, \delta_{\Delta_\nu}(\nu) =$$

$$= W(t,f) \overset{t}{\circledast} \delta_{N\Delta/2}(t) = \sum_n W\left(t - n\frac{N\Delta}{2},f\right) \quad \text{for all } t,f \; . \qquad (48)$$

The first aliasing lobe for $n = 1$ is centered at $t = N\Delta/2$.

The t extent of GTFR W(t,f) is $\pm(T/2 + 1/B)$, as seen in figure 3. In order that aliasing in t be insignificant in (48), we must have

$$\frac{T}{2} + \frac{1}{B} < \frac{N\Delta}{4} \; ; \qquad (49)$$

that is, the FFT size N must satisfy (42), as before. This is more stringent than original constraint (37), which sufficed for the unmodified TFRs. Again, an unaliased smoothed WDF can only be achieved if sampling increment Δ is smaller and if the FFT size N is larger, the exact amounts depending on the degree of smoothing desired; see figure 2 in this regard. When (42) is satisfied, we have from (48)

$$W_a(t,f) = W(t,f) \quad \text{for } |t| < N\Delta/4 \text{ , all } f \text{ .} \tag{50}$$

The combination of (50), (48), and (46) now yields smoothed WDF samples

$$W\left(t,\frac{j}{N\Delta}\right) = \frac{2}{N\Delta} \sum_n \exp\left(i2\pi\frac{2n}{N\Delta}t\right) \Phi\left(\frac{2n}{N\Delta},\frac{j}{N\Delta}\right)$$

$$\text{for } |t| < \frac{N\Delta}{4} \text{ , } \quad |j| < \frac{N}{2} \text{ .} \tag{51}$$

Finally, to convert (51) to an FFT, we restrict the t values to

$$W\left(\frac{m\Delta}{2},\frac{j}{N\Delta}\right) = \frac{2}{N\Delta} \sum_n \exp(i2\pi nm/N) \; \Phi\left(\frac{2n}{N\Delta},\frac{j}{N\Delta}\right)$$

$$\text{for } |m| < \frac{N}{2} \text{ , } \quad |j| < \frac{N}{2} \text{ .} \tag{52}$$

Again, N-point FFTs will realize the desired unaliased smoothed WDF $W(t,f)$, provided that (41) and (42) are satisfied. The ranges of integers m and j in (52) cover interval $\pm N\Delta/4$ in t and bandwidth $\pm 1/(2\Delta)$ in f. But since $N\Delta/4 > T/2 + 1/B$ and $1/(2\Delta) > F/2 + 1/D$ according to (42) and (41), respectively, these t and f ranges cover the full extent of smoothed WDF $W(t,f)$ in figure 3.

The time increment $\Delta_t = \Delta/2$ in (52) is fine enough to track $W(t,f)$ in t, since $\Delta/2 < 1/(2F)$ according to (41), while the ν

extent of the GTFRs in figure 3 is always less than $\pm F$. Also, the frequency increment $\Delta_f = 1/(N\Delta)$ in (52) is fine enough to track $W(t,f)$ in f, since $1/(N\Delta) < 1/(2T)$ according to (42), while the τ extent of the GTFRs in figure 3 is always less than $\pm T$. Also, see [2; appendix A].

If $\Phi(2n/(N\Delta),f)$ in the top line of (48) were available for all f, the approximation $W_a(t,f)$ would be aliased only in t, with period $N\Delta/2$. However, the SCF available is $\Phi_a(\nu,f)$, given by the top line of (43), and it is seen to be aliased in f, with period $1/\Delta$. The combination of these properties results in approximate WDF $W_a(t,f)$ being aliased in <u>both</u> t and f, with periods $N\Delta/2$ and $1/\Delta$, respectively. The limitations on m and j in final result (52) keep t and f within the fundamental aliasing interval. However, (52) contains <u>all</u> the infinite number of overlapping aliasing lobes centered at $t = nN\Delta/2$ and $f = k/\Delta$ for $n,k \neq 0,0$. It is only the satisfaction of (41) and (42) that keeps all these overlapping contributions small in the fundamental interval centered at 0,0.

SUMMARY

Calculation of the modified time-frequency representations, $\chi(\nu,\tau)$, $\Phi(\nu,f)$, and $W(t,f)$, at selected discrete points in the various two-dimensional planes, can be accomplished without aliasing and without losing any information, provided that the time sampling increment Δ satisfies $\Delta < 1/(F + 2/D)$ and that the FFT size N satisfies $N > 2T/\Delta + 4/(B\Delta)$. Also, it is shown in appendix A that calculation of an unaliased modified TCF $R(t,\tau)$ requires that these same constraints be satisfied.

If integrals of products of WDFs or CAFs are of interest [6], the rules on sampling rate and FFT size given here should suffice to get accurate numerical results. The aliasing lobes have been kept out of the regions of interest, thereby minimizing possible interference effects, and the information in the functions has been retained.

A summary of the operations that must be undertaken on available time data samples $\{s(k\Delta)\}$ follows: compute the spectral quantities $\overline{S}$ in (33); use these in (40) to get samples of the weighted CAF χ; employ (46) to evaluate the modified SCF Φ; and use (52) to determine the smoothed WDF W. All of these expressions use N-point FFTs.

Since the number of substantial samples of $s(t)$ is T/Δ according to (2), the FFT size N in (33) is at least twice this large; see (37) and (42). Thus, approximately half of the N array locations input to (33) will contain rather small contributions. If $s(t)$ is sampled well beyond $t = \pm T/2$, say for

$|t| > T$, these very small values can be "collapsed" into the available N bins with no loss of accuracy; see [2; page 5]. A program that incorporates all these features above is contained in appendix B. The detailed locations of the aliasing lobes of this procedure are investigated in appendix C.

Candidates for weighting $\tilde{v}(\nu,\tau)$ to be used in (40) include (12) or (20) or (25). The selection of values for parameters B, D, r, and σ will have to be made by inspection of CAF $\chi(\nu,\tau)$, which is the factor multiplying weighting $\tilde{v}(\nu,\tau)$ in (40). A check should then be made of (41) and (42) to ensure that aliasing is not significant.

APPENDIX A. EVALUATION OF MODIFIED TCF $R(t,\tau)$

The modified TCF $R(t,\tau)$ is given by (18) as the Fourier transform on ν of $\chi(\nu,\tau)$. Since $\chi(\nu,\tau)$ will only be available at increment $\Delta_\nu = 2/(N\Delta)$, as given by (40), we adopt as our approximation the trapezoidal form

$$R_a(t,\tau) \equiv \frac{2}{N\Delta} \sum_n \exp\left(i2\pi\frac{2n}{N\Delta}t\right) \chi\left(\frac{2n}{N\Delta},\tau\right) = \tag{A-1}$$

$$= \int d\nu \exp(i2\pi\nu t)\, \chi(\nu,\tau)\, \Delta_\nu\, \delta_{\Delta_\nu}(\nu) =$$

$$= R(t,\tau) \overset{t}{\circledast} \delta_{N\Delta/2}(t) = \sum_n R\left(t - n\frac{N\Delta}{2},\tau\right) \quad \text{for all } t,\tau \ . \tag{A-2}$$

The first aliasing lobe for $n = 1$ is centered at $t = N\Delta/2$.

The t extent of GTFR $R(t,\tau)$ is $\pm(T/2 + 1/B)$, as seen in figure 3. In order that aliasing be insignificant in (A-2), we must have $T/2 + 1/B < N\Delta/4$; that is, FFT size N must satisfy constraint (42), as before. In this case, we have from (A-2)

$$R_a(t,\tau) = R(t,\tau) \quad \text{for } |t| < \frac{N\Delta}{4}\ , \quad \text{all } \tau \ . \tag{A-3}$$

In particular, from (A-1) and (A-3), we get

$$R\left(\frac{k\Delta}{2},\tau\right) = \frac{2}{N\Delta} \sum_n \exp(i2\pi kn/N)\, \chi\left(\frac{2n}{N\Delta},\tau\right) \quad \text{for } |k| < \frac{N}{2}\ , \quad \text{all } \tau \ . \tag{A-4}$$

Finally, in order to use the available quantities in (40), we restrict the calculations to values

$$R\left(\frac{k\Delta}{2},m\Delta\right) = \frac{2}{N\Delta}\sum_{n}\exp(i2\pi kn/N)\,\chi\left(\frac{2n}{N\Delta},m\Delta\right) \quad \text{for } |k| < \frac{N}{2}\,, \quad |m| < \frac{N}{2}\,. \tag{A-5}$$

This procedure in (A-5) yields unaliased samples of the GTFR $R(t,\tau)$ when (42) is satisfied. It utilizes FFT operations, applied to the GTFR $\chi(\nu,\tau)$ which is available by the FFT prescription in (40). The ranges of integers k and m in (A-5) are sufficient to cover the ranges $\pm N\Delta/4$ and $\pm N\Delta/2$ in t and τ, respectively. But since $N\Delta/2 > T + 2/B$ by (42), the ranges $\pm(T/2 + 1/B)$ and $\pm(T + 2/B)$ in t and τ, respectively, are adequate to fully cover the extent of GTFR $R(t,\tau)$; see figure 3.

The time increment $\Delta_t = \Delta/2$ in (A-5) is fine enough to track $R(t,\tau)$ in t, since $\Delta/2 < 1/(2F)$ by (41), while the ν extent of the GTFRs in figure 3 is always less than $\pm F$. Similarly, increment $\Delta_\tau = \Delta$ in (A-5) is fine enough to track $R(t,\tau)$ in τ, since $\Delta < 1/(F + 2/D)$ by (41), while the f extent of the GTFRs in figure 3 is always less than $\pm(F/2 + 1/D)$.

APPENDIX B. PROGRAM FOR SMOOTHED WDF $\mathbf{W}(t,f)$

In this appendix, a program for the procedure given in (33), (40), (46), and (52) is presented in BASIC for the Hewlett Packard 9000 computer. However, in order to minimize computational effort and storage, some additional shortcuts have been employed that take advantage of the symmetry properties of the various two-dimensional functions encountered here.

We begin by observing from (5) that the SCF satisfies

$$\Phi(-\nu,f) = \Phi^*(\nu,f) \ . \tag{B-1}$$

Therefore, we can confine the calculation of $\Phi(\nu,f)$ to $\nu \geq 0$, all f. Then, from (7b), the CAF satisfies a conjugate symmetry through the origin:

$$\chi(-\nu,-\tau) = \chi^*(\nu,\tau) \ , \tag{B-2}$$

which means that $\chi(\nu,\tau)$ need be computed only for $\nu \geq 0$, all τ.

We now choose weighting $\tilde{v}(\nu,\tau)$ in (8) to possess this same origin symmetry property as in (B-2), namely

$$\tilde{v}(-\nu,-\tau) = \tilde{v}^*(\nu,\tau) \ ; \tag{B-3}$$

then it follows that the modified CAF in (8) also satisfies

$$\boldsymbol{\chi}(-\nu,-\tau) = \boldsymbol{\chi}^*(\nu,\tau) \ . \tag{B-4}$$

Again, this allows us to confine the calculation of $\boldsymbol{\chi}(\nu,\tau)$ to $\nu \geq 0$, all τ.

The modified SCF $\boldsymbol{\Phi}(\nu,f)$ is given by Fourier transform (17).

Use of (B-4) reveals that $\Phi(\nu,f)$ satisfies

$$\Phi(-\nu,f) = \Phi^*(\nu,f) \ , \tag{B-5}$$

which allows us to compute $\Phi(\nu,f)$ only for $\nu \geq 0$, all f. Then the smoothed WDF, given by (47), can be manipulated as follows:

$$W(t,f) = \int_{-\infty}^{+\infty} d\nu \ \exp(i2\pi\nu t) \ \Phi(\nu,f) = 2 \ \mathrm{Re} \int_{0}^{+\infty} d\nu \ \exp(i2\pi\nu t) \ \Phi(\nu,f) =$$

$$= 2 \ \mathrm{Re} \int_{0}^{+\infty} d\nu \ \exp(-i2\pi\nu t) \ \Phi^*(\nu,f) \ . \tag{B-6}$$

This calculation of smoothed WDF $W(t,f)$ via a forward FFT must be done for all t,f, but it utilizes $\Phi(\nu,f)$ only for $\nu \geq 0$.

If needed, calculation of modified TCF $R(t,\tau)$ can be obtained from (18) according to

$$R(t,\tau) = \int_{-\infty}^{+\infty} d\nu \ \exp(i2\pi\nu t) \ \chi(\nu,\tau) =$$

$$= \int_{0}^{+\infty} d\nu \ \exp(i2\pi\nu t) \ \chi(\nu,\tau) + \int_{0}^{+\infty} d\nu \ \exp(-i2\pi\nu t) \ \chi^*(\nu,-\tau) \ . \tag{B-7}$$

This calculation need only be done for $\tau \geq 0$, all t, since the modified TCF satisfies

$$R(t,-\tau) = R^*(t,\tau) \ , \tag{B-8}$$

which follows from (B-7) and (B-4).

In the program listed below, the user must input time sampling increment Δ and FFT size N in lines 20 and 30. The complex data samples $\{s(k\Delta)\}$ are entered via SUB Data in lines 1210 - 1360, which requires time limits K1 Δ and K2 Δ that guarantee small values of s(t) outside this time interval. The particular waveform s(t) of interest is entered in SUB S in lines 1380 - 1470 and would have to be replaced by the user for his particular application. The complex waveform s(t) should be centered at t = 0 and f = 0; but even if this is not done, an aliased version of W(t,f) always appears in the fundamental t,f interval centered at the origin, as discussed in the sequel to (52) and appendix C. The particular example given here has been shifted by t_o and f_o, for purposes of obtaining a less symmetric example to test the routines for accuracy. Also, linear frequency modulation has been included in this example in terms of parameter Alo, α_o; see [4; (84), (91), (93)], where we have also taken $a_o = 1$, $\sigma_o = 1$.

Tilted Gaussian weighting $\tilde{v}(\nu,\tau)$ in (20) and figure 4 has been incorporated in function routine DEF FNVt in lines 1490 - 1570; the user must input choices for D, B, r in lines 1500 - 1520. The result of smoothing operation (19), namely the double convolution of WDF W(t,f) with smoothing function V(t,f) in (23), can be computed in closed form for the waveform s(t) in SUB S and the weighting $\tilde{v}(\nu,\tau)$ in DEF FNVt. This result is programmed in DEF FNWdfsmooth and is based upon [4; page J-1].

Subroutine SUB Fft14 in lines 1930 - 2860 can compute an N-point FFT for values of N up to 16384. However, due to storage demands in the main program, in particular line 120 for the two-dimensional arrays Re and Im, the maximum value of N that can be accommodated in our particular computer configuration is N = 128. However, another facility with larger storage capabilities can handle N values larger than 128 if lines 110 - 120 are increased. It should be noted that this procedure in SUB Fft14 uses zero subscripts, as encountered directly in the definition of the FFT.

An error check has been performed on the entire procedure programmed here; it is indicated in the main program by the indented lines. It is included so that a user can check his program for accuracy. In an actual application to given data, the indented lines in the main program should be deleted along with SUB S and DEF FNWdfsmooth; also, SUB Data must be modified or replaced, to suit the user.

The results of this error check are listed below for several choices of fundamental parameters N and Δ. It is seen that extreme accuracy can be achieved for the larger FFT sizes N, if increment Δ is chosen appropriately.

N	Δ	maximum error in smoothed WDF W(t,f) (t_o=.11, f_o=.17)	(t_o=0, f_o=0)
8	.90	.25	.15
16	.65	.016	.010
32	.45	.14E-3	.77E-4
64	.35	.77E-9	.36E-10
128	.25	.89E-15	.89E-15

The best choices for Δ in the latter case, where t_o = 0 and f_o = 0, are 1, .72, .51, .36, .25, respectively; the corresponding maximum errors are .078, .32E-2, .41E-5, .86E-11, .89E-15, with execution times .12, .45, 1.9, 7.8, 33.3 seconds.

```
10  ! TR 8785, APPENDIX B, ALIAS-FREE SMOOTHED WDF; HALF STORAGE
20    Delta=.35                   !  TIME SAMPLING INCREMENT; (31)
30    N=64                        !  FFT SIZE <= 128
40    PRINT "Delta =";Delta;"      N =";N
50    N1=N-1
60    N2=N/2
70    N3=N2-1
80    DOUBLE N,N1,N2,N3,Ns,Js,Ks,Ms,Jn,Jm ! INTEGERS, NOT DOUBLE PREC.
90    REDIM Cos(0:N/4),Sr(0:N1),Si(0:N1),Sbr(-N2:N2),Sbi(-N2:N2)
100   REDIM X(0:N1),Y(0:N1),Re(0:N3,0:N1),Im(0:N3,0:N1)
110   DIM Cos(32),Sr(128),Si(128),Sbr(128),Sbi(128)
120   DIM X(128),Y(128),Re(63,127),Im(63,127)  !  64 X 128
130   A=2.*PI/N
140   FOR Ns=0 TO N/4
150   Cos(Ns)=COS(A*Ns)           !  QUARTER-COSINE TABLE
160   NEXT Ns
170   CALL Data(N,Delta,Sr(*),Si(*))     !  TIME DATA
180   CALL Fft14(N,Cos(*),Sr(*),Si(*))   !  SPECTRUM
190   FOR Ns=-N2 TO N2
200   Ks=Ns MODULO N              !
210   Sbr(Ns)=Sr(Ks)              !  S̄(f); (31)
220   Sbi(Ns)=Si(Ks)              !  NEEDS Delta; (33)
230   NEXT Ns
240   Dnu=2./(N*Delta)            !  nu  INCREMENT IN CAF; (40)
250   Dtau=Delta                  !  tau INCREMENT IN CAF; (40)
260   FOR Ns=0 TO N3              !  nu >= 0; APPENDIX B
270   MAT X=(0.)
280   MAT Y=(0.)
290   Jn=N2-Ns
300   FOR Js=-Jn TO Jn
310   Ks=Js+Ns
320   Ms=Js-Ns
330   Pr=Sbr(Ks)
340   Pi=Sbi(Ks)
350   Mr=Sbr(Ms)
360   Mi=Sbi(Ms)
370   Jm=Js MODULO N              !
380   X(Jm)=Pr*Mr+Pi*Mi           !  S̄(f+nu/2) S̄*(f-nu/2); (40)
390   Y(Jm)=-(Pi*Mr-Pr*Mi)        !  CONJUGATE THE FFT INPUT
400   NEXT Js
410   CALL Fft14(N,Cos(*),X(*),Y(*))  !  INTO nu,tau DOMAIN
420   Nu=Dnu*Ns                   !  nu IN WEIGHTING v~ ; (40)
430   FOR Ms=-N2 TO N3
440   Jm=Ms MODULO N
450   Tau=Dtau*Ms                 !  tau IN WEIGHTING v~
460   Vt=FNVt(Nu,Tau)             !  WEIGHTING v~
470   Re(Ns,Jm)=X(Jm)*Vt
480   Im(Ns,Jm)=-Y(Jm)*Vt         !  CONJUGATE THE FFT OUTPUT
490   NEXT Ms                     !  WEIGHTED COMPLEX AMBIGUITY FN.
500   NEXT Ns                     !  NEEDS Delta/N; (40)
510   FOR Ns=0 TO N3
520   FOR Ms=0 TO N1
530   X(Ms)=Re(Ns,Ms)
540   Y(Ms)=Im(Ns,Ms)
550   NEXT Ms
560   CALL Fft14(N,Cos(*),X(*),Y(*))  !  INTO nu,f DOMAIN
570   FOR Js=0 TO N1
580   Re(Ns,Js)=X(Js)
590   Im(Ns,Js)=Y(Js)
600   NEXT Js                     !  MODIFIED SPECTRAL CORRELATION FN.
610   NEXT Ns                     !  NEEDS Delta*Delta/N; (46)
```

```
620     FOR Js=0 TO N1
630     X(0)=Re(0,Js)
640     Y(0)=-Im(0,Js)
650     FOR Ns=1 TO N3
660     X(Ns)=Re(Ns,Js)*2.
670     Y(Ns)=-Im(Ns,Js)*2.            !  CONJUGATE THE FFT INPUT
680     NEXT Ns
690     FOR Ns=N2 TO N1
700     X(Ns)=Y(Ns)=0.                 !  ZERO MODIFIED SCF FOR nu < 0
710     NEXT Ns
720     CALL Fft14(N,Cos(*),X(*),Y(*))   !  INTO t,f DOMAIN
730     FOR Ms=0 TO N3
740     Re(Ms,Js)=X(Ms)                !  SMOOTHED WDF FOR t >= 0
750     NEXT Ms
760     FOR Ms=N2 TO N1
770     Im(Ms-N2,Js)=X(Ms)             !  SMOOTHED WDF FOR t < 0
780     NEXT Ms                        !  ARRAY Y(*) IS DISCARDED; APP. B
790     NEXT Js                        !  NEEDS 2.*Delta/(N*N); (52)
800     A=2.*Delta/(N*N)
810     MAT Re=Re*(A)                  !  ONE FINAL SCALING
820     MAT Im=Im*(A)                  !   GIVES SMOOTHED WDF
830       Big=0.
840     Dt=Delta*.5                    !  t INCREMENT IN SMOOTHED WDF; (52)
850     Df=1./(N*Delta)                !  f INCREMENT IN SMOOTHED WDF; (52)
860     GINIT
870     PLOTTER IS "GRAPHICS"
880     GRAPHICS ON
890     WINDOW -N2,N2,-N2,N2
900     LINE TYPE 3
910     MOVE -N2,0
920     DRAW N2,0
930     MOVE 0,-N2
940     DRAW 0,N2
950     PENUP
960     LINE TYPE 1
970     FOR Js=-N2 TO N3
980     Jn=Js MODULO N
990     Fs=Df*Js                       !  f IN SMOOTHED WIGNER DIST. FN.
1000    FOR Ms=-N2 TO -1
1010    Wdfsm=Im(Ms+N2,Jn)             !  SMOOTHED WDF FOR t < 0
1020    Ts=Dt*Ms                       !  t IN SMOOTHED WIGNER DIST. FN.
1030      Error=Wdfsm-FNWdfsmooth(Ts,Fs)
1040      Big=MAX(Big,ABS(Error))
1050    PLOT Ms,Js+Wdfsm
1060    NEXT Ms
1070    FOR Ms=0 TO N3
1080    Wdfsm=Re(Ms,Jn)                !  SMOOTHED WDF FOR t >= 0
1090    Ts=Dt*Ms
1100      Error=Wdfsm-FNWdfsmooth(Ts,Fs)
1110      Big=MAX(Big,ABS(Error))
1120    PLOT Ms,Js+Wdfsm
1130    NEXT Ms
1140    PENUP
1150    NEXT Js
1160      PRINT "MAXIMUM ERROR =";Big  !  MAXIMUM ERROR IN SMOOTHED WDF
1170      PRINT
1180    PAUSE
1190    END
1200    !
```

```
1210    SUB Data(DOUBLE N,REAL Delta,Sr(*),Si(*))
1220    DOUBLE Ks,Js,K1,K2             !  INTEGERS, NOT DOUBLE PRECISION
1230    MAT Sr=(0.)
1240    MAT Si=(0.)
1250    K1=-40                         !  USER MUST
1260    K2=40                          !   INPUT LIMITS
1270    FOR Ks=K1 TO K2
1280    Js=Ks MODULO N                 !  COLLAPSING
1290    Ts=Delta*Ks                    !  TIME t
1300    CALL S(Ts,Sr,Si)               !  COMPLEX DATA WAVEFORM
1310    Sr(Js)=Sr(Js)+Sr               !  DATA IS STORED IN 0:N1
1320    Si(Js)=Si(Js)+Si
1330    IF Ks=K1 THEN PRINT "WAVEFORM EDGE VALUES:  ";SQR(Sr*Sr+Si*Si);
1340    IF Ks=K2 THEN PRINT SQR(Sr*Sr+Si*Si)
1350    NEXT Ks
1360    SUBEND
1370    !
1380    SUB S(Ts,Sr,Si)                !  WAVEFORM s(t); CENTER AT t=0, f=0
1390    Alo=.92                        !  LINEAR FM
1400    To=.11                         !  CENTERED AT t=to AND
1410    Fo=.17                         !   f=fo FOR THIS EXAMPLE
1420    A=Ts-To
1430    B=2.*PI*Fo*Ts+.5*Alo*A*A
1440    E=EXP(-.5*A*A)
1450    Sr=E*COS(B)                    !  COMPLEX
1460    Si=E*SIN(B)                    !  WAVEFORM
1470    SUBEND
1480    !
1490    DEF FNVt(Nu,Tau)               !  WEIGHTING v~(nu,tau)
1500    D=3.5                          !  tau EXTENT, SECONDS
1510    B=1.1                          !  nu  EXTENT, HERTZ
1520    Rs=-.21                        !  TILT, |r| < 1
1530    V=Nu/B
1540    T=Tau/D
1550    A=V*V+T*T+2.*Rs*V*T
1560    RETURN EXP(-PI*A)              !  (20) AND FIGURE 4
1570    FNEND
1580    !
```

```
1590    DEF FNWdfsmooth(Ts,Fs)         !  SMOOTHED WDF; TR 8225, page J-1
1600    Alo=.92                        !  LINEAR FM; SEE SUB S
1610    To=.11                         !  CENTERED AT t=to AND
1620    Fo=.17                         !   f=fo FOR THIS EXAMPLE
1630    D=3.5                          !  tau EXTENT, SECONDS
1640    B=1.1                          !  nu  EXTENT, HERTZ
1650    Rs=-.21                        !  TILT, |r| < 1
1660    Q2=1.-Rs*Rs
1670    A2=1.+Alo*Alo
1680    As=2.*A2
1690    Bs=8.*PI*PI
1700    Rho=-Alo/SQR(A2)
1710    Cs=2.*PI*B*B/Q2
1720    Ds=2.*PI*D*D/Q2
1730    Lam=Rs
1740    R1=1.-Rho*Rho
1750    L1=1.-Lam*Lam
1760    Ab=As*Bs
1770    Cd=Cs*Ds
1780    Sa=SQR(Ab)
1790    Sc=SQR(Cd)
1800    A1=Ab*R1
1810    C1=Cd*L1
1820    Dc=A1+C1+As*Ds+Bs*Cs-2.*Sa*Sc*Rho*Lam
1830    N1=A1*Cs+As*C1
1840    N2=A1*Ds+Bs*C1
1850    N3=Ab*Sc*Lam*R1+Sa*Cd*Rho*L1
1860    Fac=4.*PI*B*D*SQR(PI/(Q2*Dc))
1870    Xs=Ts-To
1880    Ys=Fs-Fo
1890    Num=N1*Xs*Xs+N2*Ys*Ys+2.*N3*Xs*Ys
1900    RETURN Fac*EXP(-.5*Num/Dc)
1910    FNEND
1920    !
```

```
1930    SUB Fft14(DOUBLE N,REAL Cos(*),X(*),Y(*)) ! N<=2^14=16384; 0 SUBS
1940    DOUBLE Log2n,N1,N2,N3,N4,J,K   !  INTEGERS < 2^31 = 2,147,483,648
1950    DOUBLE I1,I2,I3,I4,I5,I6,I7,I8,I9,I10,I11,I12,I13,I14,L(0:13)
1960    IF N=1 THEN SUBEXIT
1970    IF N>2 THEN 2050
1980    A=X(0)+X(1)
1990    X(1)=X(0)-X(1)
2000    X(0)=A
2010    A=Y(0)+Y(1)
2020    Y(1)=Y(0)-Y(1)
2030    Y(0)=A
2040    SUBEXIT
2050    A=LOG(N)/LOG(2.)
2060    Log2n=A
2070    IF ABS(A-Log2n)<1.E-8 THEN 2100
2080    PRINT "N =";N;"IS NOT A POWER OF 2; DISALLOWED."
2090    PAUSE
2100    N1=N/4
2110    N2=N1+1
2120    N3=N2+1
2130    N4=N3+N1
2140    FOR I1=1 TO Log2n
2150    I2=2^(Log2n-I1)
2160    I3=2*I2
2170    I4=N/I3
2180    FOR I5=1 TO I2
2190    I6=(I5-1)*I4+1
2200    IF I6<=N2 THEN 2240
2210    A1=-Cos(N4-I6-1)
2220    A2=-Cos(I6-N1-1)
2230    GOTO 2260
2240    A1=Cos(I6-1)
2250    A2=-Cos(N3-I6-1)
2260    FOR I7=0 TO N-I3 STEP I3
2270    I8=I7+I5-1
2280    I9=I8+I2
2290    T1=X(I8)
2300    T2=X(I9)
2310    T3=Y(I8)
2320    T4=Y(I9)
2330    A3=T1-T2
2340    A4=T3-T4
2350    X(I8)=T1+T2
2360    Y(I8)=T3+T4
2370    X(I9)=A1*A3-A2*A4
2380    Y(I9)=A1*A4+A2*A3
2390    NEXT I7
2400    NEXT I5
2410    NEXT I1
```

```
2420    I1=Log2n+1
2430    FOR I2=1 TO 14
2440    L(I2-1)=1
2450    IF I2>Log2n THEN 2470
2460    L(I2-1)=2^(I1-I2)
2470    NEXT I2
2480    K=0
2490    FOR I1=1 TO L(13)
2500    FOR I2=I1 TO L(12) STEP L(13)
2510    FOR I3=I2 TO L(11) STEP L(12)
2520    FOR I4=I3 TO L(10) STEP L(11)
2530    FOR I5=I4 TO L(9) STEP L(10)
2540    FOR I6=I5 TO L(8) STEP L(9)
2550    FOR I7=I6 TO L(7) STEP L(8)
2560    FOR I8=I7 TO L(6) STEP L(7)
2570    FOR I9=I8 TO L(5) STEP L(6)
2580    FOR I10=I9 TO L(4) STEP L(5)
2590    FOR I11=I10 TO L(3) STEP L(4)
2600    FOR I12=I11 TO L(2) STEP L(3)
2610    FOR I13=I12 TO L(1) STEP L(2)
2620    FOR I14=I13 TO L(0) STEP L(1)
2630    J=I14-1
2640    IF K>J THEN 2710
2650    A=X(K)
2660    X(K)=X(J)
2670    X(J)=A
2680    A=Y(K)
2690    Y(K)=Y(J)
2700    Y(J)=A
2710    K=K+1
2720    NEXT I14
2730    NEXT I13
2740    NEXT I12
2750    NEXT I11
2760    NEXT I10
2770    NEXT I9
2780    NEXT I8
2790    NEXT I7
2800    NEXT I6
2810    NEXT I5
2820    NEXT I4
2830    NEXT I3
2840    NEXT I2
2850    NEXT I1
2860    SUBEND
```

APPENDIX C. GENERAL ALIASING PROPERTIES

No finite-duration time function can be exactly bandlimited in frequency. Therefore, all the properties presented above are approximations, their quality depending on the detailed temporal and spectral behaviors on the tails of waveform $s(t)$ and spectrum $S(f)$, respectively. In this appendix, we will derive the exact aliasing properties of the method listed in appendix B, for arbitrary values of sampling increment Δ and FFT size N. In fact, we will not even refer to a duration T or band F, nor will we limit time function $s(t)$ and spectrum $S(f)$ to be centered at $t = 0$ and $f = 0$, respectively. The following results will explain the aliasing properties of this numerical procedure.

We begin with (1), namely

$$S(f) \equiv \int dt \exp(-i2\pi ft)\ s(t) \quad \text{for all } f \ . \tag{C-1}$$

This spectrum can have arbitrary extent and lie anywhere on the f scale. For time sampling of $s(t)$ at increment Δ, define

$$\tilde{S}(f) \equiv \Delta \sum_k \exp(-i2\pi f\Delta k)\ s(k\Delta) \quad \text{for all } f \ , \tag{C-2}$$

where sums without limits are over $-\infty,\infty$. This function has period $1/\Delta$ in f and can be written as convolution

$$\tilde{S}(f) = S(f) \circledast \delta_{1/\Delta}(f) = \sum_n S\left(f - \frac{n}{\Delta}\right) \ . \tag{C-3}$$

Thus, no matter where $S(f)$ is located, a replica of it appears in $\tilde{S}(f)$ somewhere in the fundamental $\pm 1/(2\Delta)$ frequency range centered at f = 0. Of course, if the frequency extent of S(f) exceeds $1/\Delta$, there will be overlapping spectral components in $\tilde{S}(f)$ which will cause distortion; these effects are included in the following analysis.

As in (31), define bandlimited spectrum

$$\bar{S}(f) \equiv \tilde{S}(f)\ \mathrm{rect}(\Delta f) \quad \text{for all } f\ , \tag{C-4}$$

where rect(x) = 1 for $|x| < 1/2$ and zero otherwise. This function $\bar{S}(f)$ has limited extent in frequency, namely, it is nonzero only for $|f| < 1/(2\Delta)$. Therefore, using (C-2), we can limit its calculation to the values

$$\bar{S}\left(\frac{n}{N\Delta}\right) = \tilde{S}\left(\frac{n}{N\Delta}\right) = \Delta \sum_{k} \exp(-i2\pi nk/N)\ s(k\Delta) \quad \text{for } |n| < \frac{N}{2}\ . \tag{C-5}$$

The increment in frequency here is $\Delta_f = 1/(N\Delta)$, where N is an arbitrary integer, but generally large.

Guided by continuous forms (7b) and (5) for the CAF, we define here approximate CAF

$$\tilde{\chi}(\nu,\tau) \equiv \Delta_f \sum_{j} \exp(i2\pi j\Delta_f\tau)\ \bar{S}\left(j\Delta_f + \frac{\nu}{2}\right)\ \bar{S}^*\left(j\Delta_f - \frac{\nu}{2}\right) \quad \text{for all } \nu,\tau\ . \tag{C-6}$$

Since the product of $\bar{S}$ functions in (C-6) is nonzero only for $|j\Delta_f \pm \nu/2| < 1/(2\Delta)$, the infinite sum in (C-6) can be limited to $|j| < N/2$. Also, $\tilde{\chi}(\nu,\tau)$ is limited to $|\nu| < 1/\Delta$ and has period $1/\Delta_f = N\Delta$ in τ. In fact, we can develop (C-6) as

$$\tilde{\chi}(\nu,\tau) = \int df \exp(i2\pi f\tau)\ \overline{S}\left(f + \frac{\nu}{2}\right)\ \overline{S}^*\left(f - \frac{\nu}{2}\right)\ \Delta_f\ \delta_{\Delta_f}(f) =$$

$$= \chi_a(\nu,\tau) \overset{\tau}{\circledast} \delta_{N\Delta}(\tau) = \sum_n \chi_a(\nu,\tau - nN\Delta)\ , \qquad \text{(C-7)}$$

where $\chi_a(\nu,\tau)$ is the CAF of $\overline{S}(f)$. Thus, again, no matter where the waveform corresponding to $\overline{S}(f)$ is located on the time scale, a replica of its CAF, $\chi_a(\nu,\tau)$, appears in $\tilde{\chi}(\nu,\tau)$ somewhere in the interval $|\tau| < N\Delta/2$ centered at $\tau = 0$.

Since $\tilde{\chi}(\nu,\tau)$ is periodic in τ, we define the τ-limited CAF

$$\overline{\chi}(\nu,\tau) \equiv \tilde{\chi}(\nu,\tau)\ \text{rect}\left(\frac{\tau}{N\Delta}\right) \quad \text{for all } \nu,\tau\ . \qquad \text{(C-8)}$$

This function is nonzero only for $|\nu| < 1/\Delta$ and for $|\tau| < N\Delta/2$. Accordingly, using (C-6), we only calculate it for sample values

$$\overline{\chi}\left(\frac{2n}{N\Delta}, m\Delta\right) = \frac{1}{N\Delta} \sum_j \exp(i2\pi jm/N)\ \overline{S}\left(\frac{j + n}{N\Delta}\right)\ \overline{S}^*\left(\frac{j - n}{N\Delta}\right)$$

$$\text{for } |n| < \frac{N}{2}\ ,\ |m| < \frac{N}{2}\ . \qquad \text{(C-9)}$$

Furthermore, as noted under (C-6), the sum on j can be limited to $|j| < N/2$, by using the limited extent of $\overline{S}(f)$ in (C-4). The increments in (C-9) are $\Delta_\nu = 2/(N\Delta)$ and $\Delta_\tau = \Delta$.

Now define the weighted approximate CAF

$$\chi_b(\nu,\tau) \equiv \overline{\chi}(\nu,\tau)\ \tilde{v}(\nu,\tau) \quad \text{for all } \nu,\tau\ . \qquad \text{(C-10)}$$

This function is nonzero only for $|\nu| < 1/\Delta$ and $|\tau| < N\Delta/2$, in which case we limit its calculation to

$$\chi_b\left(\frac{2n}{N\Delta},m\Delta\right) = \bar{\chi}\left(\frac{2n}{N\Delta},m\Delta\right)\ \tilde{v}\left(\frac{2n}{N\Delta},m\Delta\right) \quad \text{for } |n| < \frac{N}{2}\ , \quad |m| < \frac{N}{2}\ . \qquad \text{(C-11)}$$

This result, combined with (C-9), is equivalent to (40) in the main text. The subscript b explicitly recognizes the approximate nature of this weighted CAF. In fact, use of (C-7), (C-8), and (C-10) indicates the precise form of this approximation to be

$$\chi_b(\nu,\tau) = \left[\chi_a(\nu,\tau) \overset{\tau}{\circledast} \delta_{N\Delta}(\tau)\right] \text{rect}\left(\frac{\tau}{N\Delta}\right)\ \tilde{v}(\nu,\tau) \quad \text{for all } \nu,\tau. \qquad \text{(C-12)}$$

where $\chi_a(\nu,\tau)$ is the CAF of $\overline{S}(f)$. If weighting $\tilde{v}(\nu,\tau)$ is chosen to cutoff in τ below $|\tau| = N\Delta/2$, then the rect operation in (C-12) can be removed. But, in general, this complicated expression in (C-12) describes the GTFR in the ν,τ domain.

By combining (18) and (19), the smoothed WDF can be written as a double Fourier transform of the weighted CAF. We therefore adopt, as our approximation for the smoothed WDF,

$$\tilde{W}_b(t,f) \equiv \Delta_\nu\ \Delta_\tau \sum_{nm} \exp\left(i2\pi\frac{2n}{N\Delta}t - i2\pi f m\Delta\right)\ \chi_b\left(\frac{2n}{N\Delta},m\Delta\right) \quad \text{for all } t,f\ . \qquad \text{(C-13)}$$

The function $W_b(t,f)$ has period $N\Delta/2$ in t and period $1/\Delta$ in f; therefore we only need to calculate

$$\tilde{W}_b\left(\frac{k\Delta}{2},\frac{j}{N\Delta}\right) = \frac{2}{N}\sum_{nm} \exp(i2\pi nk/N - i2\pi mj/N)\ \chi_b\left(\frac{2n}{N\Delta},m\Delta\right)$$

$$\text{for } |k| < \frac{N}{2}\ , \quad |j| < \frac{N}{2}\ . \qquad \text{(C-14)}$$

The double sum can be terminated at $\pm N/2$, as seen by reference to (C-10) and (C-11). The result in (C-14) is equivalent to a combination of (46) and (52) in the main text.

The doubly periodic nature of $\tilde{W}_b(t,f)$ is made apparent by developing (C-13) as

$$\tilde{W}_b(t,f) = \iint d\nu\, d\tau\, \exp(i2\pi\nu t - i2\pi f\tau)\, \chi_b(\nu,\tau)\, \Delta_\nu\, \delta_{\Delta_\nu}(\nu)\, \Delta_\tau\, \delta_{\Delta_\tau}(\tau) =$$

$$= W_b(t,f) \overset{tf}{\circledast} \delta_{N\Delta/2}(t)\, \delta_{1/\Delta}(f) = \sum_{nm} W_b\left(t - n\frac{N\Delta}{2}, f - \frac{m}{\Delta}\right) , \qquad \text{(C-15)}$$

where $W_b(t,f)$ is the WDF corresponding to modified CAF $\chi_b(\nu,\tau)$ in (C-12). Thus, regardless of where the energy of waveform s(t) is located in the t,f plane, a replica of the energy distribution appears in $\tilde{W}_b(t,f)$ in the fundamental rectangle $\pm N\Delta/4$ by $\pm 1/(2\Delta)$ centered at t,f = 0,0; this behavior has been verified numerically in the program in appendix B.

APPENDIX D. ROTATION OF TWO-DIMENSIONAL SMOOTHING FUNCTION

Let arbitrary weighting function $\tilde{v}(\nu,\tau)$ be expressed in terms of a normalized function $\tilde{u}(x,y)$ according to

$$\tilde{v}(\nu,\tau) = \tilde{u}(\nu/B,\tau/D) \ , \tag{D-1}$$

where B and D are some characteristics locations on the ν and τ axes, respectively. An example of a tilted Gaussian weighting is given in (20) and figure 4. The remaining two-dimensional functions related to $\tilde{u}(x,y)$ are just as in (9) - (11), namely

$$\tilde{U}(x,\beta) = \int dy \, \exp(-i2\pi\beta y) \, \tilde{u}(x,y) \ , \tag{D-2}$$

$$u(\alpha,y) = \int dx \, \exp(+i2\pi x\alpha) \, \tilde{u}(x,y) \ , \tag{D-3}$$

$$\begin{aligned} U(\alpha,\beta) &= \int dy \, \exp(-i2\pi\beta y) \, u(\alpha,y) = \\ &= \int dx \, \exp(+i2\pi x\alpha) \, \tilde{U}(x,\beta) = \\ &= \iint dx \, dy \, \exp(+i2\pi x\alpha - i2\pi\beta y) \, \tilde{u}(x,y) \ . \end{aligned} \tag{D-4}$$

It then follows that the remaining two-dimensional functions corresponding to weighting $\tilde{v}(\nu,\tau)$ in (D-1) can be expressed as

$$\begin{aligned} \tilde{V}(\nu,f) &= D \, \tilde{U}(\nu/B,Df) \ , \\ v(t,\tau) &= B \, u(Bt,\tau/D) \ , \\ V(t,f) &= BD \, U(Bt,Df) \ . \end{aligned} \tag{D-5}$$

Compare with (20) - (23) for a specific example.

Now consider rotation of normalized weighting $\tilde{u}$ by angle θ in the $\nu/B,\tau/D$ plane. Letting $C = \cos(\theta)$ and $S = \sin(\theta)$, the rotated weighting corresponding to $\tilde{v}$ is then defined as

$$\tilde{r}(\nu,\tau) = \tilde{u}\left(C\frac{\nu}{B} + S\frac{\tau}{D},\ C\frac{\tau}{D} - S\frac{\nu}{B}\right) = \tilde{v}\left(C\nu + S\frac{B}{D}\tau,\ C\tau - S\frac{D}{B}\nu\right) , \tag{D-6}$$

where we also used (D-1). The corresponding (rotated) two-dimensional smoothing function will be shown below to be given by

$$R(t,f) = BD\ U(CBt - SDf,\ CDf + SBt) = \tag{D-7}$$

$$= V\left(Ct - S\frac{D}{B}f,\ Cf + S\frac{B}{D}t\right) , \tag{D-8}$$

where we used (D-5). Thus, the two-dimensional normalized smoothing function U is rotated by angle $-\theta$ in the Bt,Df plane. This rule holds regardless of the forms of $\tilde{u}$ or U.

The two remaining functions $r(t,\tau)$ and $\tilde{R}(\nu,f)$ are not available in closed form involving any of the normalized functions, in general; for example,

$$\tilde{R}(\nu,f) = \int d\tau\ \exp(-i2\pi f\tau)\ \tilde{r}(\nu,\tau) =$$

$$= \int d\tau\ \exp(-i2\pi f\tau)\ \tilde{u}\left(C\frac{\nu}{B} + S\frac{\tau}{D},\ C\frac{\tau}{D} - S\frac{\nu}{B}\right) . \tag{D-9}$$

This latter integral requires a slice of $\tilde{u}(x,y)$ along a line not parallel to either coordinate axis; such a Fourier transform is not given simply in terms of $\tilde{U}$, u, or U. This type of result might have been anticipated by looking at the examples in (21) and (22) which contain oscillatory terms.

To derive (D-7), we employ (D-6) to obtain

$$R(t,f) = \iint d\nu\, d\tau\, \exp(i2\pi\nu t - i2\pi f\tau)\, \tilde{r}(\nu,\tau) =$$

$$= \iint d\nu\, d\tau\, \exp(i2\pi\nu t - i2\pi f\tau)\, \tilde{u}\left(C\frac{\nu}{B} + S\frac{\tau}{D},\, C\frac{\tau}{D} - S\frac{\nu}{B}\right) . \qquad \text{(D-10)}$$

Now let $x = C\nu/B + S\tau/D$, $y = C\tau/D - S\nu/B$; then $\nu/B = Cx - Sy$, $\tau/D = Cy + Sx$, for which the Jacobian is BD. Then (D-10) becomes

$$R(t,f) = BD \iint dx\, dy\, \exp[i2\pi Bt(Cx-Sy) - i2\pi Df(Cy+Sx)]\, \tilde{u}(x,y) =$$

$$= BD \iint dx\, dy\, \exp[i2\pi(CBt-SDf)x - i2\pi(CDf+SBt)y]\, \tilde{u}(x,y) . \qquad \text{(D-11)}$$

Reference to (D-4) immediately yields (D-7). (As a check, $\theta = 0$ yields

$$R(t,f) = BD\, U(Bt,Df) = V(t,f) , \qquad \text{(D-12)}$$

where we used (D-5).)

REFERENCES

[1] L. Cohen, "Time-Frequency Distributions - A Review", **Proceedings of the IEEE**, volume 77, number 7, pages 941 - 981, July 1989.

[2] A. H. Nuttall, **Alias-Free Wigner Distribution Function and Complex Ambiguity Function for Discrete-Time Samples**, NUSC Technical Report 8533, Naval Underwater Systems Center, New London, CT, 14 April 1989.

[3] B. Harms, "Computing Time-Frequency Distributions", **IEEE Transactions on Acoustics, Speech, and Signal Processing**, accepted for publication, October 1990.

[4] A. H. Nuttall, **Wigner Distribution Function: Relation to Short-Term Spectral Estimation, Smoothing, and Performance in Noise**, NUSC Technical Report 8225, Naval Underwater Systems Center, New London, CT, 16 February 1988.

[5] H. I. Choi and W. J. Williams, "Improved Time-Frequency Representation of Multicomponent Signals using Exponential Kernels", **IEEE Transactions on Acoustics, Speech, and Signal Processing**, volume ASSP-37, number 6, pages 862 - 871, June 1989.

[6] A. H. Nuttall, **Two-Dimensional Convolutions, Correlations, and Fourier Transforms of Combinations of Wigner Distribution Functions and Complex Ambiguity Functions**, NUSC Technical Report 8759, Naval Underwater Systems Center, New London, CT, 6 August 1990.

NUSC Technical Report 8827
1 February 1991

Complex Envelope Properties, Interpretation, Filtering, and Evaluation

Albert H. Nuttall

ABSTRACT

The complex envelope of a narrowband waveform y(t) typically has logarithmic singularities, due to discontinuities in y(t) or its derivatives, which have little physical significance. The complex envelope also has a very slow decay in time, due to the discontinuous spectrum associated with its very definition; this slow decay can mask weak desired features of the complex envelope. In order to suppress these undesired behaviors of the mathematically defined complex envelope, a filtered version is suggested and investigated in terms of its singularity rejection capability and better decay rate. Finally, numerical computation of the complex envelope, as well as its filtered version, by means of a fast Fourier transform (FFT) is investigated and the effects of aliasing are assessed quantitatively. A program for the latter task, utilizing an FFT procedure with collapsing, is furnished in BASIC.

TABLE OF CONTENTS

LIST OF ILLUSTRATIONS

LIST OF SYMBOLS

t	time, (1)
$y(t)$	real waveform, (1)
$a(t)$	imposed amplitude modulation, (1)
$p(t)$	imposed phase modulation, (1)
f_o	carrier frequency, (1)
$z(t)$	imposed complex modulation, (2)
f	frequency, (3)
$Z(f)$	spectrum (Fourier transform) of z(t), (3)
$Y(f)$	spectrum of y(t), (5)
$Y_+(f)$	single-sided spectrum of y(t), (6)
$U(f)$	unit step in f, (6)
$y_+(t)$	analytic waveform, (8)
$N(f)$	negative-frequency function, (9)
$n(t)$	negative-frequency waveform, (10)
Im	imaginary part, (13)
Re	real part, (14)
$y_H(t)$	Hilbert transform of y(t), (15)
$\circledast$	convolution, (15)
$e(t)$	error between Hilbert transform and quadrature, (17)
$E(f)$	error spectrum, (21)
$\underline{y}(t)$	complex envelope, (24)
$\underline{Y}(f)$	spectrum of complex envelope, (26)
$A(t)$	extracted amplitude modulation from $\underline{y}(t)$, (29), (42)
$P(t)$	extracted phase modulation from $\underline{y}(t)$, (29), (42)
$q(t)$	quadrature version of (30), (31)

$Q(f)$	spectrum of $q(t)$, (33)
$\mathrm{sgn}(f)$	$+1$ for $f > 0$, -1 for $f < 0$, (33)
$Y_H(f)$	spectrum of Hilbert transform, (33)
f_c	center frequency of $Y_+(f)$, (40), appendix A
α	exponential parameter, (45)
ϕ	phase parameter, (45)
ω	radian frequency $2\pi f$, (46)
ω_o	$2\pi f_o$, (46)
c	$\alpha - i\omega_o$, (46)
$E_1(z)$	exponential integral, (53), (64)
t_o	time of discontinuity, (77)
D	size of discontinuity, (77)
$H(f)$	lowpass filter, (83)
f_1	cutoff frequency, (83)
$G(f)$	filtered complex envelope spectrum, (84)
$g(t)$	filtered complex envelope, (85), (86)
$h(t)$	impulse response of lowpass filter $H(f)$, (85)
$g_d(t)$	desired component of filtered complex envelope, (86)
$g_u(t)$	undesired component of filtered complex envelope, (86)
$E(z)$	auxiliary exponential integral, (87)
u_n, v_n	auxiliary variables, (90), (91)
Δ	frequency increment, (102)
$\tilde{y}_+(t)$	approximation to analytic waveform $y_+(t)$, (102)
$\{\varepsilon_n\}$	sequence which is ½ for $n = 0$, 1 for $n \geq 1$, (102)
N	number of time points, size of FFT, (104), (106)
$\{z_n\}$	collapsed sequence, (105), (118)
$\tilde{\underline{y}}(t)$	approximation to complex envelope $\underline{y}(t)$, (109)

α	shift of frequency samples, (114)
$\tilde{g}_{\alpha}(t)$	approximation to filtered complex envelope, (114)
$\tilde{A}(t)$	magnitude of $\tilde{\underline{y}}(t)$, figure 8
$\tilde{P}(t)$	phase of $\tilde{\underline{y}}(t)$, figure 9
$y_e(t)$	even part of $y(t)$, (121)
$y_o(t)$	odd part of $y(t)$, (121)
$y_1(t)$	approximation to (119), (131)
$y_{2c}(t)$	approximation to (125), (134)
$y_{2s}(t)$	approximation to (126), (136)
$y_3(t)$	approximation to (127), (138)
$y_{4c}(t)$	approximation to (129), (141)
$y_{4s}(t)$	approximation to (130), (142)
$z_1(t)$	Fourier transform of single-sided $Y_r(f)$, (149)
$z_2(t)$	Fourier transform of single-sided $Y_i(f)$, (153)
β	displaced sampling time, (155)
FFT	fast Fourier transform

COMPLEX ENVELOPE PROPERTIES, INTERPRETATION, FILTERING, AND EVALUATION

INTRODUCTION

When a narrowband input excites a passband filter, the output time waveform y(t) is a narrowband process with low-frequency amplitude- and/or phase-modulations. The evaluation of this output process y(t) can entail an extreme amount of calculations if the detailed behavior of the higher-frequency carrier is tracked. A much better procedure in this case is to concentrate instead on determination of the low-frequency complex envelope of the narrowband output process y(t) and to state the carrier frequency associated with it. Then, the detailed nature of the output can be found at any time points of interest if desired, although, often, the complex envelope itself is the quantity of interest.

The complex envelope of output y(t) is determined from its spectrum (Fourier transform) Y(f) by suppressing the negative frequencies, down-shifting by the carrier frequency, and Fourier transforming back into the time domain. For a complicated input spectrum and/or filter transfer function with slowly decaying spectral skirts, these calculations can encounter a large number of data points and require large-size fast Fourier transforms (FFTs) for their direct realization. In this case, the use of collapsing or pre-aliasing [1; pages 4 - 5] can be fruitfully employed, thereby keeping storage and FFT sizes small, without any loss of accuracy. This procedure will be employed here.

As will be seen, when the complex envelope is re-applied to the one-sided carrier term and the real part taken, the exact narrowband waveform $y(t)$ is recovered. However, if the complex envelope itself is the quantity of interest, it has some undesirable features. The first problem is related to the fact that if waveform $y(t)$ has any discontinuities in time, its Hilbert transform contains logarithmic infinities, which show up in the complex envelope. The second problem is generated by the operation of truncating the negative frequencies in spectrum $Y(f)$; this creates a discontinuous spectrum which leads to a very slow decay in time of the magnitude of the complex envelope. Since numerical calculation of the complex envelope is necessarily accomplished by sampling spectrum $Y(f)$ in frequency f and performing FFTs, this slow time decay leads to significant aliasing and distortion in the time domain of the computed quantities.

Because these features in the mathematically defined complex envelope are very undesirable, there is a need to define and investigate a modified complex envelope which more nearly corresponds to physical interpretation and utility. The time discontinuities in $y(t)$ show up in $Y(f)$ as a $1/f$ decay for large frequencies, whereas the truncation of the negative frequencies of $Y(f)$ shows up as a discontinuity directly in f. Both of these spectral properties can be controlled by filtering the truncated spectral quantity, prior to transforming back to the time domain. We will address this filtered complex envelope and its efficient evaluation in this report.

When the waveform $y(t)$ is real and/or causal, its spectrum $Y(f)$ possesses special properties which enable alternative methods of calculation. Thus, it sometimes suffices to have only the real (or imaginary) part of $Y(f)$ and to employ a cosine (or sine) transform, rather than a complex exponential transform. The aliasing properties of these special transforms, when implemented by means of FFTs, will also be addressed here.

ANALYTIC WAVEFORM AND COMPLEX ENVELOPE

Waveform y(t) is real with amplitude modulation a(t) and phase modulation p(t) applied on given carrier frequency f_o; however, y(t) need not be narrowband. That is,

$$y(t) = a(t)\cos[2\pi f_o t + p(t)] = \mathrm{Re}\{z(t)\exp(i2\pi f_o t)\} , \qquad (1)$$

where complex lowpass waveform

$$z(t) \equiv a(t)\exp[ip(t)] \qquad (2)$$

will be called the <u>imposed</u> modulation. The corresponding spectrum of imposed modulation z(t) is

$$Z(f) = \int dt\, \exp(-i2\pi ft)\, z(t) . \qquad (3)$$

(Integrals without limits are from $-\infty$ to $+\infty$.) The magnitude of spectrum Z(f) is depicted in figure 1; it is generally concentrated near frequency f = 0. The graininess of the curves here is due to plotter quantization, not function discontinuities.

From (1), since waveform

$$y(t) = \frac{1}{2} z(t)\exp(i2\pi f_o t) + \frac{1}{2} z^*(t)\exp(-i2\pi f_o t) , \qquad (4)$$

its spectrum can be expressed as (see figure 1)

$$Y(f) = \frac{1}{2} Z(f-f_o) + \frac{1}{2} Z^*(-f-f_o) \; ; \quad Y(-f) = Y^*(f) . \qquad (5)$$

It will be assumed here that y(t) has no dc component; that is, Y(f) contains no impulse at f = 0.

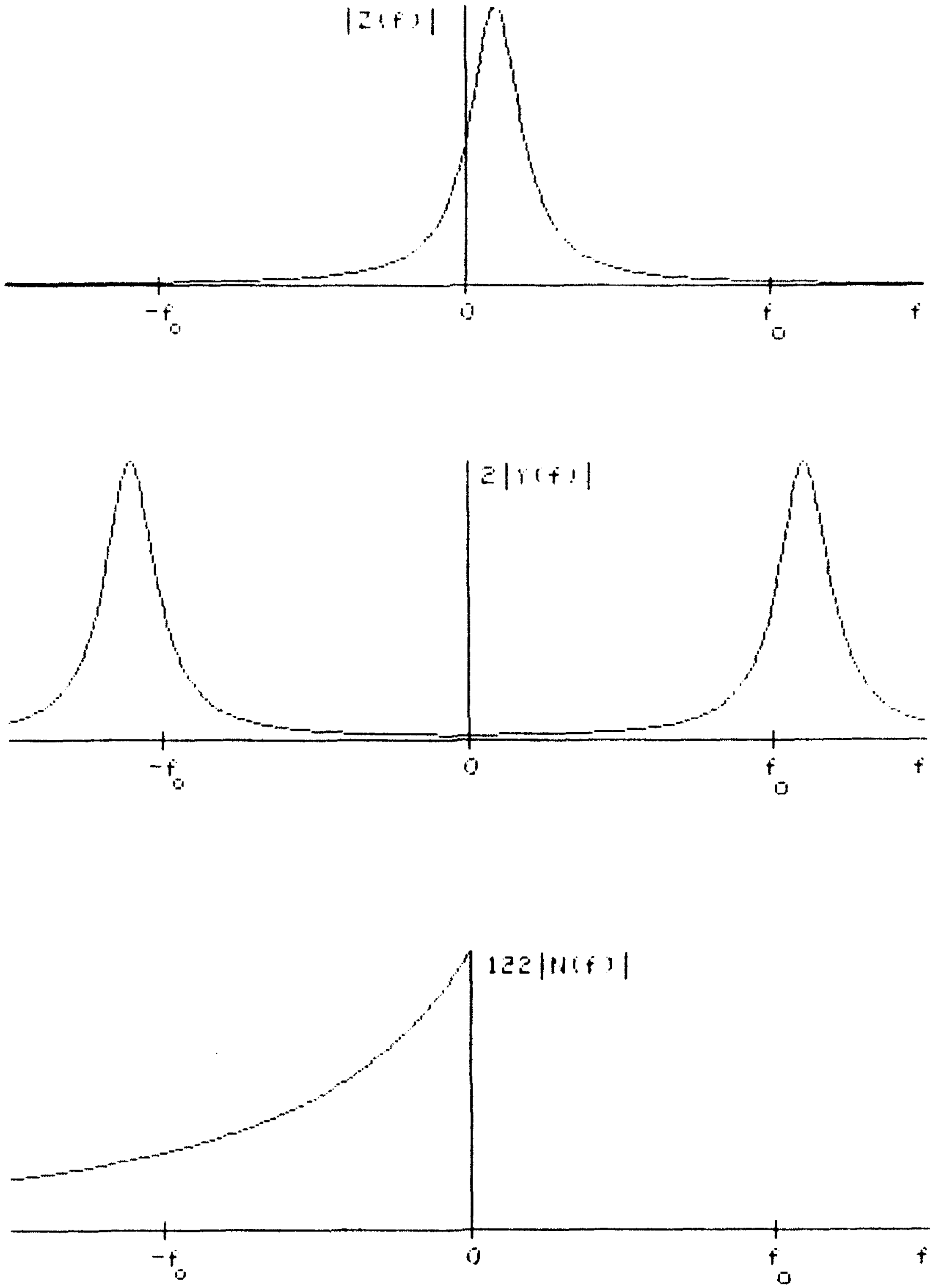

Figure 1. Spectral Quantities

ANALYTIC WAVEFORM

The single-sided (positive) frequency spectrum is defined as

$$Y_+(f) = 2\ U(f)\ Y(f) = U(f)\ Z(f-f_o) + U(f)\ Z^*(-f-f_o) = \qquad (6)$$

$$= Z(f-f_o) - U(-f)\ Z(f-f_o) + U(f)\ Z^*(-f-f_o) \quad \text{for all } f\ . \qquad (7)$$

Here, $U(x)$ is the unit step function; that is, $U(x)$ is 1 for $x > 0$ and $U(x)$ is 0 for $x < 0$. The analytic waveform corresponding to $y(t)$ is then given by Fourier transform

$$y_+(t) = \int df\ \exp(i2\pi ft)\ Y_+(f)\ . \qquad (8)$$

In order to further develop (8), we define a single-sided (negative) frequency function

$$N(f) = U(-f)\ Z(f-f_o) = \begin{Bmatrix} 0 & \text{for } f > 0 \\ Z(f-f_o) & \text{for } f < 0 \end{Bmatrix}\ , \qquad (9)$$

which can be determined directly from the spectrum $Z(f)$ of the imposed modulation $z(t)$ in (2) if f_o is known. The magnitude of $N(f)$, scaled to peak value 1, is sketched in figure 1; it is small if f_o is large, and is peaked near $f = 0$. The complex time function corresponding to (negative frequency) function $N(f)$ is

$$n(t) = \int df\ \exp(i2\pi ft)\ N(f) = \int_{-\infty}^{0} df\ \exp(i2\pi ft)\ Z(f-f_o)\ . \qquad (10)$$

With the help of (9) and (10), the single-sided spectrum $Y_+(f)$ in (7) can now be expressed as

$$Y_+(f) = Z(f-f_o) - N(f) + N^*(-f) \ , \tag{11}$$

with corresponding analytic waveform (8)

$$y_+(t) = \exp(i2\pi f_o t)\ z(t) - n(t) + n^*(t) = \tag{12}$$

$$= \exp(i2\pi f_o t)\ z(t) - i\ 2\ \mathrm{Im}\{n(t)\} \ . \tag{13}$$

That is, the analytic waveform is composed of two parts, the first of which is what we would typically desire, namely the imposed modulation (2) shifted up in frequency by f_o. The second term in (13), which is totally imaginary, is usually undesired; it can be seen from (10) and $|N(f)|$ in figure 1 to be generally rather small. There also follows immediately, from (13) and (2), the expected result

$$\mathrm{Re}\{y_+(t)\} = a(t)\ \cos[2\pi f_o t + p(t)] = y(t) \ . \tag{14}$$

Since analytic waveform $y_+(t)$ can also be expressed as

$$y_+(t) = y(t) + i\ y_H(t) = y(t) + i\ y(t) \circledast \frac{1}{\pi t} = y(t) + i\int du\ \frac{y(u)}{\pi(t-u)}, \tag{15}$$

where $y_H(t)$ is the Hilbert transform of $y(t)$ and $\circledast$ denotes convolution, (13) and (2) yield

$$y_H(t) = a(t)\ \sin[2\pi f_o t + p(t)] - 2\ \mathrm{Im}\{n(t)\} \ . \tag{16}$$

If we define (real) error waveform $e(t)$ as the difference between the Hilbert transform of (1) and the quadrature version of original waveform (1), we have

$$e(t) \equiv y_H(t) - a(t) \sin[2\pi f_o t + p(t)] = \tag{17}$$

$$= -2 \, \mathrm{Im}\{n(t)\} = i \, [n(t) - n^*(t)] = \tag{18}$$

$$= -2 \, \mathrm{Im} \int_{-\infty}^{0} df \exp(i2\pi ft) \, Z(f-f_o) = \tag{19}$$

$$= -2 \, \mathrm{Im} \left\{ \exp(i2\pi f_o t) \int_{-\infty}^{-f_o} df \exp(i2\pi ft) \, Z(f) \right\} , \tag{20}$$

where we used (16) and (10). The error spectrum is, from (18) and (9),

$$E(f) = i \, [N(f) - N^*(-f)] = \tag{21}$$

$$= \left\{ \begin{matrix} -i \, Z^*(-f-f_o) & \text{for } f > 0 \\ i \, Z(f-f_o) & \text{for } f < 0 \end{matrix} \right\} . \tag{22}$$

Then, $E(-f) = E^*(f)$. The magnitude of $E(f)$ is displayed in figure 2; it is generally small and centered about $f = 0$.

The total energy in real error waveform $e(t)$ is

$$\int dt \, [e(t)]^2 = \int df \, |E(f)|^2 =$$

$$= \int df \left[N(f) - N^*(-f) \right] \left[N^*(f) - N(-f) \right] =$$

$$= \int df \left[|N(f)|^2 + |N(-f)|^2 \right] = 2 \int df \, |N(f)|^2 =$$

$$= 2 \int_{-\infty}^{0} df \, |Z(f-f_o)|^2 = 2 \int_{-\infty}^{-f_o} df \, |Z(f)|^2 , \tag{23}$$

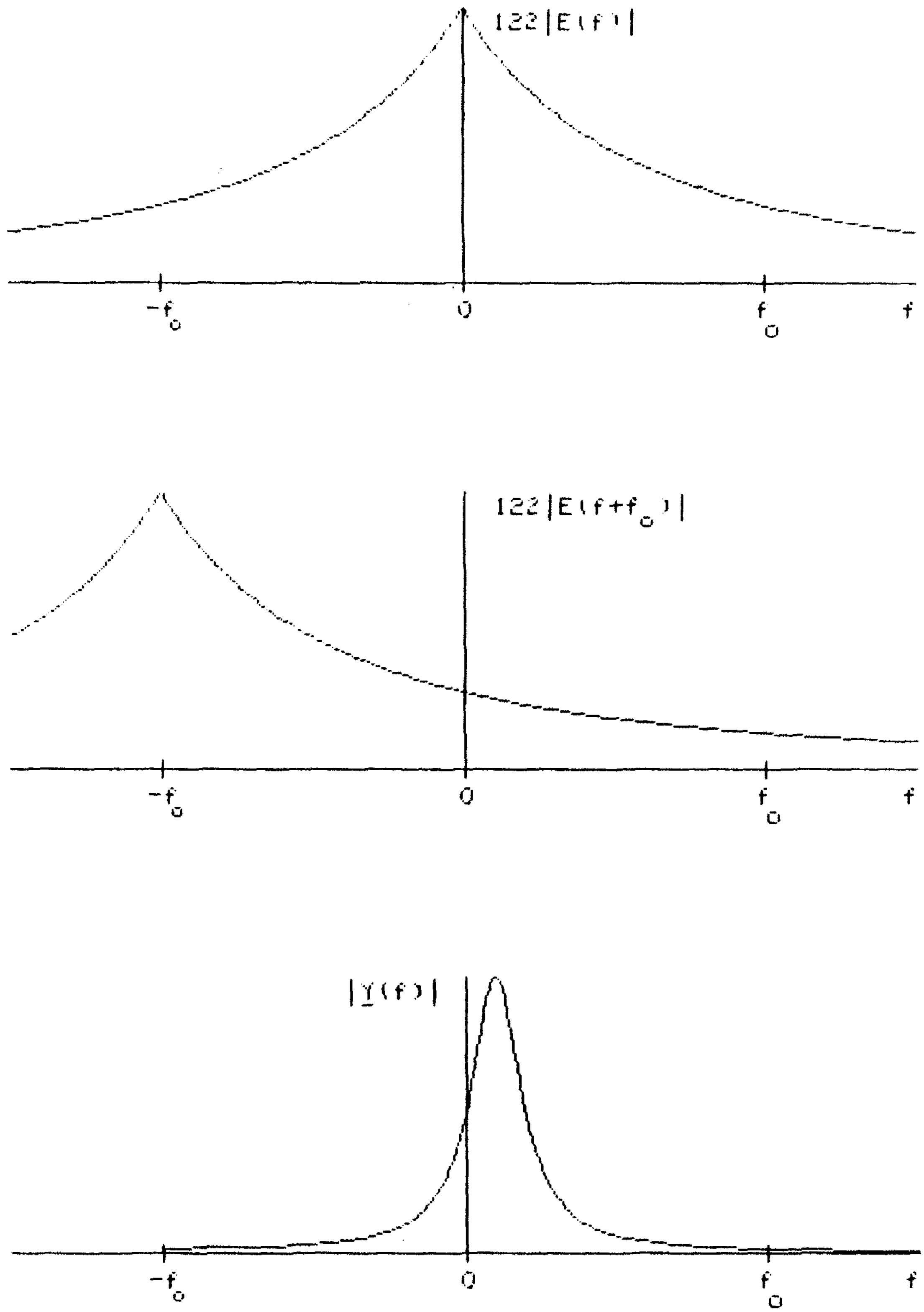

Figure 2. Error and Complex Envelope Spectra

where we used (21), the single-sided behavior of N(f), and (9). This is just twice the energy in the spectrum Z(f) of imposed modulation z(t) below frequency $-f_o$; inspection of figure 1 reveals that this quantity will usually be small.

COMPLEX ENVELOPE

The complex envelope $\underline{y}(t)$ of waveform y(t) is the frequency down-shifted version of analytic waveform $y_+(t)$:

$$\underline{y}(t) \equiv y_+(t)\,\exp(-i2\pi f_o t) = \tag{24}$$

$$= z(t) + i\,e(t)\,\exp(-i2\pi f_o t)\ , \tag{25}$$

where we used (13) and (18) and chose to downshift by f_o Hertz, the known carrier frequency in (1). Waveforms z(t) and e(t) are lowpass, as may be verified from their spectra in figures 1 and 2. The spectrum of the complex envelope is, from (25),

$$\underline{Y}(f) = Z(f) + i\,E(f+f_o)\ . \tag{26}$$

Equations (25) and (26) show that the complex envelope and its spectrum are each composed of a desired component and an error term.

The magnitudes of the complex envelope spectrum $\underline{Y}(f)$ and its error component are displayed in figure 2; $\underline{Y}(f)$ is discontinuous at $f = -f_o$ but has zero slope as $f \to -f_o$, whether from above or below. The left tail of Z(f) and shifted error spectrum, $i\,E(f+f_o)$, interact so as to yield $\underline{Y}(f) = 0$ for $f < -f_o$; this is most easily seen from a combination of (24) and (6), namely

$$\underline{Y}(f) = Y_+(f+f_o) = 2\ U(f+f_o)\ Y(f+f_o) = \quad (27)$$

$$= U(f+f_o)\ [Z(f) + Z^*(-f-2f_o)]\ . \quad (28)$$

The results for the error spectrum and energy in (22) and (23), respectively, were originally derived by Nuttall [2]; however, we have augmented those results here, to give detailed expressions for the error and complex envelope waveforms and spectra. There are no approximations in any of the above relations; they apply to waveforms with arbitrary spectra, whether carrier frequency f_o is large or small.

EXTRACTED AMPLITUDE AND PHASE MODULATIONS

It is important and useful to also make the following observations relative to the amplitude and phase modulations that can be extracted from the complex envelope $\underline{y}(t)$. Define

$$A(t) = |\underline{y}(t)|\ , \qquad P(t) = \arg\{\underline{y}(t)\}\ . \quad (29)$$

Then, from (14) and (24), the original waveform can be expressed in terms of these extracted amplitude and phase modulations as

$$y(t) = \mathrm{Re}\{\underline{y}(t)\ \exp(i2\pi f_o t)\} = A(t)\ \cos[2\pi f_o t + P(t)]\ . \quad (30)$$

However, complex-envelope modulations A(t) and P(t) in (29) and (30) are not generally equal to imposed modulations a(t) and p(t) in (1), as may be seen by reference to (25). Namely, complex envelope $\underline{y}(t)$ is equal to complex lowpass waveform z(t) in (2) only if error e(t) is zero. But the energy in waveform e(t), as given by (23), is zero only if imposed spectrum Z(f) in (3) is zero for $f < -f_o$. When Z(f) is not zero for $f < -f_o$, complex-envelope modulations A(t) and P(t) do not agree with imposed modulations a(t) and p(t), despite the ability to write y(t) in the two similar real forms (1) and (30) involving an amplitude- and phase-modulated cosine with the same f_o.

Another interesting property of form (30) is that its quadrature version is identically the Hilbert transform of y(t). This is in contrast with the quadrature version of (1) involving imposed modulations a(t) and p(t); see (17) - (20). To prove this claim, observe that the quadrature version of the last term of (30) is, using (29),

$$q(t) \equiv A(t) \sin[2\pi f_o t + P(t)] = \tag{31}$$

$$= \frac{1}{i2} [A(t) \exp(iP(t) + i2\pi f_o t) - A(t) \exp(-iP(t) - i2\pi f_o t)] =$$

$$= \frac{1}{i2}[\underline{y}(t) \exp(i2\pi f_o t) - \underline{y}^*(t) \exp(-i2\pi f_o t)] \ . \tag{32}$$

The spectrum of this waveform is

$$Q(f) = \frac{1}{i2}\left[\underline{Y}(f-f_o) - \underline{Y}^*(-f-f_o)\right] = -i[U(f)\ Y(f) - U(-f)\ Y^*(-f)] =$$

$$= \begin{Bmatrix} -i\ Y(f) & \text{for } f > 0 \\ i\ Y(f) & \text{for } f < 0 \end{Bmatrix} = -i\ \mathrm{sgn}(f)\ Y(f) = Y_H(f) \ , \tag{33}$$

where we used (27), the conjugate symmetry of Y(f), sgn(x) = +1 for x > 0 and -1 for x < 0, and (6) in the form

$$Y_+(f) = 2\ U(f)\ Y(f) = [1 + \mathrm{sgn}(f)]\ Y(f) = Y(f) + i\ Y_h(f) \ , \tag{34}$$

the latter result following from (15). Thus, (33) and (31) yield the desired result

$$y_H(t) = \frac{1}{\pi t} \circledast y(t) = q(t) = A(t) \sin[2\pi f_o t + P(t)] \; . \qquad (35)$$

This simple connection between (35) and (30) holds in general when modulations A(t) and P(t) are extracted from the complex envelope according to (29); there are no narrowband assumptions required. The more complicated connection between (16) and (1), which is applicable for the imposed modulations, involves an error term; this error is zero if and only if spectrum Z(f) in (3) is zero for $f < -f_o$.

SPECTRUM Y(f) GIVEN

All of the above results have presumed that waveform y(t) in the form (1) was available as the starting point. But there are many problems of interest where spectrum Y(f) is the initial available quantity, rather than y(t). For example, the output spectrum Y(f) of a linear filter L(f) subject to input spectrum X(f) is given by Y(f) = L(f) X(f) and can often be easily and directly computed. In this case, there are no given amplitude and phase modulations a(t) and p(t) as in (1); in fact, there is not even an obvious or unique center frequency for a given spectrum Y(f). Nevertheless, many, but not all, of the relations above hold true under appropriate definitions of the various terms.

Given spectrum $Y(f)$ with conjugate symmetry, $Y(-f) = Y^*(f)$, we begin with its corresponding real waveform

$$y(t) = \int df \exp(i2\pi ft)\, Y(f) \, . \tag{36}$$

The Hilbert transform of $y(t)$ and its spectrum are given by

$$y_H(t) = \frac{1}{\pi t} \circledast y(t) \, , \quad Y_H(f) = -i \operatorname{sgn}(f)\, Y(f) \, . \tag{37}$$

The single-sided spectrum and analytic waveform are, respectively

$$Y_+(f) = 2\, U(f)\, Y(f) = [1 + \operatorname{sgn}(f)]\, Y(f) = Y(f) + i\, Y_H(f) \, , \tag{38}$$

$$y_+(t) = 2 \int_0^\infty df \exp(i2\pi ft)\, Y(f) = y(t) + i\, y_H(t) \, . \tag{39}$$

Up to this point, all the functions are unique and nothing has changed. However, we now have to choose a "center frequency" f_c of $Y_+(f)$, since none has been specified; this (somewhat arbitrary) selection process of f_c is addressed in appendix A, to which the reader is referred at this point. Hence, we take f_c as given and define lowpass spectrum

$$\underline{Y}(f) = Y_+(f+f_c) = 2\, U(f+f_c)\, Y(f+f_c) \, . \tag{40}$$

The corresponding complex envelope is

$$\underline{y}(t) = y_+(t) \exp(-i2\pi f_c t) \, . \tag{41}$$

We define the complex-envelope amplitude and phase modulations as in (29):

$$A(t) = |\underline{y}(t)| \, , \quad P(t) = \arg\{\underline{y}(t)\} = \arg\{y_+(t)\} - 2\pi f_c t \, . \tag{42}$$

Then, from (39), (41), and (42), we have

$$y(t) = \mathrm{Re}\{y_+(t)\} = \mathrm{Re}\{\underline{y}(t)\exp(i2\pi f_c t)\} = A(t)\cos[2\pi f_c t + P(t)]. \tag{43}$$

Now when we define the quadrature version of the right-hand side of (43) in a manner similar to (31), but now employing f_c instead of (unspecified) f_o, the same type of manipulations as in (31) - (35) yield relations identical to those given above:

$$Q(f) = Y_H(f)\ , \quad y_H(t) = q(t) = A(t)\sin[2\pi f_c t + P(t)]\ . \tag{44}$$

Because the choice of center frequency f_c of single-sided spectrum $Y_+(f)$ is somewhat arbitrary (see appendix A), this makes complex envelope $\underline{y}(t)$ and its extracted phase $P(t)$ somewhat arbitrary. However, the argument, $2\pi f_c t + P(t) = \arg\{y_+(t)\}$, of (43) and (44) is <u>not</u> arbitrary, as seen directly from (41) and the uniqueness of $y_+(t)$ in (39). Furthermore, extracted amplitude modulation $A(t)$ in (42) has no arbitrariness since it is given alternatively by $|y_+(t)|$, according to (41).

Since $A(t)$ and $P(t)$ are lowpass functions, we can compute them at relatively coarse increments in time t. Then, if we want to observe the fine detail of $y(t)$, as given by (43), we can interpolate between these values of $A(t)$ and $P(t)$ and then compute the cosine in (43) at whatever t values are of interest. This practical numerical approach will reduce the number of computations of $A(t)$ and $P(t)$ required; in fact, in many applications, $A(t)$ and $P(t)$ will themselves be the desired output quantities of interest, rather than narrowband waveform $y(t)$ with all its unimportant high-frequency detail.

EXAMPLE

Consider the fundamental building block of systems with rational transfer functions, namely

$$y(t) = U(t)\exp(-\alpha t)\cos(2\pi f_o t + \phi)\ , \quad \alpha > 0\ , \quad f_o > 0\ , \tag{45}$$

where U(t) is the unit step in time t. Let

$$\omega = 2\pi f\ , \quad \omega_o = 2\pi f_o\ , \quad c = \alpha - i\omega_o\ . \tag{46}$$

Then, from (1) and (2), the imposed modulations are

$$a(t) = U(t)\exp(-\alpha t), \quad p(t) = \phi, \quad z(t) = U(t)\exp(i\phi - \alpha t)\ , \tag{47}$$

yielding, upon use of (3) and (46), spectrum

$$Z(f) = \frac{\exp(i\phi)}{\alpha + i2\pi f} = \frac{\exp(i\phi)}{\alpha + i\omega}\ . \tag{48}$$

From (5) and (48), the spectrum of y(t) is

$$Y(f) = \frac{1}{2}\left[\frac{\exp(i\phi)}{\alpha + i(\omega - \omega_o)} + \frac{\exp(-i\phi)}{\alpha + i(\omega + \omega_o)}\right]\ , \tag{49}$$

and (6) yields single-sided spectrum

$$Y_+(f) = U(f)\left[\frac{\exp(i\phi)}{\alpha + i(\omega - \omega_o)} + \frac{\exp(-i\phi)}{\alpha + i(\omega + \omega_o)}\right]\ . \tag{50}$$

Now we use (9), (48), and (46) to obtain (negative) spectrum

$$N(f) = U(-f)\,\frac{\exp(i\phi)}{c + i\omega} = \begin{Bmatrix} 0 & \text{for } f > 0 \\ \dfrac{\exp(i\phi)}{c + i\omega} & \text{for } f < 0 \end{Bmatrix}\ . \tag{51}$$

Then, from (10), the corresponding complex time waveform is

$$n(t) = \int_{-\infty}^{0} df \, \exp(i\omega t) \, \frac{\exp(i\phi)}{c + i\omega} = \frac{\exp(i\phi - ct)}{i2\pi} \int_{c-i\infty}^{c} \frac{du}{u} \exp(tu) \; . \qquad (52)$$

For $t < 0$, let $x = |t|u = -tu$, to get

$$n(t) = \frac{\exp(i\phi - ct)}{i2\pi} \int_{c|t|-i\infty}^{c|t|} \frac{dx}{x} \exp(-x) = \frac{i}{2\pi} \exp(i\phi - ct) \, E_1(c|t|) \; , \qquad (53)$$

where $E_1(z)$ is the exponential integral [3; 5.1.1]. It is important to observe and use the fact that the path of integration in the complex x-plane in (53) remains in the fourth quadrant and never crosses the negative real x-axis [3; under 5.1.6].

Also, for $t > 0$, let $x = -tu$ in (52), to get

$$n(t) = \frac{\exp(i\phi - ct)}{i2\pi} \int_{-ct+i\infty}^{-ct} \frac{dx}{x} \exp(-x) = \frac{i}{2\pi} \exp(i\phi - ct) \, E_1(-ct) \; . \qquad (54)$$

Here, the contour of integration remains in the second quadrant of the complex x-plane and again does not cross the negative real x-axis [3; under 5.1.6]. The combination of (53) and (54) now yields complex time waveform

$$n(t) = \frac{i}{2\pi} \exp(i\phi - ct) \, E_1(-ct) \quad \text{for all } t \neq 0 \; . \qquad (55)$$

Now, we use (18) to obtain real error waveform

$$e(t) = -\frac{1}{\pi}\,\mathrm{Re}\{\exp(i\phi-ct)\;E_1(-ct)\} \quad \text{for all } t \neq 0\,. \tag{56}$$

(Or we could directly use (20) with (48).) The corresponding error spectrum follows from (22), (48), and (46) as

$$E(f) = \begin{Bmatrix} \dfrac{-i\exp(-i\phi)}{c^* + i\omega} & \text{for } f > 0 \\[2ex] \dfrac{i\exp(i\phi)}{c + i\omega} & \text{for } f < 0 \end{Bmatrix}\,. \tag{57}$$

From (16), (17), (47), and (56), the Hilbert transform of y(t) is

$$y_H(t) = U(t)\exp(-\alpha t)\sin(2\pi f_o t+\phi) - \\ -\frac{1}{\pi}\,\mathrm{Re}\{\exp(i\phi-ct)\;E_1(-ct)\} \quad \text{for all } t \neq 0. \tag{58}$$

In addition, using (15) and (45), the analytic waveform is

$$y_+(t) = U(t)\exp(i\phi-ct) - i\,\frac{1}{\pi}\,\mathrm{Re}\{\exp(i\phi-ct)\;E_1(-ct)\} \\ \text{for all } t \neq 0. \tag{59}$$

The complex envelope follows from (25), (47), and (56) as

$$\underline{y}(t) = U(t)\exp(i\phi-\alpha t) - \frac{i}{\pi}\exp(-i\omega_o t)\,\mathrm{Re}\{\exp(i\phi-ct)\;E_1(-ct)\} \\ \text{for all } t \neq 0\,. \tag{60}$$

The corresponding spectrum is, from (27) and (50),

$$\underline{Y}(f) = U(f+f_o)\left[\frac{\exp(i\phi)}{\alpha + i\omega} + \frac{\exp(-i\phi)}{\alpha + i(\omega + 2\omega_o)}\right]\,. \tag{61}$$

The extracted amplitude and phase modulations A(t) and P(t) of complex envelope $\underline{y}(t)$ are now available by applying (42) to (60). Since the first term, by itself, in (60) has the imposed amplitude and phase modulations a(t) and p(t) as specified in (47), A(t) cannot possibly equal a(t), nor can P(t) equal p(t). This example is an illustration of the general property stated in the sequel to (30). The reason is that spectrum Z(f) in (48) is obviously nonzero for $f < -f_o$.

From (23) and (48), the energy in error waveform e(t) is

$$2 \int_{-\infty}^{-f_o} \frac{df}{\alpha^2 + \omega^2} = \frac{1}{2\alpha}\left[1 - \frac{2}{\pi} \arctan\left(\frac{\omega_o}{\alpha}\right)\right] . \qquad (62)$$

For comparison, the energy in desired component z(t) in complex envelope $\underline{y}(t)$ of (25) is, from (47),

$$\int_{-\infty}^{\infty} dt \, |z(t)|^2 = \frac{1}{2\alpha} . \qquad (63)$$

SINGULAR BEHAVIOR

Since [3; 5.1.11 and footnote on page 228]

$$E_1(z) = -\ln(z) - \gamma + \mathrm{Ein}(z) \ , \tag{64}$$

where Ein(z) is entire, the error waveform in (56) has a component

$$-\frac{1}{\pi}\,\mathrm{Re}\{-\exp(i\phi - ct)\,\ln(-ct)\} =$$

$$= \frac{1}{\pi}\,\mathrm{Re}\{\exp(i\phi - ct)\,[\ln(-c\,\mathrm{sgn}(t)) + \ln|t|]\quad \text{for } t \neq 0 \ , \tag{65}$$

of which the most singular component is

$$\frac{1}{\pi}\,\ln|t|\,\exp(-\alpha t)\,\cos(\omega_o t + \phi) \sim \frac{1}{\pi}\,\cos(\phi)\,\ln|t| \text{ as } t \to 0 \ . \tag{66}$$

The only situation for which this logarithmic singularity does not contribute an infinity as $t \to 0$ is when $\phi = -\pi/2$ (or $\pi/2$). That corresponds to the special case in (45) of

$$y(t) = U(t)\,\exp(-\alpha t)\,\sin(\omega_o t) \quad \text{for } \phi = -\pi/2 \ , \tag{67}$$

which is zero at $t = 0$; that is, $y(t)$ is continuous for all t. However, even for $\phi = -\pi/2$ in the first term of (66), the product $\ln|t|\,\sin(\omega_o t)$ has an infinite slope at its zero at $t = 0$, leading possibly to numerical difficulties.

The spectrum $Y(f)$ follows from (49) as

$$Y(f) = \frac{\omega_o}{\alpha^2 + \omega_o^2 + i2\alpha\omega - \omega^2} \quad \text{for } \phi = -\frac{\pi}{2} \ , \tag{68}$$

which decays as ω^{-2} as $\omega \to \pm\infty$; this spectral decay is the key issue for avoiding a logarithmic singularity in $e(t)$, $y_H(t)$, $y_+(t)$, and $\underline{y}(t)$. All values of ϕ other than $\pm\pi/2$ lead to asymptotic decay of $Y(f)$ in (49) according to $-i \cos(\phi)\, \omega^{-1}$, which leads to a logarithmic singularity in the various time functions considered here, including the complex envelope.

Continuing this special case of $\phi = -\pi/2$ in (67) and (68), we find, from (48),

$$Z(f) = \frac{-i}{\alpha + i\omega}, \qquad z(t) = U(t)\,(-i)\,\exp(-\alpha t) \quad \text{for } \phi = -\frac{\pi}{2}. \tag{69}$$

Also, there follows from (56), (58), and (60), respectively, the error, the Hilbert transform, and the complex envelope, as

$$e(t) = -\frac{1}{\pi}\,\mathrm{Im}\{\exp(-ct)\,E_1(-ct)\}, \tag{70}$$

$$y_H(t) = -U(t)\exp(-\alpha t)\cos(\omega_o t) + e(t), \tag{71}$$

$$\underline{y}(t) = U(t)\,(-i)\exp(-\alpha t) + i\exp(-i\omega_o t)\,e(t), \tag{72}$$

all for $\phi = -\pi/2$.

The asymptotic behavior of error $e(t)$ at infinity is available from [3; 5.1.51] as

$$e(t) \sim \frac{\omega_o}{\alpha^2 + \omega_o^2}\,\frac{1}{\pi t} \quad \text{as } t \to \pm\infty \quad \text{for } \phi = -\frac{\pi}{2}. \tag{73}$$

The origin behavior is available from [3; 5.1.11]:

$$e(t) \sim \begin{Bmatrix} -\frac{1}{\pi}\arctan(\omega_o/\alpha) & \text{as } t \to 0- \\ 1 - \frac{1}{\pi}\arctan(\omega_o/\alpha) & \text{as } t \to 0+ \end{Bmatrix} \quad \text{for } \phi = -\frac{\pi}{2} . \tag{74}$$

Observe that these limits in (74) at $t = \pm 0$ are both finite. Also, note the very slow decay in (73), namely $1/t$, of error $e(t)$ at infinity.

When $\phi \neq \pm\pi/2$, the generalizations to (73) and (74) are [3; 5.1.51 and 5.1.11]

$$e(t) \sim \frac{\alpha\cos\phi - \omega_o\sin\phi}{\alpha^2 + \omega_o^2}\,\frac{1}{\pi t} \quad \text{as } t \to \pm\infty , \tag{75}$$

and

$$e(t) \sim \frac{\cos\phi}{\pi}\ln|t| \quad \text{as } t \to 0 . \tag{76}$$

Now, error $e(t)$ becomes infinite at the origin and decays only as $1/t$ for large t. (If $\tan\phi = \alpha/\omega_o$, then $e(t) = O(t^{-2})$ as $t \to \pm\infty$; this corresponds to $Y(0) = 0$ in (49).)

GENERAL HILBERT TRANSFORM BEHAVIOR

The example of $y(t)$ in (45) (when $\phi \neq \pm\pi/2$) illustrates the general rule that if a time function has a discontinuity of value D at time t_o, then its Hilbert transform behaves as $D/\pi \ln|t-t_o|$ as $t \to t_o$. To derive this result, observe that

$$y(t) \sim V + \tfrac{1}{2}D \operatorname{sgn}(t-t_o) \quad \text{as } t \to t_o \ , \tag{77}$$

when $y(t)$ is discontinuous at t_o. Then, for t near t_o, the Hilbert transform of $y(t)$ is dominated by the components

$$\begin{aligned} y_H(t) \sim \frac{1}{\pi}\int_{-b}^{-\varepsilon} \frac{du}{u}\left[V + \tfrac{1}{2}D \operatorname{sgn}(t-t_o-u)\right] + \\ + \frac{1}{\pi}\int_{\varepsilon}^{b} \frac{du}{u}\left[V + \tfrac{1}{2}D \operatorname{sgn}(t-t_o-u)\right] \ , \end{aligned} \tag{78}$$

where ε is a small positive quantity and the principal value nature of the Hilbert transform integral has been utilized. The integrals involving constant V cancel; also, by breaking the integrals in (78) down into regions where sgn is positive versus negative, and watching whether $t-t_o$ is positive or negative, the terms involving $\ln(\varepsilon)$ cancel, leaving the dominant behavior

$$y_H(t) \sim \frac{D}{\pi} \ln|t-t_o| \quad \text{as } t \to t_o \ . \tag{79}$$

(The example in (66) corresponds to a discontinuity $D = \cos(\phi)$ at $t_o = 0$, as may be seen by referring to (45).) When Hilbert transform $y_H(t)$ has this logarithmic singularity (79), then so also do $y_+(t)$, $\underline{y}(t)$, and $e(t)$ at the same time location. Thus, the complex envelope corresponding to a discontinuous $y(t)$ has a logarithmic singularity.

An alternative representation for Hilbert transform $y_H(t)$ in (15) is given by

$$y_H(t) = \int df \exp(i2\pi ft) \, (-i) \, \mathrm{sgn}(f) \, Y(f) \; . \tag{80}$$

If $Y(f)$ decays to zero at $f = \pm\infty$ and if $Y(f)$ is continuous for all real f, then an integration by parts on (80) yields (due to the discontinuity of $\mathrm{sgn}(f)$) the asymptotic decay

$$y_H(t) \sim \frac{Y(0)}{\pi t} \quad \text{as } t \to \pm\infty \; . \tag{81}$$

(Results (73) and (75) are special cases of (81), when applied to example (49).) The only saving feature of this very slow decay for large t in (81) is that $Y(0)$ may be small relative to its maximum for $f \neq 0$. For example (49), $|Y(f_o)| \cong (2\alpha)^{-1}$ for $\alpha << \omega_o$, which is then much larger than $Y(0) \cong -\sin\phi/\omega_o$. In this narrowband case, the slow decay of (81) will not be overly significant in analytic waveform $y_+(t)$ until t gets rather large. If $Y(0)$ is zero, the dominant behavior is not given by (81), but instead is replaced by a $1/t^2$ dependence, with a magnitude proportional to $Y'(0)$.

GRAPHICAL RESULTS

We now take the example in (45) with parameter values $\alpha = 1\ \sec^{-1}$ and $f_o = 100$ Hz. The error e(t) in (56) is plotted versus time t in figure 3 for three different values of phase ϕ. A time sampling increment Δ_t of .02 msec was used to compute (56), since these error functions are very sharp in t, being concentrated around t = 0 where the waveform y(t) has its discontinuity. The period of the carrier frequency is $1/f_o = 10$ msec; however, the error functions vary significantly in time intervals less than 1 msec. These functions approach $-\infty$ at t = 0, according to (66), except for $\phi = -\pi/2$.

The corresponding complex envelope is given by (72); its magnitude is plotted in figure 4 over a much wider time interval. The straight line just to the right of the origin is the desired exponential decay $a(t) = \exp(-\alpha t)$, which dominates the error e(t) in this region of time. Eventually, however, for larger t or negative t, the error e(t) dominates, with its much slower decay rate. It is readily verified that the asymptotic behavior predicted by (75) is in control and very accurate near both edges of figure 4.

At the transition between the two components, the random vector addition in (72) leads to large oscillations; the period of the carrier is $1/f_o = 10$ msec, meaning that the transition oscillations in figure 4 have been grossly undersampled with the time increment Δ_t approximately 40 msec that was used. The error curve for $\phi = 0$ is much smaller than the other two examples over most of its range; however, the magnitude error goes sharply to ∞ at $t = 0$.

From (72) and figure 4, it is seen that for $\phi = -\pi/2$, the phase $P(t)$ of complex envelope $\underline{y}(t)$ is essentially $-\pi/2$ for $t > 0$, until we reach the transition. To the right of the transition, the phase of $\underline{y}(t) \exp(i\omega_o t)$ is essentially $\pi/2$ because $e(t) > 0$ for $t > 0$, for this example. For $t < 0$, the phase of $\underline{y}(t) \exp(i\omega_o t)$ is $-\pi/2$ because $e(t) < 0$ for $t < 0$. We will numerically confirm these claims later when we compute the analytic waveform and complex envelope by means of FFTs.

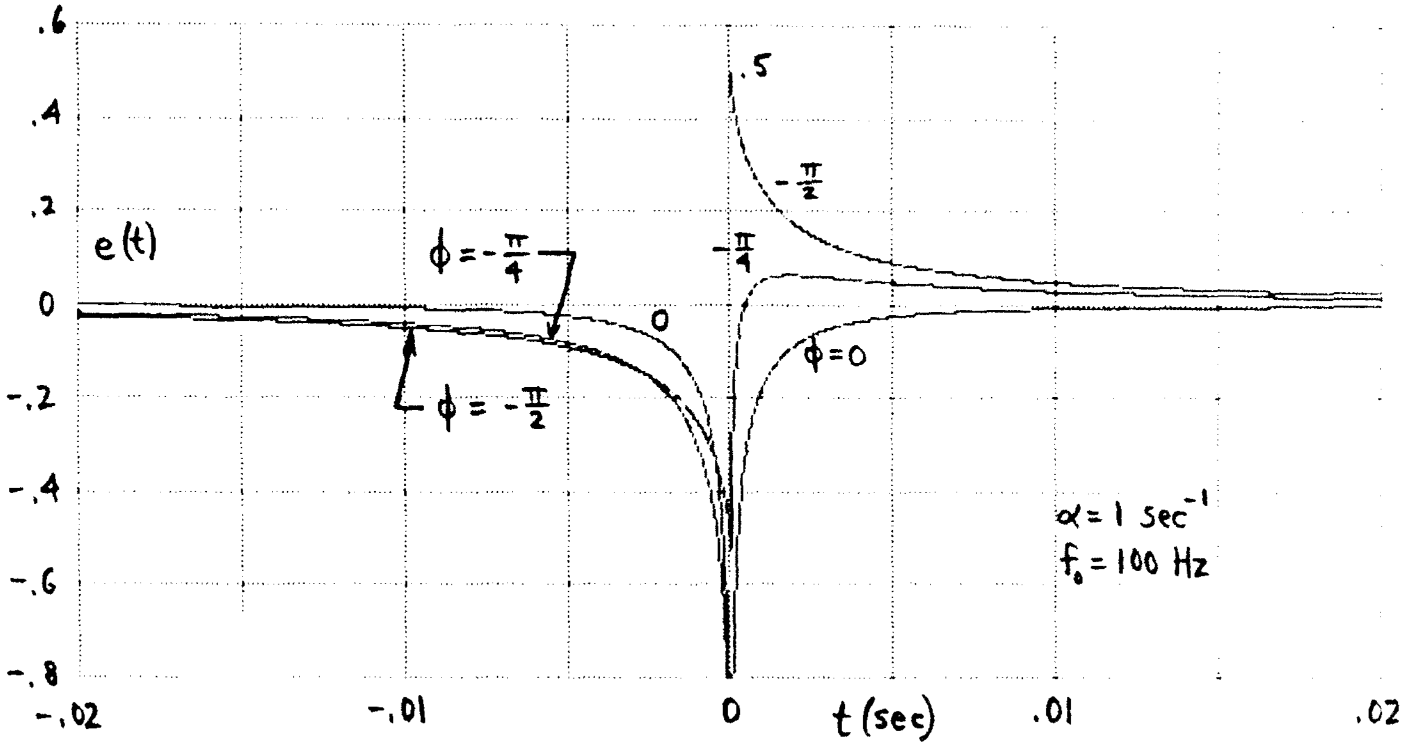

Figure 3. Error e(t) for Various ϕ

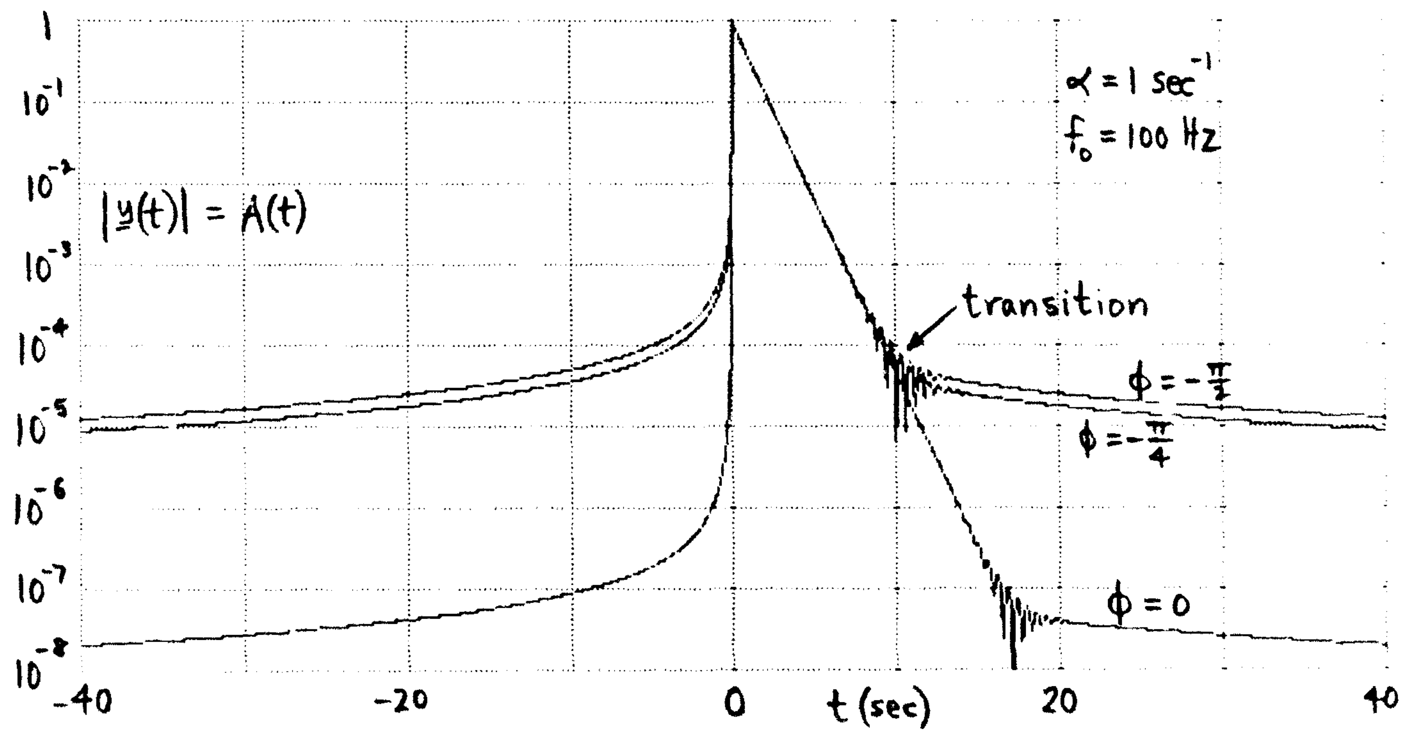

Figure 4. Complex Envelope for Various ϕ

FILTERED COMPLEX ENVELOPE

It was shown in (26) that the spectrum $\underline{Y}(f)$ of the complex envelope $\underline{y}(t)$ of a given waveform $y(t)$ with complex imposed modulation $z(t)$ is given by a desired term $Z(f)$ plus an undesired error term, namely,

$$\underline{Y}(f) = Z(f) + i\, E(f+f_o) \ . \tag{82}$$

According to figures 1 and 2, the major contribution of the first term, $Z(f)$, is centered around $f = 0$, while the undesired second term in (82) is centered about $f = -f_o$. This suggests the possibility of lowpass filtering complex envelope spectrum $\underline{Y}(f)$ in order to suppress the undesired frequency components. Also, this will eliminate or suppress the undesired logarithmic singularities present in the complex envelope $\underline{y}(t)$.

LOWPASS FILTER

To this aim, let $H(f)$ denote a lowpass filter with $H(0) = 1$ and cutoff frequency, f_1, smaller than f_o. For example, the Hann filter is characterized by

$$H(f) = \left\{ \begin{array}{ll} \cos^2\left(\frac{\pi}{2}\frac{f}{f_1}\right) & \text{for } |f| < f_1 \\ 0 & \text{otherwise} \end{array} \right\} . \tag{83}$$

The filtered complex envelope spectrum is, in general,

$$G(f) = \underline{Y}(f)\, H(f) \ . \tag{84}$$

The importance of having $f_1 < f_o$ is that filter H(f) will then smoothly cut off its response before reaching the discontinuity at $f = -f_o$ of the spectrum $\underline{Y}(f)$ of the complex envelope $\underline{y}(t)$; see (27). In this way, we can avoid the slowly decaying behavior of the complex envelope $\underline{y}(t)$ for large t, namely 1/t, which inherently accompanies its discontinuous frequency spectrum. This will prove important when we numerically evaluate the filtered complex envelope, by sampling (84) at equispaced frequencies and performing a Fourier transform into the t domain, necessarily encountering the unavoidable aliasing in time associated with such a technique.

Since the complex envelope $\underline{y}(t)$ is given by (25) as the sum of desired component z(t) and an error term, the filtered waveform corresponding to spectrum G(f) in (84) is given by

$$g(t) = \underline{y}(t) \circledast h(t) =$$

$$= z(t) \circledast h(t) + [i\ e(t) \exp(-i2\pi f_o t)] \circledast h(t) = \tag{85}$$

$$= g_d(t) + g_u(t) \ , \tag{86}$$

where $\circledast$ denotes convolution, h(t) is the impulse response of the general filter H(f) in (84), and $g_d(t)$ and $g_u(t)$ are, respectively, the desired and undesired components of the filtered complex envelope g(t). We should choose filter H(f) to be real and even; then impulse response h(t) is also real and even.

The Hann filter example in (83) could be replaced by a filter with a flatter response about f = 0 and a sharper cutoff behavior. The major features that filter H(f) should have are a fairly flat response in the Z(f) frequency range near $f = 0$, but cut off significantly before getting into the major frequency content of error term $E(f+f_o)$, which is centered about $f = -f_o$. If the given waveform y(t) in (1) is not really narrowband, there may not be any good choice of cutoff frequency f_1; that is, it may be necessary to sacrifice some of the higher frequency content of z(t) or to allow some of the error e(t) to pass.

EXAMPLE

We again consider the example given in (47) and (48), along with the Hann filter in (83). In order to evaluate the filtered complex envelope g(t) in (86), we define an auxiliary function

$$E(z) = \exp(z)\, E_1(z) , \tag{87}$$

where $E_1(z)$ is the exponential integral [3; 5.1.1]. Then, when we use the fact that (83) can be expressed as

$$H(f) = \frac{1}{2} + \frac{1}{4}\exp(i\pi f/f_1) + \frac{1}{4}\exp(-i\pi f/f_1) \quad \text{for } |f| < f_1 , \tag{88}$$

we encounter the following two integrals. First, we need the result

$$\int_{-f_1}^{f_1} df\, \frac{\exp(i\omega t + i\omega \frac{1}{2} n/f_1)}{\alpha + i2\omega_o + i\omega} = \frac{(-1)^n}{i2\pi}\Big[\exp(-i\omega_1 t)E(u_n) - \exp(i\omega_1 t)E(v_n)\Big] , \tag{89}$$

where $\omega = 2\pi f$, n is an integer, $f_1 < f_o$, and we defined

$$u_n = -(\alpha + i2\omega_o - i\omega_1)(t + \tfrac{1}{2}n/f_1) ,$$

$$v_n = -(\alpha + i2\omega_o + i\omega_1)(t + \tfrac{1}{2}n/f_1) . \qquad (90)$$

To derive this result, we let $x = -(\alpha + i2\omega_o + i\omega)(t + \tfrac{1}{2}n/f_1)$ in (89) and used [3; 5.1.1], along with the important fact that $f_1 < f_o$, which guarantees no crossing of the negative real axis of the resulting contour of integration in the complex x-plane.

Also, when we define

$$\underline{u}_n \equiv u_n(f_o{=}0) = -(\alpha - i\omega_1)(t + \tfrac{1}{2}n/f_1) ,$$

$$\underline{v}_n \equiv v_n(f_o{=}0) = -(\alpha + i\omega_1)(t + \tfrac{1}{2}n/f_1) , \qquad (91)$$

then for $f_o = 0$, we find the second integral result required, namely,

$$\int_{-f_1}^{f_1} df \, \frac{\exp(i\omega t + i\omega\frac{1}{2}n/f_1)}{\alpha + i\omega} = \frac{(-1)^n}{i2\pi}\Big[\exp(-i\omega_1 t)E(\underline{u}_n) - \exp(i\omega_1 t)E(\underline{v}_n)\Big] +$$

$$+ U(t + \tfrac{1}{2}n/f_1) \exp(-\alpha t - \tfrac{1}{2}\alpha n/f_1) . \qquad (92)$$

The extra term in the second line of (92) is due to a crossing of the negative real axis in the complex x-plane by the contour of integration when we make the substitution $x = -(\alpha + i\omega)(t + \tfrac{1}{2}n/f_1)$ in the integral of (92).

The desired component of the filtered complex envelope is given by the first term of (85) and (86), in the alternative form

$$g_d(t) = \int df \exp(i2\pi ft)\ Z(f)\ H(f) =$$

$$= \int_{-f_1}^{f_1} df \exp(i2\pi ft) \frac{\exp(i\phi)}{\alpha + i\omega} \cos^2\left(\frac{\pi}{2} \frac{f}{f_1}\right) = \tag{93}$$

$$= e^{i\phi}\left(e^{-\alpha t}\left[\frac{1}{2}U(t) + \frac{1}{4}U\left(t + \frac{1}{2f_1}\right) \exp\left(\frac{-\alpha}{2f_1}\right) + \frac{1}{4}U\left(t - \frac{1}{2f_1}\right) \exp\left(\frac{\alpha}{2f_1}\right)\right] +\right.$$

$$+ \frac{1}{i4\pi}\left(\exp(-i\omega_1 t)\left[E(\underline{u}_0) - \frac{1}{2} E(\underline{u}_1) - \frac{1}{2} E(\underline{u}_{-1})\right] -\right.$$

$$\left.\left. - \exp(i\omega_1 t)\left[E(\underline{v}_0) - \frac{1}{2} E(\underline{v}_1) - \frac{1}{2} E(\underline{v}_{-1})\right]\right)\right) . \tag{94}$$

Here, we also used (48), (88), and (92). Since the factor multiplying $\exp(i\phi)$ in (93) has conjugate symmetry in frequency f, the time function multiplying $\exp(i\phi)$ in (94) is purely real for all time t.

The undesired spectral component in (82) is given by

$$i\ E(f+f_o) = Z^*(-f-2f_o) \quad \text{for } f > -f_o\ , \tag{95}$$

where we used (22). Therefore, using restriction $f_1 < f_o$, the undesired time component in the filtered complex envelope in (86) is given, upon use of (89), by

$$g_u(t) = \int_{-f_1}^{f_1} df \exp(i2\pi ft) \frac{\exp(-i\phi)}{\alpha + i2\omega_o + i\omega} \cos^2\left(\frac{\pi}{2} \frac{f}{f_1}\right) =$$

$$= \frac{\exp(-i\phi)}{i4\pi}\left(\exp(-i\omega_1 t)\left[E(u_0) - \frac{1}{2} E(u_1) - \frac{1}{2} E(u_{-1})\right] -\right.$$

$$\left. - \exp(i\omega_1 t)\left[E(v_0) - \frac{1}{2} E(v_1) - \frac{1}{2} E(v_{-1})\right]\right) . \tag{96}$$

In contrast with (94), the time function multiplying phase factor $\exp(-i\phi)$ in (96) is complex. The total time waveform at the filter output, $g(t)$, namely the filtered complex envelope, is given by (94) plus (96), and depends on ϕ. In fact, since the magnitude of total output $g(t)$ depends on ϕ, we will look at plots of the magnitudes of components $|g_d(t)|$ and $|g_u(t)|$, neither of which depend on ϕ.

For comparison, the complex envelope itself is given by (25) in the form $\underline{y}(t) = z(t) + i\, e(t) \exp(-i2\pi f_o t)$. Since these two (unfiltered) components depend differently on phase ϕ, we shall also consider only their magnitudes $|z(t)|$ and $|e(t)|$ and compare them with filtered components $|g_d(t)|$ and $|g_u(t)|$, respectively. In particular, from (48), the desired component of the complex envelope $\underline{y}(t)$ for the example at hand is

$$z(t) = \exp(i\phi - \alpha t)\, U(t) \quad \text{for all } t\ , \tag{97}$$

while the undesired portion is given by (56) and (87) as

$$e(t) = -\frac{1}{\pi}\mathrm{Re}\{\exp(i\phi - ct)\, E_1(-ct)\} = -\frac{1}{\pi}\mathrm{Re}\{\exp(i\phi)\, \mathbf{E}(-ct)\} \tag{98}$$

for $t \neq 0$, where $c = \alpha - i\omega_o$. The magnitude of complex waveform $z(t)$ is independent of ϕ, but the magnitude of real error waveform $e(t)$ still depends on ϕ; see figure 3.

The magnitudes of $z(t)$ and $g_d(t)$ for $\alpha = 1\ \mathrm{sec}^{-1}$ and $f_1 = 40$ Hz are displayed in figure 5 on a logarithmic ordinate. The filtered complex envelope component, $g_d(t)$, drops very quickly to the left of $t = 0$ and is indistinguishable from $z(t)$ for $t > 0$; compare with figure 4. Thus, the passband of the Hann filter $H(f)$ in (83) has been taken wide enough to pass the majority of the frequency components of desired function $Z(f)$ in this example. The darkened portion of the plot just to the left of $t = 0$ corresponds to a weak amplitude-modulated 40 Hz component, which is the cutoff frequency f_1 of filter $H(f)$.

The magnitudes of $g_u(t)$ and error $e(t)$ are displayed in figure 6 for the additional choice of parameters $f_o = 100$ Hz and $\phi = -\pi/2$ rad. The peak values of these undesired components at $t = 0$ differ by over a factor of 10, through this process of filtering the complex envelope. At the same time, the skirts of filtered version $g_u(t)$ are down by several orders of magnitude relative to $e(t)$. The thick plot of $|g_u(t)|$ is again a 40 Hz component, which has been sampled at a time increment $\Delta_t = .002$ sec.

For phase $\phi = 0$ instead, original waveform $y(t)$ in (45) is discontinuous at $t = 0$, giving rise to a Hilbert transform which has a logarithmic infinity there; see (77), (78), and (79). Therefore, the magnitude of error $e(t)$ in figure 7 has an infinity at $t = 0$, whereas the filtered quantity $g_u(t)$ is finite there; in fact, $|g_u(t)|$ is independent of ϕ. Although $e(t)$ is significantly reduced in value, away from the origin, relative to figure 6, it is still larger than the filtered quantity $g_u(t)$. Since the energy in error waveform $e(t)$ is independent of ϕ (see (62)), smaller skirts in $e(t)$ can only be accompanied by a larger peak; in fact, this latter case for $e(t)$ in figure 7 has an infinite (integrable) peak at $t = 0$. By contrast, the energy in the filtered undesired component $g_u(t)$ is, from (82) and (84),

$$\int df \; |E(f+f_o)|^2 \; |H(f)|^2 \; , \tag{99}$$

which can be considerably less than the error energy, when filter $H(f)$ significantly rejects the displaced error spectrum $E(f+f_o)$.

This example points out that considerable reduction of the undesired error term in the complex envelope can be achieved through the use of lowpass filtering with an appropriate cutoff frequency, and that the undesired singularities can be significantly suppressed. Furthermore, the desired component of the complex envelope can be essentially retained. These conclusions follow if the bandwidth of the imposed modulation, $z(t)$ in (1) and (2), is small relative to the carrier frequency f_o.

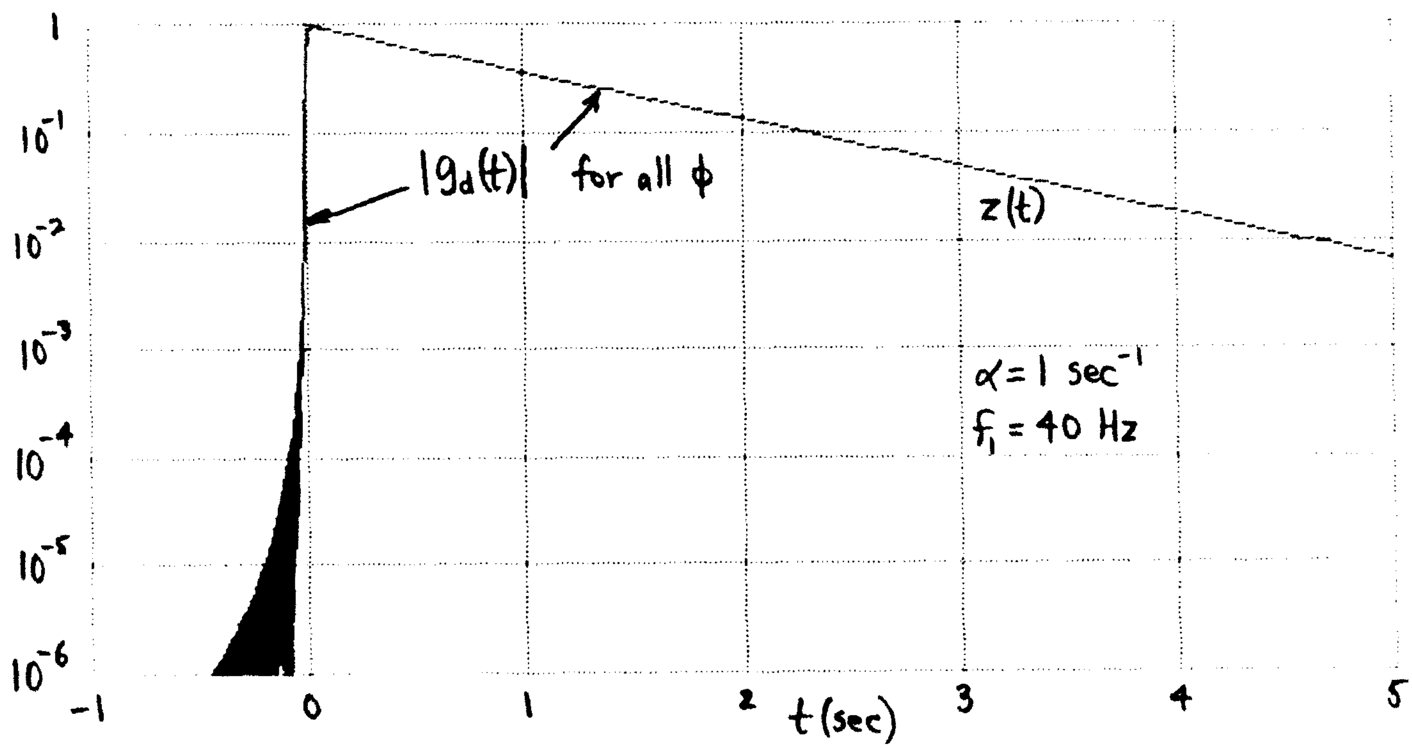

Figure 5. Filtered Complex Envelope; Desired Terms

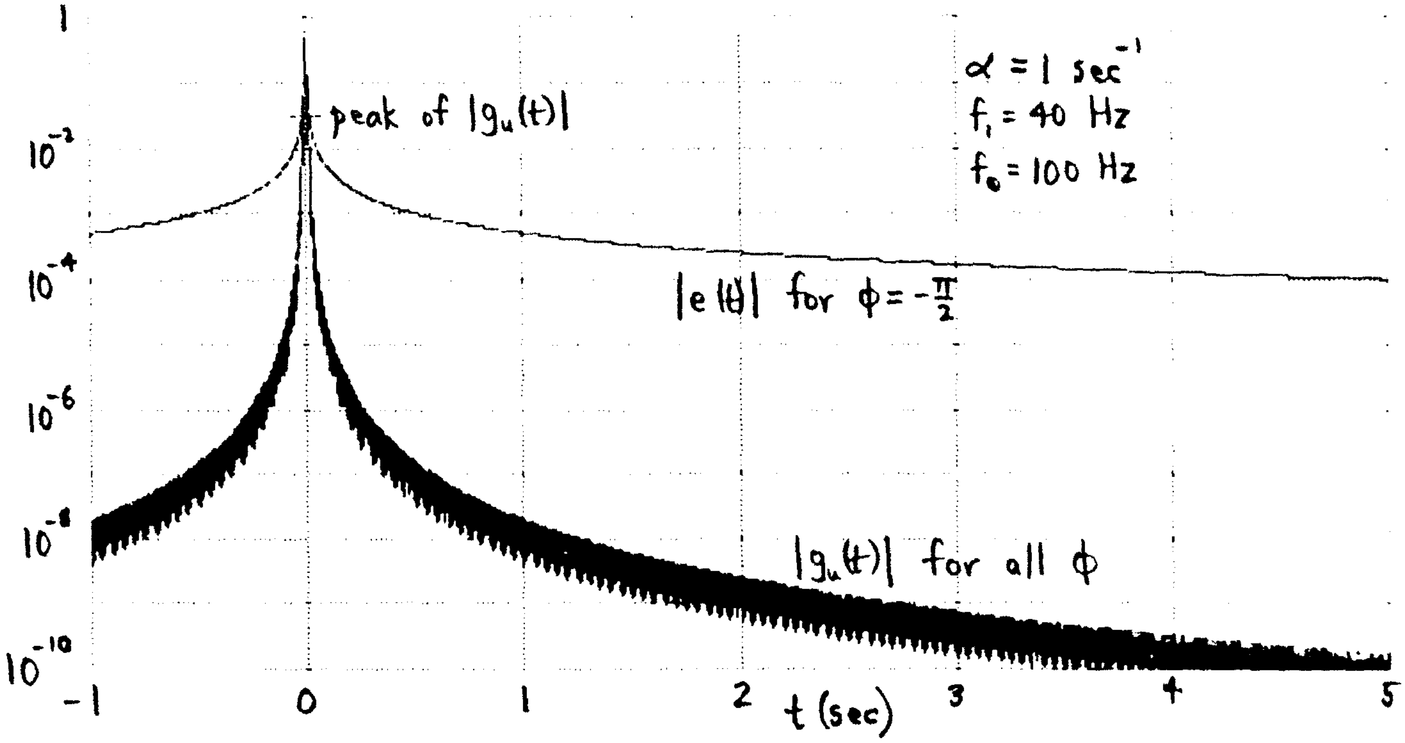

Figure 6. Filtered Complex Envelope; Undesired Terms, $\phi=-\pi/2$

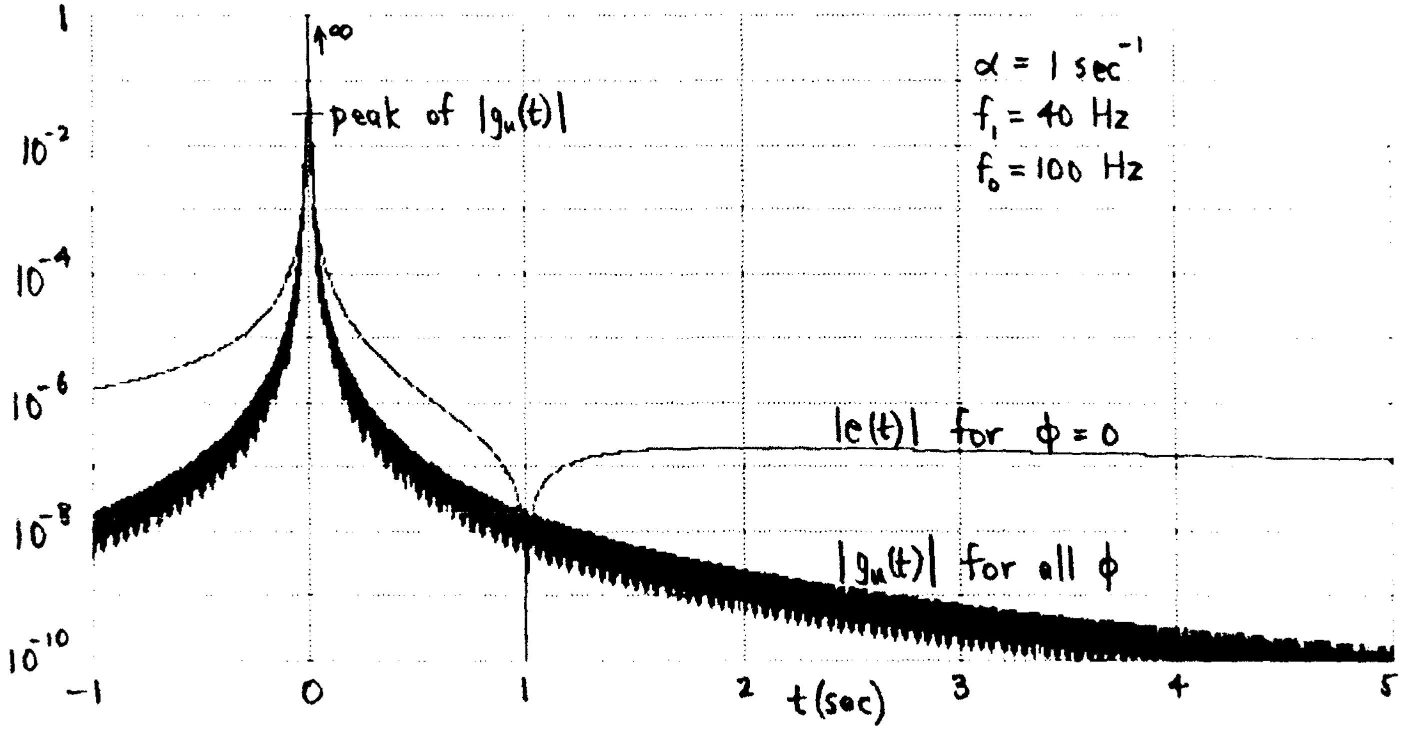

Figure 7. Filtered Complex Envelope; Undesired Terms, $\phi=0$

TRAPEZOIDAL APPROXIMATIONS TO ANALYTIC WAVEFORM, COMPLEX ENVELOPE, AND FILTERED COMPLEX ENVELOPE

In this section, we address methods of evaluating the analytic waveform and the complex envelope by means of FFTs. We start by repeating the results in (6) and (8) for the analytic waveform, that is,

$$Y_+(f) = 2\ U(f)\ Y(f)\ , \tag{100}$$

$$y_+(t) = \int df\ \exp(i2\pi ft)\ Y_+(f) = \int_0^\infty df\ \exp(i2\pi ft)\ 2\ Y(f)\ . \tag{101}$$

The trapezoidal approximation to (101) is obtained by sampling with frequency increment Δ to get

$$\tilde{y}_+(t) \equiv \Delta \sum_{n=0}^{\infty} \epsilon_n \exp(i2\pi n\Delta t)\ 2\ Y(n\Delta) = \tag{102}$$

$$= \int_0^\infty df\ \exp(i2\pi ft)\ 2\ Y(f)\ \Delta\ \delta_\Delta(f) =$$

$$= y_+(t) \circledast \delta_{1/\Delta}(t) = \sum_n y_+\left(t - \frac{n}{\Delta}\right)\ , \tag{103}$$

where sequence $\epsilon_o = \frac{1}{2}$ and $\epsilon_n = 1$ for $n \geq 1$, and summations without limits are from $-\infty$ to $+\infty$.

Notice that approximation $\tilde{y}_+(t)$ is a continuous function of time t and has period $1/\Delta$ in t. The desired term in (103) is that for $n = 0$, namely analytic waveform $y_+(t)$. Because $y_+(t)$ can contain a slowly decaying Hilbert transform component, the aliasing at separation $1/\Delta$ in (103) can lead to severe distortion in approximation $\tilde{y}_+(t)$ defined in (102).

Since $\tilde{y}_+(t)$ has period $1/\Delta$ in t, we can confine its computation to any interval of length $1/\Delta$. In particular, if we divide this interval into N equally-spaced points (where integer N is arbitrary), we can compute, from (102),

$$\tilde{y}_+\left(\frac{k}{N\Delta}\right) = \Delta \sum_{n=0}^{\infty} \varepsilon_n \exp(i2\pi nk/N)\ 2\ Y(n\Delta) \tag{104}$$

for any N contiguous values of k. If we choose the range $0 \le k \le N-1$, and if we collapse the infinite sequence in the summand of (104) according to

$$z_n = 2\Delta \sum_{j=0}^{\infty} \varepsilon_{n+jN}\ Y(n\Delta + jN\Delta) \quad \text{for } 0 \le n \le N-1 \ , \tag{105}$$

then (104) can be written precisely as

$$\tilde{y}_+\left(\frac{k}{N\Delta}\right) = \sum_{n=0}^{N-1} \exp(i2\pi nk/N)\ z_n \ . \tag{106}$$

This last result can be accomplished by means of an N-point FFT if N is highly composite. This is a very efficient method of computing the aliased version of the analytic waveform as defined by (102).

COMPLEX ENVELOPE

The center frequency f_c of single-sided spectrum $Y_+(f)$ in (100) can be found by the method described in appendix A. Then the complex envelope spectrum and waveform are, respectively,

$$\underline{Y}(f) = Y_+(f+f_c) \ , \tag{107}$$

$$\underline{y}(t) = \int df \exp(i2\pi ft)\ \underline{Y}(f) =$$

$$= \int df \exp(i2\pi ft)\ Y_+(f+f_c) = \exp(-i2\pi f_c t)\ y_+(t) \ . \tag{108}$$

The approximation to complex envelope $\underline{y}(t)$ is achieved by relating it to that for analytic waveform $y_+(t)$ according to

$$\tilde{\underline{y}}(t) \equiv \exp(-i2\pi f_c t)\ \tilde{y}_+(t) = \tag{109}$$

$$= \exp(-i2\pi f_c t)\ \Delta \sum_{n=0}^{\infty} \varepsilon_n \exp(i2\pi n\Delta t)\ 2\ Y(n\Delta) \ , \tag{110}$$

where we used (108) and (102). The continuous function $\exp(i2\pi f_c t)\ \tilde{\underline{y}}(t)$, which is just $\tilde{y}_+(t)$, has period $1/\Delta$ in t, which simplifies its calculation. Using (109), (103), and (108), there follows, for the approximation to the complex envelope,

$$\tilde{\underline{y}}(t) = \exp(-i2\pi f_c t) \sum_n y_+\left(t - \frac{n}{\Delta}\right) = \sum_n \underline{y}\left(t - \frac{n}{\Delta}\right) \exp(-i2\pi f_c n/\Delta) \ . \tag{111}$$

The desired term in (111), for n = 0, is complex envelope $\underline{y}(t)$. The n-th term has a time delay (aliasing) of n/Δ and a phase shift of $n2\pi f_c/\Delta$ radians, which is arbitrary because frequency sampling increment Δ in (102) is unrelated to center frequency f_c of $Y_+(f)$ in (100).

Sample values of complex envelope approximation $\tilde{\underline{y}}(t)$ can be obtained from (110) as

$$\tilde{\underline{y}}\left(\frac{k}{N\Delta}\right) = \exp\left(-i2\pi f_c \frac{k}{N\Delta}\right) \Delta \sum_{n=0}^{\infty} \varepsilon_n \exp(i2\pi nk/N) \; 2 \; Y(n\Delta) \; . \tag{112}$$

Again, the infinite sum in (112) can be collapsed and realized as an N-point FFT; see (104) - (106). The phase factor $p_k = \exp(-i2\pi f_c k/(N\Delta))$ can be computed via recurrence $p_k = p_{k-1} \exp(-i2\pi f_c/(N\Delta))$.

FILTERED COMPLEX ENVELOPE

The spectrum of the filtered complex envelope is given by (84) as $G(f) = \underline{Y}(f) \; H(f)$. The filtered complex envelope waveform is

$$g(t) = \int df \; \exp(i2\pi ft) \; G(f) = \underline{y}(t) \circledast h(t) \tag{113}$$

and has low sidelobes and rapid decay in t, when filter H(f) is chosen appropriately.

The approximation to g(t) adopted here will be generalized slightly in order to allow for frequency-shifted sampling. Specifically, we define

$$\tilde{g}_\alpha(t) \equiv \int df \exp(i2\pi ft)\, G(f)\, \Delta\, \delta_\Delta(f - \alpha) = \tag{114}$$

$$= \Delta \sum_n \exp(i2\pi[n\Delta + \alpha]t)\, G(n\Delta + \alpha) \ . \tag{115}$$

The function $\exp(-i2\pi\alpha t)\ \tilde{g}_\alpha(t)$ has period $1/\Delta$ in t, which allows us to confine its calculation to any convenient period.

The behavior of approximation $\tilde{g}_\alpha(t)$ in (114) follows as

$$\tilde{g}_\alpha(t) = g(t) \circledast [\exp(i2\pi\alpha t)\ \delta_{1/\Delta}(t)] =$$

$$= g(t) \circledast \sum_n \exp(i2\pi\alpha n/\Delta)\ \delta\left(t - \frac{n}{\Delta}\right) =$$

$$= \sum_n \exp(i2\pi\alpha n/\Delta)\ g\left(t - \frac{n}{\Delta}\right) \ . \tag{116}$$

This is the aliased version of the filtered complex envelope. The desired term, for $n = 0$, is the filtered complex envelope $g(t)$, independent of the choice of frequency shift α. Shift α is arbitrary and could be taken as $-f_c$ if desired.

Samples of $\tilde{g}_\alpha(t)$ are available from (115) according to

$$\tilde{g}_\alpha\left(\frac{k}{N\Delta}\right) = \Delta \exp\left(i2\pi\alpha \frac{k}{N\Delta}\right) \sum_n \exp(i2\pi nk/N)\ G(n\Delta + \alpha) \ , \tag{117}$$

which we can limit to $0 \le k \le N-1$ due to the periodicity of $\tilde{g}_\alpha(t)$. Again, the infinite sum on n can be converted to an N-point FFT without error, by collapsing into the finite sequence

$$z_n = \Delta \sum_j G(n\Delta + \alpha + jN\Delta) \quad \text{for } 0 \le n \le N-1 \ . \tag{118}$$

The remaining phasor $\exp(i2\pi\alpha k/(N\Delta))$ in (117) can be quickly obtained via recursion on k.

GRAPHICAL RESULTS

The same fundamental example introduced in (45) will be used here, again with $\alpha = 1 \text{ sec}^{-1}$ and $f_o = 100$ Hz. For phase $\phi = -\pi/2$, FFT size N = 1024, and a frequency increment of $\Delta = 1/80$ Hz, the magnitude of $\tilde{y}(t)$, namely $\tilde{A}(t)$, is displayed in figure 8 over the $1/\Delta = 80$ sec period centered at t = 0. This selection of the time period has been purposely made the same as that used in figure 4, for easy comparison of results. The major difference between the $\phi = -\pi/2$ result in figure 4 and figure 8 is that the aliasing in the latter case causes the curve to have a jagged behavior and to droop in the neighborhood of $t = \pm 40$ sec. However, other examples could well have the aliasing increase near the edges of the period. A total of 88,000 samples of Y(f) at frequency increment Δ were taken in computation of (104); the collapsing in (106) resulted in storage of only N = 1024 complex numbers and the ability to use a single relatively small N-point FFT. A program for the evaluation of the complex envelope by means of an FFT with collapsing is furnished in appendix B; the FFT uses a zero-subscripted array in direct agreement with the mathematical definition of the FFT.

The corresponding phase, $\tilde{P}(t) = \arg\{\tilde{y}(t)\}$, of the aliased complex envelope is given in figure 9. The phase is approximately $-\pi/2$ for $0 \le t \le 10$ sec, as expected, since in this limited time interval, the error is not the dominant term. However, over the rest of the period, the error term does dominate and it has an $\exp(-i\omega_o t)$ behavior, where $f_o = 100$; see (25) and figure 3. Thus, the time sampling increment $\Delta_t = 1/(N\Delta) = .078$ sec is grossly inadequate to track this high-frequency term, and we get virtually random samples of the phase of the complex exponential $\exp(-i\omega_o t)$.

To confirm the phase behavior outside the (0,10) sec interval, we have plotted the phase of $\underline{y}(t) \exp(i\omega_o t) = y_+(t)$ in figure 10 as found by the FFT procedure above. To the right of $t = 10$, the phase is approximately $\pi/2$, in agreement with the fact that $e(t)$ is real and positive for $t > 0$; see figure 3 and (25). For time $t < 0$, the phase is $-\pi/2$ because $e(t) < 0$ for $t < 0$. The oscillatory behavior at both edges of the period, namely, for $30 < |t| < 40$, is due to aliasing from adjacent lobes indicated by (103) and (111).

When ϕ is changed to 0 and everything else is kept unchanged, the result for the magnitude of complex envelope aliased version $\tilde{\underline{y}}(t)$ is plotted in figure 11. Comparison with the exact results in figure 4 reveals a very dramatic increase in aliasing, in fact, by <u>two</u> orders of magnitude. The reason for this considerable increase can be seen from figure 3 and (75); namely, the error $e(t)$ is unipolar for $\phi = 0$ and it decays very slowly. Whereas for figure 8, the alternating character of the overlapping aliased error lobes led to a cancellation near $t = \pm 40$ sec, the opposite situation occurred in figure 11, leading to a considerable build-up of the aliasing effect.

The corresponding phase of $\tilde{y}(t)$, $\tilde{P}(t)$, is plotted in figure 12. Its value is zero in the region $0 \le t \le 10$, as expected, since the desired term, $\exp(-\alpha t)$, dominates here. Outside this region, the situation is the same as explained above with respect to figure 9. We have not plotted the counterpart to figure 10 because no one error lobe dominates anywhere on the time scale; the result is a phase plot that looks random over the entire period of (-40,40) sec.

When the complex envelope spectrum is filtered according to the Hann filter in (83) - (86), the results for the sampled filtered complex envelope waveform, obtained by means of the collapsed FFT in (117) and (118) with $\alpha = 0$, are given in figures 13 and 14. There were 6400 frequency samples taken of $G(f)$ with increment $\Delta = 1/80$ Hz and an FFT size of $N = 1024$ was utilized; see appendix B. A comparison of the magnitudes in figures 13 and 5 reveals virtually identical results; namely, the error and its inherent accompanying aliasing, that was present in figure 8, is absent from figure 13.

The corresponding phase plot of the FFT output is displayed in figure 14. In the region $0 \le t \le 24$ sec, where the desired $\exp(-\alpha t)$ term dominates, the FFT output phase is equal to the value of $\phi = -\pi/2$ for this example. When this example was rerun for $\phi = 0$, similar high quality results were obtained, except that the FFT output phase was zero. The benefits of filtering the complex envelope spectrum are well illustrated by the results of figures 13 and 14.

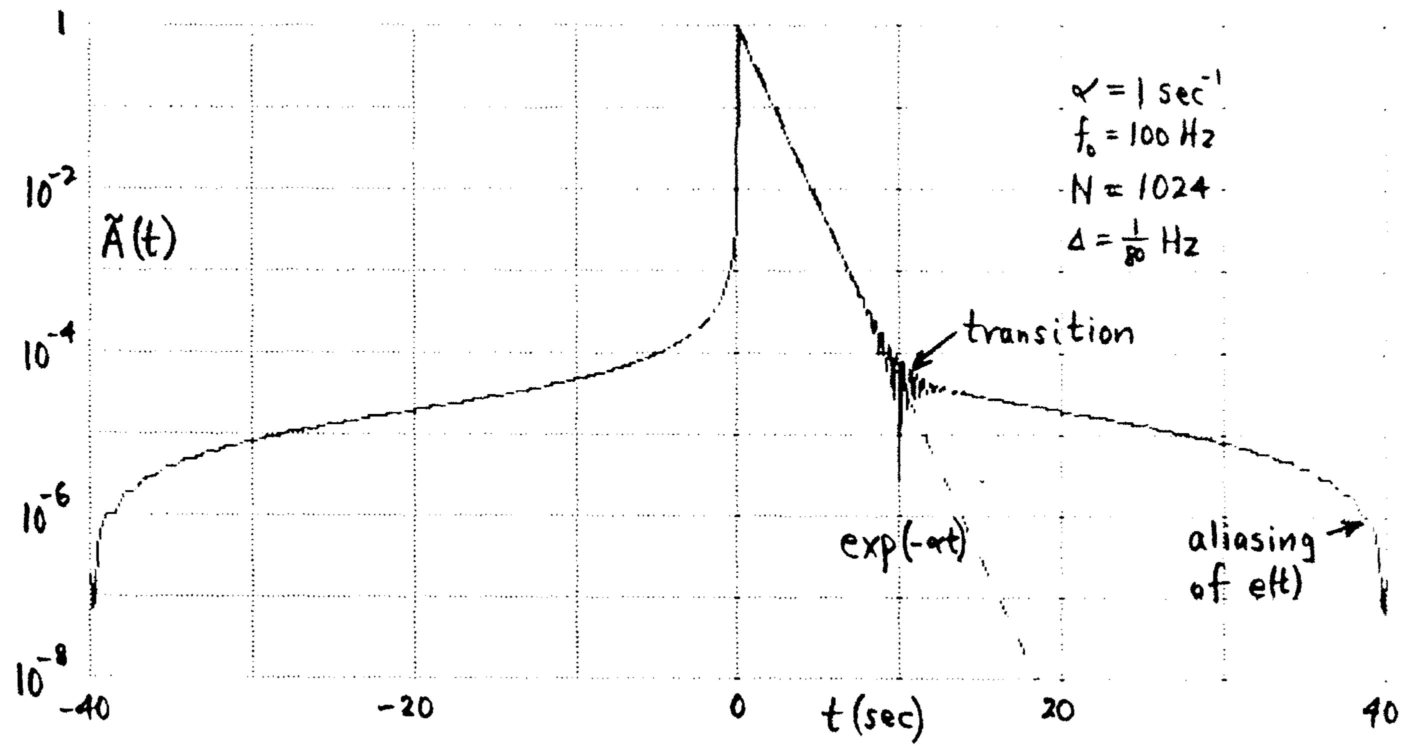

Figure 8. Magnitude of Complex Envelope via FFT, $\phi=-\pi/2$

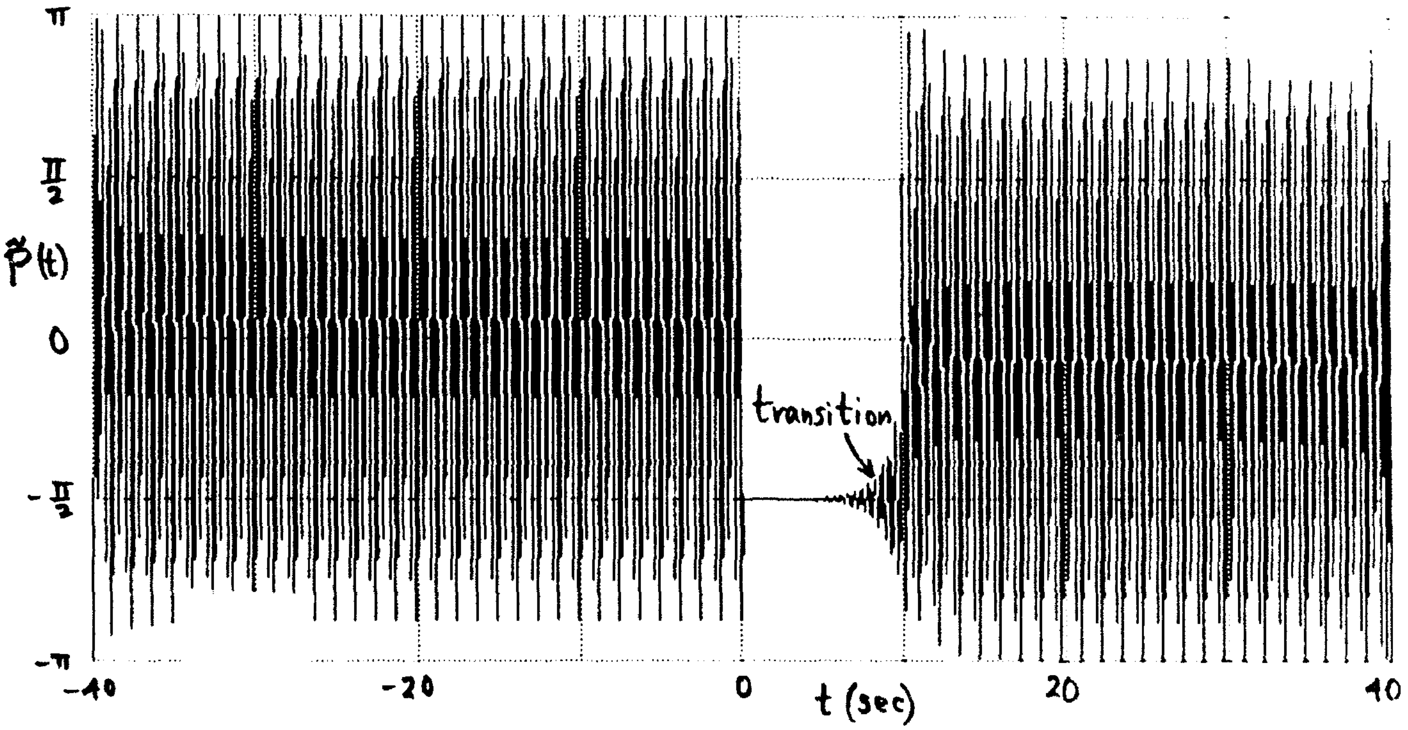

Figure 9. Phase of Complex Envelope via FFT, $\phi=-\pi/2$

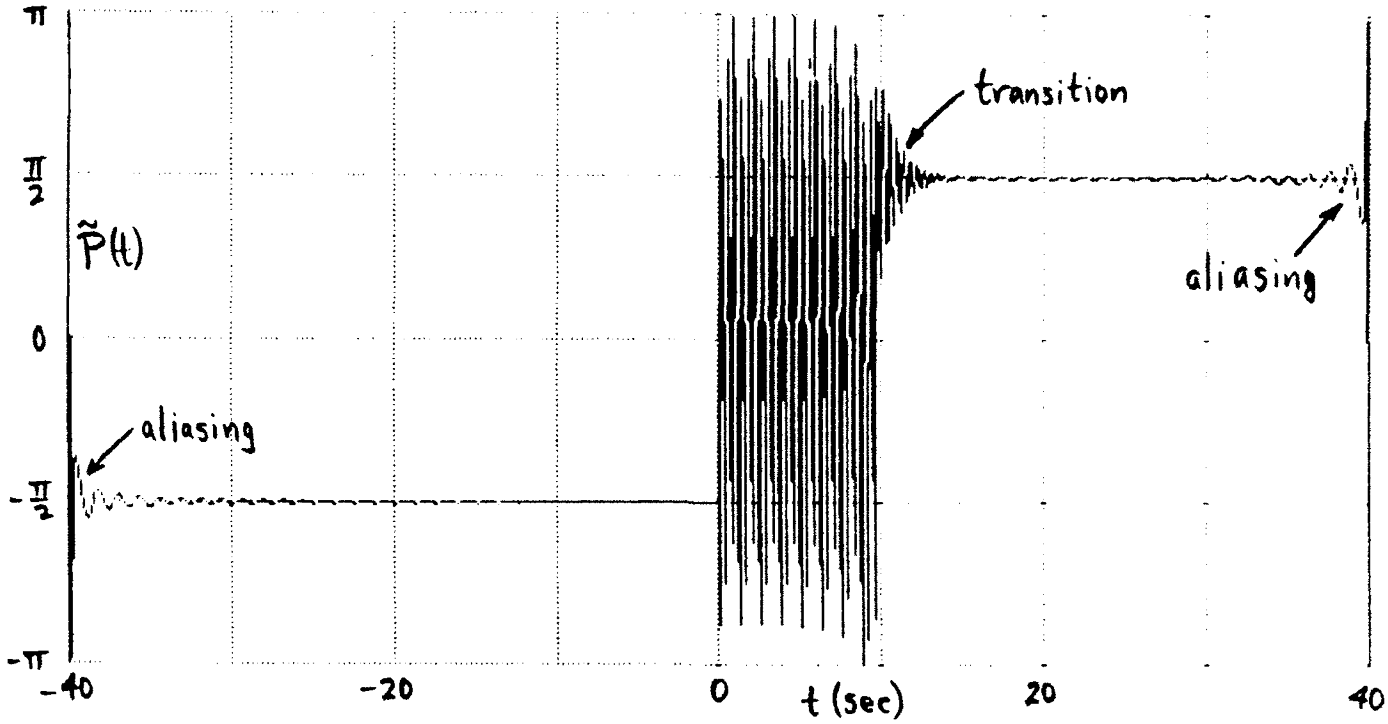

Figure 10. Phase of Analytic Waveform via FFT, $\phi=-\pi/2$

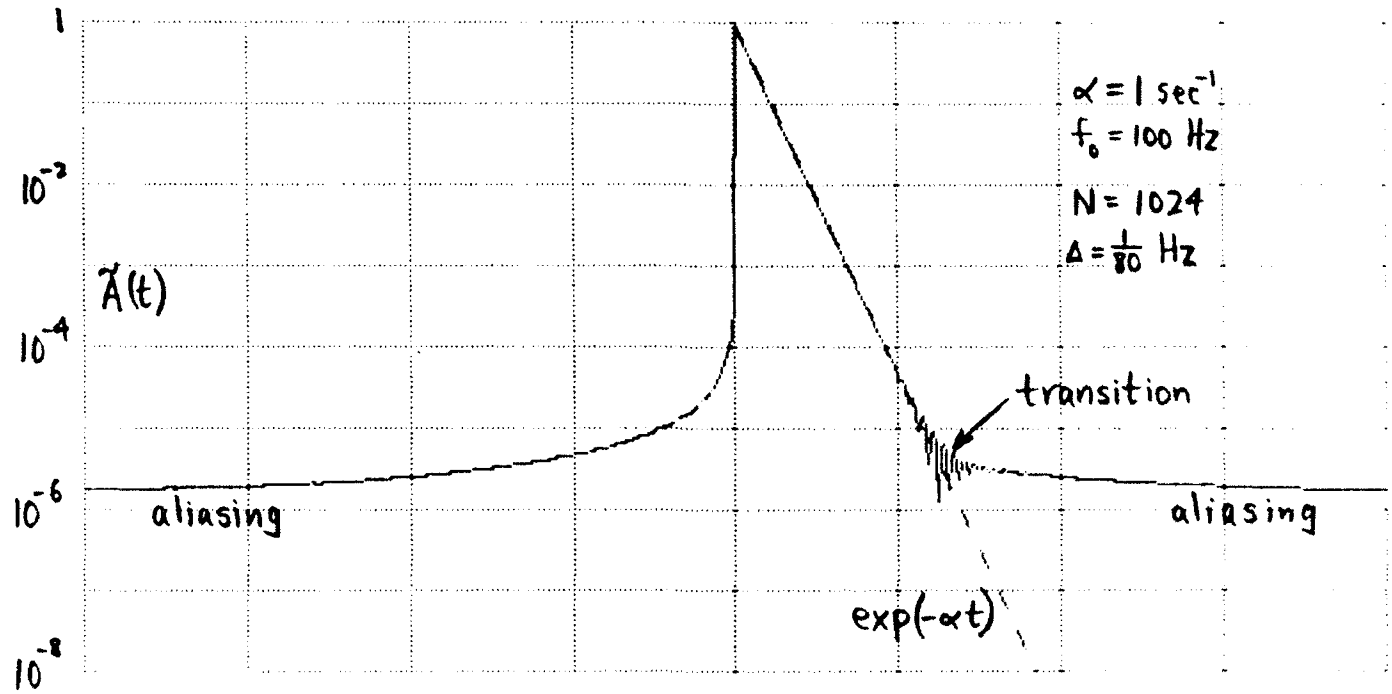

Figure 11. Magnitude of Complex Envelope via FFT, $\phi=0$

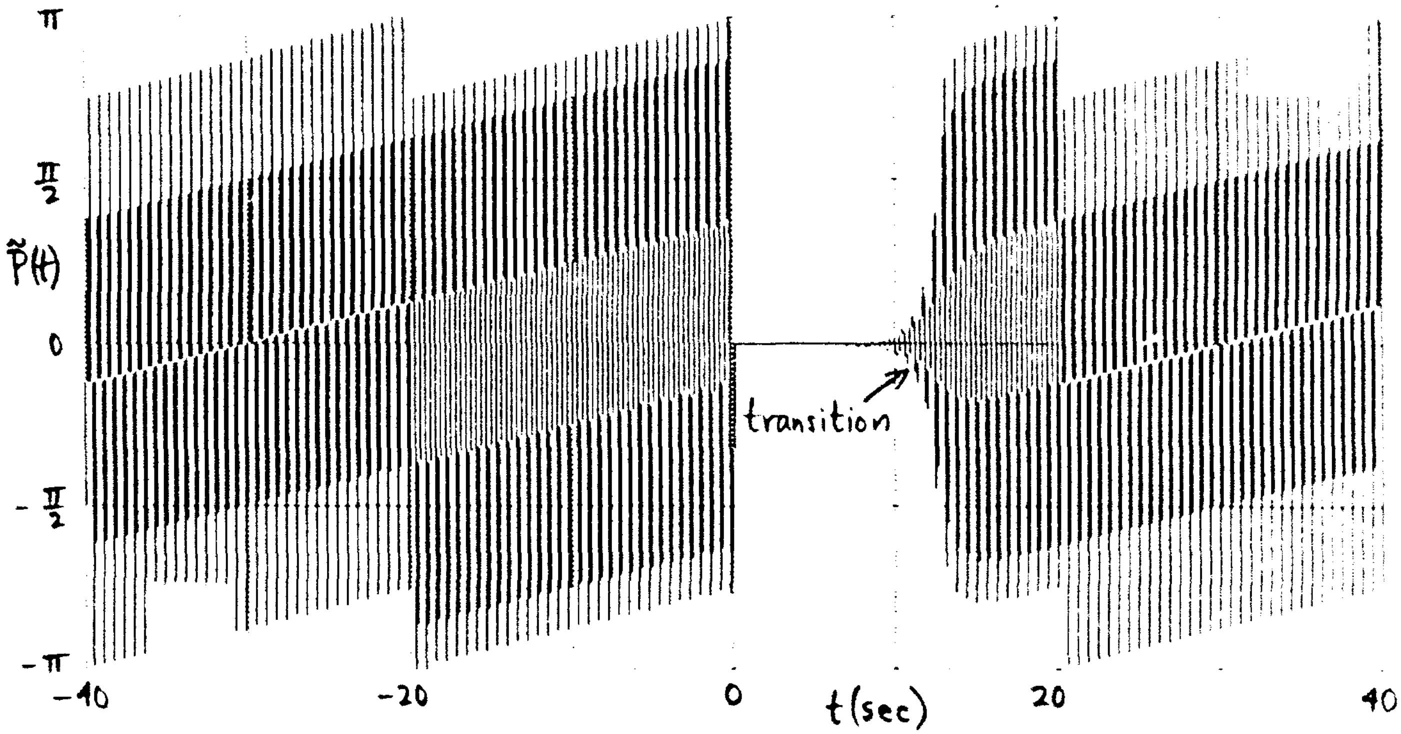

Figure 12. Phase of Complex Envelope via FFT, $\phi=0$

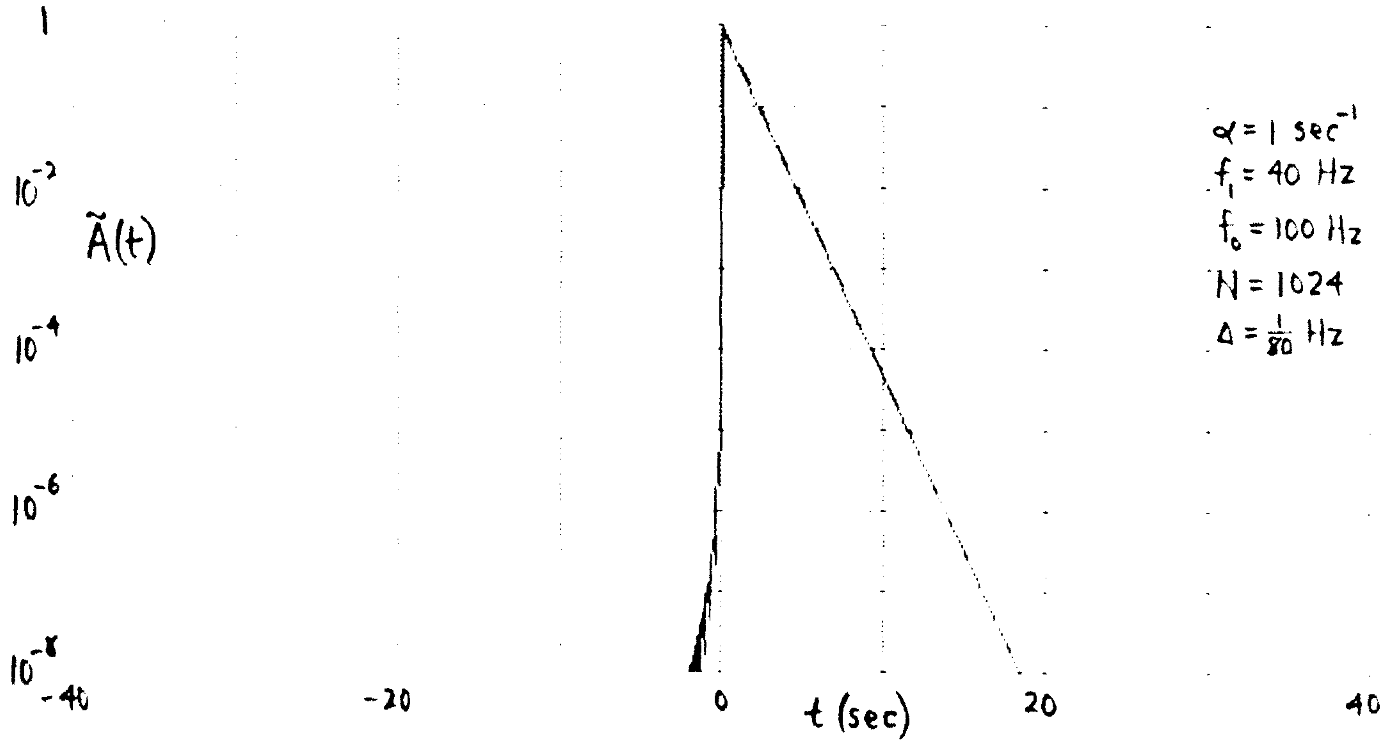

Figure 13. Magnitude of Filtered Complex Envelope via FFT, $\phi=-\pi/2$

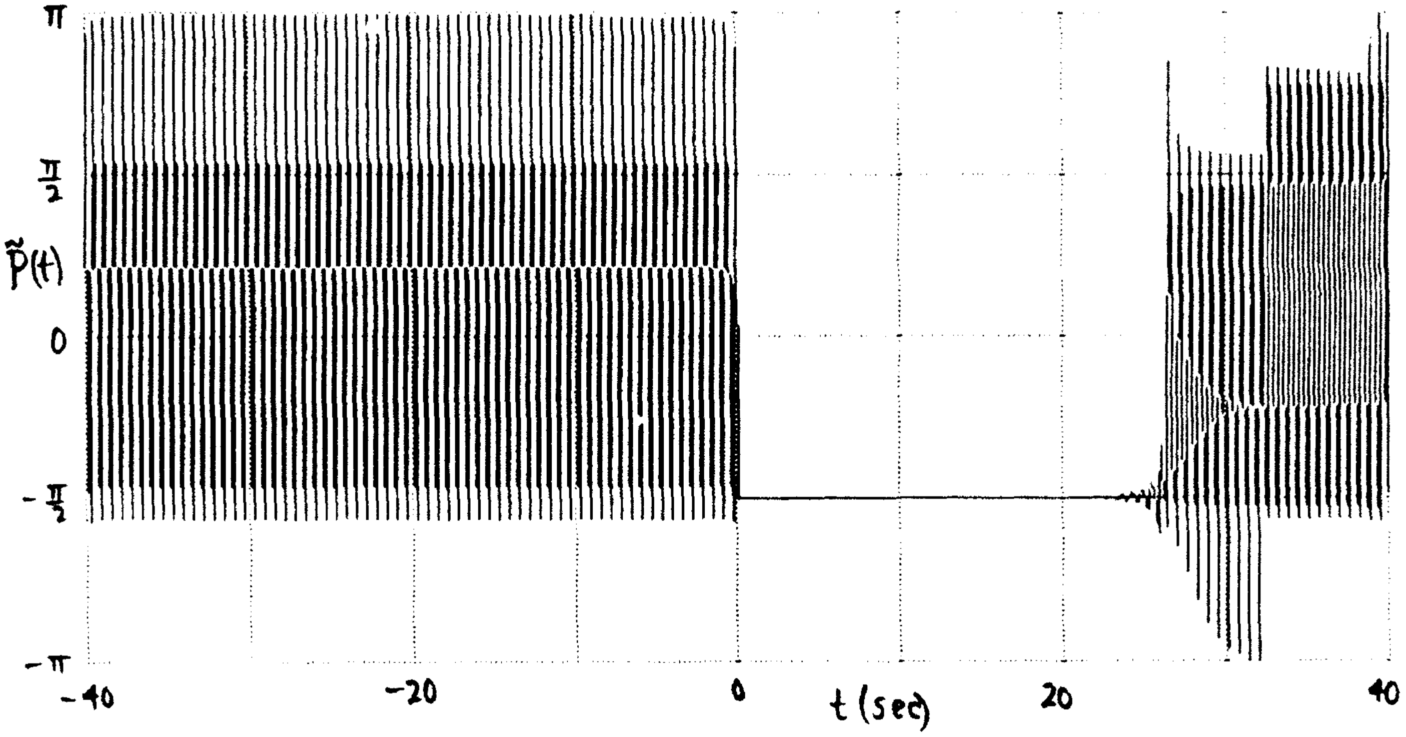

Figure 14. Phase of Filtered Complex Envelope via FFT, $\phi=-\pi/2$

ALIASING PROPERTIES OF COSINE AND SINE TRANSFORMS

If a time function is causal, it can be obtained from its Fourier transform either by a cosine or a sine transform. However, when these integral transforms are approximated, by means of sampling the frequency function and using some integration rule like trapezoidal, the "alias-free" interval in the time domain is approximately halved, as shown below. This does not necessarily mean that these transform alternatives should be discarded, because a more rapidly decaying integrand can be useful, but it does point out a cautionary feature in their use and the need to consider the tradeoff between aliasing and truncation error.

GENERAL TIME FUNCTION

In general, complex time function $y(t)$ is obtained from its Fourier transform $Y(f)$ according to

$$y(t) = \int df \exp(i2\pi ft)\, Y(f) = \tag{119}$$

$$= \int df \cos(2\pi ft)\, Y(f) + i \int df \sin(2\pi ft)\, Y(f) = \tag{120}$$

$$= y_e(t) + y_o(t) \quad \text{for all } t \, , \tag{121}$$

where complex functions $y_e(t)$ and $y_o(t)$ are the even and odd parts of function $y(t)$, respectively.

CAUSAL COMPLEX TIME FUNCTION

Now suppose that $y(t)$ is causal, but possibly complex; then

$$y(t) = 0 \quad \text{for } t < 0 . \tag{122}$$

Then, letting $t = -a$, $a > 0$, we have, from (122) and (121),

$$0 = y(-a) = y_e(-a) + y_o(-a) = y_e(a) - y_o(a) \quad \text{for } a > 0 . \tag{123}$$

That is,

$$y_o(a) = y_e(a) \quad \text{for } a > 0 . \tag{124}$$

Therefore, from (121) and (120), we have two alternatives for a causal complex time function $y(t)$:

$$y(t) = 2 \int df \cos(2\pi ft)\, Y(f) \quad \text{for } t > 0 , \tag{125}$$

and

$$y(t) = i2 \int df \sin(2\pi ft)\, Y(f) \quad \text{for } t > 0 . \tag{126}$$

We need complex function $Y(f)$ for negative as well as positive frequency arguments f, in order to determine causal complex function $y(t)$, but we can utilize either a cosine or a sine transform.

NONCAUSAL REAL TIME FUNCTION

Now suppose instead that y(t) is real, but noncausal. Then, since spectrum $Y(-f) = Y^*(f)$, we can express (119) as

$$y(t) = 2 \text{ Re} \int_0^\infty df \exp(i2\pi ft)\, Y(f) = \tag{127}$$

$$= 2\int_0^\infty df \cos(2\pi ft)\, Y_r(f) - 2\int_0^\infty df \sin(2\pi ft)\, Y_i(f) \quad \text{for all } t. \tag{128}$$

The first term in (128) is even part $y_e(t)$, while the second term in (128) is odd part $y_o(t)$; see (121). In this case of a real time function y(t), we need complex function Y(f) only for $f > 0$.

CAUSAL REAL TIME FUNCTION

Now let y(t) be both causal and real. Then using property $Y(-f) = Y^*(f)$ in (125) and (126), we obtain

$$y(t) = 4 \int_0^\infty df \cos(2\pi ft)\, Y_r(f) \quad \text{for } t > 0 \text{ ,} \tag{129}$$

and

$$y(t) = -4 \int_0^\infty df \sin(2\pi ft)\, Y_i(f) \quad \text{for } t > 0 \text{ .} \tag{130}$$

Here, we need either $Y_r(f)$ or $Y_i(f)$, and then only for positive frequency arguments f. Also, a cosine or a sine transform will suffice for determination of y(t).

ALIASING PROPERTIES

The above relations have all assumed that spectrum $Y(f)$ is available for all continuous f. Now we will address the effects of only having samples of $Y(f)$ available at frequency increment Δ. We begin with the trapezoidal approximation to (119):

$$y_1(t) \equiv \Delta \sum_n \exp(i2\pi n\Delta t)\, Y(n\Delta) \quad \text{for all } t\ . \tag{131}$$

The approximation $y_1(t)$ is periodic in t with period $1/\Delta$. It can be expressed exactly as

$$y_1(t) = \int df \exp(i2\pi ft)\, Y(f)\, \Delta\, \delta_\Delta(f) = \tag{132}$$

$$= y(t) \circledast \delta_{1/\Delta}(t) = \sum_n y\left(t - \frac{n}{\Delta}\right) \quad \text{for all } t\ . \tag{133}$$

That is, approximation $y_1(t)$ is an aliased version of desired waveform $y(t)$, with displacements $1/\Delta$ in time. This result holds for any complex waveform $y(t)$ and has been used repeatedly in the analyses above.

The second approximation of interest is obtained from the cosine transform in (125), which applies for causal complex $y(t)$ in the form

$$y_{2c}(t) \equiv 2\Delta \sum_n \cos(2\pi n\Delta t)\, Y(n\Delta) \quad \text{for all } t\ . \tag{134}$$

$y_{2c}(t)$ also has period $1/\Delta$ in t and can be developed as follows:

$$y_{2c}(t) = \Delta \sum_n [\exp(i2\pi n\Delta t) + \exp(-i2\pi n\Delta t)]\; Y(n\Delta) =$$

$$= \int df\; [\exp(i2\pi ft) + \exp(-i2\pi ft)]\; Y(f)\; \Delta\; \delta_\Delta(f) =$$

$$= [y(t) + y(-t)] \circledast \delta_{1/\Delta}(t) = 2\, y_e(t) \circledast \delta_{1/\Delta}(t) =$$

$$= \sum_n \left[y\left(t - \frac{n}{\Delta}\right) + y\left(\frac{n}{\Delta} - t\right)\right] \quad \text{for all } t\ . \tag{135}$$

That is, sampling of the cosine transform in (125) results in aliasing of $y(t)$ plus its mirror image $y(-t)$, <u>even when</u> $y(t)$ is causal. This will restrict useful results in $y_{2c}(t)$ to a region approximately <u>half</u> as large as that given by (131) and (133), where the sampled exponential transform was used. Even when we restrict calculation of approximation $y_{2c}(t)$ to the region $(0,1/\Delta)$, we are contaminated by the mirror image lobe $y(1/\Delta - t)$ and by the usual lobe $y(t + 1/\Delta)$ extending from $t = -1/\Delta$ into the desired region.

A similar situation exists for using a sampled version of the sine transform for causal complex $y(t)$ in (126); namely, consider the approximation

$$y_{2s}(t) \equiv i2\Delta \sum_n \sin(2\pi n\Delta t)\; Y(n\Delta) \quad \text{for all } t\ . \tag{136}$$

Then

$$y_{2s}(t) = \Delta \sum_n [\exp(i2\pi n\Delta t) - \exp(-i2\pi n\Delta t)]\ Y(n\Delta) =$$

$$= \int df\ [\exp(i2\pi ft) - \exp(-i2\pi ft)]\ Y(f)\ \Delta\ \delta_\Delta(f) =$$

$$= [y(t) - y(-t)] \circledast \delta_{1/\Delta}(t) = 2\ y_o(t) \circledast \delta_{1/\Delta}(t) =$$

$$= \sum_n \left[y\left(t - \frac{n}{\Delta}\right) - y\left(\frac{n}{\Delta} - t\right)\right] \quad \text{for all } t\ . \qquad (137)$$

Here, for the approximate sine transform, twice the odd part of causal complex y(t) is aliased with separations $1/\Delta$ in time, thereby again leading to a clear region only about half that attainable from (131) and (133). We will return to these apparently undesirable transform properties below and find them useful when we consider a causal real time function.

The next approximation is for the noncausal real waveform result in (127); namely, letting $\varepsilon_o = \frac{1}{2}$ and $\varepsilon_n = 1$ for $n \geq 1$, we have trapezoidal approximation

$$y_3(t) \equiv 2\ \mathrm{Re}\ \Delta \sum_{n=0}^{\infty} \varepsilon_n \exp(i2\pi n\Delta t)\ Y(n\Delta) \quad \text{for all } t\ . \qquad (138)$$

Then

$$y_3(t) = 2\ \mathrm{Re} \int_0^{\infty} df\ \exp(i2\pi ft)\ Y(f)\ \Delta\ \delta_\Delta(f) =$$

$$= \int df\ \exp(i2\pi ft)\ Y(f)\ \Delta\ \delta_\Delta(f) = \sum_n y\left(t - \frac{n}{\Delta}\right) \quad \text{for all } t\ , \qquad (139)$$

just as in (133). Thus, the combination of the cosine and sine transforms in (128) does not additionally damage the aliasing behavior associated with sampling. In practice, we would use the real part of the exponential transform as given by (127). The same result, (139), follows when the cosine and sine transforms in (128) are individually directly approximated by the trapezoidal rule and the results added together.

The two final approximations of interest come from sampling the results for causal real y(t) in (129) and (130); from (129), define approximation

$$y_{4c}(t) \equiv 4\Delta \sum_{n=0}^{\infty} \varepsilon_n \cos(2\pi n\Delta t)\ Y_r(n\Delta) \quad \text{for all } t\ , \tag{140}$$

which has period $1/\Delta$ in t. Now we develop (140) as

$$\begin{aligned} y_{4c}(t) &= 2\Delta \sum_n \cos(2\pi n\Delta t)\ Y_r(n\Delta) = \\ &= 2 \int df\ \cos(2\pi ft)\ Y_r(f)\ \Delta\ \delta_\Delta(f) = \\ &= 2 \int df\ \exp(i2\pi ft)\ Y_r(f)\ \Delta\ \delta_\Delta(f) = \\ &= \int df\ \exp(i2\pi ft)\ [Y(f) + Y^*(f)]\ \Delta\ \delta_\Delta(f) = \\ &= y(t) \circledast \delta_{1/\Delta}(t) + y^*(-t) \circledast \delta_{1/\Delta}(t) = \\ &= \sum_n y\left(t - \frac{n}{\Delta}\right) + \sum_n y\left(\frac{n}{\Delta} - t\right) = 2\ y_e(t) \circledast \delta_{1/\Delta}(t) \quad \text{for all } t, \end{aligned} \tag{141}$$

where we used the real character of $y(t)$.

This end result is identical to (135); however, approximation $y_{4c}(t)$ in (140) uses only the real part $Y_r(f)$ of the complex function $Y(f)$, whereas $y_{2c}(t)$ in (134) requires the complete complex function $Y(f)$ for a causal complex $y(t)$. Since it is possible to have complex functions $Y(f)$ which have rapidly decaying real parts and slower decaying imaginary parts, (140) affords the possibility of getting a smaller truncation error than (134), when $y(t)$ is causal real and when both sums are carried out to the same frequency limit, because both sums must be terminated in practice. Whether the reduction in the usable "alias-free" region, dictated by (141), can be traded off against a smaller truncation error associated with use of only the real part $Y_r(f)$ in (140), depends on the particular example under investigation. In any event, (140) affords an alternative to consider for causal real $y(t)$.

The final approximation comes about by sampling (130):

$$y_{4s}(t) \equiv -4\Delta \sum_{n=1}^{\infty} \sin(2\pi n\Delta t)\; Y_i(n\Delta) \quad \text{for all } t \,, \tag{142}$$

which has period $1/\Delta$ in t. In the usual fashion, we find

$$y_{4s}(t) = -2\Delta \sum_n \sin(2\pi n\Delta t)\ Y_i(n\Delta) =$$

$$= -2 \int df \sin(2\pi ft)\ Y_i(f)\ \Delta\ \delta_\Delta(f) =$$

$$= i2 \int df \exp(i2\pi ft)\ Y_i(f)\ \Delta\ \delta_\Delta(f) =$$

$$= \int df \exp(i2\pi ft)\ [Y(f) - Y^*(f)]\ \Delta\ \delta_\Delta(f) =$$

$$= y(t) \circledast \delta_{1/\Delta}(t) - y^*(-t) \circledast \delta_{1/\Delta}(t) = 2\ y_o(t) \circledast \delta_{1/\Delta}(t) =$$

$$= \sum_n y\left(t - \frac{n}{\Delta}\right) - \sum_n y\left(\frac{n}{\Delta} - t\right) \quad \text{for all } t . \tag{143}$$

Here, we used the real character of y(t).

The end result in (143) is identical to (137); however, $y_{4s}(t)$ in (142) only requires knowledge of the imaginary part $Y_i(f)$ of complex function Y(f), whereas $y_{2s}(t)$ in (136) requires the complete complex function Y(f) for a causal complex y(t). This is due to the fact that (129) and (130) apply only to causal real y(t), whereas (125) and (126) apply to causal complex y(t). Since there exist complex functions Y(f) which have more rapidly decaying imaginary parts than real parts, the opportunity arises to reduce the truncation error by employing (142) instead of (136), when y(t) is causal and real. The comments in the sequel to (141), regarding the trade-off between truncation error and a reduced alias-free region, are again applicable.

This procedure, of using only the imaginary part of a Fourier transform because it decays faster than the real part, was utilized to advantage in [4; pages 4 - 6] and was based upon an earlier result in [5; (15)]. The very rapid decay of the imaginary part far outweighed the aliasing; see [4; page 6].

EVALUATION BY MEANS OF FFTs

If periodic function $y_1(t)$ in (131) is evaluated at the equally spaced time points $k/(N\Delta)$ for $k=0$ to $N-1$, which suffice to cover one period, we obtain

$$y_1\left(\frac{k}{N\Delta}\right) = \Delta \sum_n \exp(i2\pi nk/N)\ Y(n\Delta) = \tag{144}$$

$$= \Delta \sum_{n=0}^{N-1} \exp(i2\pi nk/N)\ z_n \ , \tag{145}$$

where $\{z_n\}$, $0 \le n \le N-1$, is the collapsed version of sequence $\{Y(n\Delta)\}$, $-\infty < n < \infty$. No approximations are involved in this collapsing procedure from (144) to (145). Relation (145) can be accomplished by means of an N-point FFT if N is highly composite.

In a similar fashion, (140) yields samples of the cosine transform as

$$y_{4c}\left(\frac{k}{N\Delta}\right) = 4\Delta \sum_{n=0}^{\infty} \varepsilon_n \cos(2\pi nk/N)\; Y_r(n\Delta) =$$

$$= 4\Delta \; \mathrm{Re} \sum_{n=0}^{\infty} \exp(i2\pi nk/N)\; \varepsilon_n \; Y_r(n\Delta) = \tag{146}$$

$$= 4\Delta \; \mathrm{Re} \sum_{n=0}^{N-1} \exp(i2\pi nk/N)\; z_n \;, \tag{147}$$

where $\{z_n\}$, $0 \le n \le N-1$, is the collapsed version of sequence $\{\varepsilon_n \; Y_r(n\Delta)\}$, $0 \le n < \infty$.

Since (147) will likely be realized as the real part of an FFT output, the question arises as to the interpretation and utility of the total complex FFT output in (147). To this aim, we rewrite $y_{4c}(t)$ in (146) (in its continuous time version) as

$$y_{4c}(t) = \mathrm{Re}\; 4 \int_0^{\infty} df \; \exp(i2\pi ft)\; Y_r(f)\; \Delta \; \delta_\Delta(f) =$$

$$= \mathrm{Re}\{z_1(t) \circledast \delta_{1/\Delta}(t)\} \;, \tag{148}$$

where we define, for all t, Fourier transform

$$z_1(t) = 4 \int_0^{\infty} df \; \exp(i2\pi ft)\; Y_r(f) =$$

$$= \int_0^{\infty} df \; \exp(i2\pi ft)\; [2Y(f) + 2Y^*(f)] =$$

$$= y_+(t) + y_+^*(-t) = [\underline{y}(t) + \underline{y}^*(-t)]\; \exp(i2\pi f_c t) =$$

$$= y(t) + y(-t) + i[y_H(t) - y_H(-t)] \;. \tag{149}$$

That is, $y_{4c}(t)$ is the real part of the aliased version of $z_1(t)$, which itself is composed of the analytic waveform $y_+(t)$ and its mirror image. Thus, not only is $z_1(t)$ aliased according to (148), but in addition, $z_1(t)$ contains terms which will further overlap and thereby confuse the values of $y_{4c}(t)$ in the fundamental range $(0,1/\Delta)$. (Of course, the real part of $z_1(t)$ in (149) for $t > 0$ is, as expected, just $y(t)$ for this causal real case.)

Finally, sampling the sine transform of $Y_i(f)$ in (142) yields

$$y_{4s}\left(\frac{k}{N\Delta}\right) = -\,4\Delta \sum_{n=1}^{\infty} \sin(2\pi nk/N)\; Y_i(n\Delta) =$$

$$= -\,4\Delta\ \mathrm{Im} \sum_{n=1}^{\infty} \exp(i2\pi nk/N)\; Y_i(n\Delta) = \tag{150}$$

$$= -\,4\Delta\ \mathrm{Im} \sum_{n=0}^{N-1} \exp(i2\pi nk/N)\; z_n\ , \tag{151}$$

where $\{z_n\}$, $0 \le n \le N-1$, is the collapsed version of sequence $\{Y_i(n\Delta)\}$, $1 \le n < \infty$. Relation (151) can be realized as an N-point FFT of which only the imaginary part is kept for $0 \le k \le N-1$.

As above, the interpretation of the complete complex output of the FFT in (151) is furnished by returning to the continuous version of the sampled $y_{4s}(t)$ in (150). We express it as

$$y_{4s}(t) = -\ \mathrm{Im}\ 4 \int_0^{\infty} df\ \exp(i2\pi ft)\; Y_i(f)\ \Delta\ \delta_\Delta(f) =$$

$$= \mathrm{Im}\{z_2(t) \circledast \delta_{1/\Delta}(t)\}\ , \tag{152}$$

where we define, for all t, Fourier transform

$$z_2(t) = - 4 \int_0^\infty df \exp(i2\pi ft) \; Y_i(f) =$$

$$= i \int_0^\infty df \exp(i2\pi ft) \; [2Y(f) - 2Y^*(f)] =$$

$$= i[y_+(t) - y_+^*(-t)] = i[\underline{y}(t) - \underline{y}^*(-t)] \exp(i2\pi f_c t) = \qquad (153)$$

$$= i[y(t) - y(-t)] - y_H(t) - y_H(-t) \; . \qquad (154)$$

Again, the aliasing of $z_2(t)$ in (152) and the mirror image of the analytic waveform and complex envelope in (153) will serve to confuse the usefulness of $z_2(t)$. The imaginary part of $z_2(t)$ in (154) for $t > 0$ is just $y(t)$, as expected, for this causal real waveform.

DISPLACED SAMPLING

If displaced samples of a waveform are desired, such as at time locations $(k+\beta)/(N\Delta)$ in (145), where $0 < \beta < 1$, we can obtain them via an N-point FFT as follows: from (131),

$$y_1\left(\frac{k+\beta}{N\Delta}\right) = \Delta \sum_n \exp(i2\pi nk/N)\, \exp(i2\pi n\beta/N)\, Y(n\Delta) = \tag{155}$$

$$= \Delta \sum_{n=0}^{N-1} \exp(i2\pi nk/N)\, z_n \quad \text{for } 0 \le k \le N-1 , \tag{156}$$

where $\{z_n\}$, $0 \le n \le N-1$, is the collapsed version of sequence $\{\exp(i2\pi n\beta/N)\, Y(n\Delta)\}$, $-\infty < n < \infty$. That is, we have to load up the arrays containing $\{z_n\}$ with phase-shifted versions of the original sequence $\{Y(n\Delta)\}$ and then perform the N-point FFT. Calculation of phasor $p_n = \exp(i2\pi n\beta/N)$ in (155) can take advantage of recursion $p_n = p_{n-1} \exp(i2\pi\beta/N)$.

SUMMARY

The advantages of filtering the complex envelope spectrum by means of a suitable lowpass filter are significant in some instances. The singular behavior of the complex envelope waveform is eliminated by utilizing a filter which cuts off at finite frequencies, while the slow decay in the time domain of the complex envelope is circumvented by using a filter with a smoothly tapered cutoff that prevents any discontinuities in the complex envelope spectrum from contributing.

The use of an FFT to evaluate the filtered complex envelope is then an attractive efficient approach because the inherent time aliasing associated with frequency sampling has been greatly suppressed. Also, the very rapidly varying singular components of the complex envelope have been eliminated, allowing for a lower time-sampling rate, that is, smaller FFT sizes.

When two waveforms, each with its own imposed amplitude- and phase-modulations, are convolved, such as encountered in the narrowband excitation of a passband filter, the output complex envelope is given exactly by the convolution of the individual complex envelopes. Although the convolution of the two (complex) imposed modulations is often a good approximation to the output complex envelope, it has an error term. This analysis is presented in appendix C.

APPENDIX A. DETERMINATION OF CENTER FREQUENCY

Suppose we are given spectrum $Y(f)$ of (narrowband) real waveform $y(t)$, but the center frequency of $Y(f)$ is not obvious or is unknown. The analytic waveform is still uniquely given by

$$y_+(t) = \int df \exp(i2\pi ft)\, Y_+(f) = 2 \int_0^\infty df \exp(i2\pi ft)\, Y(f) \ . \qquad \text{(A-1)}$$

Make a guess at initial frequency f_i near the center of $Y_+(f)$. Then compute the initial down-shifted waveform

$$y_i(t) \equiv \exp(-i2\pi f_i t)\, y_+(t) = 2 \int_{-f_i}^\infty df \exp(i2\pi ft)\, Y(f+f_i) \ . \qquad \text{(A-2)}$$

Compute initial phase $P_i(t) = \arg\{y_i(t)\}$ and then unwrap $P_i(t)$. Select time t in the interval T of interest and fit a straight line $\alpha + \beta t$ to the unwrapped phase $P_i(t)$ over T. Compute frequency

$$f_c = f_i + \frac{\beta}{2\pi} \ ; \qquad \text{(A-3)}$$

this is the center frequency of $y_+(t)$ for $t \in T$. Another selection of a different time interval could lead to a somewhat different center frequency; there is no unique center frequency of an arbitrarily given spectrum $Y(f)$.

The complex envelope is then

$$\underline{y}(t) = \exp(-i2\pi f_c t)\, y_+(t) \ . \qquad \text{(A-4)}$$

The "physical" envelope or extracted amplitude modulation is

$$A(t) = |\underline{y}(t)| = |y_+(t)| = |y_i(t)| \ , \tag{A-5}$$

which is independent of the choice of f_i or f_c. The extracted phase of complex envelope $\underline{y}(t)$ is

$$P(t) = \arg\{\underline{y}(t)\} = \arg\{y_+(t) \exp(-i2\pi f_c t)\} = P_i(t) - \beta t \ , \tag{A-6}$$

where we used (A-4) and (A-2). Functions $y_i(t)$ and $P_i(t)$ have already been computed and can be used to evaluate the envelope A(t) and phase P(t). The real waveform is

$$y(t) = \mathrm{Re}\{y_+(t)\} = \mathrm{Re}\{\underline{y}(t) \exp(i2\pi f_c t)\} = A(t) \cos[2\pi f_c t + P(t)], \tag{A-7}$$

in terms of chosen center frequency f_c and amplitude and phase modulations A(t) and P(t), respectively. Although f_c and P(t) are not unique, the argument of the cosine and the waveform y(t) in (A-7) are unique, as may be seen by the first equality in (A-7). All of these relations hold for time $t \in T$.

If the fit of the straight line $\alpha + \beta t$ to initial unwrapped phase $P_i(t)$ over interval T is via minimum error energy, then we find

$$\beta = \frac{\mu_o \nu_1 - \mu_1 \nu_o}{\mu_o \mu_2 - \mu_1^2} \ , \qquad \mu_n = \int_T dt \ t^n \ , \qquad \nu_n = \int_T dt \ t^n \ P_i(t) \ . \tag{A-8}$$

There is no need to explicitly compute α, although it should be included in the error energy minimization in order to afford a better fit.

APPENDIX B. PROGRAM FOR FILTERED COMPLEX ENVELOPE VIA FFT

The program listed below actually computes the unfiltered complex envelope by means of an FFT. In order to convert it to one which will compute the filtered complex envelope, remove lines 220 - 320 and replace them by the following lines:

```
220     F1=40.                  !  CUTOFF FREQUENCY < Fo
230     H1=.5*PI/F1
240     M1=M*F1/Fo
250     FOR Ms=-M1 TO M1        !  -F1 < F < F1
260     J=Ms MODULO N           !  COLLAPSING
270     F=Df*Ms                 !  FREQUENCY f
280     CALL Y(F+Fo,Al,Wo,Cp,Sp,Yr,Yi) !SHIFTED FREQUENCY FUNCTION
290     Cos=COS(H1*F)
300     H=Cos*Cos               !  REAL LOWPASS HANN FILTER
310     X(J)=X(J)+Yr*H
320     Y(J)=Y(J)-Yi*H          !  CONJUGATE INPUT INTO FFT
```

```
 10  ! COMPLEX ENVELOPE VIA SHIFTED FREQUENCY FUNCTION
 20    Al=1                    !  DAMPING ALPHA
 30    Fo=100                  !  CARRIER FREQUENCY
 40    Phi=-PI/2               !  PHASE
 50    M=8000                  !  NUMBER OF SAMPLES FOR F < 0; LINE 270
 60    N=1024                  !  SIZE OF FFT; ZERO SUBSCRIPT
 70    REDIM Cos(0:N/4),X(0:N-1),Y(0:N-1)
 80    DIM Cos(1024),X(4096),Y(4096)
 90    DOUBLE M,N,N2,J,Ms      !  INTEGERS, NOT DOUBLE PRECISION
100    N2=N/2
110    A=2.*PI/N
120    FOR J=0 TO N/4
130    Cos(J)=COS(A*J)         !  QUARTER-COSINE TABLE IN Cos(*)
140    NEXT J
150    Cp=COS(Phi)
160    Sp=SIN(Phi)
170    Wo=2*PI*Fo
180    Df=Fo/M                 !  FREQUENCY INCREMENT
190    Dt=1./(N*Df)            !  TIME INCREMENT ON COMPLEX ENVELOPE
200    MAT X=(0.)
210    MAT Y=(0.)
220    Ms=-M
230    J=Ms MODULO N
240    CALL Y(0.,Al,Wo,Cp,Sp,Yr,Yi)   !   Y(0)
250    X(J)=.5*Yr
260    Y(J)=-.5*Yi             !  CONJUGATE INPUT TO FFT
270    FOR Ms=-M+1 TO M*10 !  NOTICE UPPER LIMIT ON FREQUENCY
280    J=Ms MODULO N           !  COLLAPSING
290    F=Df*Ms                 !  FREQUENCY f
300    CALL Y(F+Fo,Al,Wo,Cp,Sp,Yr,Yi)   !   SHIFTED FREQUENCY FUNCTION
310    X(J)=X(J)+Yr
320    Y(J)=Y(J)-Yi            !  CONJUGATE INPUT TO FFT
330    NEXT Ms
```

```
340   MAT X=X*(2.*Df)
350   MAT Y=Y*(2.*Df)                    !    *       CONJUGATE
360   CALL Fft14(N,Cos(*),X(*),Y(*))     !  y (t)     OF COMPLEX
370   GINIT                              !  -         ENVELOPE
380   PLOTTER IS "GRAPHICS"
390   GRAPHICS ON
400   WINDOW -N2,N2,-8,0                 !  CENTER PLOT AT TIME t = 0
410   LINE TYPE 3
420   GRID N/8,1
430   LINE TYPE 4
440   MOVE 0,0
450   Ts=Dt*N/4
460   DRAW N/4,LGT(EXP(-A1*Ts))
470   PENUP
480   LINE TYPE 1
490   FOR Ms=-N2 TO N2
500   J=Ms MODULO N
510   X=X(J)
520   Y=Y(J)
530   T=X*X+Y*Y              !  MAGNITUDE SQUARED COMPLEX ENVELOPE
540   IF T>0. THEN 570
550   PENUP
560   GOTO 580
570   PLOT Ms,LGT(T)*.5      !  MAGNITUDE OF COMPLEX ENVELOPE
580   NEXT Ms
590   PENUP
600   PAUSE
610   GCLEAR
620   GRAPHICS ON
630   WINDOW -N2,N2,-PI,PI
640   LINE TYPE 3
650   GRID N/8,PI/2
660   LINE TYPE 1
670   FOR Ms=-N2 TO N2               !  PLOT COMPLEX ENVELOPE PHASE
680   J=Ms MODULO N
690   PLOT Ms,FNArg(X(J),-Y(J))      !  CONJUGATE THE FFT OUTPUT
700   NEXT Ms
710   PENUP
720   PAUSE
730   GCLEAR
740   GRAPHICS ON
750   LINE TYPE 3
760   GRID N/8,PI/2
770   LINE TYPE 1
780   FOR Ms=-N2 TO N2
790   J=Ms MODULO N
800   Ts=Ms*Dt               !  TIME t
810   Cos=COS(Wo*Ts)         !  SHIFT PHASE THE
820   Sin=SIN(Wo*Ts)         !  COMPLEX ENVELOPE BY Wo Ts
830   X=X(J)
840   Y=-Y(J)                !  CONJUGATE THE FFT OUTPUT
850   PLOT Ms,FNArg(X*Cos-Y*Sin,X*Sin+Y*Cos)
860   NEXT Ms
870   PENUP
880   PAUSE
890   END
900   !
```

```
910    DEF FNArg(X,Y)        !  PRINCIPAL ARG(Z)
920    IF X=0. THEN RETURN .5*PI*SGN(Y)
930    A=ATN(Y/X)
940    IF X>0. THEN RETURN A
950    IF Y<0. THEN RETURN A-PI
960    RETURN A+PI
970    FNEND
980    !
990    SUB Y(F,A1,Wo,Cp,Sp,Yr,Yi)  !  SPECTRAL FUNCTION
1000   W=2.*PI*F
1010   T=W-Wo
1020   D=A1*A1+T*T
1030   R1=(Cp*A1+Sp*T)/D
1040   I1=(Sp*A1-Cp*T)/D
1050   T=W+Wo
1060   D=A1*A1+T*T
1070   R2=(Cp*A1-Sp*T)/D
1080   I2=(-Sp*A1-Cp*T)/D
1090   Yr=.5*(R1+R2)
1100   Yi=.5*(I1+I2)
1110   SUBEND
1120   !
1130   SUB Fft14(DOUBLE N,REAL Cos(*),X(*),Y(*)) ! N<=2^14=16384; 0 SUBS
1140   DOUBLE Log2n,N1,N2,N3,N4,J,K    !  INTEGERS < 2^31 = 2,147,483,648
1150   DOUBLE I1,I2,I3,I4,I5,I6,I7,I8,I9,I10,I11,I12,I13,I14,L(0:13)
1160   IF N=1 THEN SUBEXIT
1170   IF N>2 THEN 1250
1180   A=X(0)+X(1)
1190   X(1)=X(0)-X(1)
1200   X(0)=A
1210   A=Y(0)+Y(1)
1220   Y(1)=Y(0)-Y(1)
1230   Y(0)=A
1240   SUBEXIT
1250   A=LOG(N)/LOG(2.)
1260   Log2n=A
1270   IF ABS(A-Log2n)<1.E-8 THEN 1300
1280   PRINT "N =";N;"IS NOT A POWER OF 2; DISALLOWED."
1290   PAUSE
1300   N1=N/4
1310   N2=N1+1
1320   N3=N2+1
1330   N4=N3+N1
1340   FOR I1=1 TO Log2n
1350   I2=2^(Log2n-I1)
1360   I3=2*I2
1370   I4=N/I3
1380   FOR I5=1 TO I2
1390   I6=(I5-1)*I4+1
1400   IF I6<=N2 THEN 1440
1410   A1=-Cos(N4-I6-1)
1420   A2=-Cos(I6-N1-1)
1430   GOTO 1460
1440   A1=Cos(I6-1)
1450   A2=-Cos(N3-I6-1)
1460   FOR I7=0 TO N-I3 STEP I3
1470   I8=I7+I5-1
1480   I9=I8+I2
```

```
1490    T1=X(I8)
1500    T2=X(I9)
1510    T3=Y(I8)
1520    T4=Y(I9)
1530    A3=T1-T2
1540    A4=T3-T4
1550    X(I8)=T1+T2
1560    Y(I8)=T3+T4
1570    X(I9)=A1*A3-A2*A4
1580    Y(I9)=A1*A4+A2*A3
1590    NEXT I7
1600    NEXT I5
1610    NEXT I1
1620    I1=Log2n+1
1630    FOR I2=1 TO 14
1640    L(I2-1)=1
1650    IF I2>Log2n THEN 1670
1660    L(I2-1)=2^(I1-I2)
1670    NEXT I2
1680    K=0
1690    FOR I1=1 TO L(13)
1700    FOR I2=I1 TO L(12) STEP L(13)
1710    FOR I3=I2 TO L(11) STEP L(12)
1720    FOR I4=I3 TO L(10) STEP L(11)
1730    FOR I5=I4 TO L(9) STEP L(10)
1740    FOR I6=I5 TO L(8) STEP L(9)
1750    FOR I7=I6 TO L(7) STEP L(8)
1760    FOR I8=I7 TO L(6) STEP L(7)
1770    FOR I9=I8 TO L(5) STEP L(6)
1780    FOR I10=I9 TO L(4) STEP L(5)
1790    FOR I11=I10 TO L(3) STEP L(4)
1800    FOR I12=I11 TO L(2) STEP L(3)
1810    FOR I13=I12 TO L(1) STEP L(2)
1820    FOR I14=I13 TO L(0) STEP L(1)
1830    J=I14-1
1840    IF K>J THEN 1910
1850    A=X(K)
1860    X(K)=X(J)
1870    X(J)=A
1880    A=Y(K)
1890    Y(K)=Y(J)
1900    Y(J)=A
1910    K=K+1
1920    NEXT I14
1930    NEXT I13
1940    NEXT I12
1950    NEXT I11
1960    NEXT I10
1970    NEXT I9
1980    NEXT I8
1990    NEXT I7
2000    NEXT I6
2010    NEXT I5
2020    NEXT I4
2030    NEXT I3
2040    NEXT I2
2050    NEXT I1
2060    SUBEND
```

APPENDIX C. CONVOLUTION OF TWO WAVEFORMS

Suppose real waveform $x(t)$ excites passband filter $H(f)$ with real impulse response $h(t)$. Then, the output is

$$Y(f) = H(f)\,X(f) , \qquad y(t) = h(t) \circledast x(t) . \tag{C-1}$$

The single-sided output spectrum is

$$Y_+(f) = 2\,U(f)\,Y(f) = 2\,U(f)\,H(f)\,X(f) = \frac{1}{2}\,H_+(f)\,X_+(f) . \tag{C-2}$$

The corresponding output analytic waveform is exactly

$$y_+(t) = \frac{1}{2}\,h_+(t) \circledast x_+(t) , \tag{C-3}$$

which is just (one-half of) the convolution of the individual analytic waveforms.

If the center frequency of $Y_+(f)$ is f_c (see appendix A), then the spectrum of the output complex envelope is, using (C-2),

$$\underline{Y}(f) = Y_+(f+f_c) = \frac{1}{2}\,H_+(f+f_c)\,X_+(f+f_c) = \frac{1}{2}\,\underline{H}(f)\,\underline{X}(f) , \tag{C-4}$$

where we have taken the <u>same</u> center frequency, f_c, for $H_+(f)$ as well as $X_+(f)$. This relation in (C-4) is exact; it involves <u>no narrowband approximations</u>. The output complex envelope corresponding to (C-4) is then exactly

$$\underline{y}(t) = \frac{1}{2}\,\underline{h}(t) \circledast \underline{x}(t) . \tag{C-5}$$

That is, the complex envelope of the convolution of any two waveforms is equal to (one-half of) the convolution of the two individual complex envelopes, irrespective of their frequency contents.

Now suppose that $x(t)$ is given in terms of some complex <u>imposed</u> modulation $x_i(t)$ according to

$$x(t) = \mathrm{Re}\{x_i(t)\ \exp(i2\pi f_c t)\}\ , \tag{C-6}$$

which allows for amplitude-modulation as well as phase-modulation. The spectrum of $x(t)$ can then be expressed as

$$X(f) = \frac{1}{2}\ [X_i(f-f_c) + X_i^*(-f-f_c)]\ . \tag{C-7}$$

Also, suppose that filter impulse response $h(t)$ is expressible in a similar form according to

$$h(t) = \mathrm{Re}\{h_i(t)\ \exp(i2\pi f_c t)\}\ , \tag{C-8}$$

with corresponding transfer function

$$H(f) = \frac{1}{2}\ [H_i(f-f_c) + H_i^*(-f-f_c)]\ . \tag{C-9}$$

The filter output spectrum then follows from (C-1), (C-7), and (C-9) as

$$\begin{aligned} Y(f) = \frac{1}{4}\ [&H_i(f-f_c)\ X_i(f-f_c) + H_i^*(-f-f_c)\ X_i^*(-f-f_c) + \\ &+ H_i^*(-f-f_c)\ X_i(f-f_c) + H_i(f-f_c)\ X_i^*(-f-f_c)\ ]\ . \end{aligned} \tag{C-10}$$

By inverse Fourier transforming the individual terms, the corresponding waveform to (C-10) is found to be exactly

$$y(t) = \mathrm{Re}\{\exp(i2\pi f_c t)\ [y_a(t) + y_b(t)]\}\ , \tag{C-11}$$

where

$$y_a(t) = \frac{1}{2} h_i(t) \circledast x_i(t) \ , \tag{C-12}$$

and

$$y_b(t) = \frac{1}{2} [h_i^*(t) \exp(-i4\pi f_c t)] \circledast x_i(t) \ . \tag{C-13}$$

Relation (C-12) states that component $y_a(t)$ of output $y(t)$ in (C-11) is just the convolution of the two complex imposed modulations $h_i(t)$ and $x_i(t)$. However, (C-11) and (C-13) reveal that there is an additional term in $y(t)$, which requires the convolution of a relatively high-frequency component, namely $\exp(-i4\pi f_c t)$. Since this latter term, $y_b(t)$, will often be small due to this oscillatory integrand, we may neglect it in many circumstances.

A good way of assessing the importance of the $y_b(t)$ term in (C-11) is to observe that it is due to the second line of the spectrum in (C-10); the first line in (C-10) corresponds to $y_a(t)$. Since $H_i(f)$ and $X_i(f)$ are generally lowpass functions of frequency, the function $H_i(-f-f_c)$ in (C-10) is centered around $f = -f_c$, while the $X_i(f-f_c)$ term peaks near $f = f_c$. The separation of these two functions is approximately $2f_c$ on the f axis; if this separation is somewhat greater than the bandwidths of H_i and X_i, then there is inconsequential overlap of any of the frequency components in the second line of (C-10). This leads to a small value for $y_b(t)$ for all t and we can neglect its effect relative to $y_a(t)$ in (C-11).

REFERENCES

[1] A. H. Nuttall, **Alias-Free Wigner Distribution Function and Complex Ambiguity Function for Discrete-Time Samples**, NUSC Technical Report 8533, Naval Underwater Systems Center, New London, CT, 14 April 1989.

[2] A. H. Nuttall, "On the Quadrature Approximation to the Hilbert Transform of Modulated Signals", **Proceedings IEEE**, volume 54, number 10, pages 1458 - 1459, October 1966.

[3] **Handbook of Mathematical Functions**, U. S. Department of Commerce, National Bureau of Standards, Applied Mathematics Series, Number 55, U. S. Government Printing Office, Washington, DC, June 1964.

[4] A. H. Nuttall and B. Dedreux, **Exact Operating Characteristics for Linear Sum of Envelopes of Narrowband Gaussian Process and Sinewave**, NUSC Technical Report 7117, Naval Underwater Systems Center, New London, CT, 11 January 1984.

[5] A. H. Nuttall, "Alternative Forms and Computational Considerations for Numerical Evaluation of Cumulative Probability Distributions Directly From Characteristic Functions," **Proceedings IEEE**, Volume 58, Number 11, pages 1872 - 1873, November 1970. Also in NUSC Report Number NL-3012, Naval Underwater Systems Center, New London, CT, 12 August 1970.

SUBJECT MATTER INDEX